Magnetic Resonance Imaging in Parkinsons's disease and related disoders

Surova, Yulia

2018

Document Version:
Publisher's PDF, also known as Version of record

Magnetic Resonance Imaging in Parkinson's disease and related disorders

Magnetic Resonance Imaging in Parkinson's disease and related disorders

Yulia Surova

LUND
UNIVERSITY

DOCTORAL DISSERTATION
by due permission of the Faculty of Medicine, Lund University, Sweden.
To be defended at Föreläsningssal 4 C-block University Hospital of Lund on
Friday, Mars 23, 2018 at 13:00 p.m.

Faculty opponent
professor Lars Forsgren

Organization LUND UNIVERSITY	Document name DOCTORAL DISSERTATION
	Date of issue September 1, 2017
Author(s) Yulia Surova	Sponsoring organization

Title and subtitle

Magnetic Resonance Imaging in Parkinson's disease and related disorders

Abstract

Objectives: To identify diagnostic and prognostic biomarkers in the cerebral white (WM) and the deep grey matter (GM) in patients with Parkinson's disease (PD) and atypical parkinsonian syndromes (APS) using magnetic resonance imaging (MRI).

Methods: Patients with a clinical diagnosis of PD, multiple system atrophy (MSA) and progressive supranuclear palsy (PSP) were included in the study. Patients and controls underwent standardized clinical assessment and testing regarding motor and cognitive function. All patients underwent MRI, including Diffusion tensor imaging (DTI), Diffusion tensor tractography (DTT), Diffusion kurtosis imaging (DKI), Neurite density Imaging (NDI), morphometric analyses and susceptibility weighted imaging (SWI).

Results:

In paper I we assessed both global and regional changes in larger cerebral WM tracts of patients with PD, MSA-P, and PSP, employing DTT. We found that the anterior portion of the corpus callosum is a promising region for detection of neurodegenerative changes in patients with PSP, as well as for differential diagnosis between PSP and PD.

In paper II we investigated the disease specific changes in the basal ganglia, the thalamus, the pons, the midbrain, and the dentato-rubro-thalamic tract (DRTT) of patients with PD, MSA-P, and PSP, using DTI and morphometric analyses. We found that patients with PSP, but not PD or MSA-P, exhibit signs of structural abnormalities in the thalamus and in the DRTT. We also found that these disease-specific changes are associated with disease stage and impaired motor function.

In paper III we investigated if changes in subcortical nuclei, brainsteam and WM tracts measured by DKI and NDI could differentiate between PD and controls, and between phenotypes, such as postural instability gait difficulty (PIGD) and tremor dominant (TD) PD. We found that patients with PD exhibit diffusion MRI (dMRI) changes in the putamen, the thalamus, and the superior longitudinal fasciculus associated with worse disease severity. However, the dMRI changes were not sufficiently specific to improve the diagnostic work-up of PD.

In paper IV we investigated longitudinal dMRI measures over a two year period in PD. The study indicates that in PD microstructural changes in the putamen occur selectively over a two-year period and can be detected with DKI.

In paper V we evaluated the use of quantitative susceptibility mapping (QSM) for clinical diagnostics in PD, PSP and MSA. PSP showed higher susceptibility in the globus pallidus, substantia nigra, red nucleus and dentate nucleus compared to all other groups, and higher putaminal susceptibility compared to PD and controls. MSA showed higher putaminal susceptibility compared to PD and controls, and higher susceptibility in the substantia nigra and dentate nucleus compared to PD. Discriminant analysis between PSP and all other groups combined, a sensitivity of 91% and specificity of 97% was achieved. Using all regions to separate MSA from all other groups combined, a sensitivity of 70% and specificity of 93% was noted. We also found correlations between disease severity measured by motor part of unified PD raiting scale (UPDRS-III) and putaminal susceptibility in PD.

Key words: Magnetic Resonance Imaging, Parkinson's disease, tractography, Diffusional Kurtosis, quantitative susceptibility mapping

Classification system and/or index terms (if any)

Supplementary bibliographical information	Language English
ISSN and key title 1652-8220	ISBN 978-91-7619-590-1
Recipient's notes	Number of pages 98 / Price / Security classification

Magnetic Resonance Imaging in Parkinson's disease and related disorders

Yulia Surova

LUND
UNIVERSITY

Lund University, Faculty of Medicine Doctoral Dissertation Series 2018:23

ISBN 978-91-7619-590-1
ISSN 1652-8220

Printed in Sweden by Media-Tryck, Lund University
Lund 2018

MADE IN SWEDEN

Table of Contents

Original papers

I. Surova Y**,** Szczepankiewicz F, Lätt J, Nilsson M, Eriksson B, Leemans A, Hansson O, van Westen D, Nilsson C. Assessment of global and regional diffusion changes along white matter tracts in parkinsonian disorders by MR tractography. *PLoS One*. 2013 Jun 13;8(6)

II. Surova Y**,** Nilsson M, Lätt J, Lampinen B, Lindberg O, Hall S, Widner H, Nilsson C, van Westen D, Hansson O. Disease-specific structural changes in thalamus and dentatorubrothalamic tract in progressive supra nuclear palsy. Surova Y et al. *Neuroradiology*. 2015 Nov 57(11):1079-91

III. Surova Y**,** Lampinen B, Nilsson M, Lätt J, Hall S, Widner H, Swedish BioFINDER study, van Westen D, Hansson O. Alterations of diffusion kurtosis and neurite density measures in deep grey matter and white matter in Parkinson's disease. *PLoS One*. 2016 Jun 30;11(6)

IV. Surova Y**,** Lampinen B, Nilsson M, Lätt J, Hall S, Widner H, Swedish BioFINDER study, van Westen D, Hansson O. Alteration of putaminal kurtosis in longitudinal study in Parkinson's disease. *Neuroradiology.* 2018 March 60(3):247-254

V. Sjöström H, Surova Y, Nilsson M, Granberg T, Westman E, van Westen D, Svenningsson P, Hansson O. Quantitative susceptibility mapping (QSM) in parkinsonism – potentially improving diagnostic. *Neurology* under revision

Abbreviations

ADC	Apparent diffusional coefficient
CBD	Corticobasal degeneration
CC	Corpus callosum
CG	Cingulum
CSF	Cerebrospinal fluid
CST	Corticospinal tract
DKI	Diffusion kurtosis imaging
DLB	Dementia with Lewy bodies
dMRI	Diffusion magnetic resonance imaging
DTI	Diffusion tensor imaging
GM	Grey matter
MCP	Middle cerebellar peduncles
MMSE	Mini Mental State Examination
MSA	Multiple System Atrophy
NDI	Neurite density imaging
NODDI	Neurite orientation dispersion and density imaging
PD	Parkinson's disease
PET	Positron emission tomography
PIGD	Postural instability gait difficulty
QSM	Quantitative susceptibility mapping
PSP	Progressive supranuclear palsy
PIGD	Postural instability and gait difficulty
SWI	Susceptibility-weighted imaging
SPECT	Single-photon emission computed tomography
RBD	Rapid eye sleep behavioural disorder
SCP	Superior cerebellar peduncle
SLF	Superior longitudinal fasciculus
TD	Tremor dominant
UPDRS	Unified Parkinson's disease rating scale
	Mathematical symbols
AAC	Apparent area coefficient
FA	Fractional anisotropy
f_{ic}	Neurite density index
f_{iso}	Partial fraction of free water
ES	Effect size
MD	Mean diffusivity
MK	Mean kurtosis
Dr	Radial diffusivity
Da	Axial diffusivity

Populärvetenskaplig sammanfattning

Parkinsons sjukdom (PS) är den näst vanligaste neurodegenerativa sjukdomen, där nervsystemet bryts ned, och dess betydelse ökar när befolkningen åldras. Sjukdomen belastar patienter, anhöriga och samhället. Läkemedel som kan stoppa sjukdomen saknas. Misslyckade resultat från stora kliniska läkemedelsprövningar speglar bl.a. bristen på metoder för tidig sjukdomsdiagnostik. Hjärnavbildning med Single-photon emission computed tomography (SPECT) och Positron emission tomography (PET) kan användas för att detektera brist på dopaminceller vid PS, men strålning och höga kostnader begränsar deras kliniska användbarhet, liksom att förändringarna inte är specifika för PS utan även ses vid s.k. atypisk parkinsonism (progressiv supranuclear paralys (PSP) och multipel system atrofi (MSA). Magnetisk resonanstomografi (MRT, eng. MRI) av hjärna är allmänt tillgänglig och säker bildhanteringsmodalitet, fast den inte kan påvisa tecken till PS.

Diffusion MRT (dMRT), en MRT-sekvens, vilken avbildar mikrostrukturen i normal och patologisk vävnad baserad på vattenmolekylernas möjlighet till spontan mikroskopisk rörelse som man kallar för diffusion. I områden i hjärna med tät packade celler blir diffusionen långsam i alla riktningar, medan i cellstrukturer som är extremt avlånga, exempelvis nervfibrer, kan diffusionshastigheten skilja sig mellan olika riktningar. Diffusion kan också förändras om celler eller nervtrådar i hjärna angripas av en PS, PSP, MSA eller och ersättas med förändrad vävnad. Med dMRT kan vi mäta dessa förändringar och använda denna information både för diagnostik och för uppföljning av behandlingar.

Studier I-IV undersökte hur bra dMRT är på att skilja på patienter med PS från PSP och MSA. Studie I och II visade att patienter med PSP till skillnad från patienter med MSA och PS hade en förtunning av en främre del av en nervbana som hette corpus callosum (CC), en nervbana i hjärnstammen samt förändringar i thalamus mitt i hjärnan. Förändringarna korrelerade med kliniska skalor som avspeglade nedsatt motorik och balans hos patienter. Studie III visade att med dMRT kan man skilja på patienter med PS från friska kontroller med hjälp av förändringar i putamen, thalamus och i en nervbana som hette superior långitudinell fasciculus (SLF). De förändringarna var dock inte tillräcklig specifika för PS, eftersom att de fanns även hos patienter med MSA och PSP. Studie IV undersökte om det fanns dMRT förändringar vid PS efter 2 år och om de har samband med sjukdoms aktivitet. Studien visade att patienter med PS till skillnad från friska kontroller har förändringar i putamen efter 2 år. Dessa förändringar var ganska modesta men korrelerade med hur mycket läkemedel patienten tar mot PS.

En annan MRT-sekvens är så kallad Susceptibility weighted imaging (eng. SWI) användes i Studie V. SWI avspeglar järninlagring i hjärna. Vid neurodegenerativa sjukdomar som PS, PSP och MSA lagras järn i vissa strukturer specifikt. Studie V

påvisade att vid PSP lagrades mera järn i nucleus ruber, substantia nigra (SN) och pallidum jämfört med MSA och PS. MSA patienter lagrade mera järn i putamen jämfört med PS däremot. Vi tror att igenom att använda SWI sekvens vid MRT kan man med ganska hög sannolikhet skilja på patienter med PS från PSP och MSA.

Avhandlingens konklusion är att både dMRT och SWI har högre känslighet för att påvisa mikrostrukturella förändringar och järninlagring än konventionell MRT. Både dMRT och SWI har visat en viss potential för att skilja på patienter med PSP från övriga patienter med parkinsonistiska symtom. Studierna har gett lovande resultat, men större prospektiva och longitudinella studier behövs för att bekräfta den resultaten, och se om att de även är användbara tidigt i sjukdomen.

Introduction

Parkinsonism

Parkinsonism is a constellation of symptoms and signs. The definition used in this thesis is the United Kingdom Parkinson's Disease Society Brain Bank (UK PDSBB) definition: bradykinesia plus at least one of the following: 4-6 Hz rest tremor, muscular rigidity or postural instability not caused by primary visual, vestibular, cerebellar or proprioceptive dysfunction (Gibb and Lees 1988). Parkinsonism can be idiopathic or secondary. The idiopathic causes of parkinsonism are Parkinson's disease (PD) and the atypical parkinsonian syndromes (APS): MSA, PSP, and Corticobasal degeneration (CBD), and dementia with Lewy bodies (DLB) (Stamelou and Hoeglinger 2013). Apart from these sporadic neurodegenerative disorders, parkinsonism has also been described in a variety of other sporadic and hereditary neurodegenerative conditions such as frontotemporal dementia (FTD), Alzheimer's disease (AD), and Perry syndrome (Stamelou and Hoeglinger 2013). There are several possible causes of secondary parkinsonism, e.g. vascular injuries in the basal ganglia, encephalitis, side effects of medications (e.g. antipsychotic medications) (Ham, Cha et al. 2015), and traumatic brain injury (Bhidayasiri, Chotipanich et al. 2012).

Overview of idiopathic parkinsonian disorders

A common feature of the idiopathic parkinsonian disorders is the diminishing production of dopamine due to the degeneration of dopaminergic neurons in the SN. In the APS the degeneration is more widespread and also affects the post-synaptic neurons in the striatum thus leading to less responsiveness to treatment with dopaminergic drugs. The APS severely reduces life expectancy while PD has a more limited influence. Moreover, the early differential diagnosis of patients with APS, which would be important for clinical purposes (e.g., prognosis and treatment) and research purposes, is poor (Stamelou and Hoeglinger 2013). Unfortunately, there are no curative or disease-modifying treatments for any of the idiopathic parkinsonian disorders.

Parkinson's disease

PD is a common, chronic and progressive neurodegenerative condition. It is estimated to affect 100-180 people per 100,000 of the population and has an annual incidence of 4-20 per 100,000 people (Conditions 2006). The prevalence of PD rises sharply with age, from a mean of 41.51 per 100,000 in these aged 40-49 years to 1,902.98 per 100,000 in these aged over 80 years (Pringsheim, Jette et al. 2014). The prevalence and incidence are higher in men than in women.
The diagnosis of PD is primarily clinical, based on history and examination (Conditions 2006). The cardinal motor symptoms of PD are bradykinesia, rigidity, rest tremor and postural and gait disturbance (Rodriguez-Oroz, Jahanshahi et al. 2009). Non-motor symptoms and co-morbid syndromes in PD include cognitive impairment, depression, olfactory dysfunction, sleep disorders, constipation, genitourinary dysfunction, etc. (Barone, Antonini et al. 2009). Cognitive dysfunction occurs in 15-20% of early stage, untreated PD patients and may eventually be found in 40-80% of patients following long-term observation (Hely, Reid et al. 2008, Calabresi, Castrioto et al. 2013, Lin and Wu 2015).

The precise mechanism accounting for the decrease in dopamine-producing neurons is not fully understood. An early pathologic hallmark of PD is a decline in dopamine-producing neurons in the SN pars compacta (SNpc) (Saladin 2009). Impulses from this region of the midbrain, through projection to the corpus striatum, is essential for the regulation of normal movement. The striatum is the main input region of the basal ganglia for cortical information and plays an important role in motor control (Figure 1). Post-mortem pathology studies of PD patients' brains show that even mildly affected patients have lost about 60% of their dopamine-producing neurons in the SN (Greffard, Verny et al. 2006). It is this loss that account for the approximately 80% loss of dopamine in the corpus striatum in advanced patients (Zigmond 2002).

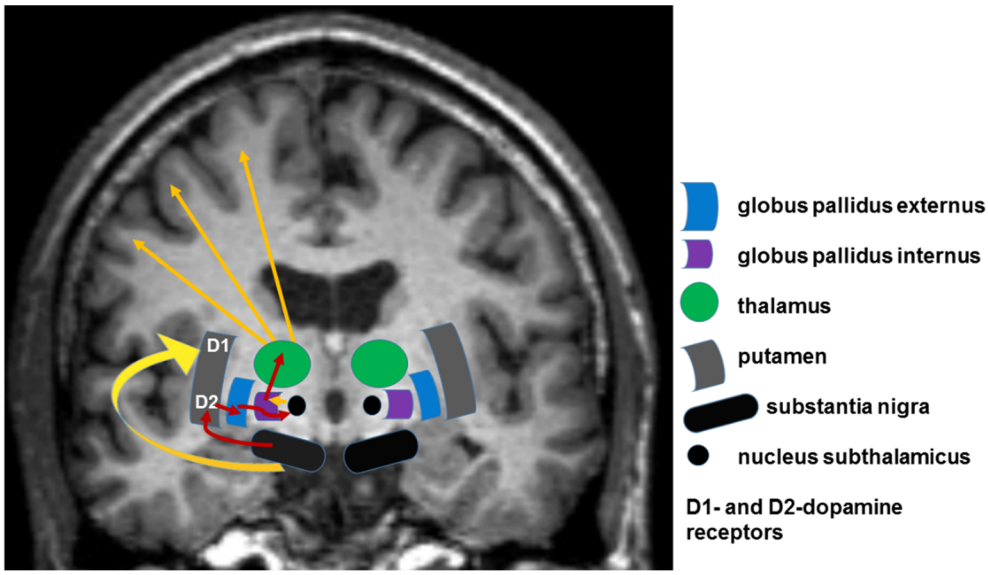

Figure 1
Schematic illustration of basal ganglia circuit. Red arrows means suppression, yellow arrows means induction. Patient from *BioFINDER* study.

Other non-dopaminergic neurotransmitter systems including acetylcholine, serotonin and noradrenaline neurons are also involved in PD (Duty 2012).
The pathological hallmark of PD is the presence of neuronal inclusions called Lewy bodies (Spillantini, Crowther et al. 1998). These structures contain misfolded aggregates of α-synuclein and ubiquitin. The Braak hypothesis suggests that α-synuclein inclusions may first accumulate in peripheral nerve tissue and subsequently spread to involve the midbrain and the cortex (Braak, Del Tredici et al. 2003). Attention is now being given to the importance of axonal degeneration in the neuropathophysiology of PD. Particularly, axonopathy precedes cell body death of nigral dopaminergic projection neurons. This is referred to as "dying-back degeneration" (Burke and O'Malley 2013). Note that axons in the brain, both myelinated and unmyelinated, traverse the brain in white matter (WM). Some implications of this axonal degeneration are that neuroimaging of WM and WM tracts, would be expected to show changes in PD, including in early stages.
While gene mutations account for as many as 15-20% of PD cases, a genetic predispositions associated with an environmental trigger may be a far more common cause (Wichmann 2002, Poewe and Mahlknecht 2009). The best documented and most widely investigated genetic causes are mutations in the *LRRK2* (coding for leucine-rich repeat kinase 2), *SNCA* (coding for α-synuclein) and parkin genes (Zigmond 2002).

Multiple system atrophy

MSA is a sporadic adult-onset neurodegenerative disease. It is characterised clinically by parkinsonism, cerebellar features and autonomic failure in varying combinations, and pathologically by the presence of neuronal loss, gliosis and a-synuclein positive oligodendroglial cytoplasmic inclusions in a selection of structures (Jellinger and Wenning 2016). These include supratentorially the striatum (particularly posterior putamen) and SN, infratentorially the inferior olives, pons and cerebellum, and the spinal cord intermediolateral cell columns and Onuf's nucleus (Jellinger and Wenning 2016). Consensus criteria are now widely used for a clinical diagnosis of MSA (Gilman, Wenning et al. 2008). There is agreement between Consensus Criteria and post-mortem confirmation of diagnosis (Iodice, Lipp et al. 2012, Figueroa, Singer et al. 2014).

The annual incidence of MSA is of 3 per 100,000 for subjects aged 50-99 years (Bower, Maraganore et al. 1997). The estimated prevalence of MSA is between 2 to 5 cases per 100,000 population (Schrag, Ben-Shlomo et al. 1999, Tison, Yekhlef et al. 2000). Mean age of symptom onset is 63.4 years (Wenning, Geser et al. 2013). Median survival from symptom onset in a prospective study was 8-10 years (Wenning, Geser et al. 2013, Low, Reich et al. 2015).

MSA is classified according to the predominant phenotype at onset into MSA-parkinsonism (MSA-P) or MSA-cerebellar type (MSA-C).

MSA-P is characterized by parkinsonism, and/or an irregular jerky postural and action tremor, postural instability and falls (usually within three years of motor onset), pyramidal signs, rapid progression regardless of dopaminergic treatment (Watanabe, Saito et al. 2002, Wenning, Colosimo et al. 2004), stimulus-sensitive cortical myoclonus, hemiballism and chorea, and dystonia unrelated to dopaminergic therapy (Quinn 1989, Wenning, Colosimo et al. 2004).

MSA-C is characterized by gait ataxia, limb ataxia, cerebellar scanning dysarthria, and cerebellar disturbances of eye movements (Wenning, Colosimo et al. 2004).
A greater than 50% response to levodopa was reported for only 1.5% of MSA patients. The cause of MSA is unknown, although likely linked to alterations in α-synuclein with subsequent formation of glial cytoplasmic inclusions and selective neuronal pathology (Ubhi, Low et al. 2011, Kuzdas-Wood, Stefanova et al. 2014). Familial MSA has been reported rarely. Whole-genome sequencing and linkage analysis of a sample obtained from a member of a multiplex family in whom MSA had been diagnosed on autopsy revealed a homozygous mutation (M78V–V343A/M78V–V343A) and compound heterozygous mutations (R337X/V343A) in *COQ2* in two multiplex families (Multiple-System Atrophy Research 2013).

Progressive supranuclear palsy

PSP is another disabling and fatal neurodegenerative disorder for which no disease-modifying treatment is available. Pathological diagnosis is defined by the presence of neuronal loss and gliosis together with abnormally phosphorylated 4R-tau protein in neurofibrillary tangles and tufted astrocytes in a characteristic distribution involving the globus pallidum, subthalamic nucleus, dentate nucleus, SN, midbrain, pons, medulla oblongata and, to a varying degree, frontal cortex (Williams and Lees 2009, Respondek, Stamelou et al. 2014).

The PSP course is one of relentless progression, increasing disability and death with a median survival of 5-10 years from onset of symptoms. PSP incidence was estimated to be 0.3-0.4 per 100,000 (Golbe, Davis et al. 1988). Estimates of PSP prevalence varies between 0.15 per 100,000 (Golbe, Davis et al. 1988) and 6.4 per 100,000 (2.3-10.6) (Schrag, Ben-Shlomo et al. 1999). Mean age of symptom onset is 63 (Bensimon, Ludolph et al. 2009).

The Movement Disorder Society (MDS) have recently developed the new PSP clinical diagnostic criteria (Hoglinger, Respondek et al. 2017). Four functional domains identified as clinical predictors of PSP: ocular motor dysfunction, postural instability, akinesia, and cognitive dysfunction. Within each of these domains, MDS proposed three clinical features that contribute different levels of diagnostic certainty. Combinations of these features define the diagnostic criteria, stratified by three degrees of diagnostic certainty: probable PSP, possible PSP, and suggestive of PSP. Clinical clues and imaging findings represent supportive features. Classic presentation of PSP is termed Richardson's syndrome (PSP-RS) (Williams, de Silva et al. 2005). PSP-RS is characterized by axial rigidity, retrocollis, early onset of postural instability and falls, supranuclear vertical gaze palsy, and cognitive dysfunction (Williams, de Silva et al. 2005). Other PSP variants include initial predominance of ocular motor dysfunction (PSP-OM), postural instability (PSP-PI), Parkinsonism resembling idiopathic PD (PSP-P), frontal lobe cognitive or behavioral presentations (PSP-F), including behavioral variant frontotemporal dementia (bvFTD), progressive gait freezing (PSP-PGF), corticobasal syndrome (PSP-CBS), primary lateral sclerosis (PSP-PLS), cerebellar ataxia (PSP-C), and speech/language disorders (PSP-SL), including nonfluent/agrammatic primary progressive aphasia (nfaPPA) and progressive apraxia of speech (AOS) (Hoglinger, Respondek et al. 2017). A retrospective study on autopsy-confirmed patients showed that only 24% of the PSP cases presented as PSP-RS, while more than half of the cases either had overlapping features of several phenotypes or could not be classified as one of the phenotypes already described (Respondek, Stamelou et al. 2014).

A genome-wide association study demonstrated two independent variants in the microtubule-associated protein tau gene *MAPT*, affecting risk for PSP, and

identified three significant novel genes conferring PSP risk (Hoglinger, Melhem et al. 2011).

Evaluation of auxiliary tests in differential diagnosis of parkinsonism

The differential diagnosis of parkinsonism is a major challenge for clinicians and movement disorder specialists, especially in the early stage of the disease. The American Academy of Neurology systematic review and practice parameter published in 2006 found insufficient evidence to support or refute the value of neurodiagnostic tests for distinguishing PD from other parkinsonism, including MRI, ultrasound of the brain parenchyma, ^{18}F-fluorodeoxyglucose (FDG) PET, urodynamics, autonomic testing, and urethral or anal electromyography (Suchowersky, Reich et al. 2006). While these techniques have continued to advance (Perlmutter and Norris 2014), the diagnosis of PD remains predominantly clinical (Perlmutter and Norris 2014).

SPECT/PET

SPECT is commonly used for PD diagnosis (Booth, Nathan et al. 2015). SPECT employs radioisotopes such as ^{123}I or ^{99m}Tc that have long half-lives and therefore do not require an on-site cyclotron. SPECT imaging using ^{123}I (^{123}I-FP-CIT-SPECT) provides information based on local binding of presynaptic dopamine transporters (DaT) with ^{123}I, which has been shown to be highly correlated with PD progression (Booth, Nathan et al. 2015). This binding measure is quantitative and assesses the spatial distribution of DaT. Most studies that use ^{123}I-FP-CIT-SPECT have focused on the striatum (i.e., putamen and caudate) (Booij, Tissingh et al. 1997, Benamer, Patterson et al. 2000, Antonini, Benti et al. 2003, Spiegel, Hellwig et al. 2007). Researchers have reported that PD has markedly reduced DaT levels in the striatum, which are correlated with disease progression and clinical scores (Booij, Tissingh et al. 1997, Benamer, Patterson et al. 2000, Antonini, Benti et al. 2003, Spiegel, Hellwig et al. 2007).

DaT SPECT has not been confirmed to be useful in differentiating APS from PD (Ghaemi, Hilker et al. 2002), significant striatal DaT loss is found in APS as well as in PD (Pirker, Asenbaum et al. 2000, Varrone, Marek et al. 2001). DaT SPECT is however useful in excluding essential tremor (Antonini, Moresco et al. 2001), drug-induced parkinsonism (Seifert and Wiener 2013), vascular parkinsonism (Brigo, Matinella et al. 2014), and AD (Hilker, Thomas et al. 2005, Bohnen, Kaufer et al. 2006).

PET has a higher resolution and sensitivity compared with SPECT. PET employs radioisotopes such as ^{11}C, ^{18}F, and ^{15}O that have relatively short half-lives and require a nearby cyclotron to provide the necessary radioisotopes.

^{18}F-DTBZ PET and ^{18}F-AV-133 PET explore the characteristics of vesicular monoamine transporter type 2 (VMAT2). ^{18}F-DTBZ PET demonstrated that the reduction of VMAT2 availability was obviously correlated with the severity of disease in patients with PD (Hsiao, Weng et al. 2014).

^{18}F-AV-133 PET demonstrated similar performance in differentiation PD from control, and a better correlation to clinical characteristics than that of ^{99m}Tc-TRODAT-1 SPECT (Hsiao, Weng et al. 2014). PET imaging using ^{18}F-FP-CIT (^{18}FP-CIT PET) measures DaT binding. Study with FDG PET and ^{18}FP-CIT PET demonstrated a significant relationship between loss of dopaminergic input to the caudate nucleus and the expression of a cognition-related disease network in unmedicated PD patients (Niethammer, Tang et al. 2013).

PET shows decreased ^{18}F-FDOPA tracer uptake in the caudate and putamen in patients with early PD compared with controls (Teune, Bartels et al. 2010, Pavese 2012).

FDG PET shows preserved or raised glucose metabolism of lentiform nucleus in PD, while it is reduced in most APS (Eckert, Tang et al. 2008, Brooks 2010). In an autopsy cohort including 7 PSP patients (all PSP-RS), the most common FDG PET findings were hypometabolism of the thalamus (100%), caudate (86%), midbrain (86%), and frontal lobes (71%) (Zalewski, Botha et al. 2014). PSP-RS tends to show greater frontal hypometabolism than PD and MSA (Klein, de Jong et al. 2005), with visual assessments of frontal hypometabolism producing good sensitivity (76%) and specificity (98%) for PSP-RS (Tripathi, Dhawan et al. 2013).

In summary, SPECT/PET has a role in diagnosis of parkinsonism but is relatively expensive, with limited availability, and requires radioactive tracers.

Magnetic resonance imaging

Conventional MRI is achievable, feasible, non-invasive examination that uses magnetic fields to create images of the body by detecting spin properties of nuclei. Most MRI studies are based on ^{1}H nuclei of hydrogen atoms (protons) found endogenously throughout the body.

The classic domain of conventional MRI is the exclusion of structural lesions that may cause secondary, symptomatic parkinsonism, such as normal pressure hydrocephalus, multiple sclerosis, or tumors. Cerebrovascular damage due to small vessel disease and infarctions, such as vascular parkinsonism, is perhaps the most common form of secondary parkinsonism, and abnormal structural MRI findings are present in up to 90 to 100% of these cases (Kalra, Grosset et al. 2010). In

idiopathic PD without concomitant cerebral disease, structural MRI is usually normal, at least early in the disease course.

In MSA, T2- weighted sequences may reveal the atrophy of the putamen, pons, and middle cerebellar peduncles (MCP) (Gilman, Wenning et al. 2008, Massano, Costa et al. 2008, Brooks, Seppi et al. 2009). Signal changes include hypointensity of the posterior putamen (also described as a slit-like void), a hyperintense lateral putaminal rim (sensitivity 44.4%)(Feng, Huang et al. 2015), and hyperintensities of the MCP (Figure 2). The "hot cross bun sign" refers to hyperintense T2 signal in the shape of a cross within the pons that arises from degeneration of transverse pontocerebellar fibers (Gilman, Wenning et al. 2008, Massano, Costa et al. 2008, Brooks, Seppi et al. 2009).

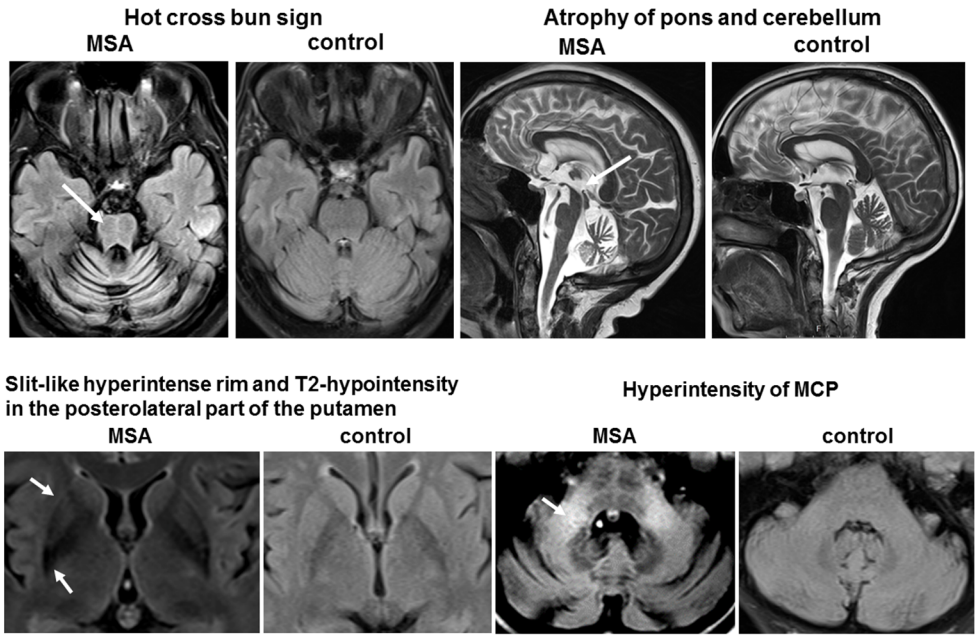

Figure 2
Structural MRI demonstrating the morphological characteristics of a clinically verified MSA patient from *BioFINDER* study. Top left sagittal slice shows the hot cross bun sign of the pons. Top right sagittal slice through the midbrain shows reduced volume of pons and cerebellum. Bottom left axial slice obvious putaminal atrophy, along with the slit-like hyperintense rim (arrow heads) and T2-hypointensity in the posterolateral part of the putamen (arrows). Bottom right sagittal image show hyperintense signal of middle cerebellar peduncle (MCP) (modified from reference (Gilman, Wenning et al. 2008, Massano, Costa et al. 2008, Brooks, Seppi et al. 2009)).

In PSP, structural MRI allows visual assessment of midbrain atrophy, midbrain or the presence of specific morphological markers such as the “hummingbird” sign (atrophy of dorsal midbrain resembles hummingbird’s head and bill in midsagittal plane) (Kato, Arai et al. 2003), “Mickey Mouse” sign (rounded rather than rectangular midbrain peduncles in axial planes) (Massey, Micallef et al. 2012) and

"morning glory" sign (concavity of the lateral margin of the midbrain tegmentum in axial planes) (Adachi, Kawanami et al. 2004) (Figure 3). These signs support the clinical diagnosis of PSP (Whitwell, Hoglinger et al. 2017).

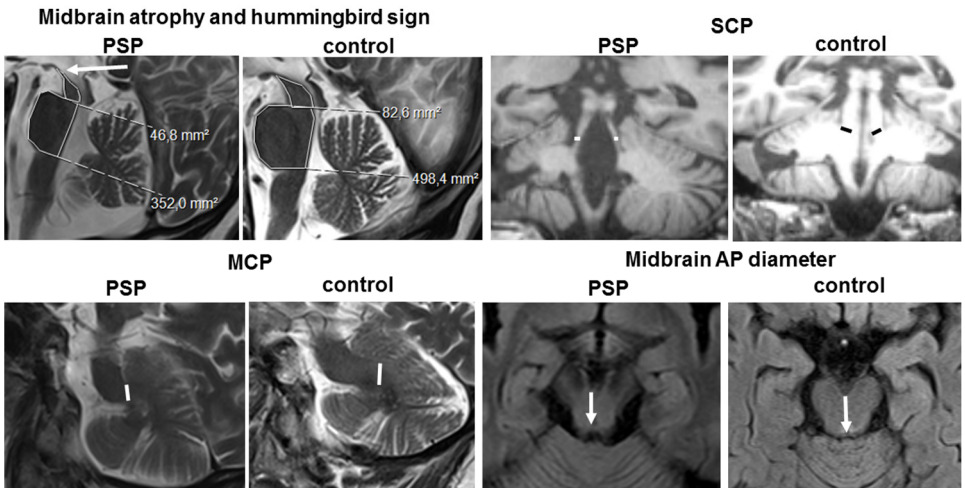

Figure 3
Structural MRI demonstrating the morphological characteristics of neuropathological verified PSP patient from the *BioFINDER* study. Top left sagittal slice shows the hummingbird sign with atrophy of the dorsal midbrain and relative preservation of the pons. Top middle axial slice through the midbrain shows rounded midbrain peduncles (Mickey Mouse sign) and concavity of the lateral margin of the midbrain tegmentum (morning glory sign [arrow]). Top right axial slice shows example measurements of the midbrain anteroposterior (AP) diameter. Bottom left and middle sagittal and right axial images show midbrain, and pons area, superior cerebellar peduncle (SCP) width, and middle cerebellar peduncle (MCP) width (modified from reference(Moller, Kassubek et al. 2017)).

In a published study, MRI from neuropathologically confirmed PSP (n = 22), MSA (n = 13), PD (n = 7), and CBD (n = 6), and controls (n = 9) were assessed blinded to clinical details and systematically rated for reported abnormalities. Radiological assessment of MRI was correct in 72.7% PSP cases and 76.9% MSA cases (Massey, Micallef et al. 2012). The "hummingbird" and "morning glory" signs were highly specific for PSP, and "the MCP sign" and "hot cross bun" for MSA, but sensitivity was lower (up to 68.4%) and characteristic findings may not be present even at autopsy (Massey, Micallef et al. 2012).

Morphometric Magnetic Resonance Imaging

Magnetic resonance volumetric (MRV) allows for the quantitative assessment of brain atrophy. MRV is performed in a semiautomated manner by defining a priori regions-of-interest (ROI). Employing this ROI-based approach, a variety of volume ratio indices have been proposed to assist in the differential diagnosis of parkinsonian syndromes. In PSP-RS, the midbrain-pons area (Cosottini, Ceravolo et al. 2007) and the MR Parkinsonism Index (MRPI = pons/midbrain area ratio x

the MCP/SCP width ratio) (Quattrone, Nicoletti et al. 2008) are the most reliable biomarkers. Diagnostic sensitivity and specificity values are typically high (>80 up to 90%) for differentiating PSP-RS from controls and from MSA and PD (Whitwell, Hoglinger et al. 2017). In MSA, pontocerebellar volume loss was reported (Paviour, Price et al. 2006). In contrast, regional volumes usually are normal in PD (Paviour, Price et al. 2006, Messina, Cerasa et al. 2011). It has been suggested, however, that atrophy of the SN may be present in APS (Kashihara, Shinya et al. 2011) as well as in early-stage PD (Ziegler, Wonderlick et al. 2013). That said, SN atrophy does not reliably distinguish PD from APS (Jesse, Kassubek et al. 2012).

Brain atrophy can also be assessed at the whole-brain level. Voxel-based morphometry (VBM) is a fully automated and rater-independent approach that does not necessitate the a priori delineation of ROIs, but relies on whole-brain voxel-wise comparisons (Ashburner and Friston 2000). Using VBM, several groups have reported cortical atrophy mainly in temporal associative, limbic, paralimbic, frontal, and parietal regions in PD (Biundo, Formento-Dojot et al. 2011, Pereira, Ibarretxe-Bilbao et al. 2012). Cortical atrophy in clinical practice is observed mainly in advanced PD. Two recent meta-analyses (Shi, Zhong et al. 2013, Yang, Shao et al. 2014) investigated atrophy patterns of the cerebral WM and gray matter (GM) in PSP patients. Subjects showed consistent WM reductions in the pons, midbrain, and adjacent to the basal ganglia (Yang, Shao et al. 2014). GM loss was observed in the thalamus, midbrain, basal ganglia, and insular and frontal cortices (Shi, Zhong et al. 2013). In MSA, volume loss of putamen (Hauser, Luft et al. 2006, Minnerop, Specht et al. 2007), as well as of sensorimotor, premotor, frontal, and insular cortices is common (Brenneis, Boesch et al. 2006, Minnerop, Specht et al. 2007). In CBD, asymmetric cortical atrophy may be discerned, whereas subcortical atrophy is often less severe compared with other APS (Boxer, Geschwind et al. 2006, Josephs, Whitwell et al. 2008).

VBM can differentiate between idiopathic PD and APS, with sufficient specificity and sensitivity (Focke, Helms et al. 2011), but there remains substantial overlap at the individual level. VBM is therefore not yet established in routine clinical practice.

Diffusion weighted imaging

Diffusion weighted imaging (DWI) is a form of MRI based upon measuring the random Brownian motion of water molecules within a voxel of tissue. Brownian motion, or molecular diffusion is the random displacement of molecules in a fluid, as the molecules are agitated by thermal energy. The phenomenon is named after botanist Robert Brown who, in 1827, observed and described the spontaneous motion of pollen grains dispersed in water (Brown 1828). In the early 20th century, Albert Einstein revisited the phenomenon and published a paper that explained in

detail how the motion that Brown had observed was the result of pollen being moved by individual water molecules (Einstein 1905).

In the human body, water displacement is random as long as the medium is homogenous and there are no barriers, such as in the ventricles in the brain. However, biological tissue is heterogeneous and consists of boundaries that will hinder the mobility of water molecules, such as cell membranes, organelles and other macromolecular structures. Thus, the diffusivity is affected and the displacement is no longer random – a fact that is exploited in diffusion MRI (dMRI).

The image acquisition of dMRI is based on pulsed gradient spin echo (Stejskal and Tanner 1965). Its principle is the application of bipolar magnetic gradients; the first gradient pulse dephases and the second pulse rephases the magnetization of protons in a specific volume element (i.e. voxel). For stationary elements, such as macromolecules, the pulses induced by both gradients will cancel out. However, for non-stationary particles, such as diffusing water molecules, some of them will have moved between the pulses. As a consequence, the rephasing will be incomplete and signal will be lost. The magnitude of signal loss is thus an indirect measure of water diffusivity in the tissue. The diffusion-weighted signal from a voxel of MRI data represents the summation of the effects that all the microstructures in that voxel have on diffusing water molecules (Umesh Rudrapatna, Wieloch et al. 2014). However, many different micro-environments may lead to similar diffusion-weighted signals, making it unspecific (Mulkern, Haker et al. 2009, Yablonskiy and Sukstanskii 2010).

The diffusion of water is rather isotropic in GM (i.e. equal in all directions), but anisotropic in WM (i.e. expressing a principal diffusion direction)(Moseley, Cohen et al. 1990) (Figure 4). The anisotropic diffusion in WM is due to the parallel organization of axons, where water diffusion is hindered perpendicular to the axons but allowed to move more freely along the direction of the axons. This finding lead to the development of Diffusion tensor imaging (DTI), which measures the anisotropic diffusion in order to visualize and assess the nervous pathways (Basser, Mattiello et al. 1994, Basser, Mattiello et al. 1994). Axonal damage and cell loss, as commonly observed in neurodegenerative diseases, lead to an increase in molecule movement, and consequently, the apparent diffusion coefficient (ADC).

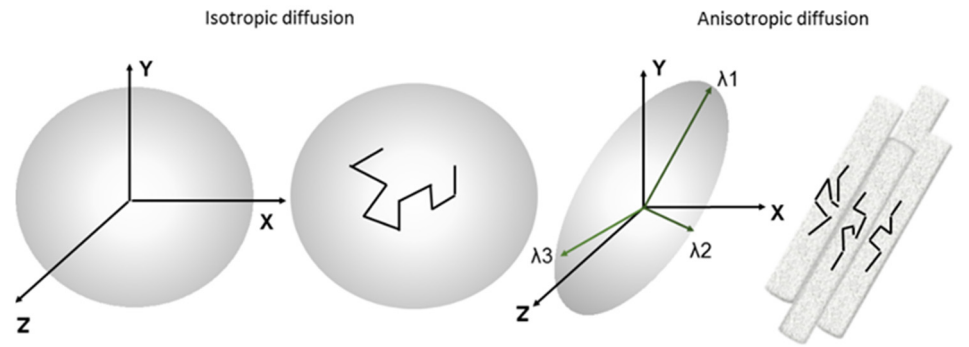

Figure 4
Schematic illustration of diffusion principles. Left: Isotropic diffusion = equal diffusion in all directions, illustrated as a sphere. Right: Anisotropic diffusion = a principal diffusional direction (λ_1) and smaller perpendicular diffusivities (λ_2 and λ_3), illustrated as a tensor.

DTI provides additional quantitative information about the average diffusivity within one voxel (mean diffusivity, MD) and directionality of diffusion (fractional anisotropy, FA) (Figure 5).

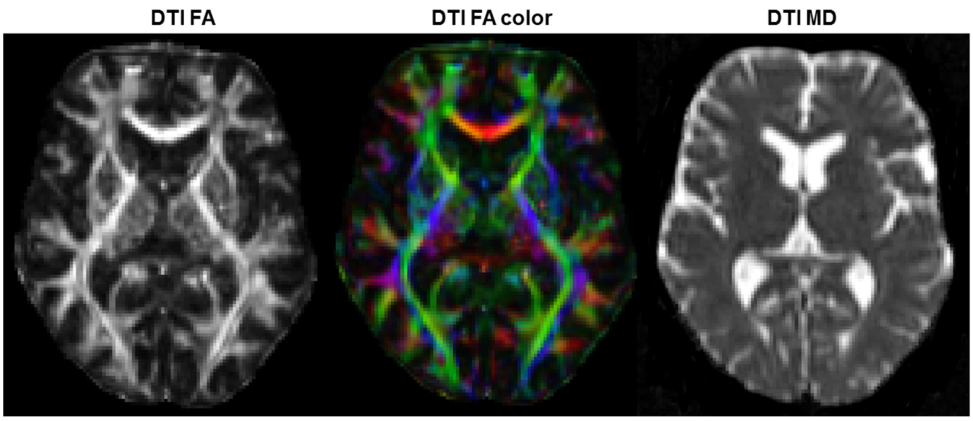

Figure 5
Diffusion tensor imaging parameter maps. DTI fractional anisotropy, FA; DTI FA color maps; DTI mean diffusivity, MD. Patient from *BioFINDER* study.

Compared with conventional MRI techniques, dMRI provides a major advantage to detect early, subtle structural changes that might not be apparent on conventional MRI (Vaillancourt, Spraker et al. 2009).

In contrast to the three magnetic field gradient directions of DWI, six or more gradient directions are required for DTI. This allows for the assessment of not only the MD (Le Bihan 2003, Alexander, Lee et al. 2007, Madden, Bennett et al. 2012) but also the magnitudes of diffusivities in different directions. The diffusion pattern

of a voxel is illustrated as a tensor, based on three orthogonal principal eigenvectors that are ordered by the magnitudes of their corresponding eigenvalues, i.e. $\lambda_1 > \lambda_2 > \lambda_3$ (Figure 4).

Diffusion tensor imaging (DTI)

- A non-invasive, in vivo MRI technique
- Detects the size and direction of water diffusion
- Diffusion is larger parallel to axons and hindered perpendicular to axons
- DTI provide information about the location and integrity of WM pathways

The magnitude of the principal diffusion direction, λ_1, corresponds to diffusion parallel to the axons: λ_1 = axial diffusivity (Da).

The mean λ_2 and λ_3 corresponds to diffusion perpendicular to the axons: $(\lambda_2 + \lambda_3)/2$ = radial diffusivity (Dr).

The mean of all eigenvalues corresponds to the MD: $(\lambda_1 + \lambda_2 + \lambda_3)/3$ = MD.

FA is a measure of the level of anisotropy on a scale from 0 to 1:

$$FA = \sqrt{\frac{3}{2}\frac{(\lambda_1 - MD)^2 + (\lambda_2 - MD)^2 + (\lambda_3 - MD)^2}{\lambda_1^2 + \lambda_2^2 + \lambda_3^2}}$$

MD and FA describe complementary information about the diffusion of water. FA is referred to as a summary measure of microstructural integrity. While FA is highly sensitive to microstructural changes, it is not very specific to the type of change and it is highly advisable to also include other DTI measures in any analysis. MD, which is the directionally averaged, inverse measure of the membrane density and fluid viscosity and is very similar for both GM and WM (Alexander, Hurley et al. 2011) (Figure 4). MD is sensitive to cellularity, edema, and necrosis. It is important to understand that noise in the measured signals can lead to overestimates of the diffusion anisotropy, particularly in more isotropic regions (Pierpaoli and Basser 1996).

Diffusion tensor tractography (DTT) is the application of DTI that can visualize WM tracts and can be derived based on the tensor information provided by DTI. The diffusion is greater along the direction of the axons than perpendicular to them. By connecting voxels based on their principal diffusion direction, WM pathways can be reconstructed to visualize large-scale structural connections of the brain

(Wakana, Jiang et al. 2004, Farquharson, Tournier et al. 2013, Abhinav, Yeh et al. 2014, Bach, Laun et al. 2014).

To this date, most clinical studies have used either deterministic tractography (DTG) (Figure 6) or probabilistic tractography (PTG) (Figure 7).

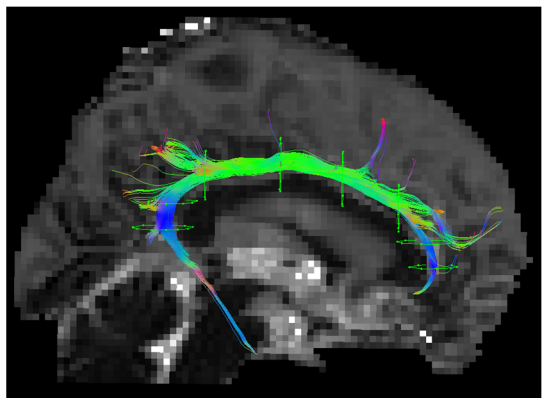

Figure 6
Deterministic tractography of the frontal and parietal cingulum (CG) on each side was performed using colour-coded FA-maps (Surova, Szczepankiewicz et al. 2013). First, two rerion of interests (ROIs) were placed in the transversal plane to select the anterior part of the CG, which runs parallel to the genu of the corpus callosum (CC); the most rostral part was not included. Then four ROIs were placed in the coronal plane at equal intervals along the superior part of the CG. Finally, two ROIs were placed in the transversal plane defining the posterior CG where it arches around the splenium of the CC. The descending part of the CG was not included.

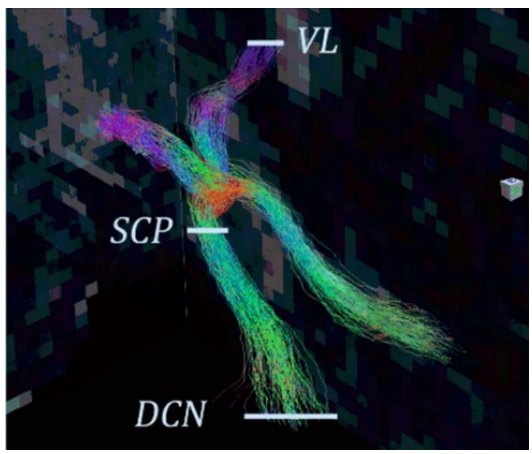

Figure 7
Probabilistic tractography (PTG) of the dentate-rubro-thalamic tract (DRTT). For PTG of the DRTT, its inferior and superior part were constructed each using a seed region of interest (ROI) placed in the deep cerebellar nuclei (DCN) and the ventral anterior and ventral lateral nuclei of the thalamus (VAVL) of the contralateral thalamus, respectively, and also includes a ROI in the superior cerebellar peduncle (SCP) (Surova, Nilsson et al. 2015). The left and right DRTT were then constructed by combining the inferior and superior DRTT into one tract, selecting fibers passing through ROIs in these three locations, DCN, SCP, and VAVL. All tracts were visually inspected.

In DTG, the orientation within a voxel is assumed to be precisely known. A tract is produced by defining a start point and applying an algorithm linking voxels with similar diffusion directions. The advantage of DTG are relatively fast and simple calculations with a clear delineation of fiber tracts. The main limitations are operator-dependency, difficulties resolving curving, crossing or kissing tracts and subjectivity in assign to a reconstructed trajectory (Jones 2008).

In contrast to DTG, PTG calculates the uncertainty of diffusion orientation within each voxel. It then traces a large number of possible pathways (Jones 2008). The result is a probability distribution of connections and, by selecting an appropriate threshold below which connections are discarded as unlikely, tracts can be outlined. PTG is less likely to exclude voxels with low FA due to, for example, crossing fibers or scan artifacts.

The most common tractography methods in the literature are ROI-methods where the reconstructed tracts are manually selected for analysis, based on preexisting anatomical knowledge (Figures 6, 7).

DTI measures can also be extracted and assessed by group-comparison methods, such as VBM and tract-based spatial statistics (TBSS) (Figure 8).

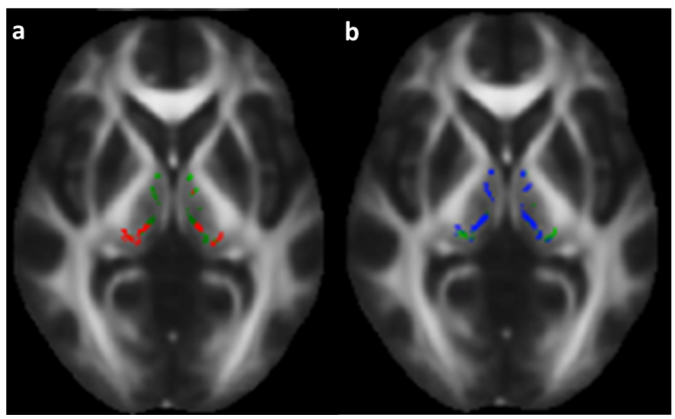

Figure 8
Results of the TBSS analysis in the thalamus (Surova, Nilsson et al. 2015). Areas in thalamus with significantly decreased FA (a) and increased MD (b) in patients with PSP when compared to healthy controls (HC). Results of the TBSS analysis in the thalamus, showing regions of significant decreased FA (red voxels) and increased MD (blue voxels) in patients with PSP when compared to (HC). Green voxels are voxels on the TBSS-skeleton where no significance was found.

There are advantages and disadvantages in most such methods. First, the voxel size of DTI scans is much larger than the axons. A regular imaging voxel of 1-2 mm in each dimension will contain several hundred thousands of axons which have diameters of 0.16-9 µm. Hence, within a specific voxel there may be part of more

than one WM pathway, with different directions (crossing or "kissing" pathways), or change in direction (curving).

Group-comparisons methods include a registration of all subjects' scans to a common space. Registration may perform poorly for structures with certain anatomical properties, for example structures that vary anatomically between subjects, that are relatively small, or that are localized in areas prone to image artifacts. Examples of image artefacts include susceptibility artifacts, caused by magnetic field gradients near boundaries of tissues.

Carefully hand-drawn ROIs in original diffusion space have the advantage of adapting to changes between scans, but potentially suffer from subjectivity/user-error. Smith et al. (2006) (Smith, Jenkinson et al. 2006) compared inter-scan and inter-subject variability between TBSS, VBM and manual ROIs and found that TBSS resulted in the lowest variance for most structures while manual ROIs had the lowest variance for some structures.

The biological relevance of dMRI in PD was studied in animal models, with diffusion changes in the SN being the focus of interest. Studies of Boska et al. and Hasan et al. showed an association between decreased FA and depletion of dopamine neurons in the SN (Boska, Hasan et al. 2007, Soria, Aguilar et al. 2011). However, other animal studies show FA to increase over longer time periods (Van Camp, Blockx et al. 2009), see below. The administration of 1-methyl-4-phenyl-1,2,3,6-tetrahydropyridine (MPTP) in a murine model of PD demonstrated increased Dr and Da or decreased FA within 7 days following MPTP administration (Boska, Hasan et al. 2007). Other animal models demonstrate opposite changes in FA and MD as well (Boska, Hasan et al. 2007, Van Camp, Blockx et al. 2009, Soria, Aguilar et al. 2011).

In summary, dMRI techniques such as DTI have enabled detailed investigation of brain tissue integrity. The integrity is quantified by MD, FA and Dr and Da. MD reflects general molecule mobility, FA directionality, whereas Da and Dr describe diffusion strength along its main and transverse axis, respectively. There are different data-analysis technique such as DTG and PTG, whole brain and ROI-based analyses.

DKI is an extension of DTI that has been suggested to show higher sensitivity and specificity than DTI in detecting and differentiating alterations of tissue microstructure (Cheung, Hui et al. 2009, Grossman, Ge et al. 2012). DKI provides DTI-based parameters as the MD and FA and unique parameters that describe the degree to which the water diffusion is non-Gaussian. These are mean diffusional kurtosis (MK), axial kurtosis, and radial kurtosis (Alexander, Hurley et al. 2011) (Figure 9).

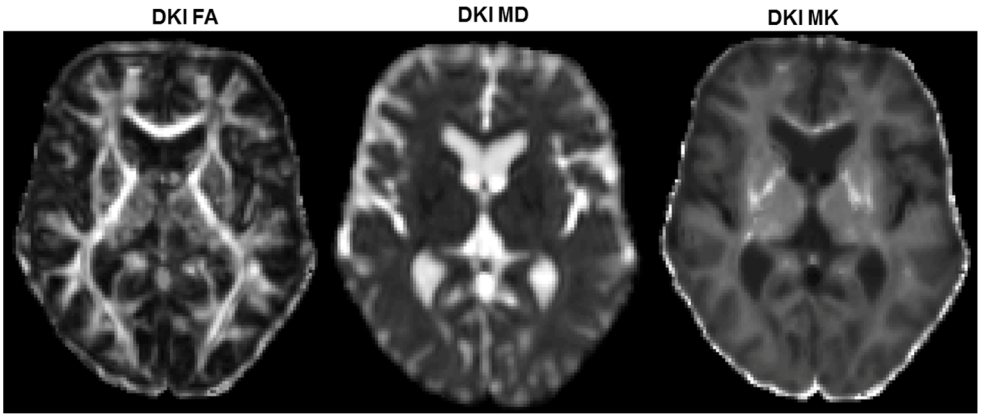

Figure 9.
Diffusion kurtosis imaging parameter maps. DKI fractional anisotropy, FA; DKI mean diffusivity, MD; DKI mean kurtosis, MK.

MK is regarded an index of the complexity of tissue microstructure such as the density, orientation, and degree of organization of cell membranes, axon sheaths, and myelin layers (Latt, Nilsson et al. 2013). DKI parameters can potentially be more effective in elucidating cerebral GM changes (Jensen, Helpern et al. 2005). The group size requirements in DKI as compared to DTI are expected to be higher, since diffusional kurtosis can only be probed at relatively high b-values with higher signal attenuation (Szczepankiewicz, Latt et al. 2013). DKI may be preferable to DTI in tissue where the DTI model is invalid, for example, in regions with complex fiber organization (Szczepankiewicz, Latt et al. 2013).

The advantages offered by DKI over DTI have been reported in several recent studies. In an experimental traumatic brain injury model in rats Zhuo et al. (Zhuo, Xu et al. 2012) observed the continued sensitivity of MK to structural tissue changes even into sub-acute stages, when DTI parameters had re-normalized. Raab et al. reported that gliomas of two different grades could be separated only by using MK values (Raab, Hattingen et al. 2010). Vanhoutte et al. reported the suitability of DKI metrics to detect amyloid deposition in a mouse model of AD, when plain DTI metrics failed to do this (Vanhoutte, Pereson et al. 2013). These studies indicate that kurtosis parameters bring in original information, which DTI parameters may not be able to provide. Furthermore, studies on brain maturation (Cheung, Hui et al. 2009), temporal lobe epilepsy (Gao, Zhang et al. 2012) have reported the enhanced sensitivity of DKI parameters over DTI parameters in discerning differences in tissue status. In a transgenic Huntington rat model study Blockx et al. combined use of kurtosis and DTI parameters proved to be advantageous in detecting tissue changes (Blockx, De Groof et al. 2012). These observations indicate that kurtosis

parameters can discriminate healthy from abnormal tissue under various pathophysiological conditions.

Diffusion kurtosis imaging (DKI)

- A non-invasive, in vivo dMRI technique, that extends DTI
- Suggested to show higher sensitivity and specificity than DTI
- Mean kurtosis (MK) can be related to axonal water fraction and the tortuosity of the extracellular space in WM
- MK may be preferable that DTI in regions with complex fiber organization

Although many previous studies in PD have used DTI to examine nigrostriatal degeneration, they have been unable to attain sufficient diagnostic accuracy and reliability to justify the introduction of DTI in routine clinical practice or as part of interventional clinical studies. Neurite orientation dispersion and density imaging (NODDI) is a model for estimating the structure and orientation of neurites by using an orientation-dispersed cylinder model and the Watson distribution (Zhang, Schneider et al. 2012, Lampinen 2015).

A promising tool for future evaluation of nigrostriatal degeneration is the recently published data of using NODDI in PD. Using NODDI Kamagata et al. (Kamagata, Hatano et al. 2015) found lower neurite density indices (f_{ic} in Paper III) in the contralateral SNpc and putamen in PD patients. It was supposed that this might be an indirect measure of nigrostriatal microstructural changes such as cell loss, morphological changes in dendritic length, and loss of dendritic spines and could be associated with disease severity in PD. However, low signal-to-noise ratio (SNR) in iron-rich structures can influence NODDI parameters (Kamagata, Hatano et al. 2015). We have developed a modified version of this concept, NDI (Lampinen 2015), explored in Paper III.

Neurite orientation dispersion density imaging (NODDI)

- A non-invasive, in vivo dMRI technique
- NODDI estimates microstructure more specifically than DTI
- Assumes intra-, extracellular, and cerebrospinal fluid (CSF) biophysical tissue model for each voxel
- Neurite density index (f_{ic}) and the orientation dispersion are parameters that separately contribute to changes in FA

Other MRI methods

T2- and T2*- (or the transverse relaxation rate R2* where R2*= (1/T2*)) weighted MRI are sensitive to the presence of paramagnetic iron, which is found in the SN. Because of this sensitivity to iron, T2- and T2*-weighted imaging of the SN were among MRI studies of PD (Tuite, Mangia et al. 2013). These studies have shown precise imaging of the SN, including the nigrosomes (Schwarz, Afzal et al. 2014). Qualitative/quantitative MR changes in the SN do not discriminate between different forms of parkinsonism (Rizzo, Zanigni et al. 2016).

Susceptibility weighted imaging (SWI)

- Exploits the magnetic properties of iron content of tissues
- Use magnitude and phase images
- Phase images can enhance contrast to local changes in magnetic susceptibility
- Ferritin causes a phase shift in the local field that correlate with the amount of iron deposition
- Quantitative susceptibility mapping (QSM) is a technique where phase MRI data is processed to yield susceptibility maps.

SWI is another technique that exploits the magnetic properties of iron content of tissues by using magnitude and phase images from a T2*-weighted gradient-echo sequence. However, compared with a standard T2* sequence, SWI use thin sections with a 3D acquisition to avoid background field T2* signal intensity loss. Moreover, phase images can enhance contrast to local changes in magnetic susceptibility, therefore, yielding increased sensitivity in detecting local changes in iron content (Reichenbach, Venkatesan et al. 1997, Haacke, Xu et al. 2004, Haacke, Cheng et al. 2005). Nonheme iron, usually in the form of ferritin, is a highly paramagnetic molecule, which causes a phase shift in the local field correlated with the amount of iron deposition (Ogg, Langston et al. 1999, Haacke, Cheng et al. 2005). An example of SWI in SN and red nucleus is shown in Figure 10.

In vivo iron quantification using MRI relaxometry (T2*, R2*) or SWI consistently demonstrates increased iron levels in SN in PD relative to HC (Table 1). Results of iron quantification in the caudate nucleus, putamen and globus pallidus appear highly heterogeneous (Table 1). However, several studies have observed relationships between increased nigral iron accumulation, disease duration and motor severity. SWI has also demonstrated the absence of nigrosomes in PD (Schwarz, Afzal et al. 2014).

Table 1
MRI relaxometry (T2*,R2*) or susceptibility-weighted imaging (SWI) in vivo studies in PD from the literature.

First author	Year	Comparisons	MRI method	Main results
Antonini(Antonini, Leenders et al. 1993)	1993	30 PD : 33 HC postmortem	T2	Decreased T2 in SN, caudate nucleus, putamen in PD
Ryvlin(Ryvlin, Broussolle et al. 1995)	1995	45 PD : 45 HC	T2	Decreased T2 in SN, putamen, pallidum in PD
Graham(Graham, Paley et al. 2000)	2000	25 PD : 14 HC	R(2)*and R(2)'	Increased R(2)*and R(2)' relaxation rates in SN, decreased R(2)' in putamen in PD
Kosta(Kosta, Argyropoulou et al. 2006)	2006	40 PD : 40 HC	T2	Decreased T2 in SN, increased in putamen and globus pallidum in PD
Martin(Martin, Wieler et al. 2008)	2008	26 PD: 13 HC	R(2)*	Increased R(2)* in SN pars compacta in PD
Wallis(Wallis, Paley et al. 2008)	2008	70 PD: 10 HC	R(2)'	Increased in SN and putamen in PD
Zhang(Zhang, Zhang et al. 2010)	2010	40 PD : 26 HC	SWI	Increased iron in SN in PD
Wang(Wang, Butros et al. 2012)	2012	16 PD: 8 MSA-P : 44 HC	SWI	Increased iron in putamen in MSA-P : PD
Jin(Jin, Wang et al. 2012)	2012	87 PD : 50 HC	SWI	Increased iron i SN
Bunzeck(Jin, Wang et al. 2012)	2013	20 PD : 20 HC	Volume, R2* and MT value	Decreased volume and MT value in SN in PD
Martin-Bastida(Martin-Bastida, Lao-Kaim et al. 2017)	2017	70 PD : 20 HC	SWI	Increased iron in SN in PD

HC, healthy controls; PD, Parkinson's disease; SN, substantia nigra; SWI, Susceptibility weighted imaging.

Increased nigral iron accumulation in PD appears to be stratified according to disease motor severity and correlates with symptoms related to dopaminergic neurodegeneration (Martin-Bastida, Lao-Kaim et al. 2017). This semi-quantitative in vivo iron assessment could prove useful for objectively monitoring PD progression, especially in clinical trials concerning iron chelation therapies.

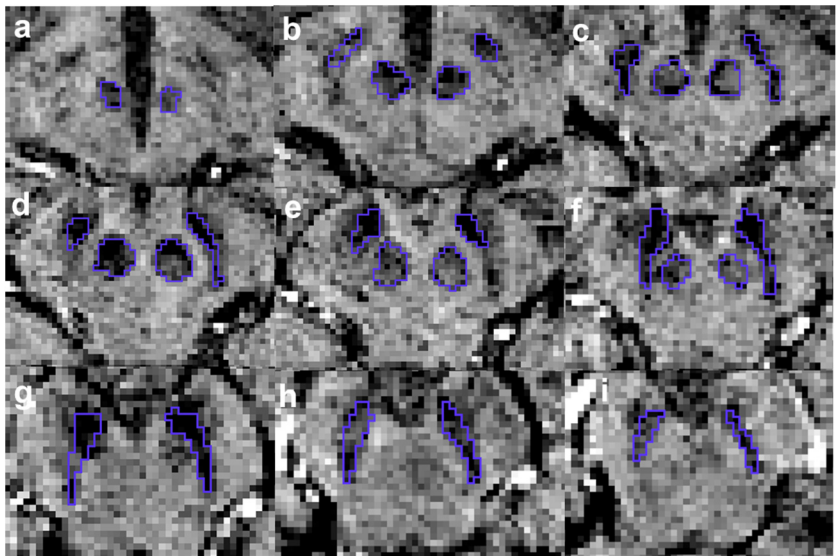

Figure 10
Susceptibility weighted imaging (SWI) of the substantia nigra (SN) and red nucleus of patient with PD from the *BioFINDER* study. Representative consecutive slices showing ROI placement in the red nucleus and SN on SWI maps.

Quantitative susceptibility mapping (QSM) is a technique where phase MRI data is processed to yield susceptibility maps. The quantitative maps correlate well to tissue iron content (Langkammer, Schweser et al. 2012). Iron accumulation is common in neurodegenerative disorders. QSM has shown improved imaging of the subthalamic nucleus and globus pallidus interna (Liu, Eskreis-Winkler et al. 2013) and has been used to investigate changes in the SN in PD (Barbosa, Santos et al. 2015, Murakami, Kakeda et al. 2015). While QSM is commonly gathered through dedicated data acquisition, routine clinical SWI sequence may be used for quantitative measurements. Sjöström et al. has previously showed that PSP and MSA exhibit characteristic susceptibility patterns in a retrospective pilot study using such data (Sjostrom, Granberg et al. 2017).

Neuromelanin-sensitive imaging has observed decreased volumes of SNpc and locus coeruleus (Castellanos et al., 2015), or decreased signals in locus coeruleus (Garcia-Lorenzo et al., 2013), indicating loss of dopaminergic neuromelanin containing neurons in these regions in PD.

Results of perfusion MRI, proton MR spectroscopy (Groger, Bender et al. 2013), and functional MRI (fMRI) have been used diagnostically in parkinsonism (Tuite, Mangia et al. 2013, Holtbernd and Eidelberg 2014, Kahan, Urner et al. 2014, Pyatigorskaya, Gallea et al. 2014).

Al-Bachari et al. (Al-Bachari, Parkes et al. 2014) examined neurovascular status and cerebral blood flow in PD through arterial spin labeling (ASL) measures of arterial arrival time (AAT). Widespread regions of the brain showed prolongation of AAT. A combined ASL and morphometric study observed a pattern of "parietal cortical thinning and reduced precuneus perfusion" that appeared even in mild PD (Madhyastha, Askren et al. 2015). ASL perfusion indicated subthalamic nucleus hyperconnectivity with primary motor cortex and precuneus regions (Fernandez-Seara, Mengual et al. 2015).

Finally, many MR studies have provided a combination of both qualitative and quantitative findings (Rizzo, Zanigni et al. 2016) or the integration of multimodal MRI (Eckert, Tang et al. 2008, Rae, Correia et al. 2012, Nair, Tan et al. 2013, Surova, Nilsson et al. 2015).

In summary, MRI in PD investigations is a noninvasive approach and does not expose subjects to radiation. This safety profile, along with excellent spatial and temporal resolution and wide availability, has led to widespread applications of MRI for structural and functional neuroimaging investigations of PD.

Cognitive screening

Mild cognitive impairment (MCI) occurs in 20-50% of PD patients (PD-MCI) (Goldman, Holden et al. 2015) and frequently progresses to dementia (Pedersen, Larsen et al. 2013). The point prevalence of dementia is 31.5% in PD (Aarsland, Zaccai et al. 2005). Patients with PD had almost six-fold increased risk of dementia compared to HC. As a potential treatable conditions the identification of PD-MCI and dementia in PD (PDD) is urgent.

Typically for PD cognitive decline is in executive function, includes planning, attention, working memory, and task set-shifting. The hippocampus degenerates in later stages of PD and leads to memory impairment and other cognitive dysfunction in later stages of PD. Typically for PSP are behavioral changes (include apathy, irritability, childishness, and impulsivity), executive dysfunction, memory, visuospatial, and language and social cognitive deficits (Hoglinger, Respondek et al. 2017). Cognitive disturbances in MSA include a wide spectrum from mild single domain deficits to impairments in multiple domains and even to frank dementia in some cases (Stankovic, Krismer et al. 2014). Frontal-executive dysfunction is the most common presentation, while memory and visuospatial functions may also be impaired (Stankovic, Krismer et al. 2014).

When investigating cognitive function *in PD*, a neuropsychological test should include tests of memory, executive function, visuospatial function, and language function (Goldman, Holden et al. 2015). Previous studies have shown that the Montreal Cognitive Assessment (MoCA) test is a better screening method for cognitive impairment due to PD, than Mini mental state examination test (MMSE)

(Biundo, Weis et al. 2016). After clinical and neuropsychological assessment, a cognitive diagnosis of not impaired, PD-MCI, or PDD is recommended to be assigned at a clinical consensus conference (Cholerton, Zabetian et al. 2013), in accordance with MDS recommendations (Goldman, Holden et al. 2013, Goldman, Holden et al. 2015).

In PSP, three cognitive screening tests have been demonstrated to differentiate between patients with PSP and individuals with other neurodegenerative conditions including APS: Dementia Rating Scale (DRS)(Dubois, Slachevsky et al. 2000, Bak, Rogers et al. 2005), Addenbrooke's Cognitive Examination (ACE) and Frontal Assessment Battery at bedside (FAB) (Dubois, Slachevsky et al. 2000, Paviour, Winterburn et al. 2005, Brown, Lacomblez et al. 2010). FAB with a cut-off of 15 was shown to differentiate patients with PSP from individuals with PD or MSA (Paviour, Winterburn et al. 2005). A 24-item Frontal Behavioral Inventory (FBI) (Kertesz, Davidson et al. 1997), neuropsychological investigation (Cummings, Mega et al. 1994), clinical tests (e.g. applause sign) (Somme, Gomez-Esteban et al. 2013) and various other neuropsychological test batteries can be used in PSP, but they are not specific. No single test distinguishes PSP from other related disorders.

In MSA, cognitive impairment is present more frequently than previously considered (Stankovic, Krismer et al. 2014). Today, there is lack of consensus about which test is best suited to assess cognition in patients with MSA. In according to a position statement by the Neuropsychology Task Force of the MDS MSA (MODIMSA) Study Group, executive functions and fluency are the most commonly affected, while attention, memory and visuospatial domains are sometimes impaired, and language mostly spared (Stankovic, Krismer et al. 2014). MODIMSA made a summary of the methods and results of the neuropsychological studies assessing cognitive functions in MSA (Stankovic, Krismer et al. 2014). Dementia in MSA patients used to be diagnosed with PDD criteria (Kim, Jeon et al. 2013), DSM-IV criteria (Kitayama, Wada-Isoe et al. 2009) or cut-off values of the Clinical Dementia Rating Scale (Chang, Chang et al. 2009, Kitayama, Wada-Isoe et al. 2009) or Mattis Dementia Rating Scale (Chang, Chang et al. 2009).

Cerebrospinal fluids and blood-based biomarkers

Neurofilament light chain (NfL) protein in cerebrospinal fluid (CSF) is a promising marker for APS. Studies have previously shown that the CSF concentration of NfL is increased in APS but not in PD (Constantinescu, Rosengren et al. 2010, Herbert, Aerts et al. 2015) and that NfL in CSF can discriminate between PD and APS with a high degree of diagnostic accuracy (Abdo, Bloem et al. 2007, Hall, Ohrfelt et al. 2012, Magdalinou, Paterson et al. 2015). In a recent study Hansson et al. (Hansson, Janelidze et al. 2017) showed that quantification of blood NfL concentration can be used to distinguish PD from APS and thus might consequently be included in the diagnostic workup of patients with parkinsonism.

Conclusion

Differential diagnosis of parkinsonism relies on the clinical exam. The role of conventional structural MRI is largely limited to the exclusion of structural lesions causing secondary parkinsonism. dMRI has higher sensitivity to discern subtle microstructural changes than conventional MRI, and has shown some potential in the separation of APS from PD. Studies employing novel MRI techniques have provided promising results, but larger prospective studies are required to determine the merits of these techniques in the differential diagnosis of parkinsonian syndromes. The integration of neuroimaging and CSF/blood biomarkers could allow for more accurate differential diagnosis than a single approach.

Aim

Study I

1. To investigate whether there are global and regional changes in larger WM tracts in patients with PD, MSA-P, and PSP, compared to HC, employing DTT.
2. To study if DTT can be used in the differential diagnosis between PSP and PD, and also between PSP and MSA.

Study II

1. To investigate the presence of disease-specific changes in the basal ganglia, thalamus, pons, midbrain, and dentate-rubro-thalamic tract (DRTT) of patients with PD, MSA-P, and PSP, using DTI and morphometric analyses.

Study III

1. To explore whether DKI and NDI can be used to assess the basal ganglia, thalamus, pons and midbrain using tractography of selected WM tracts in PD.
2. To investigate whether there are differences in DKI and NDI parameters between postural instability gait difficulty (PIGD) and tremor dominant (TD) phenotypes of PD.

Study IV

1. To explore whether there are dMRI changes over 2 years in DKI parameters of WM and deep GM of patients with PD and if these correlate with disease progression.

Study V

1. To evaluate the use of QSM for clinical diagnostics in PD, PSP and MSA.

Subjects and methods

Study participants

The common base for the papers in this thesis were two case-control studies of patients with idiopathic parkinsonism and controls. The studied cases were sampled from the South Region of Sweden, a catchment area with 1.3 million inhabitants (http://www.scb.se), and were investigated for sub classification of different forms of parkinsonism.

Cohort 1, the studied cases were selected retrospectively, in accordance with defined inclusion and exclusion criteria (Litvan, Agid et al. 1996, Litvan, Hauw et al. 1996, Gelb, Oliver et al. 1999, Gilman, Low et al. 1999), from patients who visited the Neurology and Memory Clinics at Skåne University Hospital and Landskrona Hospital, Sweden, during 4 years (2008-2011). HC, age- and sex-matched, were recruited from the Swedish population registry and had no previous neurologic or psychiatric diseases. Clinical evaluation, including a fixed protocol for neurological signs, formed the basis for inclusion in the study. The clinical diagnosis used was the diagnosis obtained at the 12-month follow-up visit. The medical records and the results of auxiliary test were analyzed in Papers I and II.

Cohort 2, the studied cases were included in the prospective and longitudinal Swedish *BioFINDER* study (www.biofinder.se) in Papers II-V (Hall, Surova et al. 2015). These study participants were recruited from the Neurology Clinic at Skåne University Hospital, Sweden, between 2008 and 2016. The study participants underwent assessment by a medical doctor with experience in movement disorders and a registered nurse using a large battery of rating scales. Overview of clinical tests used in Papers II-V were summarized in Table 2.

Table 2
Overview of clinical tests used in cohort 2 Papers II-V.

	Paper II	Paper III	Paper IV	Paper V
Cognitive tests				
MMSE (Folstein, Folstein et al. 1975)	√	√	√	√
AQT (Nielsen, Wiig et al. 2004)	√	√	√	
ADAS-Cog (Mohs and Cohen 1988)	√	√	√	
Motor tests				
UPDRS (Fahn 1987)	√	√	√	√
H&Y (Hoehn 1967)	√	√	√	√
S&E (Schwab 1969)	√	√	√	
CAPSIT-PD test (Hagell 2000)		√		
The timed up and go test (Podsiadlo and Richardson 1991)	√	√	√	
Tandem gait (Fregly 1974)	√	√	√	
PSPRS (Golbe and Ohman-Strickland 2007)	√			

ADAS-Cog, the memory subtests of the Alzheimer's Disease Assessment Scale; AQT, Quick Test of Cognitive Speed; CAPSIT, Core Assessment Program for Surgical Interventional Therapies H&Y, Hoehn and Yahr staging scale; MMSE, Mini Mental State Examination; PSPRS, PSP rating scale; S&E, Schwab and England activities of daily living scale; UPDRS, Unified Parkinson's Disease Rating Scale.

A thorough medical history is taken and the patients undergo physical examination regarding symptoms of PD and APS according to criteria as well as exclusion criteria (Litvan, Agid et al. 1996, Litvan, Hauw et al. 1996, Gelb, Oliver et al. 1999, Gilman, Low et al. 1999). Levodopa equivalent daily dose (LEDD) is calculated (Tomlinson, Stowe et al. 2010). Controls underwent the same extensive testing. Individuals with overt signs of parkinsonism or cognitive symptoms were not included in the studies. Blood and CSF samples were obtained at baseline and biannually.

In Paper III an empirical groupings was made into TD, PIGD and indeterminate PD. The method used by Jankovic et al. (Jankovic, McDermott et al. 1990) applied. The sum of UPDRS 'tremor items' (arm tremor by history, rest tremor of face, arms, legs, postural and action tremor of arms by examination) was divided by the sum of UPDRS 'PIGD' items (postural instability and gait by examination and walking, freezing and falls by history). This ratio indicates PD subtypes as follows: ≤1.0 is classified as PIGD, >1.5 is classified as tremor dominant and 1.0-1.5 is indeterminate.

To ensure standardization, dMRI were performed on PD patients (Papers III-V, and the *derivation cohort* Paper II) during "on" medication state, or fully responding to their PD medications (in the "on" state). At the time of testing, none of the patients exhibited any dyskinesia, dystonia, or other signs of involuntary movement.

The patients from the Swedish *BioFINDER* cohort will be followed for up to 10 years. At baseline and at the 2, 4, 6 and 10 year follow-up, the study participants undergo the examination as listed above. At the 1, 3 and 8 year follow up patients are assessed with a shorter visit with a research nurse. *BioFINDER* study participants undergo assessment using other battery of rating scales not included in the thesis: 1-minute Animal Fluency test (Sebaldt, Dalziel et al. 2009), 1 minute Letter S Fluency test (Isella, Mapelli et al. 2014), Clock drawing test (Shulman 2000), The International Quality Of Life Assessment (IQOLA) (Gandek, Ware et al. 1998), SF-12, Walk-12 (Holland, O'Connor et al. 2006), SCOPA-AUT (Visser, Marinus et al. 2004), SCOPA-Sleep (Marinus, Visser et al. 2003), FACIT-FS (Cella and Webster 1997), HADS (Zigmond and Snaith 1983).

Table 3
Chart over follow-up routines in the study.

	Baseline	1 year	2 years	3 years	4 years	6 years	8 years	10 years
Medical Doctor	√		√		√	√		√
Registered nurse	√	√	√	√	√	√	√	√
Medical history	√		√		√	√		√
UPDRS I-IV	√	√	√	√	√	√	√	√
Hoehn & Yahr scale	√		√		√	√		√
CAPSIT-PD test	√		√		√	√		√
Timed Up and Go	√		√		√	√		√
Tandem Gait	√		√		√	√		√
MMSE	√	√	√	√	√	√	√	√
ADAS-Cog	√		√		√	√		√
AQT	√	√	√	√	√	√	√	√
Animal Fluency	√		√		√	√		√
Letter-S Fluency	√		√		√	√		√
Clock drawing test	√		√		√	√		√
CSF	√		√		√	√		√
Blood samples	√		√		√	√		√
Ortostatic blood pressure	√	√	√	√	√	√	√	√
Questionnaires	√		√		√	√		√
MRI	√		√		√	√		√

ADAS-Cog, the memory subtests of the Alzheimer's Disease Assessment Scale; AQT, Quick Test of Cognitive Speed UPDRS, Unified Parkinson's Disease Rating Scale; CAPSIT, Core Assessment Program for Surgical Interventional Therapies; CSF, cerebrospinal fluid.

Patients also undergo MRI at baseline and there after every other year (Table 3). Orthostatic blood pressure measures annually (Gilman, Wenning et al. 2008) (Table 3).

Overall research plan

Overview of design of the studies is presented in Table 4.

Table 4
Overview of the design of the studies.

Paper	I	II	III	IV	V
Design	Retrospectiv case-control cross-sectional study	Retro and prospectiv case-control cross-section study	Prospectiv case-control cross-section study	Prospectiv case-control cross-section longitudinal study	Prospectiv case-control cross-section study
Study population	Patients from the Neurology and Memory Clinics at Skåne University Hospital and Landskrona Hospital, 2008-2011	*Derivation cohort* from *BioFINDER study* *Validation cohort* from Paper I	Patients were consequently included between 2008 and 2016 from the prospective and longitudinal Swedish *BioFINDER* study (www.biofinder.se) at the Skåne University hospital, Lund, Sweden		
Participants	PD, n=10, PSP, n=16, MSA, n=12, controls, n=16	*Derivation cohort*: PSP, n=8, controls, n= 30. *Validation cohort*: PD, n=10, PSP, n=27, MSA, n=11, controls, n=21	PD, n=105, controls, n=44, PSP, n=10, MSA, n=11	PD, n=76, controls, n=38, who had done MRI two years apart	PD, n=133, controls, n=44, PSP, n=11, MSA, n=10
Statistical analysis	Descriptiv and analytic statistic (Fisher's Exact test, Kruskall-Wallis test, Mann-Whitney U-test with Bonferroni correction, univariate binary logistic regression analysis, ROC analysis)	Descriptiv and analytic statistic (Fisher's Exact test, Kruskall-Wallis test, Mann-Whitney U-test with Bonferroni correction, binary logistic regression analysis, ROC analysis; Spearman's rho. Threshold-Free Cluster Enhancement of FSL Randomize (v 2.9), effect sizes)	Descriptiv and analytic statistic (Pearson's χ^2 test, Mann-Whitney U-test, ANCOVA, univariate binary logistic regression analysis, ROC analysis; Spearman's rho)	Descriptiv and analytic statistic (Pearson's χ^2 test, ANOVA, Mann-Whitney U-test, ANCOVA, univariate binary logistic regression analysis; R2 Linear and Spearman's rho)	Descriptiv and analytic statistic (Pearson's χ^2 test, ANCOVA, AUC, discriminant analysis, for the pairwise comparisons Bonferroni correction; Pearson partial correlation tests)

Sperman's rho, Spearman's rank correlation coeficient; R2 Linear, Linear regressions analys; ROC, receiver operator characteristic curve analysis.

Methods

For Papers I and II (*derivation cohort*) dMRI were performed on a 3 T Philips Intera MR scanner (Table 5). For Paper II (*validation cohort*), Papers III-V dMRI were performed on a 3 T Siemens Skyra MR scanner (Table 5).

Table 5
Parameters of data acquisition and processing papers I-V.

		DTI parameters									
Paper	**MRI Scanner**	**Channels head coil**	**EPI sequence, TE/TR [ms/ms]**	**Diffusion encoding,**	***b* values [s/mm^2]**	**voxel size [mm^3]**	**Slices**	**Parallell imaging factor**	**acquisition time [min.s]**	**FOV, [mm^3]**	**Partial Fourier factor**
I	3 T Philips Achieva	8	single -shot 90 / 7900	48	0 and 800	2×2×2	60	2.5	6.5	256×256×120	No data
II, derivation cohort	3 T Siemens Skyra	20	single -shot 70/75 00	30	0 and 1000	2×2×2		2	4.2	294×294×120	6/8
II, validation cohort	3 T Philips Achieva	8	single -shot 90/79 00	48	0 and 800	2×2×2	60	2.5	6.5	256×256×120	No data
III-IV	3 T Siemens Skyra	20	single -shot 103 / 8100	6, 6, 20, and 64	0, 250, 500, 1000, and 2750	2.3×2.3×2.3		2	14	294×294×120	6/8
V	3 T Siemens Skyra	20	27/20	ND	ND	0.86 x 0.86 x 1.5 (SWI) 1 x 1 x 1 (volumetric analysis)	ND	ND	ND	ND	ND

EPI, Echo planar imaging; FOV, Field-of-view, ND, non-defined.

Structural MRI assessment

All patients and controls in Paper II were examined by dMRI, included T1- and T2-weighted images (Table 5).

DTI-data post-processing

In Papers I and II, subject motion and eddy-current correction was performed in ElastiX (Klein, Staring et al. 2010), as implemented in ExploreDTI (Leemans 2009), taking the b-matrix reorientation into account (Leemans and Jones 2009).

In Papers III and IV, motion and eddy current distortions were corrected using an extrapolation-based method for improved high b-value performance (Nilsson 2014).

Tractography

For Paper I, whole-brain DTG was carried out using ExploreDTI (Leemans 2009), with FA and angular threshold values of 0.2 and 30^{o}, respectively. Multiple ROIs were selected on the directionally color-coded FA images to dissect the cortico-spinal tract (CST), CC, CG and MCP. Regional evaluation comprised projection of FA, MD, Dr, apparent area coefficient (AAC) onto a calculated mean tract and extraction of their values along each structure.

For Paper II, the PTG method with constrained spherical deconvolution (CSD) (Tournier JD 2012), was carried out using MRtrix (Brain Research Institute, Melbourne, Australia, http://www.brain.org.au/software/) (Tournier, Calamante et al. 2007), to model multiple fiber orientations in each voxel of DRTT (Figure 7).

For Paper III, CSD (Tournier JD 2012) was carried out. The ROIs used to define the seed region for each tract, and to segment the tract based on logical operations, were defined in MNI152 standard-space (Mazziotta, Toga et al. 2001), and warped back to native space utilizing the warp-fields generated by FLIRT and FNIRT (Andersson 2012).

Region-of-interest methods

For Papers II-IV, ROIs were drawn manually in the nucleus caudatus, putamen, globus pallidus, thalamus, red nucleus, SN, pons and midbrain.

The manual tracing was performed in 1) the b0 image and 2) a T1-weighted image registered to the FA image.

For Paper II, semi-automatic segmentation was performed based on the FA-skeleton algorithm in the TBSS (v 1.03), part of the FRMIB Software Library (FSL), for tractography of thalamus (Figure 8). FA an MD maps were registered onto the 1 mm^3 FMRIB58 FA template in MNI152 standard space, using the linear and nonlinear registration tools FLIRT and FNIRT (Andersson 2012, Andersson 2012).

Before registration, the diffusion maps were masked with the FSL Brain Extraction Tool (BET) (Smith 2002). The normalized maps were skeletonized by projection onto the FMRIB58 template skeleton. Finally, the skeletonized maps were masked to include only voxels from the thalamus. The masking was done using the left and right thalamus regions in the MNI152 space Harvard-Oxford subcortical atlas, together with the requirement that the MD of the normalized maps must be less than unity in the control subjects of the *derivation cohort* (Smith, Jenkinson et al. 2004).

Morphometric analysis

For Paper II *derivation cohort* volumetric data were acquired using a MPRAGE sequence with TR/TE 7/3 ms, flip angle 9°, resolution 1×1×1 mm^3 and in *validation cohort* using a T1-weighted TFE sequence with TR/TE 8/4 ms, flip angle 10°, resolution 1×1×1 mm^3. VBM was performed with FIRST (Patenaude, Smith et al. 2011). Correction for intracranial volume was achieved by multiplying each volume with the scaling factor that estimates the scaling between the subject's image and standard space and that is provided by the SIENAX toolbox (Buckner, Head et al. 2004).

The diameter and area of the midbrain and pons, the midsagittal slice were assessed according to Oba et al. (Oba, Yagishita et al. 2005).

DKI-data analysis

For Papers III and IV DKI analysis was performed to obtain maps of FA, MK, and MD (Figure 9), using in-house developed software which fitted the diffusion and kurtosis tensors by nonlinear optimization as in Lätt et al. (Latt, Nilsson et al. 2013). The fitting only allowed positive values of the diffusion tensor eigenvalues. In a small number of voxels where the kurtosis was below zero, the fitting was repeated after additional smoothing was performed.

NDI-data analysis

For Paper III NDI analysis (Lampinen 2015), a simplification of the NODDI analysis (Zhang, Schneider et al. 2012), was performed to obtain maps of the f_{ic} and the partial fraction of free water (f_{iso}) (see Paper III for more exhaustive descriptions).

SWI-data analysis

In Paper V the phase and magnitude data was processed using an in-house pipeline consisting of FSL (version 5.0.8, http://www.fmrib.ox.ac.uk/fsl), MATLAB (version R2015a, MathWorks, Natick, USA) and STISuite (version 2.2, Duke University, Durham, North Carolina, USA). These methods are more extensively described and illustrated in a previous study (Sjostrom, Granberg et al. 2017). To

summarize, brain masks were created using FSL-BET on the magnitude images (Smith 2002). The masks were then three-dimensionally eroded to ensure that no extra-cerebral tissue was present within the mask. The masks were applied to the phase images which were unwrapped using Laplacian techniques and thereafter processed using the Variable-kernel Sophisticated Harmonic Artifact Reduction on Phase data method (V-SHARP) to remove unwanted background phase. Finally, the inverse solution from field to source was calculated using the improved sparse linear equation and least-squares method (iLSQR) (Li, Wu et al. 2011, Wu, Li et al. 2012, Li, Avram et al. 2014, Li, Wang et al. 2015) (see Paper V for more exhaustive descriptions).

Statistical analysis

Descriptive statistics was used for group comparisons in all studies. The distribution of data was described by mean, standard deviation (SD), effect size (ES) (Paper I), coefficient of variation (CV) of diffusion parameters (Papers II and III).

For **comparisons of differences between groups** Fisher's Exact test was used in Papers I and II (demographic and clinical categorical variables). Proportions were compared using Pearson's χ^2 test (Papers III-V). The Kruskall-Wallis test followed by the Mann-Whitney U-test were used for continuous data. An adjustment for multiple comparisons was made using Bonferroni correction (Papers I, II and V). For the dMRI parameter comparisons that came out significant using non-parametric testing, tried in a one-way analysis of covariance (ANCOVA) that was also conducted in order to control for the effects of gender and age (Papers III and IV).

For analysis of **correlation** between dMRI data and clinical scales, Spearman's rank correlation coefficient was used (Papers II-IV). Pearson partial correlation tests were conducted to test for correlations between susceptibility levels and clinical scales, and between disease duration and susceptibility levels (Paper V).

A **prediction model** based on univariate binary logistic regression analysis adjusted for age and sex was performed with diffusion parameter values that were significantly different between groups based on the results of Mann-Whitney U-test (Papers I and II) and on the results of ANCOVA (Paper III). The sensitivity, specificity and the optimal cutoff level of DTI values chosen by the models were calculated with receiver operator characteristic curve analysis (ROC).

Statistical processing of TBSS data was performed using Threshold-Free Cluster Enhancement of FSL Randomize (v 2.9), with 7500 permutations for the null distribution.

Intra-rater reliability of manual ROI-analysis was applied in all studies. ROIs were redrawn 8 weeks later on the same images, by the same investigator (intra-

rater variability > 0.9 for all ROIs), and the average values from paired ROIs were used for analysis. The image-presentation order was randomized, and the investigator was blinded to the order. The reliability of the ROI-placement procedures in Paper IV was calculated using the intraclass correlations coefficient (ICC) estimates and their 95% confident intervals were calculated based on a mean-rating (k = 1), single measures, absolute-agreement and 2-way mixed effects model (Koo and Li 2016).

Statisticians from FoU-centrum Skåne, Skåne University Hospital, were consulted for Papers I-III of the thesis.

Ethical considerations

The studies in of this thesis were approved by the Regional Ethics Committee for Research of Lund University and performed according to statutes of the Declaration of Helsinki. Informed oral and written consent was obtained from all subjects prior to inclusion in the studies.

All studies included non-invasive MRI and was considered safe for the participants, because there are no known risks of MRI in humans. All MRI scans, of patients and controls, were clinically assessed by a neuroradiologist in order to detect pathological findings.

Results

Paper I

This study was performed to assess alterations in measures of DTT in parkinsonism, exploring the potential role of DTI in diagnosis and as a candidate biomarker.

Patients and controls

In Paper I, participants from cohort 1 were used. During the inclusion period 54 study participants were included. At the 12-month follow-up visit the clinical diagnoses were: 10 PD (definite PD), 12 MSA-P (11 unspecified, probable MSA-P or possible MSA-P, 1 definite MSA-P), 16 PSP (15 unspecified, probable PSP or possible PSP, 1 definite PSP). Demographic and clinical data of patients and HC are reported in Table 6.

Table 6 Demographic characteristic Papers I-V.

Papers	Controls	PD	MSA	PSP	Controls	PD	MSA	PSP
	Mean age				Gender female:male			
I	67 (63–73)	68 (59–70)	63 (56–75)	68 (65–72)	7:9	4:6	8:4	9:7
II, derivation cohort	69 (67–72)	-	-	70 (68–75)	16:14	-	-	4:4
II, validation cohort	69 (65–76)	68 (59–70)	64 (56–76)	68 (65–71)	9:12	4:6	7:4	13:14
III	68 (59–72)	69 (62–74)	64 (57–71)	71 (70–76)	25:19	61:44	6:5	5:5
IV	67 (59–72)	66 (59–72)	-	-	16:22	52:24	-	-
V	66.0 ± 7.8	66.9 ± 9.6	63.4 ± 11.4	72.2 ± 5.5	26:18	48:86	6:4	6:5

All values expressed as medians, values in parenthesis indicate 25–75 percentiles.

The median disease duration at diagnosis (MRI investigation) was 4.5 (PD), 3.0 (MSA-P), 3.5 (PSP) years. There were no significant differences in age, gender ratio or disease duration between the PD, MSA-P and PSP groups.

Diffusion parameters

The most prominent differences were detected in FA, MD and Dr values in the CC in patients with PSP compared with both PD and controls. In addition, PSP patients showed a significantly lower AAC in the CG (ES = 1.9) and higher MD in the CST (ES = .8) compared to PD. There were no significant differences between PSP and MSA-P patients. We also found significantly higher AAC in the CG (ES = 1.5) of patients with PD compared to controls. MSA patients showed a significantly higher Dr in the CST (ES = 1.3) compared to PD. There was an increase in MD (ES = 0.8) and decrease in AAC in the MCP (ES = 1.2) in MSA compared to PD patients, which did not reach statistical significance. The median values of diffusion data and AAC for the whole tracts are summarized in Table 2 (Paper I).

Concerning the regional analysis along WM tracts, there were consistent variations of the DTT parameters along each tract, as determined by visual inspection, which were very similar in the different patient groups and controls. Each tract and parameter had its characteristic "2D-profile" along its length (Figure 2, Paper I). The exception was the diffusion values from CC in the PSP group that differed significantly in shape from the other groups. For all parameters, there were differences in FA and Dr values between the left and right CG (Figure 3, Paper I) and, to a lesser degree, for MD in the CST (data not shown), which were consistent throughout the control and patient groups.

Although all statistically significant differences between controls and disease groups are depicted in Figure 2 (Paper I), only continuous changes encompassing more than 2 cm along a tract were considered of significance for further analysis. There was a trend towards lower AAC in both the MSA and PSP groups in MCP, which was not significant (Figure 2, Paper I). In PSP, significant changes were seen for AAC in the CG and for MD in the CST. However, the most striking finding was a marked increase in MD and Dr, and a corresponding reduction of FA, in the anterior and central parts of the CC in PSP.

Diagnostic accuracy of diffusion parameters in CC, CST, CG in PSP.

Based on the Mann-Whitney *U*-test, five models of univariate binary logistic regression analysis were performed in order to test the potential of using diffusion parameters for differential diagnosis of PD and PSP. AAC in the CG, MD in the CST, MD in the CC, Dr in the CC and FA in the CC were included in the models, see Statistical analysis. A summary of the results is shown in Table 3 (Paper I), with details of each comparison given below.

Logistic regression analysis confirmed that the AAC in the CG, the MD in CST and the MD in the CC could significantly ($p < .025$) discriminate PSP from PD (Table 3, Paper I). The sensitivity and specificity for all these parameters, calculated using a ROC curve analysis, showed the optimal cutoff levels (with an area under the ROC

curve (AUC) of .85-.88) to discriminate PSP from PD with a sensitivity of 81-94% and a specificity of 80%. This correctly classified 80-87% of PSP and PD subjects.

To further evaluate the differences in regional values of diffusion parameters along WM tracts demonstrated above, diffusion parameters from the anterior and posterior part of CC were compared separately. The MD in the anterior part of CC, tested in the model of binary logistic regression, age and sex adjusted, showed significantly increased values in PSP vs PD, as was seen for the MD in the whole CC. MD in the posterior part of the CC did not reach significance in the binary logistic regression model. However, bee swarm box plots showed substantial overlap between the different groups (Figure 4, Paper I).

Paper II

Paper II was performed to assess alterations in measures of DTI in parkinsonism in a *derivation cohort*, to confirm results in *validation cohort*, and to explore the potential role of DTI in diagnosis and as a candidate biomarker.

Patients and controls

Age, gender, and disease duration were similar in the PD, MSA-P, and PSP groups in both *deviation cohort* (=cohort 2) and *validation cohort* (=cohort 1) (Table 6 thesis and Table 1, Paper II).

Diffusion parameters

a) ROI analysis

In the *derivation cohort*, we found that patients with PSP have increased MD in the whole thalamus, the thalamic nuclei (VAVL and LPVP) and the midbrain (Table 2, Paper II).

Significant changes of MD (increase with 9-12%) were found in the caudate head, thalamus, VAVL, LPVP and midbrain in PSP. Values of FA were reduced with 12–19% for the SCP and midbrain in PSP patients.

In the *validation cohort* patients with PSP showed higher MD values in the whole thalamus, the VAVL nuclei of the thalamus and the midbrain compared to controls, patients with PD and patients with MSA-P (Table 2, Paper II). Patients with MSA-P displayed higher MD values in the pons than controls and patients with PD, but not compared to patients with PSP (Table 2, Paper II). The values of MD in PSP were increased with 6-9% in the putamen, thalamus, VAVL, LPVP, and pons, and

with 12-15% for midbrain, SCP and red nucleus. Values of FA in PSP were reduced with 5-6% in the putamen and VAVL, with 11-15% in midbrain and SCP.

In the patients with PSP, MD changes in the thalamus did not correlate with volumetric measurements in any of the cohorts.

b) TBSS

In the *derivation cohort*, PSP patients showed significantly higher MD than controls in 75% of the skeletonized voxels in the thalamus (Figure 8).

In the *validation cohort*, patients with PSP were found to have a higher MD in the thalamus than controls (75% significant voxels). In the *derivation cohort* a higher MD was also found in the PSP group compared to both PD (67% significant voxels) and MSA-P (53% significant voxels). Furthermore, a reduced FA was observed in PSP vs controls in both cohorts, and in PSP vs PD in the derivation cohort (30-50% significant voxels).

c) Tractography of the DRTT

As many of the changes in diffusion parameters in patients with PSP observed above were localized in structures associated with the DRTT (i.e. SCP, midbrain, and ventral thalamus), PTG of this tract was performed. In the *derivation cohort*, elevation in MD and reduction of FA was seen in patients with PSP, even though it only reached significance on the right side ($p < .05$) (Figure 3 panels c-d, Supplemental table 2, Paper II).

Value of FA was reduced with 19% and value of MD was increased with 14% for right DRTT in PSP patients. Similar to the *derivation cohort*, tractography of the DRTT in patients with PSP in the *validation cohort* exhibited reduced FA and increased MD in the DRTT on both sides when compared to both controls and patients with PD or MSA-P (Figure 3 panels c-d, Supplemental table 2, Paper II). The values of FA were reduced with 21-28% and values of MD in PSP were increased with 24-29% in the left and right DRTT.

Volumetric measurements

The volumes of the thalamus, the putamen and the globus pallidus were reduced in patients with PSP in both cohorts (Supplemental table 1, Paper II). The midbrain area was reduced in patients with PSP when compared to PD, MSA-P, and control subjects (Supplemental table 1, Paper II). In patients with MSA-P (*validation cohort* only), the volumes of the putamen, and the globus pallidus were reduced (Supplemental table 1, Paper II). Only the thalamic volume and the midbrain area were specifically reduced in PSP.

Correlation between clinical scales and diffusion parameters of thalamus and DRTT in PSP

In the *derivation cohort* increased MD in the whole thalamus, VAVL and LPVP correlated with increased disease stage (H&Y) and with reduced rating scores of activities of daily living (S&E) (Spearman's Rho= – .732-.756, $p < .05$). Very similar findings were obtained in the *validation cohort*. There was a negative correlation between MD and disease stage (H&Y) in PSP patients in the *validation cohort*, similar to that in the *derivation cohort*, for values obtained in the whole thalamus and in the VAVL nuclei (Spearman's Rho = .456 and .431, $p = .017$ and $p = .025$, respectively). Further, higher MD in the LPVP correlated negatively with functional measures of activity of daily living (S&E) (Spearman's Rho = – .467 and – .489, $p = .014$ and $p = .01$, respectively).

The thalamic volume correlated with neither S&E nor H&Y (both cohorts).

In the *derivation cohort* the patients with PSP were also assessed with other clinical rating scales including UPDRS and the PSPRS. We found that worse motor performance (UPDRS-3) was associated with increased MD in the whole thalamus, VAVL and LPVP (Spearman's Rho = .714-.772, $p < .05$) and reduced FA in the whole thalamus (Spearman's Rho= – .762, $p = .028$). Impaired balance (Tandem Gait Test) correlated with increased MD in the whole thalamus, VAVL, LPVP, but also with MD in the right DRTT (Spearman's Rho = .791-.828, $p < .05$). Further, we found significant correlations between diffusion changes in thalamus (whole thalamus and VAVL) and the items in the PSPRS (Table 3, Paper II).

As depicted in figure 4 (Paper II) linear regression showed highly significant positive linear correlation between MD in the thalamus in patients with PSP and the PSPRS total score and strong negative linear relationship between FA in the thalamus in PSP and the PSPRS total score.

Diagnostic accuracy of diffusion parameters of the midbrain, DRTT and thalamus in PSP

Diffusion parameters from the *validation cohort*, that showed the most extensive differences between PSP and other diagnostic groups, were tested separately in the ROC analysis for diagnostic accuracy (Table 4, Paper II).

When using the MD in the midbrain we found that it could differentiate PSP from controls with an AUC of .86, PSP from MSA-P and PD with an AUC of .90, PSP from all groups .88 (Table 4, Paper II).

When using the MD in the right DRTT we found that it could differentiate PSP from controls with an AUC of .95 (Table 4, Paper II). Similar results were obtained when

PSP separated from MSA-P and PD (Table 4, Paper II) and when PSP separated from all groups (Table 4, Paper II).

When using MD in the thalamus we found that it could differentiate PSP from controls with an AUC of .77 (Table 4, Paper II). Similar results were obtained when PSP separated from MSA-P and PD (Table 4, Paper II) and when PSP separated from all groups (Table 4, Paper II).

Paper III

Paper III was performed to assess alterations in measures of DKI in parkinsonism, exploring the potential role of DKI in diagnosis and as a candidate biomarker.

Patients and controls

Total 149 study participants (cohort 2) (Table 6, thesis). The PD and HC groups did not differ significantly by age, but there was a significant difference in gender distribution (Pearson's χ^2 test = 5.4, $p < .05$), with a higher proportion of men in the PD group (Table 6, thesis and Table 1, Paper III).

47 patients (45%) were of PIGD subtype, 50 patients (48%) were of TD subtype and 8 patients (8%) were of intermediate type. The PIGD group performed worse on tests reflecting gait and balance (timed up and go and tandem gait tests) and a cognitive function (AQT) compared to the TD group.

Diffusion parameters

Differences in dMRI parameters in PD compared to HC

Table 2 (Paper III) shows the comparisons in GM structures between PD and HC. In the putamen, MD was increased with 8% and FA was decreased with 9% in PD compared to HC (Mann-Whitney U test, $p < .003$; ANCOVA, $p < .005$). The PD group also exhibited a 6% decrease of the MK in the putamen compared to HC (Mann-Whitney U test, $p < .05$; ANCOVA, $p < .001$). In the thalamus, MD was increased with 4%, and FA was decreased with 3%, in PD compared to HC (Mann-Whitney U test, $p < .05$; ANCOVA, $p < .001$, $p < .05$, respectively). There were no significant age- and gender-adjusted differences in dMRI parameters in the caudate head or the pons between the two groups. There were no significant differences ($p < .05$, ANCOVA) in NDI parameters in the caudate head, thalamus, putamen, and pons found in PD. In the caudate head, the f_{iso} was decreased with 2% and in the thalamus, f_{iso} was increased with 2% in PD ($p < .05$, Mann-Whitney U test, $p > .05$, ANCOVA).

The comparisons in WM tracts between PD and HC are presented in Tables 3 and 4 (Paper III).

In **SLF**, the MD was increased with 4% and f_{iso} was increased with 9% (Mann-Whitney U test and ANCOVA, $p < .05$) in PD. In CST, f_{ic} was significantly decreased with 3% (Mann Whitney U test and ANCOVA, $p < .05$ both) (Table 4, Paper III).

Differences in dMRI parameters in PIGD compared to TD

The comparisons in GM structures between PIGD and TD are shown in Table 2 (Paper III). Compared to TD, patients with the PIGD phenotype exhibited a 7% increase in MD in the putamen (Mann-Whitney U test, $p < .01$). The difference remained significant after adjusting for age (ANCOVA, $p < .05$). There were no differences in dMRI parameters in the analyzed WM tracts between the two groups (data not shown).

Correlations between clinical scores and dMRI parameters in PD

Next we analyzed correlations between the dMRI parameters that were changed in PD compared to HC (according to the analyses above) with clinical measures of motor and cognitive function.

Putamen: Increased MD correlated significantly with a worse motor function, as measured by H&Y ($Rs = .297$, $p < .005$), UPDRS-III motor score ($Rs = .192$, $p < .05$), tandem gait ($Rs = .439$, $p < .001$), and timed up and go ($Rs = .443$, $p < .001$) tests (Figure 2, Paper III).

MK correlated negatively with the disease duration ($Rs = -.206$, $p < .05$). Furthermore, increased MD correlated with impaired cognitive speed and attention, as measured by AQT ($Rs = .219$, $p < .05$). Decreased MK was associated with reduced memory performance, as measured by ADAS-Cog item 3 ($Rs = .258$, $p < .01$). In summary, a high MD and a low MK in the putamen are associated with more severe motor and cognitive symptomatology.

Thalamus: Increased MD correlated significantly with a worse motor speed and balance, as measured by the CAPSIT-PD test ($Rs = -.243$, $p < .05$), tandem gait and timed up and go tests ($Rs = .222$, $p = .05$ and $Rs = .399$, $p < .001$, respectively, Figure 2, Paper III). Decreased FA also correlated negatively with timed up and go test ($Rs = -.226$, $p < .05$).

SLF: Increased MD correlated significantly with the worsening of the motor function, as measured by H&Y, UPDRS-III motor score, tandem gate, timed up and go tests and the cognitive function, as measured by AQT and ADAS-Cog ($Rs = .204$-$.358$, $p < .05$). Increased f_{iso} correlated significantly with the worsening of the motor function, as measured by tandem gate and timed up and go tests and the

cognitive function, as measured by ADAS-Cog (Rs = .205-.325, $p < .05$). Increased f_{iso} correlated significantly with the worsening of the cognitive function as measured by MMSE (Rs = −.202, $p < .05$). In the caudate head and thalamus, f_{iso} did not correlate neither with disease duration nor with clinical scales.

Differences in dMRI parameters in PD compared to PSP or MSA

To study whether the observed differences in dMRI parameters were specific for PD, we also investigated the same parameters in patients with PSP and MSA and compared these values to the ones obtained in the PD group. The results are given in Table 5 (Paper III).

In summary, only FA and MK of putamen seem to be specifically changed in PD where both these parameters are reduced indicating microstructural damage. All of the other changes observed in PD were also found to be changed in PSP and MSA in the same direction and often even more pronounced such as MD in the thalamus or putamen.

Diagnostic accuracy of the studied dMRI parameters in identification of PD

Based on the ANCOVA test, the univariate binary logistic regression analysis were performed in order to test the potential of dMRI parameters for the differential diagnosis of PD vs. HC. MD and MK in the putamen were included in the models, see Statistical analysis. A summary of the results is shown in Paper III Supplement (Supplemental Table 1, Paper III).

Logistic regression analysis confirmed that the MD and MK in the putamen could significantly ($p < .05$) discriminate PD from HC. The sensitivity and specificity for these parameters, calculated using a ROC curve analysis, showed the optimal cutoff level of .79 for MD and of 1.18 for MK in putamen (with an AUC of .62-.65) to discriminate PD from HC with a sensitivity and specificity of around 60%.

Paper IV

IV was performed to assess alterations in measures of DKI in parkinsonian syndromes over two years, exploring the potential role of DKI in diagnosis and as a candidate biomarker.

Patients and controls

Table 6 (thesis) and Table 1 (Paper IV) shows the demographic and clinical characteristics of HC and patients with PD at baseline and after two years. There

was no group difference in age but there was a significant difference in gender distribution (Pearson's χ^2 test = 7.2, p = .009), with a higher proportion of men in the PD group.

The PD group had higher UPDRS III total and sub-scores (p < .001) compared with HC. An effect of time was found for the MMSE (p = .006), due to an increase in the HC group over the two years, and for LEDD in the PD group (p < .001), amounting to a daily LEDD increase by approximately 35% (180 mg). There were no other significant changes in any other clinical or demographic data over time (Table 1, Paper IV).

ROI method analysis of the deep grey matter

Changes in DKI parameters were observed in both PD patients and controls over the two-year period. Specifically, reductions in MD and increases in MK and FA were found in many brain regions (Online Resource 3, Paper IV). However, when comparing the changes in dMRI parameters in PD over two years to the changes observed in controls over the same time period, we only found a decrease in FA in the putamen in PD (ANCOVA, $\beta = -.248$, p = .001). Figure 1 (in Paper IV) illustrates FA changes in the putamen for PD and HC. There were no other significant longitudinal changes observed in PD when compared to controls, including in the white matter (Online Resource 3, Paper IV).

TBSS analysis of white matter

There were no significant longitudinal changes in either MD, FA or MK in the WM observed in PD patients compared to controls.

Correlation between clinical and DKI changes

Two-year change in FA in the putamen in PD patients correlated with LEDD at baseline (R2 Linear = – .184; Rs = – .399, p < .0001) (Figure 2, Paper IV) and LEDD at follow-up (data not shown). No correlations were found between DKI parameters and UPDRS III, H&Y, and MMSE. Also no correlations were found between change in DKI parameters versus change in UPDRS III, H&Y, and MMSE.

Analysis of white matter hyperintensities (WMH)

The amount of WMHs did not show any statistically significant difference between controls and patients with PD (data not shown).

Paper V

Iron accumulation is common in neurodegenerative disorders and QSM has been used to investigate changes in PD.

Patients and controls

The demographics of the participants are presented in Table 1 (Paper V) and Table 6 (thesis). There was no significant difference in age ($F_{3,195}$ = 1.842, p = .141 assessed by one-way ANOVA) between the groups. There was a difference in gender distribution (p = .026 assessed by Pearson's χ^2 test), with more male participants in the PD group, thus a one-way ANCOVA was used to correct for gender and age in the group comparisons.

Group differences

As shown in Figure 2 (Paper V) there were significant group differences in all ROIs; globus pallidus ($F_{3,193}$ = 6.474, p < .001), putamen ($F_{3,193}$ = 32.920, p < .001), SN ($F_{3,193}$ = 22.968, p < .001), red nucleus ($F_{3,193}$ = 43.137, p < .001) and dentate nucleus ($F_{3,193}$ = 26.291, p < .001). Significant effects of age were found in the putamen (p < .001), red nucleus (p < .001) and dentate nucleus (p = .004). No significant effects of gender were found in any of the regions. Further analyses revealed that the PSP group showed higher susceptibility in the red nucleus compared to all other groups (all p-values < 10^-4) and in globus pallidus, putamen, SN and the dentate nucleus compared to PD and HC (all p-values < .0001). We also found higher putaminal susceptibility in MSA compared to PD (p < .0001) and HC (p < .0001), and higher susceptibility in SN (p = .0006) and the dentate nucleus (p < .0001) compared to PD. We found no significant differences between the PD group and the control group in any of the ROI. Representative susceptibility maps of the different groups are presented in Figure 3 (Paper V).

Diagnostic performance

Diagnostic performance in the different regions between the groups was evaluated using the area under ROC-curves, AUC. Cut-off levels were chosen to yield a differentiation as close to perfect as possible by selecting the point on the ROC curve closest to the upper left corner. The ROC-curves and associated results are reported in Figure 4A-F (Paper V). To further investigate diagnostic accuracy, we also performed discriminant analysis between each of the three patient groups and the controls, using all of the five ROI. In the discriminant analysis, prior probabilities were set to "all groups equal" to correct for unbalanced group sizes. In classifying PSP vs. PD, we found a sensitivity of 100%, a specificity of 97 % and a total of 97.2% cases correctly classified. With leave-one-out cross-validation (LOOCV),

results were unchanged. When classifying PSP vs. MSA, a sensitivity of 90.9% and a specificity of 90 % were achieved, with 90.5% of cases correctly classified. In the LOOCV of this classification we found a sensitivity of 81.8%, a specificity of 90 % and a total of 85.7% cases correctly classified. Results from all discriminant analyses are reported in Table 2 (Paper V).

Correlations between susceptibility and clinical scores

In the PD group, we evaluated correlations between susceptibility levels in the different regions and the clinical scores from UPDRS-III and H&Y ratings. Due to the small number of subjects with PSP and MSA, no correlation tests were carried out in these groups. For this analysis, we used Pearson partial correlation while controlling for age, gender and disease duration. There was a significant correlation between putaminal susceptibility and UPDRS-III in the PD ($R = .213$, $p = .015$). The remaining tests between susceptibility levels and UPDRS-III or H&Y did not show any significant correlations. We also assessed correlations between disease duration and regional susceptibility while controlling for age and gender. In these tests, we found significant correlations in the PD group in the globus pallidus ($R = .198$, $p = .023$) and in the SN ($R = .251$, $p = .004$). Plots of the significant correlations are shown in Figure 4G-I (Paper V).

Discussion

Methodological Considerations

Case ascertainment and representativeness of included patients

All of the included studies in this thesis fulfil the criteria for an optimal case-control study (Song and Chung 2010) can be considered to provide Level 3 Evidence Based Medicine (Song and Chung 2010). Patients were included if they fulfilled the strict eligibility criteria. The selection process would probably limit generalizability of our findings to a more “prototypical" case of PS. Thus, the use of diagnostic criteria with a sensitivity 76-84% for PD (Ward and Gibb 1990), of 66% for PSP (Litvan, Agid et al. 1996) and 92% for MSA (Osaki, Ben-Shlomo et al. 2009) might potentially exclude patients with less typical presentation of PD, PSP and MSA. More other, PD patients with more aggressive PD disease yielding DBS treatment, were excluded because of a higher risk to get complication to the MRI investigation that could be accepted by Helsinki Declaration. This selection might have biased the study and may have led to the lack of the positive association between diffusion changes and clinical scales scores. Specifically, the sensitivity of clinical diagnostic criteria for PSP (Litvan, Agid et al. 1996), used in this study, is limited for variant PSP syndromes with presentations other than Richardson's syndrome.

Although all patients fulfilled clinical research criteria for diagnosis of their respective disorder, they might still vary substantially in disease stage, rate of progression and clinical symptoms. Patients were selected from a variety of sources including hospital patients, patients in a physician's practice, and clinic patients. Neurologically HC were selected from the same population source (Skåne region). The lack of autopsy confirmed diagnosis is an obvious limitation of all papers included in this thesis. The other limitation is that the cases were selected mostly from one hospital in the region, which affects generalizability of the results.

Paper I and validation cohort paper II

Prospective hospital-based case ascertainment was combined with a confirmed diagnosis on autopsy in two patients (cohort 1). Retrospective methods were used for H&Y and S&E scale scores, and assessed based on the medical records. This latter reduces the quality of the patient’s evaluation compared to face-to-face

assessment. Moreover, no clinical scales were applied prospectively, thus no correlation between clinical and dMRI parameters was possible. Diagnoses were validated at the hospital where baseline imaging and radiology reports were assessed. The individual age and gender matching strategy was used when controls were selected from the Swedish population registry. All main study results were age-adjusted, because dMRI parameters change with age.

In summary, cohort I are likely representative of most cases with parkinsonism, especially those with autopsy-confirmed diagnoses. Retrospective clinical scales assessment needs to be taken into account.

Paper II derivation cohort and papers III-V

Prospective hospital- and clinical practice-based case ascertainment and no retrospective methods were used (cohort 2). Clinical follow-up protocol of *BioFINDER* study facilitates re-evaluation of the clinical diagnosis to achieve as correct diagnosis as possible. Another important aspect is that patients diagnosed with structural lesions at baseline (stroke, meningioma, normal pressure hydrocephalus) were excluded from the studies, that could influence how representative the diagnostic potential is for the "general" PS population. Neurologically HC were recruited, who did not have any objective cognitive or parkinsonian symptoms. Controls were mostly recruited on a convenience manner from spouses, relatives and friends of patients, using matching, which refers to selecting controls so that they are similar to cases in age and gender. The evaluation of scales was made mostly by physicians and nurses trained to examine patients with PD and APS. It would have been preferable to record video film of the patient being examined according to UPDRS-III protocol (Fahn 1987) that would be examined by a second movement disorder specialist (Song and Chung 2010). These biases decrease the internal validity of the investigation and should be carefully addressed and reduced in the study design. Another limitation is that parkinsonism was required to be included in the study. Some patients in the early stages of MSA and PSP may have no signs or only very subtle signs of parkinsonism and thus were not referred for possible inclusion in our project.

In summary, cohort II represents patients affected mostly by parkinsonism, which together with interviewer bias needs to be taken into account when interpreting the study results.

Radiological characteristics

In all papers, dMRI estimations was made by specialist in Neurology, trained in DTI/tractography analysis, blinded to the clinical diagnosis. Therefore the reproducibility of the measurements was uncertain. Rater bias was prevented by blinding, and the intra-rater variability coefficient was calculated and reported. All

MRI scans were made and assessed at the same center, which increases the accuracy of assessments.

The issue of WMH in the thesis

WMH of presumed vascular origin are a common finding in brain MRI scans of healthy elderly individuals and patients with parkinsonism (Bohnen and Albin 2011) and can contribute to cognitive decline due to micro-vascular changes (Deary, Leaper et al. 2003, Slawek, Roszmann et al. 2013). Parameters obtained from the dMRI, such as FA and MD, can demonstrate alterations in axonal microstructure, with several studies showing that MD increases and FA decreases in areas of visible WM degeneration such as that commonly observed in WMH (Bastin, Clayden et al. 2009). The aim of our study was not to differentiate diffusion changes in WM secondary to PD from WM changes secondary to concomitant vascular pathology. Thus neither patients nor HC with WMH were ruled out from Papers I-V. In Papers II and IV, WMH were rated according to the scales of Fazekas (Fazekas, Chawluk et al. 1987) and Wahlund (Wahlund, Barkhof et al. 2001) and compared. WMH burden was higher among PD patients compared to HC, but did not show any statistically significant difference. However, this approach does not strictly demonstrate that there is relationship between WMH and diffusion parameters in the PD group. Also, if relationship between WMH and diffusion parameters is shown, the problem remains to interpret the origin of the WMH, which with increasing magnetic field strengths become more complex and difficult to define by visual inspection (Bohnen and Albin 2011). Unless patients die unexpectedly and undergo a post mortem follow-up, determining the origin of the WMH in single case will be by inference, and this remains a potentially biasing factor in this and similar studies.

Sensitivity and specificity assessment

Paper I-II

WM tract degeneration has been demonstrated to be a striking feature of PSP-RS, with abnormalities observed predominantly in the SCP, cerebellum, body of the CC, CG, and premotor aspects of the SLF (Introduction thesis). The majority of these WM tracts show greater degeneration in PSP-RS compared with PD and MSA-P.

Little data are currently available on the diagnostic utility of DTI measures, although the CC (Ito, Makino et al. 2008) and (Agosta, Galantucci et al. 2014) show high sensitivity and specificity in differentiating PSP-RS and PD. In Paper I we obtained moderate sensitivity and specificity (around 80%) for MD in the anterior CC in the differential diagnosis of PD from PSP. Ito et al. had compatible with our results: in differentiating PSP from PD, evaluation of FA in the prefrontal CC had 85.7% sensitivity, 65.5% specificity and 69.4% accuracy (Ito, Makino et al. 2008).

The diagnostic value of DTI measures to differentiate PSP-RS and MSA-P is unclear (Whitwell, Hoglinger et al. 2017). In Paper II when using the MD in the midbrain, DRTT and thalamus we found that it could differentiate PSP from PD and MSA-P with 77-92% sensitivity and specificity (Table 4, Paper II). Additionally, we could validate these results in two cohorts using two different scanners (Paper II), constituting a strong point of this paper.

In summary, DTI abnormalities are striking in PSP-RS, compared to PD and MSA, with abnormalities observed predominantly in the SCP, cerebellum, body of the CC, CG, and premotor aspects of the SLF. Our data is limited for variant PSP syndromes with presentations other than PSP-RS. More other, data are needed on the utility of DTI measures in autopsy-confirmed PSP. In according to MDS criteria, only DTI of SCP fulfill the low level of reliability and therefore have the potential to be useful diagnostic biomarkers (Table 3 in Whitwell at al.) (Whitwell, Hoglinger et al. 2017). The issue of whether DTI measurements can be translated into clinical practice is also unclear, because there is little standardization of methods across studies and no established diagnostic cut points for these measurements.

Paper III

We obtained low sensitivity and specificity for DKI measures (around 60%) in the differential diagnosis of PD from HC. The results of this study deviates from Wang et al. (Wang, Lin et al. 2011) showed higher sensitivity and specificity of MK in putamen (around 88%) in the differential diagnosis of PD from HC. Compared to Wang et al., we also investigated patients with PSP and MSA and compared DKI values to the ones obtained in the PD group (Table 5, Paper III). Only FA and MK of putamen seem to be specifically changed in PD. All of the other changes observed in PD were also found to be changed in PSP and MSA in the same direction, constituting a strong point of this paper.

Compared to Wang et al. that demonstrated high sensitivity and specificity of MK in the SN (around 80-100%) (Wang, Yang et al. 2015), we could confirm the strong impact of the low SNR on the artificial changes in FA, MD and MK in the SN, red nucleus, globus pallidus, and midbrain. The SNR was approximately 50% of that in the thalamus, and 25-35% of that in WM (S1 File, S1 Figure Paper III). Thus the artificial changes in FA, MD and MK in basal ganglia most probably refer mostly to iron accumulation in these iron-rich structures than to gliosis. As such, for accurate quantification of basal ganglia by dMRI one should achieve a sufficient SNR.

In summary, the low sensitivity and specificity of DKI measurements need to be taken into account when interpreting the study results.

Paper V

When comparing PSP to PD, we find a diagnostic performance with sensitivity 91% and specificity 97% in the SN, sensitivity 100% and specificity 91% in the red nucleus, and sensitivity 91% and specificity 90% in the dentate nucleus. The diagnostic performance is increased when including susceptibility levels from all studied regions in discriminant analyses where we have shown a sensitivity of 100% and specificity of 97% using LOOCV, for differentiating PSP from PD.

In summary, we find these levels of diagnostic performance impressive and reviewing literature we find that these results are comparable to the performance of midbrain-pons area and MRPI measurements (Whitwell, Hoglinger et al. 2017). Combining morphological analyses such as the MRPI with QSM to potentially increase the diagnostic accuracy even further is an interesting direction for future studies.

General discussion

Expert examination is a fundament in diagnosis of PD in according to the MDS Clinical Diagnostic Criteria for Parkinson's disease (MDS-PD Criteria) (Postuma, Berg et al. 2015). The MDS criteria were designed to be broadly applicable without need for ancillary diagnostic testing (Postuma, Berg et al. 2015). Nonetheless, in certain contexts, such as other pathologies causing neurodegenerative or secondary parkinsonism (MSA, PSP, subcortical arteriosclerotic encephalopathy, and so forth), or in the absence of a true progressive parkinsonian disorder (essential tremor, dystonic tremor, and so forth) ancillary testing may be necessary to resolve uncertain cases. Such diagnostic biomarkers must have 80% specificity or more for the differential diagnosis of parkinsonism (compared with gold-standard clinical or clinico-pathologic diagnosis) (Postuma, Berg et al. 2015). In this thesis we have studied how advanced MRI techniques can improve differential diagnosis of parkinsonian syndromes and serve as candidate biomarkers, facilitating diagnosis and used for monitoring of disease progression.

Cross-sectional studies

In Papers I-IV we cover several aspects of the application of dMRI in the diagnosis/differential diagnosis of parkinsonism. By using manual ROI and TBSS analysis of WM and GM in PD we observed that dMRI could not be used in isolation, because of the low specificity.

Most studies on humans, including Papers I-IV in the present thesis, show nigral MD to be unaltered in PD (Vaillancourt, Spraker et al. 2009, Peran, Cherubini et al.

2010, Du, Lewis et al. 2011, Zhan, Kang et al. 2012). In a systematic review and meta-analysis of Cochrane and Ebmeier (Cochrane and Ebmeier 2013) of a total of 21 studies, 9 studies measured FA in the SN. All except 1 found a reduction in FA in comparison with HC. The reduction was statistically significant in 7. ES for the reduction in FA pooled for the 9 ROI studies, with a total of 193 patients with PD and 195 HC, showed a large mean ES (20.64, 95% confidence interval 20.86 to 20.42, p = .0001). One study in PD showed no correlation between FA in the SN and nigrostriatal binding ratios of dopamine ligands (Harper 2011). Thus, the evidence for decreased FA being related to degeneration of nigral dopamine neurons in PD is unconvincing.

Nevertheless**,** elevated FA in SN can be explained by inflammation and gliosis (Boska, Hasan et al. 2007, Van Camp, Blockx et al. 2009), where the infiltration of gliotic cells creates a more directional diffusion but prevents an increase in MD. Another explanation could be that the proportion of fibers in adjacent longitudinal tracts relative to the shrinking nuclei, increases directionality (Lenfeldt, Larsson et al. 2015). The variability between studies may also be due to subtle changes in ROIs which may or may not include nigrosome 1 or Lewy bodies. Lenfeldt et al. (Lenfeldt, Larsson et al. 2015) showed that FA is an incomplete measure of nigral diffusion differences as it does not account for changes in diffusion directions. It is unknown if nigral diffusion alterations in PD are solely related to magnitudes or if distorted diffusion directions are also involved.

In the differential diagnosis, the most striking DWI (DTI is a specific type of modelling of DWI datasets) changes are seen in *PSP-RS*, which shows elevated ADC (MD in DTI) values in putamen, caudate, globus pallidus, midbrain, SCP, and prefrontal and precentral WM (Seppi, Schocke et al. 2003, Nicoletti, Lodi et al. 2006, Paviour, Thornton et al. 2007, Nicoletti, Tonon et al. 2008, Tsukamoto, Matsusue et al. 2012). *PD patients*, compared with PSP-RS, typically show lower ADC values in the putamen, caudate nucleus, globus pallidus, SCP, and midbrain (Seppi, Schocke et al. 2003, Nicoletti, Lodi et al. 2006, Tsukamoto, Matsusue et al. 2012, Prodoehl, Li et al. 2013) with one study obtaining high sensitivity (90%) and specificity (100%) to differentiate PSP-RS from PD using values from the putamen (Seppi, Schocke et al. 2003) and another obtaining 100% sensitivity and specificity using the SCP (Nicoletti, Tonon et al. 2008). *MSA-P* patients, compared with PSP-RS, has lower ADC values in the caudate nucleus (Tsukamoto, Matsusue et al. 2012) and SCP (Nicoletti, Tonon et al. 2008, Tsukamoto, Matsusue et al. 2012) but higher values in the MCP (Paviour, Thornton et al. 2007, Wadia, Howard et al. 2013), cerebellum (Nicoletti, Rizzo et al. 2013), and putamen (Baudrexel, Seifried et al. 2014). Sensitivity and specificity values for differentiating PSP-RS from MSA-P are high using DWI of the SCP (sensitivity, 96.4%; specificity, 93.3%103).

WM tract degeneration in parkinsonism has been demonstrated to be prominent feature in PSP-RS. In PSP-RS, abnormalities were observed mostly in the SCP, cerebellum, body of the CC, CG, WM, the thalamus, and premotor aspects of the SLF (Erbetta, Mandelli et al. 2009, Knake, Belke et al. 2010, Wang, Wai et al. 2010, Canu, Agosta et al. 2011, Whitwell, Avula et al. 2011, Whitwell, Master et al. 2011, Saini, Bagepally et al. 2012, Whitwell, Xu et al. 2012, Tessitore, Giordano et al. 2014, Worker, Blain et al. 2014, Meijer, van Rumund et al. 2015, Piattella, Upadhyay et al. 2015, Surova, Nilsson et al. 2015). The majority of these WM tracts show greater degeneration in PSP-RS compared with PD (Blain, Barker et al. 2006, Erbetta, Mandelli et al. 2009, Agosta, Galantucci et al. 2014, Worker, Blain et al. 2014, Surova, Nilsson et al. 2015) and MSA-P (Blain, Barker et al. 2006, Worker, Blain et al. 2014, Surova, Nilsson et al. 2015). Little data are currently available on the diagnostic utility of DTI measures, although the CC (Ito, Makino et al. 2008) and SCP (Agosta, Galantucci et al. 2014) show high sensitivity and specificity in differentiating PSP-RS and PD. Thus, DTI measures in PSP-RS have the potential to be useful diagnostic biomarkers (Whitwell, Hoglinger et al. 2017).
The diagnostic value of DTI measures to differentiate PSP-RS and MSA-P is unclear. Moreover, data are needed on the DTI measures in autopsy-confirmed PSP, PD, and MSA.

We did not find any clear diagnostic utility of DKI analysis of GM when identifying PD. Our finding deviate from Wang et al. (Wang, Lin et al. 2011), as mentioned above. Further, Kamagata et al. showed reduced MK in the frontal, parietal, occipital, right temporal WM, posterior corona radiata and SLF in a PD group compared with a control group when using TBSS (Kamagata, Tomiyama et al. 2014). These changes were not observed in Papers III-IV. However, the PD patients in the present study had slightly shorter disease duration, which could explain these discrepancies. Considered together, the results might suggest that alterations of MK in GM and WM probably might not improve the diagnostic work-up of early PD. However, such alterations may be related to the disease severity of PD since we found that MK of putamen in PD patients correlate with disease duration and cognitive performance. Future longitudinal studies are needed to improve sensitivity and specificity (>80%) of DKI for the clinical diagnosis of PD at the individual level, the utility for early clinical PD diagnosis, when patients have mild or nonspecific symptoms and signs before they meet clinical criteria for the PD. Another issue to consider when determining the value of DKI biomarkers in PD is how well the DKI would translate into clinical practice in PD. Ideally they should be relatively inexpensive, convenient, safe, widely available, and comparable across different centers.

There are three main shortcomings in DTI/DKI studies parkinsonism. *To begin*, there are differences in data acquisition. The interplay between selected image acquisition parameters and factors including SNR (Paper III Supplement

Supplemental Methods), image resolution, and image distortion influences the accuracy of the diffusion tensor estimation and thus the results derived. *Next*, ROI-based analysis can fail to detect important differences outside of the selected regions and their definition may be subject to user bias. Voxel-based analysis techniques, conversely, can be biased toward false positive errors due to multiple comparisons since they essentially perform voxel-by-voxel statistical comparisons throughout the whole brain (Vaillancourt, Spraker et al. 2009, Zhang, Yu et al. 2011). Issues with smoothing and spatial normalization may lead to inaccuracies. *Lastly*, in all studies so far clinical diagnostic criteria were used for patient selection without neuropathological verification thus misdiagnosis cannot be excluded. The stage of a patient's disease, either early or advanced, may influence DTI findings.

In summary, whether dMRI measurements can be translated into clinical practice is unclear, because there is little standardization of methods across studies and no established diagnostic cutoff points for these measurements (Whitwell, Hoglinger et al. 2017). Today DTI measures in parkinsonism have the potential to be useful diagnostic biomarkers only in PSP-RS (Whitwell, Hoglinger et al. 2017), especially in cerebral WM studies. Our results further high-light this fact. Interpretation of the DTI/DKI alterations in parkinsonism in terms of their underlying microstructural origins in GM is difficult. To fully understand FA alterations in SN, animal models of reduced cell number in SN are not enough, as there are contradictory conclusions on how FA reacts to this reduction (Boska, Hasan et al. 2007, Van Camp, Blockx et al. 2009). Future studies must establish what diffusion measures mean morphologically in GM, before we can explain the opposite observations made in SN in parkinsonism (Lenfeldt, Larsson et al. 2015).

Longitudinal study

Because of the onset and progression of symptoms in PD reflect the involvement of successively larger areas of the brain, it is crucial to include both baseline and follow-up data. Our longitudinal two-year DKI study (Paper IV) of a relatively large cohort of PD patients provides evidence that DKI can be used to detect disease progression in PD patients. To our knowledge, today there are no DKI study in parkinsonism. Longitudinal DTI studies in PD have so far reported inconclusive results: both increased and decreased FA in the SN, and also increased MD in the SN, thalamus, midbrain, frontal WM (Table 7). The results of the current DKI study deviates from previous DTI longitudinal reports (Rossi, Ruottinen et al. 2014, Lenfeldt, Larsson et al. 2015, Ofori, Pasternak et al. 2015, Chan, Ng et al. 2016, Loane, Politis et al. 2016, Zhang, Wu et al. 2016) (Table 7).

Table 7
Longitudinal DTI studies in PD.

First author	Year	Comparisons	Method	Main results
Rossi(Rossi, Ruottinen et al. 2014)	2014	25 PD vs 19 HC	$R2^*$, T2 DWI, SWI TBSS	Tendency to decreasing FA in the genu of corpus callosum and bilaterally in corona radiata in PD.
Lenfedt(Lenfeldt, Larsson et al. 2015)	2015	122 PD vs 34 HC	DTI	Increased FA in the substantia nigra in PD. The left middle cerebellar peduncle had increased FA and AD and decreased MD and RD compared to the right in PD.
Ofori(Ofori, Pasternak et al. 2015)	2015	19 PD vs 25 HC	DTI free-water	Free-water diffusion increased in SN in PD
Chan(Chan, Ng et al. 2016)	2016	46 PD	DTI	Increased MD in all brain regions, decreased FA in frontal WM, and increased FA in posterior putamen, thalamus, SN in PD
Loane(Loane, Politis et al. 2016)	2016	14 PD vs 18 HC	DTI	Decreased FA in the SN in PD
Zhang(Zhang, Wu et al. 2016)	2016	122 PD vs 50 HC	Multicenter DTI	Decreased FA, increased Dr and Da in SN, midbrain, thalamus in PD

DTI, Diffusion Tensor Imaging; HC, healthy controls; Dr, radial diffusivity; Da, axial diffusivity; PD, Parkinson's disease; SN, substantia nigra; SWI, Susceptibility weighted imaging; TBSS, tract based spatial statistics analysis; DWI, diffusional weighted imaging.

Overall, studies have previously detected an alteration in FA in SN in patients with PD (Lenfeldt, Larsson et al. 2015, Loane, Politis et al. 2016, Zhang, Wu et al. 2016). There were differences in the ROIs studied and the acquisition and analysis characteristics of the studies. Most intriguing is the study of Zhang et al. (Zhang, Wu et al. 2016) that in one year's DTI study demonstrated reduced FA in the SN with 3.6±1.4% per year from baseline, and increased Dr and Da in the thalamus (with 8.0±2.9% per year and 4.0±1.5% per year, respectively). These numbers are extremely large and most probably are driven by differences in technical characteristics of dMRI in different centres (16 US sites, 5 European, 1 Australian). We suppose that standardized protocol of dMRI studies will minimize the interplay between selected image acquisition parameters and factors including SNR, image resolution, and image distortion. Moreover, upgrades in software (MR scanner) should be taken into account in longitudinal dMRI studies, unlike in cross-sectional studies. Our experience indicate that the measurement of diffusion parameters can be influenced by changing MR scanner and study results corrected accordingly.

In summary, as has been addressed above DKI has potential to show disease progression in PD. However, the longitudinal changes are modest and need to be reproduced in other cohorts. Further work relating these imaging biomarkers to histopathologic findings especially at early stages in disease is required to understand fully the pathologic processes. Lastly, imaging findings related to changing MR scanner might fluctuate from baseline to follow-up imaging sessions.

Those longitudinal changes in imaging findings lead to bias that are inherent in the imaging process and thus should be taken into consideration.

Applicability of Clinical results

Neuroimaging studies in this thesis has improved our understanding of the neurobiology of the PSP but has not given many confirmed diagnostic biomarkers. Not all PSP can be identified. Nevertheless DTI/DTT measures could prove to be valuable in the differential diagnosis of PSP from PD. Findings concerning other forms of PSP than PSP-RS are lacking here. Although more work is needed to provide and validate standardized measures of the kind that could be used in diagnostic criteria. DKI measures are sensitive to parkinsonism, but specificity is low, and thus they are less useful in ruling out other parkinsonian syndromes. More work is required to assess the value of DTI and DKI measures in PSP and in autopsy-confirmed cases to determine whether they could be useful valid biomarkers. Capturing the PD, PSP and MSA in its earliest phase, do MRI and then follow patients over time to see what kind of disease they will develop will also be critical for developing well-validated biomarkers.

SWI/QSM imaging techniques is exciting, but more is needed to truly understand the biological basis SWI signal in PSP and MSA. According to our results in Paper V, susceptibility in deep nuclei seems promising in the diagnostics of APS, especially in PSP were both high sensitivity and specificity was achieved. Correlations between susceptibility and disease severity within groups might indicate a possibility that QSM could be valuable in monitoring disease progression and in clinical trials. However, these are early days of SWI/QSM imaging in APS, and we expect our understanding of this biomarkers to increase other the coming years.

Conclusions

Diffusion tensor imaging and tractography in PSP

- DTT analysis of diffusion parameters along WM tracts can demonstrate disease-specific regional WM changes in PSP.
- The anterior portion of the CC was identified as a promising region for detection of neurodegenerative changes in patients with PSP, as well as for differential diagnosis between PSP and PD.
- Patients with PSP, but not PD or MSA-P, exhibit signs of structural abnormalities in the thalamus and in the DRTT.
- However, future prospective and longitudinal studies are needed to evaluate whether dMRI can be used to reliably detect PSP during the early stages of the disease, and whether all different forms can be detected with equally high accuracy.

Diffusion kurtosis imaging in PD

- PD patients exhibit microstructural changes in the putamen, the thalamus, and the SLF, which are associated with worse disease severity.
- DKI changes are not sufficiently specific to improve the diagnostic work-up of PD.

Neurite density imaging

- We could not demonstrate any significant differences between PD patients and controls using neurite density imaging.

Longitudinal diffusion kurtosis imaging

- The study indicates that in PD microstructural changes in the putamen occur selectively over a two-year period and can be detected with DKI. However, the longitudinal changes are modest and need to be reproduced in other cohorts.

Susceptibility weighted imaging

- We showed different patterns of brain susceptibility between PD, MSA and PSP, reflecting underlying regional differences in pathological processes and brain iron accumulation.
- We believe that these differences in susceptibility, particularly in the mesencephalic region, could be of great use in the diagnostics of parkinsonism, especially when faced with the diagnostic challenge of separating PSP from other parkinsonian disorders and healthy individuals.
- Today QSM cannot be used clinically because of the problem of advanced software where the terms of use allow for research and not clinical.

Future perspectives

A major challenge faces future dMRI studies is to improve sensitivity for all variants PSP presentations, and achieving high specificity versus alternative diagnoses such as PD, MSA with predominant parkinsonism (MSA-P), CBD or alternative proteinopathies. The later will ideally require the inclusion of all patients with parkinsonism to the prospective study with dMRI. There is also a need to optimize the design of dMRI studies in PD, such as better characterization (Dubois, Slachevsky et al. 2000, Goldman, Holden et al. 2015, Biundo, Weis et al. 2016) and selection of groups of patients with PD that would provide more homogeneous groups for investigations.

Also, to further investigate the temporal changes in dMRI parameters, further longitudinal studies over a long period of time are needed. These kind of studies will improve group-level dMRI findings and could probably be translated into useful biomarkers.

The next step is to demonstrate useful sensitivity and specificity of dMRI (>80%) for the clinical diagnosis at the individual patient level (Whitwell, Hoglinger et al. 2017). More studies are needed to improve specificity to the dMRI results, like the latest approach of our group (Szczepankiewicz, Lasic et al. 2015, Lampinen, Szczepankiewicz et al. 2017). Specifically, it was suggested that the micro FA (μFA) and order parameter (OP) may complement FA by independently quantifying the microscopic anisotropy and the level of orientation coherence. The interpretation of dMRI parameters should also be informed and substantiated by independent validation.

Paper V presented promising results about QSM as a possible objective diagnostic tool for differential diagnosis between PD, PSP and MSA. The predictive model based on QSM measures should be repeated, confirmed and possibly modified based on a larger patient cohort. Clinical applications of QSM are currently not feasible because the available software (such as STISuite as we used, or MEDI, etc.) have terms of use that allow for research only. Proper implementation must fulfil requirements for Conformité Européenne (CE) marking and have an interface that is compatible with existing picture archiving and communication systems (PACS).

Acknowledgements

I wish to express my warmest gratitude to all the persons who had contributed to this thesis. My special and most sincere thanks to:

My supervisor, Professor Oskar Hansson. You have introduced me to the world of science with great care and a sure instinct. In many things, I have come to depend on your honest advice, your extensive knowledge and resourcefulness. Thank you for this scientific journey.

My co-supervisor, docent Danielle van Westen, for constructive support and enthusiasm, scientific advice, guidance through the long journey of this project from its conception to its completions, and always providing prompt feedback to my ideas and questions.

My co-supervisor, assistant professor Markus Nilsson, for your never-ending patience when explaining biophysics and statistics to a clinician, for help in matters of imaging analysis and re-analysis x 1000.

My co-supervisor, Professor Håkan Widner, for introduction and sharing with me of you great clinical experience of patients with movement disorders and for your patience.

My co-supervisor and mentor, docent Christer Nilsson, for making the railway for my first manuscript, for ten years continuous encouraging debriefing and your warm support and clinical expertise.

The collaboration with biophysics in Lund has been CRUCIAL for this thesis, both hardworking, exciting and inspiring. Thanks to Filip Szczepankiewicz, Björn Lampinen, Jimmy Lätt, Peter Mannfolk, also thanks for Olof Lindberg for collaboration with Huddinge and Alexandr Leemans for collaboration with University Medical Center of Utrecht, Netherlands.

To the research nurses, Jan Reimer and Ann Johansson, for organizing the administration in this study. Particularly I wish to thank Katarina Johansson for a great example of humanity and generosity when working with senior patients.

To research colleagues Irina Dragancea, Sara Hall and Maria Strandberg, for you gave me Ariadne's Thread.

To Henrik Sjöström, for productive collaboration with Karolinska Institutet, and also to Ruben Smith, Sebastian Palmqvist, Niklas Mattsson, Mattis Jalakas for discussions and friendship.

To Gesine Paul-Visse, Lars Wictor, Andreas Puschmann, Carl Rosenblad, Klas Wictorin, and Prof. Per Odin, for many stimulating discussions of patients with parkinsonism within the movement disorder team.

To all my colleagues at the Department of Neurology, for your support and friendship.

I wish to thank all patients who participated in this study, their caregivers, and all these who participated as control subjects. I am grateful to the ALF committee, BAGADILICO and MULTIPARK research networks, The Swedish Parkinson Academy, The Swedish Parkinson Foundation.

My very special thanks go to

my mother Lidia, for her unlimited warm support during all these years,

to my wonderful children Ivan and Sophia – you are the most important miracles in my life, thanks for reminding me that a listening of the music you playing can be more exciting that formatting a thesis,

and to Nasser, for you loving support during these years, and for your understanding even during the times when many hours were spent with research.

References

Aarsland, D., J. Zaccai and C. Brayne (2005). "A systematic review of prevalence studies of dementia in Parkinson's disease." Mov Disord **20**(10): 1255-1263.

Abdo, W. F., B. R. Bloem, W. J. Van Geel, R. A. Esselink and M. M. Verbeek (2007). "CSF neurofilament light chain and tau differentiate multiple system atrophy from Parkinson's disease." Neurobiol Aging **28**(5): 742-747.

Abhinav, K., F. C. Yeh, S. Pathak, V. Suski, D. Lacomis, R. M. Friedlander and J. C. Fernandez-Miranda (2014). "Advanced diffusion MRI fiber tracking in neurosurgical and neurodegenerative disorders and neuroanatomical studies: A review." Biochim Biophys Acta **1842**(11): 2286-2297.

Adachi, M., T. Kawanami, H. Ohshima, Y. Sugai and T. Hosoya (2004). "Morning glory sign: a particular MR finding in progressive supranuclear palsy." Magn Reson Med Sci **3**(3): 125-132.

Agosta, F., S. Galantucci, M. Svetel, M. J. Lukic, M. Copetti, K. Davidovic, A. Tomic, E. G. Spinelli, V. S. Kostic and M. Filippi (2014). "Clinical, cognitive, and behavioural correlates of white matter damage in progressive supranuclear palsy." J Neurol **261**(5): 913-924.

Al-Bachari, S., L. M. Parkes, R. Vidyasagar, M. F. Hanby, V. Tharaken, I. Leroi and H. C. Emsley (2014). "Arterial spin labelling reveals prolonged arterial arrival time in idiopathic Parkinson's disease." Neuroimage Clin **6**: 1-8.

Alexander, A. L., S. A. Hurley, A. A. Samsonov, N. Adluru, A. P. Hosseinbor, P. Mossahebi, P. M. Tromp do, E. Zakszewski and A. S. Field (2011). "Characterization of cerebral white matter properties using quantitative magnetic resonance imaging stains." Brain Connect **1**(6): 423-446.

Alexander, A. L., J. E. Lee, M. Lazar and A. S. Field (2007). "Diffusion tensor imaging of the brain." Neurotherapeutics **4**(3): 316-329.

Andersson, J. L. R., Smith, S, Jenkinson, M. (2012). Non-linear optimisation.

Andersson, J. L. R., Smith, S, Jenkinson, M. (2012). Non-linear registration, aka Spatial normalisation, FMRIB Technical Report TR07JA2. 2007b. http://www.fmrib.ox.ac.uk/analysis/techrep Accessed 3 September 2012.

Antonini, A., R. Benti, R. De Notaris, S. Tesei, A. Zecchinelli, G. Sacilotto, N. Meucci, M. Canesi, C. Mariani, G. Pezzoli and P. Gerundini (2003). "123I-Ioflupane/SPECT binding to striatal dopamine transporter (DAT) uptake in patients with Parkinson's disease, multiple system atrophy, and progressive supranuclear palsy." Neurol Sci **24**(3): 149-150.

Antonini, A., K. L. Leenders, D. Meier, W. H. Oertel, P. Boesiger and M. Anliker (1993). "T2 relaxation time in patients with Parkinson's disease." Neurology **43**(4): 697-700.

Antonini, A., R. M. Moresco, C. Gobbo, R. De Notaris, A. Panzacchi, P. Barone, S. Calzetti, A. Negrotti, G. Pezzoli and F. Fazio (2001). "The status of dopamine nerve terminals in Parkinson's disease and essential tremor: a PET study with the tracer [11-C]FE-CIT." Neurol Sci **22**(1): 47-48.

Ashburner, J. and K. J. Friston (2000). "Voxel-based morphometry--the methods." Neuroimage **11**(6 Pt 1): 805-821.

Bach, M., F. B. Laun, A. Leemans, C. M. Tax, G. J. Biessels, B. Stieltjes and K. H. Maier-Hein (2014). "Methodological considerations on tract-based spatial statistics (TBSS)." Neuroimage **100**: 358-369.

Bak, T. H., T. T. Rogers, L. M. Crawford, V. C. Hearn, P. S. Mathuranath and J. R. Hodges (2005). "Cognitive bedside assessment in atypical parkinsonian syndromes." J Neurol Neurosurg Psychiatry **76**(3): 420-422.

Barbosa, J. H., A. C. Santos, V. Tumas, M. Liu, W. Zheng, E. M. Haacke and C. E. Salmon (2015). "Quantifying brain iron deposition in patients with Parkinson's disease using quantitative susceptibility mapping, R2 and R2." Magn Reson Imaging **33**(5): 559-565.

Barone, P., A. Antonini, C. Colosimo, R. Marconi, L. Morgante, T. P. Avarello, E. Bottacchi, A. Cannas, G. Ceravolo, R. Ceravolo, G. Cicarelli, R. M. Gaglio, R. M. Giglia, F. Iemolo, M. Manfredi, G. Meco, A. Nicoletti, M. Pederzoli, A. Petrone, A. Pisani, F. E. Pontieri, R. Quatrale, S. Ramat, R. Scala, G. Volpe, S. Zappulla, A. R. Bentivoglio, F. Stocchi, G. Trianni, P. D. Dotto and P. s. group (2009). "The PRIAMO study: A multicenter assessment of nonmotor symptoms and their impact on quality of life in Parkinson's disease." Mov Disord **24**(11): 1641-1649.

Basser, P. J., J. Mattiello and D. LeBihan (1994). "Estimation of the effective self-diffusion tensor from the NMR spin echo." J Magn Reson B **103**(3): 247-254.

Basser, P. J., J. Mattiello and D. LeBihan (1994). "MR diffusion tensor spectroscopy and imaging." Biophys J **66**(1): 259-267.

Bastin, M. E., J. D. Clayden, A. Pattie, I. F. Gerrish, J. M. Wardlaw and I. J. Deary (2009). "Diffusion tensor and magnetization transfer MRI measurements of periventricular white matter hyperintensities in old age." Neurobiol Aging **30**(1): 125-136.

Baudrexel, S., C. Seifried, B. Penndorf, J. C. Klein, M. Middendorp, H. Steinmetz, F. Grunwald and R. Hilker (2014). "The value of putaminal diffusion imaging versus 18-fluorodeoxyglucose positron emission tomography for the differential diagnosis of the Parkinson variant of multiple system atrophy." Mov Disord **29**(3): 380-387.

Benamer, H. T., J. Patterson, D. J. Wyper, D. M. Hadley, G. J. Macphee and D. G. Grosset (2000). "Correlation of Parkinson's disease severity and duration with 123I-FP-CIT SPECT striatal uptake." Mov Disord **15**(4): 692-698.

Bensimon, G., A. Ludolph, Y. Agid, M. Vidailhet, C. Payan, P. N. Leigh and N. S. Group (2009). "Riluzole treatment, survival and diagnostic criteria in Parkinson plus disorders: the NNIPPS study." Brain **132**(Pt 1): 156-171.

Bhidayasiri, R., C. Chotipanich, J. Joutsa, S. Tepmongkol, N. Wannachai, J. Johansson, W. Juiklom and J. O. Rinne (2012). "Boxing and Parkinson disease: a link or a myth? An 18F-FDOPA PET/CT study in retired Thai traditional boxers." Parkinsonism Relat Disord **18**(5): 694-696.

Biundo, R., P. Formento-Dojot, S. Facchini, A. Vallelunga, L. Ghezzo, L. Foscolo, F. Meneghello and A. Antonini (2011). "Brain volume changes in Parkinson's disease and their relationship with cognitive and behavioural abnormalities." J Neurol Sci **310**(1-2): 64-69.

Biundo, R., L. Weis, S. Bostantjopoulou, E. Stefanova, C. Falup-Pecurariu, M. G. Kramberger, G. J. Geurtsen, A. Antonini, D. Weintraub and D. Aarsland (2016). "MMSE and MoCA in Parkinson's disease and dementia with Lewy bodies: a multicenter 1-year follow-up study." J Neural Transm (Vienna) **123**(4): 431-438.

Blockx, I., G. De Groof, M. Verhoye, J. Van Audekerke, K. Raber, D. Poot, J. Sijbers, A. P. Osmand, S. Von Horsten and A. Van der Linden (2012). "Microstructural changes observed with DKI in a transgenic Huntington rat model: evidence for abnormal neurodevelopment." Neuroimage **59**(2): 957-967.

Bohnen, N. I. and R. L. Albin (2011). "White matter lesions in Parkinson disease." Nat Rev Neurol **7**(4): 229-236.

Bohnen, N. I., D. I. Kaufer, R. Hendrickson, L. S. Ivanco, B. J. Lopresti, G. M. Constantine, A. Mathis Ch, J. G. Davis, R. Y. Moore and S. T. Dekosky (2006). "Cognitive correlates of cortical cholinergic denervation in Parkinson's disease and parkinsonian dementia." J Neurol **253**(2): 242-247.

Booij, J., G. Tissingh, G. J. Boer, J. D. Speelman, J. C. Stoof, A. G. Janssen, E. C. Wolters and E. A. van Royen (1997). "[123I]FP-CIT SPECT shows a pronounced decline of striatal dopamine transporter labelling in early and advanced Parkinson's disease." J Neurol Neurosurg Psychiatry **62**(2): 133-140.

Booth, T. C., M. Nathan, A. D. Waldman, A. M. Quigley, A. H. Schapira and J. Buscombe (2015). "The role of functional dopamine-transporter SPECT imaging in parkinsonian syndromes, part 2." AJNR Am J Neuroradiol **36**(2): 236-244.

Boska, M. D., K. M. Hasan, D. Kibuule, R. Banerjee, E. McIntyre, J. A. Nelson, T. Hahn, H. E. Gendelman and R. L. Mosley (2007). "Quantitative diffusion tensor imaging detects dopaminergic neuronal degeneration in a murine model of Parkinson's disease." Neurobiol Dis **26**(3): 590-596.

Bower, J. H., D. M. Maraganore, S. K. McDonnell and W. A. Rocca (1997). "Incidence of progressive supranuclear palsy and multiple system atrophy in Olmsted County, Minnesota, 1976 to 1990." Neurology **49**(5): 1284-1288.

Boxer, A. L., M. D. Geschwind, N. Belfor, M. L. Gorno-Tempini, G. F. Schauer, B. L. Miller, M. W. Weiner and H. J. Rosen (2006). "Patterns of brain atrophy that differentiate corticobasal degeneration syndrome from progressive supranuclear palsy." Arch Neurol **63**(1): 81-86.

Braak, H., K. Del Tredici, U. Rub, R. A. de Vos, E. N. Jansen Steur and E. Braak (2003). "Staging of brain pathology related to sporadic Parkinson's disease." Neurobiol Aging **24**(2): 197-211.

Brenneis, C., S. M. Boesch, K. E. Egger, K. Seppi, C. Scherfler, M. Schocke, G. K. Wenning and W. Poewe (2006). "Cortical atrophy in the cerebellar variant of multiple system atrophy: a voxel-based morphometry study." Mov Disord **21**(2): 159-165.

Brigo, F., A. Matinella, R. Erro and M. Tinazzi (2014). "[(1)(2)(3)I]FP-CIT SPECT (DaTSCAN) may be a useful tool to differentiate between Parkinson's disease and vascular or drug-induced parkinsonisms: a meta-analysis." Eur J Neurol **21**(11): 1369-e1390.

Brooks, D. J. (2010). "Imaging approaches to Parkinson disease." J Nucl Med **51**(4): 596-609.

Brooks, D. J., K. Seppi and M. S. A. Neuroimaging Working Group on (2009). "Proposed neuroimaging criteria for the diagnosis of multiple system atrophy." Mov Disord **24**(7): 949-964.

Brown, R. (1828). "A brief account of microscopic observations made on the particles contained in the pollen of plants." London and Edinburgh philosophical magazine and journal of science **4**: 161-173.

Brown, R. G., L. Lacomblez, B. G. Landwehrmeyer, T. Bak, I. Uttner, B. Dubois, Y. Agid, A. Ludolph, G. Bensimon, C. Payan, N. P. Leigh and N. S. Group (2010). "Cognitive impairment in patients with multiple system atrophy and progressive supranuclear palsy." Brain **133**(Pt 8): 2382-2393.

Buckner, R. L., D. Head, J. Parker, A. F. Fotenos, D. Marcus, J. C. Morris and A. Z. Snyder (2004). "A unified approach for morphometric and functional data analysis in young, old, and demented adults using automated atlas-based head size normalization: reliability and validation against manual measurement of total intracranial volume." Neuroimage **23**(2): 724-738.

Burke, R. E. and K. O'Malley (2013). "Axon degeneration in Parkinson's disease." Exp Neurol **246**: 72-83.

Calabresi, P., A. Castrioto, M. Di Filippo and B. Picconi (2013). "New experimental and clinical links between the hippocampus and the dopaminergic system in Parkinson's disease." Lancet Neurol **12**(8): 811-821.

Cella, D. and K. Webster (1997). "Linking outcomes management to quality-of-life measurement." Oncology (Williston Park) **11**(11A): 232-235.

Chan, L. L., K. M. Ng, C. S. Yeoh, H. Rumpel, H. H. Li and E. K. Tan (2016). "Putaminal Diffusivity Correlates With Disease Progression in Parkinson's Disease: Prospective 6-Year Study." Medicine (Baltimore) **95**(6): e2594.

Chang, C. C., Y. Y. Chang, W. N. Chang, Y. C. Lee, Y. L. Wang, C. C. Lui, C. W. Huang and W. L. Liu (2009). "Cognitive deficits in multiple system atrophy correlate with frontal atrophy and disease duration." Eur J Neurol **16**(10): 1144-1150.

Cheung, M. M., E. S. Hui, K. C. Chan, J. A. Helpern, L. Qi and E. X. Wu (2009). "Does diffusion kurtosis imaging lead to better neural tissue characterization? A rodent brain maturation study." Neuroimage **45**(2): 386-392.

Cholerton, B. A., C. P. Zabetian, J. F. Quinn, K. A. Chung, A. Peterson, A. J. Espay, F. J. Revilla, J. Devoto, G. S. Watson, S. C. Hu, K. L. Edwards, T. J. Montine and J. B. Leverenz (2013). "Pacific Northwest Udall Center of excellence clinical consortium: study design and baseline cohort characteristics." J Parkinsons Dis **3**(2): 205-214.

Cochrane, C. J. and K. P. Ebmeier (2013). "Diffusion tensor imaging in parkinsonian syndromes: a systematic review and meta-analysis." Neurology **80**(9): 857-864.

Conditions, N. C. C. f. C. (2006). Parkinson's Disease: National Clinical Guideline for Diagnosis and Management in Primary and Secondary Care. London, Royal College of Physicians (UK).

Constantinescu, R., L. Rosengren, B. Johnels, H. Zetterberg and B. Holmberg (2010). "Consecutive analyses of cerebrospinal fluid axonal and glial markers in Parkinson's disease and atypical Parkinsonian disorders." Parkinsonism Relat Disord **16**(2): 142-145.

Cosottini, M., R. Ceravolo, L. Faggioni, G. Lazzarotti, M. C. Michelassi, U. Bonuccelli, L. Murri and C. Bartolozzi (2007). "Assessment of midbrain atrophy in patients with progressive supranuclear palsy with routine magnetic resonance imaging." Acta Neurol Scand **116**(1): 37-42.

Cummings, J. L., M. Mega, K. Gray, S. Rosenberg-Thompson, D. A. Carusi and J. Gornbein (1994). "The Neuropsychiatric Inventory: comprehensive assessment of psychopathology in dementia." Neurology **44**(12): 2308-2314.

Deary, I. J., S. A. Leaper, A. D. Murray, R. T. Staff and L. J. Whalley (2003). "Cerebral white matter abnormalities and lifetime cognitive change: a 67-year follow-up of the Scottish Mental Survey of 1932." Psychol Aging **18**(1): 140-148.

Du, G., M. M. Lewis, M. Styner, M. L. Shaffer, S. Sen, Q. X. Yang and X. Huang (2011). "Combined R2* and diffusion tensor imaging changes in the substantia nigra in Parkinson's disease." Mov Disord **26**(9): 1627-1632.

Dubois, B., A. Slachevsky, I. Litvan and B. Pillon (2000). "The FAB: a Frontal Assessment Battery at bedside." Neurology **55**(11): 1621-1626.

Duty, S. (2012). "Targeting glutamate receptors to tackle the pathogenesis, clinical symptoms and levodopa-induced dyskinesia associated with Parkinson's disease." CNS Drugs **26**(12): 1017-1032.

Eckert, T., C. Tang, Y. Ma, N. Brown, T. Lin, S. Frucht, A. Feigin and D. Eidelberg (2008). "Abnormal metabolic networks in atypical parkinsonism." Mov Disord **23**(5): 727-733.

Einstein, A. (1905). "Über die von der molekularkinetischen Theorie der Wärme geforderte Bewegung von in ruhenden Flüssigkeiten suspendierten Teilchen." Annalen der Physik **322**: 549-560.

Fahn, S., Elton RL, Members of the UPDRS development committee (1987). Unified Parkinson's Disease Rating Scale. Recent developments in Parkinson's Disease, vol 2. S. Fahn, Marsden CD, Goldstein M, Calne DB. Florham Park, NJ, Macmillan Healthcare Information**:** 153-163.

Farquharson, S., J. D. Tournier, F. Calamante, G. Fabinyi, M. Schneider-Kolsky, G. D. Jackson and A. Connelly (2013). "White matter fiber tractography: why we need to move beyond DTI." J Neurosurg **118**(6): 1367-1377.

Fazekas, F., J. B. Chawluk, A. Alavi, H. I. Hurtig and R. A. Zimmerman (1987). "MR signal abnormalities at 1.5 T in Alzheimer's dementia and normal aging." AJR Am J Roentgenol **149**(2): 351-356.

Feng, J. Y., B. Huang, W. Q. Yang, Y. H. Zhang, L. M. Wang, L. J. Wang and X. L. Zhong (2015). "The putaminal abnormalities on 3.0T magnetic resonance imaging:

can they separate parkinsonism-predominant multiple system atrophy from Parkinson's disease?" Acta Radiol **56**(3): 322-328.

Fernandez-Seara, M. A., E. Mengual, M. Vidorreta, G. Castellanos, J. Irigoyen, E. Erro and M. A. Pastor (2015). "Resting state functional connectivity of the subthalamic nucleus in Parkinson's disease assessed using arterial spin-labeled perfusion fMRI." Hum Brain Mapp **36**(5): 1937-1950.

Figueroa, J. J., W. Singer, A. Parsaik, E. E. Benarroch, J. E. Ahlskog, R. D. Fealey, J. E. Parisi, P. Sandroni, J. Mandrekar, V. Iodice, P. A. Low and J. H. Bower (2014). "Multiple system atrophy: prognostic indicators of survival." Mov Disord **29**(9): 1151-1157.

Focke, N. K., G. Helms, S. Scheewe, P. M. Pantel, C. G. Bachmann, P. Dechent, J. Ebentheuer, A. Mohr, W. Paulus and C. Trenkwalder (2011). "Individual voxel-based subtype prediction can differentiate progressive supranuclear palsy from idiopathic Parkinson syndrome and healthy controls." Hum Brain Mapp **32**(11): 1905-1915.

Folstein, M. F., S. E. Folstein and P. R. McHugh (1975). ""Mini-mental state". A practical method for grading the cognitive state of patients for the clinician." J Psychiatr Res **12**(3): 189-198.

Fregly, A. R. (1974). Vestibular ataxia and its measurement in man. Handbook of Sensory Physiology. K. HH. Berlin, Springer**:** 321-360.

Gandek, B., J. E. Ware, N. K. Aaronson, G. Apolone, J. B. Bjorner, J. E. Brazier, M. Bullinger, S. Kaasa, A. Leplege, L. Prieto and M. Sullivan (1998). "Cross-validation of item selection and scoring for the SF-12 Health Survey in nine countries: results from the IQOLA Project. International Quality of Life Assessment." J Clin Epidemiol **51**(11): 1171-1178.

Gao, Y., Y. Zhang, C. S. Wong, P. M. Wu, Z. Zhang, J. Gao, D. Qiu and B. Huang (2012). "Diffusion abnormalities in temporal lobes of children with temporal lobe epilepsy: a preliminary diffusional kurtosis imaging study and comparison with diffusion tensor imaging." NMR Biomed **25**(12): 1369-1377.

Gelb, D. J., E. Oliver and S. Gilman (1999). "Diagnostic criteria for Parkinson disease." Arch Neurol **56**(1): 33-39.

Ghaemi, M., R. Hilker, J. Rudolf, J. Sobesky and W. D. Heiss (2002). "Differentiating multiple system atrophy from Parkinson's disease: contribution of striatal and midbrain MRI volumetry and multi-tracer PET imaging." J Neurol Neurosurg Psychiatry **73**(5): 517-523.

Gibb, W. R. and A. J. Lees (1988). "The relevance of the Lewy body to the pathogenesis of idiopathic Parkinson's disease." J Neurol Neurosurg Psychiatry **51**(6): 745-752.

Gilman, S., P. A. Low, N. Quinn, A. Albanese, Y. Ben-Shlomo, C. J. Fowler, H. Kaufmann, T. Klockgether, A. E. Lang, P. L. Lantos, I. Litvan, C. J. Mathias, E. Oliver, D. Robertson, I. Schatz and G. K. Wenning (1999). "Consensus statement on the diagnosis of multiple system atrophy." J Neurol Sci **163**(1): 94-98.

Gilman, S., G. K. Wenning, P. A. Low, D. J. Brooks, C. J. Mathias, J. Q. Trojanowski, N. W. Wood, C. Colosimo, A. Durr, C. J. Fowler, H. Kaufmann, T. Klockgether, A. Lees, W. Poewe, N. Quinn, T. Revesz, D. Robertson, P. Sandroni, K. Seppi and M.

Vidailhet (2008). "Second consensus statement on the diagnosis of multiple system atrophy." Neurology **71**(9): 670-676.

Golbe, L. I., P. H. Davis, B. S. Schoenberg and R. C. Duvoisin (1988). "Prevalence and natural history of progressive supranuclear palsy." Neurology **38**(7): 1031-1034.

Golbe, L. I. and P. A. Ohman-Strickland (2007). "A clinical rating scale for progressive supranuclear palsy." Brain **130**(Pt 6): 1552-1565.

Goldman, J. G., S. Holden, B. Bernard, B. Ouyang, C. G. Goetz and G. T. Stebbins (2013). "Defining optimal cutoff scores for cognitive impairment using Movement Disorder Society Task Force criteria for mild cognitive impairment in Parkinson's disease." Mov Disord **28**(14): 1972-1979.

Goldman, J. G., S. Holden, B. Ouyang, B. Bernard, C. G. Goetz and G. T. Stebbins (2015). "Diagnosing PD-MCI by MDS Task Force criteria: how many and which neuropsychological tests?" Mov Disord **30**(3): 402-406.

Graham, J. M., M. N. Paley, R. A. Grunewald, N. Hoggard and P. D. Griffiths (2000). "Brain iron deposition in Parkinson's disease imaged using the PRIME magnetic resonance sequence." Brain **123 Pt 12**: 2423-2431.

Greffard, S., M. Verny, A. M. Bonnet, J. Y. Beinis, C. Gallinari, S. Meaume, F. Piette, J. J. Hauw and C. Duyckaerts (2006). "Motor score of the Unified Parkinson Disease Rating Scale as a good predictor of Lewy body-associated neuronal loss in the substantia nigra." Arch Neurol **63**(4): 584-588.

Groger, A., B. Bender, I. Wurster, G. L. Chadzynski, U. Klose and D. Berg (2013). "Differentiation between idiopathic and atypical parkinsonian syndromes using three-dimensional magnetic resonance spectroscopic imaging." J Neurol Neurosurg Psychiatry **84**(6): 644-649.

Grossman, E. J., Y. Ge, J. H. Jensen, J. S. Babb, L. Miles, J. Reaume, J. M. Silver, R. I. Grossman and M. Inglese (2012). "Thalamus and cognitive impairment in mild traumatic brain injury: a diffusional kurtosis imaging study." J Neurotrauma **29**(13): 2318-2327.

Haacke, E. M., N. Y. Cheng, M. J. House, Q. Liu, J. Neelavalli, R. J. Ogg, A. Khan, M. Ayaz, W. Kirsch and A. Obenaus (2005). "Imaging iron stores in the brain using magnetic resonance imaging." Magn Reson Imaging **23**(1): 1-25.

Haacke, E. M., Y. Xu, Y. C. Cheng and J. R. Reichenbach (2004). "Susceptibility weighted imaging (SWI)." Magn Reson Med **52**(3): 612-618.

Hagell, P. (2000). "Timed tests in the clinical assessment of motor function in Parkinson's disease." J Neurosci Nurs **32**(6): 331-336.

Hall, S., A. Ohrfelt, R. Constantinescu, U. Andreasson, Y. Surova, F. Bostrom, C. Nilsson, W. Hakan, H. Decraemer, K. Nagga, L. Minthon, E. Londos, E. Vanmechelen, B. Holmberg, H. Zetterberg, K. Blennow and O. Hansson (2012). "Accuracy of a panel of 5 cerebrospinal fluid biomarkers in the differential diagnosis of patients with dementia and/or parkinsonian disorders." Arch Neurol **69**(11): 1445-1452.

Hall, S., Y. Surova, A. Ohrfelt, H. Zetterberg, D. Lindqvist and O. Hansson (2015). "CSF biomarkers and clinical progression of Parkinson disease." Neurology **84**(1): 57-63.

Ham, J. H., J. Cha, J. J. Lee, G. M. Baek, M. K. Sunwoo, J. Y. Hong, N. Y. Shin, Y. H. Sohn, J. M. Lee and P. H. Lee (2015). "Nigrostriatal dopamine-independent resting-state functional networks in Parkinson's disease." Neuroimage **119**: 296-304.

Hansson, O., S. Janelidze, S. Hall, N. Magdalinou, A. J. Lees, U. Andreasson, N. Norgren, J. Linder, L. Forsgren, R. Constantinescu, H. Zetterberg, K. Blennow and F. s. Swedish Bio (2017). "Blood-based NfL: A biomarker for differential diagnosis of parkinsonian disorder." Neurology **88**(10): 930-937.

Harper, L., Newman, E., Hadley, D., Grosset, D (2011). "Validation of reduced fractional anisotropy measures in the substantia nigra of Parkinson patients using DAT imaging." Proceedings of the ISMRM: 19:11.

Hauser, T. K., A. Luft, M. Skalej, T. Nagele, T. T. Kircher, D. T. Leube and J. B. Schulz (2006). "Visualization and quantification of disease progression in multiple system atrophy." Mov Disord **21**(10): 1674-1681.

Hely, M. A., W. G. Reid, M. A. Adena, G. M. Halliday and J. G. Morris (2008). "The Sydney multicenter study of Parkinson's disease: the inevitability of dementia at 20 years." Mov Disord **23**(6): 837-844.

Herbert, M. K., M. B. Aerts, M. Beenes, N. Norgren, R. A. Esselink, B. R. Bloem, H. B. Kuiperij and M. M. Verbeek (2015). "CSF Neurofilament Light Chain but not FLT3 Ligand Discriminates Parkinsonian Disorders." Front Neurol **6**: 91.

Hilker, R., A. V. Thomas, J. C. Klein, S. Weisenbach, E. Kalbe, L. Burghaus, A. H. Jacobs, K. Herholz and W. D. Heiss (2005). "Dementia in Parkinson disease: functional imaging of cholinergic and dopaminergic pathways." Neurology **65**(11): 1716-1722.

Hoehn, M. M., Yahr MD (1967). "Parkinsonism: onset, progression and mortality." Neurology **17**: 427-442.

Hoglinger, G. U., N. M. Melhem, D. W. Dickson, P. M. Sleiman, L. S. Wang, L. Klei, R. Rademakers, R. de Silva, I. Litvan, D. E. Riley, J. C. van Swieten, P. Heutink, Z. K. Wszolek, R. J. Uitti, J. Vandrovcova, H. I. Hurtig, R. G. Gross, W. Maetzler, S. Goldwurm, E. Tolosa, B. Borroni, P. Pastor, P. S. P. G. S. Group, L. B. Cantwell, M. R. Han, A. Dillman, M. P. van der Brug, J. R. Gibbs, M. R. Cookson, D. G. Hernandez, A. B. Singleton, M. J. Farrer, C. E. Yu, L. I. Golbe, T. Revesz, J. Hardy, A. J. Lees, B. Devlin, H. Hakonarson, U. Muller and G. D. Schellenberg (2011). "Identification of common variants influencing risk of the tauopathy progressive supranuclear palsy." Nat Genet **43**(7): 699-705.

Hoglinger, G. U., G. Respondek, M. Stamelou, C. Kurz, K. A. Josephs, A. E. Lang, B. Mollenhauer, U. Muller, C. Nilsson, J. L. Whitwell, T. Arzberger, E. Englund, E. Gelpi, A. Giese, D. J. Irwin, W. G. Meissner, A. Pantelyat, A. Rajput, J. C. van Swieten, C. Troakes, A. Antonini, K. P. Bhatia, Y. Bordelon, Y. Compta, J. C. Corvol, C. Colosimo, D. W. Dickson, R. Dodel, L. Ferguson, M. Grossman, J. Kassubek, F. Krismer, J. Levin, S. Lorenzl, H. R. Morris, P. Nestor, W. H. Oertel, W. Poewe, G. Rabinovici, J. B. Rowe, G. D. Schellenberg, K. Seppi, T. van Eimeren, G. K. Wenning, A. L. Boxer, L. I. Golbe, I. Litvan and P. S. P. S. G. Movement Disorder Society-endorsed (2017). "Clinical diagnosis of progressive supranuclear palsy: The movement disorder society criteria." Mov Disord **32**(6): 853-864.

Holland, A., R. J. O'Connor, A. J. Thompson, E. D. Playford and J. C. Hobart (2006). "Talking the talk on walking the walk: a 12-item generic walking scale suitable for neurological conditions?" J Neurol **253**(12): 1594-1602.

Holtbernd, F. and D. Eidelberg (2014). "The utility of neuroimaging in the differential diagnosis of parkinsonian syndromes." Semin Neurol **34**(2): 202-209.

Hsiao, I. T., Y. H. Weng, C. J. Hsieh, W. Y. Lin, S. P. Wey, M. P. Kung, T. C. Yen, C. S. Lu and K. J. Lin (2014). "Correlation of Parkinson disease severity and 18F-DTBZ positron emission tomography." JAMA Neurol **71**(6): 758-766.

Hsiao, I. T., Y. H. Weng, W. Y. Lin, C. J. Hsieh, S. P. Wey, T. C. Yen, M. P. Kung, C. S. Lu and K. J. Lin (2014). "Comparison of 99mTc-TRODAT-1 SPECT and 18 F-AV-133 PET imaging in healthy controls and Parkinson's disease patients." Nucl Med Biol **41**(4): 322-329.

Iodice, V., A. Lipp, J. E. Ahlskog, P. Sandroni, R. D. Fealey, J. E. Parisi, J. Y. Matsumoto, E. E. Benarroch, K. Kimpinski, W. Singer, T. L. Gehrking, J. A. Gehrking, D. M. Sletten, A. M. Schmeichel, J. H. Bower, S. Gilman, J. Figueroa and P. A. Low (2012). "Autopsy confirmed multiple system atrophy cases: Mayo experience and role of autonomic function tests." J Neurol Neurosurg Psychiatry **83**(4): 453-459.

Isella, V., C. Mapelli, C. Siri, D. De Gaspari, G. Pezzoli, A. Antonini, M. Poletti, U. Bonuccelli, M. Vista and I. M. Appollonio (2014). "Validation and attempts of revision of the MDS-recommended tests for the screening of Parkinson's disease dementia." Parkinsonism Relat Disord **20**(1): 32-36.

Ito, S., T. Makino, W. Shirai and T. Hattori (2008). "Diffusion tensor analysis of corpus callosum in progressive supranuclear palsy." Neuroradiology **50**(11): 981-985.

Jankovic, J., M. McDermott, J. Carter, S. Gauthier, C. Goetz, L. Golbe, S. Huber, W. Koller, C. Olanow, I. Shoulson and et al. (1990). "Variable expression of Parkinson's disease: a base-line analysis of the DATATOP cohort. The Parkinson Study Group." Neurology **40**(10): 1529-1534.

Jellinger, K. A. and G. K. Wenning (2016). "Multiple system atrophy: pathogenic mechanisms and biomarkers." J Neural Transm (Vienna) **123**(6): 555-572.

Jensen, J. H., J. A. Helpern, A. Ramani, H. Lu and K. Kaczynski (2005). "Diffusional kurtosis imaging: the quantification of non-gaussian water diffusion by means of magnetic resonance imaging." Magn Reson Med **53**(6): 1432-1440.

Jesse, S., J. Kassubek, H. P. Muller, A. C. Ludolph and A. Unrath (2012). "Signal alterations of the basal ganglia in the differential diagnosis of Parkinson's disease: a retrospective case-controlled MRI data bank analysis." BMC Neurol **12**: 163.

Jin, L., J. Wang, H. Jin, G. Fei, Y. Zhang, W. Chen, L. Zhao, N. Zhao, X. Sun, M. Zeng and C. Zhong (2012). "Nigral iron deposition occurs across motor phenotypes of Parkinson's disease." Eur J Neurol **19**(7): 969-976.

Jones, D. K. (2008). "Studying connections in the living human brain with diffusion MRI." Cortex **44**(8): 936-952.

Josephs, K. A., J. L. Whitwell, D. W. Dickson, B. F. Boeve, D. S. Knopman, R. C. Petersen, J. E. Parisi and C. R. Jack, Jr. (2008). "Voxel-based morphometry in autopsy proven PSP and CBD." Neurobiol Aging **29**(2): 280-289.

Kahan, J., M. Urner, R. Moran, G. Flandin, A. Marreiros, L. Mancini, M. White, J. Thornton, T. Yousry, L. Zrinzo, M. Hariz, P. Limousin, K. Friston and T. Foltynie (2014). "Resting state functional MRI in Parkinson's disease: the impact of deep brain stimulation on 'effective' connectivity." Brain **137**(Pt 4): 1130-1144.

Kalra, S., D. G. Grosset and H. T. Benamer (2010). "Differentiating vascular parkinsonism from idiopathic Parkinson's disease: a systematic review." Mov Disord **25**(2): 149-156.

Kamagata, K., T. Hatano, A. Okuzumi, Y. Motoi, O. Abe, K. Shimoji, K. Kamiya, M. Suzuki, M. Hori, K. K. Kumamaru, N. Hattori and S. Aoki (2015). "Neurite orientation dispersion and density imaging in the substantia nigra in idiopathic Parkinson disease." Eur Radiol.

Kamagata, K., H. Tomiyama, T. Hatano, Y. Motoi, O. Abe, K. Shimoji, K. Kamiya, M. Suzuki, M. Hori, M. Yoshida, N. Hattori and S. Aoki (2014). "A preliminary diffusional kurtosis imaging study of Parkinson disease: comparison with conventional diffusion tensor imaging." Neuroradiology **56**(3): 251-258.

Kashihara, K., T. Shinya and F. Higaki (2011). "Reduction of neuromelanin-positive nigral volume in patients with MSA, PSP and CBD." Intern Med **50**(16): 1683-1687.

Kato, N., K. Arai and T. Hattori (2003). "Study of the rostral midbrain atrophy in progressive supranuclear palsy." J Neurol Sci **210**(1-2): 57-60.

Kertesz, A., W. Davidson and H. Fox (1997). "Frontal behavioral inventory: diagnostic criteria for frontal lobe dementia." Can J Neurol Sci **24**(1): 29-36.

Kim, H. J., B. S. Jeon, Y. E. Kim, J. Y. Kim, Y. K. Kim, C. H. Sohn, J. Y. Yun, S. Jeon, J. M. Lee and J. Y. Lee (2013). "Clinical and imaging characteristics of dementia in multiple system atrophy." Parkinsonism Relat Disord **19**(6): 617-621.

Kitayama, M., K. Wada-Isoe, Y. Irizawa and K. Nakashima (2009). "Assessment of dementia in patients with multiple system atrophy." Eur J Neurol **16**(5): 589-594.

Klein, R. C., B. M. de Jong, J. J. de Vries and K. L. Leenders (2005). "Direct comparison between regional cerebral metabolism in progressive supranuclear palsy and Parkinson's disease." Mov Disord **20**(8): 1021-1030.

Klein, S., M. Staring, K. Murphy, M. A. Viergever and J. P. Pluim (2010). "elastix: a toolbox for intensity-based medical image registration." IEEE Trans Med Imaging **29**(1): 196-205.

Koo, T. K. and M. Y. Li (2016). "A Guideline of Selecting and Reporting Intraclass Correlation Coefficients for Reliability Research." J Chiropr Med **15**(2): 155-163.

Kosta, P., M. I. Argyropoulou, S. Markoula and S. Konitsiotis (2006). "MRI evaluation of the basal ganglia size and iron content in patients with Parkinson's disease." J Neurol **253**(1): 26-32.

Kuzdas-Wood, D., N. Stefanova, K. A. Jellinger, K. Seppi, M. G. Schlossmacher, W. Poewe and G. K. Wenning (2014). "Towards translational therapies for multiple system atrophy." Prog Neurobiol **118**: 19-35.

Lampinen, B., F. Szczepankiewicz, J. Martensson, D. van Westen, P. C. Sundgren and M. Nilsson (2017). "Neurite density imaging versus imaging of microscopic anisotropy in diffusion MRI: A model comparison using spherical tensor encoding." Neuroimage **147**: 517-531.

Lampinen, B., van Westen D, Ståhlberg F, Lätt J, Hansson O, Nilsson M (2015). "Neurite Density Imaging (NDI): rapid acquisition and estimation of the intracellular volume fraction." Proceedings of the ISMRM: 2772.

Langkammer, C., F. Schweser, N. Krebs, A. Deistung, W. Goessler, E. Scheurer, K. Sommer, G. Reishofer, K. Yen, F. Fazekas, S. Ropele and J. R. Reichenbach (2012). "Quantitative susceptibility mapping (QSM) as a means to measure brain iron? A post mortem validation study." Neuroimage **62**(3): 1593-1599.

Latt, J., M. Nilsson, R. Wirestam, F. Stahlberg, N. Karlsson, M. Johansson, P. C. Sundgren and D. van Westen (2013). "Regional values of diffusional kurtosis estimates in the healthy brain." J Magn Reson Imaging **37**(3): 610-618.

Le Bihan, D. (2003). "Looking into the functional architecture of the brain with diffusion MRI." Nat Rev Neurosci **4**(6): 469-480.

Leemans, A., Jeurissen B, Sijbers J, Jones DK. (2009). "ExploreDTI: a graphical toolbox for processing, analyzing, and visualizing diffusion MR data.

." In: Proceedings of the ISMRM: 3537.

Leemans, A. and D. K. Jones (2009). "The B-matrix must be rotated when correcting for subject motion in DTI data." Magn Reson Med **61**(6): 1336-1349.

Lenfeldt, N., A. Larsson, L. Nyberg, R. Birgander and L. Forsgren (2015). "Fractional anisotropy in the substantia nigra in Parkinson's disease: a complex picture." Eur J Neurol **22**(10): 1408-1414.

Li, W., A. V. Avram, B. Wu, X. Xiao and C. Liu (2014). "Integrated Laplacian-based phase unwrapping and background phase removal for quantitative susceptibility mapping." NMR Biomed **27**(2): 219-227.

Li, W., N. Wang, F. Yu, H. Han, W. Cao, R. Romero, B. Tantiwongkosi, T. Q. Duong and C. Liu (2015). "A method for estimating and removing streaking artifacts in quantitative susceptibility mapping." Neuroimage **108**: 111-122.

Li, W., B. Wu and C. Liu (2011). "Quantitative susceptibility mapping of human brain reflects spatial variation in tissue composition." Neuroimage **55**(4): 1645-1656.

Lin, C. H. and R. M. Wu (2015). "Biomarkers of cognitive decline in Parkinson's disease." Parkinsonism Relat Disord **21**(5): 431-443.

Litvan, I., Y. Agid, D. Calne, G. Campbell, B. Dubois, R. C. Duvoisin, C. G. Goetz, L. I. Golbe, J. Grafman, J. H. Growdon, M. Hallett, J. Jankovic, N. P. Quinn, E. Tolosa and D. S. Zee (1996). "Clinical research criteria for the diagnosis of progressive supranuclear palsy (Steele-Richardson-Olszewski syndrome): report of the NINDS-SPSP international workshop." Neurology **47**(1): 1-9.

Litvan, I., Y. Agid, J. Jankovic, C. Goetz, J. P. Brandel, E. C. Lai, G. Wenning, L. D'Olhaberriague, M. Verny, K. R. Chaudhuri, A. McKee, K. Jellinger, J. J. Bartko, C. A. Mangone and R. K. Pearce (1996). "Accuracy of clinical criteria for the diagnosis of progressive supranuclear palsy (Steele-Richardson-Olszewski syndrome)." Neurology **46**(4): 922-930.

Litvan, I., J. J. Hauw, J. J. Bartko, P. L. Lantos, S. E. Daniel, D. S. Horoupian, A. McKee, D. Dickson, C. Bancher, M. Tabaton, K. Jellinger and D. W. Anderson (1996). "Validity and reliability of the preliminary NINDS neuropathologic criteria for

progressive supranuclear palsy and related disorders." J Neuropathol Exp Neurol **55**(1): 97-105.

Liu, T., S. Eskreis-Winkler, A. D. Schweitzer, W. Chen, M. G. Kaplitt, A. J. Tsiouris and Y. Wang (2013). "Improved subthalamic nucleus depiction with quantitative susceptibility mapping." Radiology **269**(1): 216-223.

Loane, C., M. Politis, Z. Kefalopoulou, N. Valle-Guzman, G. Paul, H. Widner, T. Foltynie, R. A. Barker and P. Piccini (2016). "Aberrant nigral diffusion in Parkinson's disease: A longitudinal diffusion tensor imaging study." Mov Disord **31**(7): 1020-1026.

Low, P. A., S. G. Reich, J. Jankovic, C. W. Shults, M. B. Stern, P. Novak, C. M. Tanner, S. Gilman, F. J. Marshall, F. Wooten, B. Racette, T. Chelimsky, W. Singer, D. M. Sletten, P. Sandroni and J. Mandrekar (2015). "Natural history of multiple system atrophy in the USA: a prospective cohort study." Lancet Neurol **14**(7): 710-719.

Madden, D. J., I. J. Bennett, A. Burzynska, G. G. Potter, N. K. Chen and A. W. Song (2012). "Diffusion tensor imaging of cerebral white matter integrity in cognitive aging." Biochim Biophys Acta **1822**(3): 386-400.

Madhyastha, T. M., M. K. Askren, P. Boord, J. Zhang, J. B. Leverenz and T. J. Grabowski (2015). "Cerebral perfusion and cortical thickness indicate cortical involvement in mild Parkinson's disease." Mov Disord **30**(14): 1893-1900.

Magdalinou, N. K., R. W. Paterson, J. M. Schott, N. C. Fox, C. Mummery, K. Blennow, K. Bhatia, H. R. Morris, P. Giunti, T. T. Warner, R. de Silva, A. J. Lees and H. Zetterberg (2015). "A panel of nine cerebrospinal fluid biomarkers may identify patients with atypical parkinsonian syndromes." J Neurol Neurosurg Psychiatry **86**(11): 1240-1247.

Marinus, J., M. Visser, J. J. van Hilten, G. J. Lammers and A. M. Stiggelbout (2003). "Assessment of sleep and sleepiness in Parkinson disease." Sleep **26**(8): 1049-1054.

Martin-Bastida, A., N. P. Lao-Kaim, C. Loane, M. Politis, A. A. Roussakis, N. Valle-Guzman, Z. Kefalopoulou, G. Paul-Visse, H. Widner, Y. Xing, S. T. Schwarz, D. P. Auer, T. Foltynie, R. A. Barker and P. Piccini (2017). "Motor associations of iron accumulation in deep grey matter nuclei in Parkinson's disease: a cross-sectional study of iron-related magnetic resonance imaging susceptibility." Eur J Neurol **24**(2): 357-365.

Martin, W. R., M. Wieler and M. Gee (2008). "Midbrain iron content in early Parkinson disease: a potential biomarker of disease status." Neurology **70**(16 Pt 2): 1411-1417.

Massano, J., F. Costa and G. Nadais (2008). "Teaching neuroImage: MRI in multiple system atrophy: "hot cross bun" sign and hyperintense rim bordering the putamina." Neurology **71**(15): e38.

Massey, L. A., C. Micallef, D. C. Paviour, S. S. O'Sullivan, H. Ling, D. R. Williams, C. Kallis, J. L. Holton, T. Revesz, D. J. Burn, T. Yousry, A. J. Lees, N. C. Fox and H. R. Jager (2012). "Conventional magnetic resonance imaging in confirmed progressive supranuclear palsy and multiple system atrophy." Mov Disord **27**(14): 1754-1762.

Mazziotta, J., A. Toga, A. Evans, P. Fox, J. Lancaster, K. Zilles, R. Woods, T. Paus, G. Simpson, B. Pike, C. Holmes, L. Collins, P. Thompson, D. MacDonald, M. Iacoboni, T. Schormann, K. Amunts, N. Palomero-Gallagher, S. Geyer, L. Parsons, K. Narr, N.

Kabani, G. Le Goualher, D. Boomsma, T. Cannon, R. Kawashima and B. Mazoyer (2001). "A probabilistic atlas and reference system for the human brain: International Consortium for Brain Mapping (ICBM)." Philos Trans R Soc Lond B Biol Sci **356**(1412): 1293-1322.

Messina, D., A. Cerasa, F. Condino, G. Arabia, F. Novellino, G. Nicoletti, M. Salsone, M. Morelli, P. L. Lanza and A. Quattrone (2011). "Patterns of brain atrophy in Parkinson's disease, progressive supranuclear palsy and multiple system atrophy." Parkinsonism Relat Disord **17**(3): 172-176.

Minnerop, M., K. Specht, J. Ruhlmann, N. Schimke, M. Abele, A. Weyer, U. Wullner and T. Klockgether (2007). "Voxel-based morphometry and voxel-based relaxometry in multiple system atrophy-a comparison between clinical subtypes and correlations with clinical parameters." Neuroimage **36**(4): 1086-1095.

Mohs, R. C. and L. Cohen (1988). "Alzheimer's Disease Assessment Scale (ADAS)." Psychopharmacol Bull **24**(4): 627-628.

Moller, L., J. Kassubek, M. Sudmeyer, R. Hilker, E. Hattingen, K. Egger, F. Amtage, E. H. Pinkhardt, G. Respondek, M. Stamelou, F. Moller, A. Schnitzler, W. H. Oertel, S. Knake, H. J. Huppertz and G. U. Hoglinger (2017). "Manual MRI morphometry in Parkinsonian syndromes." Mov Disord **32**(5): 778-782.

Moseley, M. E., Y. Cohen, J. Kucharczyk, J. Mintorovitch, H. S. Asgari, M. F. Wendland, J. Tsuruda and D. Norman (1990). "Diffusion-weighted MR imaging of anisotropic water diffusion in cat central nervous system." Radiology **176**(2): 439-445.

Mulkern, R. V., S. J. Haker and S. E. Maier (2009). "On high b diffusion imaging in the human brain: ruminations and experimental insights." Magn Reson Imaging **27**(8): 1151-1162.

Multiple-System Atrophy Research, C. (2013). "Mutations in COQ2 in familial and sporadic multiple-system atrophy." N Engl J Med **369**(3): 233-244.

Murakami, Y., S. Kakeda, K. Watanabe, I. Ueda, A. Ogasawara, J. Moriya, S. Ide, K. Futatsuya, T. Sato, K. Okada, T. Uozumi, S. Tsuji, T. Liu, Y. Wang and Y. Korogi (2015). "Usefulness of quantitative susceptibility mapping for the diagnosis of Parkinson disease." AJNR Am J Neuroradiol **36**(6): 1102-1108.

Nair, S. R., L. K. Tan, N. Mohd Ramli, S. Y. Lim, K. Rahmat and H. Mohd Nor (2013). "A decision tree for differentiating multiple system atrophy from Parkinson's disease using 3-T MR imaging." Eur Radiol **23**(6): 1459-1466.

Nicoletti, G., R. Lodi, F. Condino, C. Tonon, F. Fera, E. Malucelli, D. Manners, M. Zappia, L. Morgante, P. Barone, B. Barbiroli and A. Quattrone (2006). "Apparent diffusion coefficient measurements of the middle cerebellar peduncle differentiate the Parkinson variant of MSA from Parkinson's disease and progressive supranuclear palsy." Brain **129**(Pt 10): 2679-2687.

Nicoletti, G., G. Rizzo, G. Barbagallo, C. Tonon, F. Condino, D. Manners, D. Messina, C. Testa, G. Arabia, A. Gambardella, R. Lodi and A. Quattrone (2013). "Diffusivity of cerebellar hemispheres enables discrimination of cerebellar or parkinsonian multiple system atrophy from progressive supranuclear palsy-Richardson syndrome and Parkinson disease." Radiology **267**(3): 843-850.

Nicoletti, G., C. Tonon, R. Lodi, F. Condino, D. Manners, E. Malucelli, M. Morelli, F. Novellino, S. Paglionico, P. Lanza, D. Messina, P. Barone, L. Morgante, M. Zappia, B. Barbiroli and A. Quattrone (2008). "Apparent diffusion coefficient of the superior cerebellar peduncle differentiates progressive supranuclear palsy from Parkinson's disease." Mov Disord **23**(16): 2370-2376.

Nielsen, N. P., E. H. Wiig, S. Warkentin and L. Minthon (2004). "Clinical utility of color-form naming in Alzheimer's disease: preliminary evidence." Percept Mot Skills **99**(3 Pt 2): 1201-1204.

Niethammer, M., C. C. Tang, Y. Ma, P. J. Mattis, J. H. Ko, V. Dhawan and D. Eidelberg (2013). "Parkinson's disease cognitive network correlates with caudate dopamine." Neuroimage **78**: 204-209.

Nilsson, M., Szczepankiewicz F, van Westen D, Hansson O (2014). "Motion and eddy-current correction in high b-value diffusion MRI: Systematic registration errors and how to avoid them." Proceedings of the ISMRM: 2569.

Oba, H., A. Yagishita, H. Terada, A. J. Barkovich, K. Kutomi, T. Yamauchi, S. Furui, T. Shimizu, M. Uchigata, K. Matsumura, M. Sonoo, M. Sakai, K. Takada, A. Harasawa, K. Takeshita, H. Kohtake, H. Tanaka and S. Suzuki (2005). "New and reliable MRI diagnosis for progressive supranuclear palsy." Neurology **64**(12): 2050-2055.

Ofori, E., O. Pasternak, P. J. Planetta, H. Li, R. G. Burciu, A. F. Snyder, S. Lai, M. S. Okun and D. E. Vaillancourt (2015). "Longitudinal changes in free-water within the substantia nigra of Parkinson's disease." Brain **138**(Pt 8): 2322-2331.

Ogg, R. J., J. W. Langston, E. M. Haacke, R. G. Steen and J. S. Taylor (1999). "The correlation between phase shifts in gradient-echo MR images and regional brain iron concentration." Magn Reson Imaging **17**(8): 1141-1148.

Osaki, Y., Y. Ben-Shlomo, A. J. Lees, G. K. Wenning and N. P. Quinn (2009). "A validation exercise on the new consensus criteria for multiple system atrophy." Mov Disord **24**(15): 2272-2276.

Patenaude, B., S. M. Smith, D. N. Kennedy and M. Jenkinson (2011). "A Bayesian model of shape and appearance for subcortical brain segmentation." Neuroimage **56**(3): 907-922.

Pavese, N. (2012). "PET studies in Parkinson's disease motor and cognitive dysfunction." Parkinsonism Relat Disord **18 Suppl 1**: S96-99.

Paviour, D. C., S. L. Price, M. Jahanshahi, A. J. Lees and N. C. Fox (2006). "Regional brain volumes distinguish PSP, MSA-P, and PD: MRI-based clinico-radiological correlations." Mov Disord **21**(7): 989-996.

Paviour, D. C., J. S. Thornton, A. J. Lees and H. R. Jager (2007). "Diffusion-weighted magnetic resonance imaging differentiates Parkinsonian variant of multiple-system atrophy from progressive supranuclear palsy." Mov Disord **22**(1): 68-74.

Paviour, D. C., D. Winterburn, S. Simmonds, G. Burgess, L. Wilkinson, N. C. Fox, A. J. Lees and M. Jahanshahi (2005). "Can the frontal assessment battery (FAB) differentiate bradykinetic rigid syndromes? Relation of the FAB to formal neuropsychological testing." Neurocase **11**(4): 274-282.

Pedersen, K. F., J. P. Larsen, O. B. Tysnes and G. Alves (2013). "Prognosis of mild cognitive impairment in early Parkinson disease: the Norwegian ParkWest study." JAMA Neurol **70**(5): 580-586.

Peran, P., A. Cherubini, F. Assogna, F. Piras, C. Quattrocchi, A. Peppe, P. Celsis, O. Rascol, J. F. Demonet, A. Stefani, M. Pierantozzi, F. E. Pontieri, C. Caltagirone, G. Spalletta and U. Sabatini (2010). "Magnetic resonance imaging markers of Parkinson's disease nigrostriatal signature." Brain **133**(11): 3423-3433.

Pereira, J. B., N. Ibarretxe-Bilbao, M. J. Marti, Y. Compta, C. Junque, N. Bargallo and E. Tolosa (2012). "Assessment of cortical degeneration in patients with Parkinson's disease by voxel-based morphometry, cortical folding, and cortical thickness." Hum Brain Mapp **33**(11): 2521-2534.

Perlmutter, J. S. and S. A. Norris (2014). "Neuroimaging biomarkers for Parkinson disease: facts and fantasy." Ann Neurol **76**(6): 769-783.

Pierpaoli, C. and P. J. Basser (1996). "Toward a quantitative assessment of diffusion anisotropy." Magn Reson Med **36**(6): 893-906.

Pirker, W., S. Asenbaum, G. Bencsits, D. Prayer, W. Gerschlager, L. Deecke and T. Brucke (2000). "[123I]beta-CIT SPECT in multiple system atrophy, progressive supranuclear palsy, and corticobasal degeneration." Mov Disord **15**(6): 1158-1167.

Podsiadlo, D. and S. Richardson (1991). "The timed "Up & Go": a test of basic functional mobility for frail elderly persons." J Am Geriatr Soc **39**(2): 142-148.

Poewe, W. and P. Mahlknecht (2009). "The clinical progression of Parkinson's disease." Parkinsonism Relat Disord **15 Suppl 4**: S28-32.

Postuma, R. B., D. Berg, M. Stern, W. Poewe, C. W. Olanow, W. Oertel, J. Obeso, K. Marek, I. Litvan, A. E. Lang, G. Halliday, C. G. Goetz, T. Gasser, B. Dubois, P. Chan, B. R. Bloem, C. H. Adler and G. Deuschl (2015). "MDS clinical diagnostic criteria for Parkinson's disease." Mov Disord **30**(12): 1591-1601.

Pringsheim, T., N. Jette, A. Frolkis and T. D. Steeves (2014). "The prevalence of Parkinson's disease: a systematic review and meta-analysis." Mov Disord **29**(13): 1583-1590.

Prodoehl, J., H. Li, P. J. Planetta, C. G. Goetz, K. M. Shannon, R. Tangonan, C. L. Comella, T. Simuni, X. J. Zhou, S. Leurgans, D. M. Corcos and D. E. Vaillancourt (2013). "Diffusion tensor imaging of Parkinson's disease, atypical parkinsonism, and essential tremor." Mov Disord **28**(13): 1816-1822.

Pyatigorskaya, N., C. Gallea, D. Garcia-Lorenzo, M. Vidailhet and S. Lehericy (2014). "A review of the use of magnetic resonance imaging in Parkinson's disease." Ther Adv Neurol Disord **7**(4): 206-220.

Quattrone, A., G. Nicoletti, D. Messina, F. Fera, F. Condino, P. Pugliese, P. Lanza, P. Barone, L. Morgante, M. Zappia, U. Aguglia and O. Gallo (2008). "MR imaging index for differentiation of progressive supranuclear palsy from Parkinson disease and the Parkinson variant of multiple system atrophy." Radiology **246**(1): 214-221.

Quinn, N. (1989). "Disproportionate antecollis in multiple system atrophy." Lancet **1**(8642): 844.

Raab, P., E. Hattingen, K. Franz, F. E. Zanella and H. Lanfermann (2010). "Cerebral gliomas: diffusional kurtosis imaging analysis of microstructural differences." Radiology **254**(3): 876-881.

Rae, C. L., M. M. Correia, E. Altena, L. E. Hughes, R. A. Barker and J. B. Rowe (2012). "White matter pathology in Parkinson's disease: the effect of imaging protocol differences and relevance to executive function." Neuroimage **62**(3): 1675-1684.

Reichenbach, J. R., R. Venkatesan, D. A. Yablonskiy, M. R. Thompson, S. Lai and E. M. Haacke (1997). "Theory and application of static field inhomogeneity effects in gradient-echo imaging." J Magn Reson Imaging **7**(2): 266-279.

Respondek, G., M. Stamelou, C. Kurz, L. W. Ferguson, A. Rajput, W. Z. Chiu, J. C. van Swieten, C. Troakes, S. Al Sarraj, E. Gelpi, C. Gaig, E. Tolosa, W. H. Oertel, A. Giese, S. Roeber, T. Arzberger, S. Wagenpfeil, G. U. Hoglinger and P. S. P. S. G. Movement Disorder Society-endorsed (2014). "The phenotypic spectrum of progressive supranuclear palsy: a retrospective multicenter study of 100 definite cases." Mov Disord **29**(14): 1758-1766.

Rizzo, G., S. Zanigni, R. De Blasi, D. Grasso, D. Martino, R. Savica and G. Logroscino (2016). "Brain MR Contribution to the Differential Diagnosis of Parkinsonian Syndromes: An Update." Parkinsons Dis **2016**: 2983638.

Rodriguez-Oroz, M. C., M. Jahanshahi, P. Krack, I. Litvan, R. Macias, E. Bezard and J. A. Obeso (2009). "Initial clinical manifestations of Parkinson's disease: features and pathophysiological mechanisms." Lancet Neurol **8**(12): 1128-1139.

Rossi, M. E., H. Ruottinen, T. Saunamaki, I. Elovaara and P. Dastidar (2014). "Imaging brain iron and diffusion patterns: a follow-up study of Parkinson's disease in the initial stages." Acad Radiol **21**(1): 64-71.

Ryvlin, P., E. Broussolle, H. Piollet, F. Viallet, Y. Khalfallah and G. Chazot (1995). "Magnetic resonance imaging evidence of decreased putamenal iron content in idiopathic Parkinson's disease." Arch Neurol **52**(6): 583-588.

Saladin, K. (2009). Anatomy & Physiology: The utility of Form and Function. New York, NY: MvGraw-Hill Companies, Inc.

Schrag, A., Y. Ben-Shlomo and N. P. Quinn (1999). "Prevalence of progressive supranuclear palsy and multiple system atrophy: a cross-sectional study." Lancet **354**(9192): 1771-1775.

Schwab, R. S., England AC. (1969). Projection technique for evaluating surgery in Parkinson's disease. Third Symposium of Parkinson's disease. . F. J. Gillingham, Donaldson IML. Edinburgh, E & S Livingstone**:** 152-157.

Schwarz, S. T., M. Afzal, P. S. Morgan, N. Bajaj, P. A. Gowland and D. P. Auer (2014). "The 'swallow tail' appearance of the healthy nigrosome - a new accurate test of Parkinson's disease: a case-control and retrospective cross-sectional MRI study at 3T." PLoS One **9**(4): e93814.

Sebaldt, R., W. Dalziel, F. Massoud, A. Tanguay, R. Ward, L. Thabane, P. Melnyk, P. A. Landry and B. Lescrauwaet (2009). "Detection of cognitive impairment and dementia using the animal fluency test: the DECIDE study." Can J Neurol Sci **36**(5): 599-604.

Seifert, K. D. and J. I. Wiener (2013). "The impact of DaTscan on the diagnosis and management of movement disorders: A retrospective study." Am J Neurodegener Dis **2**(1): 29-34.

Seppi, K., M. F. Schocke, R. Esterhammer, C. Kremser, C. Brenneis, J. Mueller, S. Boesch, W. Jaschke, W. Poewe and G. K. Wenning (2003). "Diffusion-weighted imaging discriminates progressive supranuclear palsy from PD, but not from the parkinson variant of multiple system atrophy." Neurology **60**(6): 922-927.

Shi, H. C., J. G. Zhong, P. L. Pan, P. R. Xiao, Y. Shen, L. J. Wu, H. L. Li, Y. Y. Song, G. X. He and H. Y. Li (2013). "Gray matter atrophy in progressive supranuclear palsy: meta-analysis of voxel-based morphometry studies." Neurol Sci **34**(7): 1049-1055.

Shulman, K. I. (2000). "Clock-drawing: is it the ideal cognitive screening test?" Int J Geriatr Psychiatry **15**(6): 548-561.

Sjostrom, H., T. Granberg, E. Westman and P. Svenningsson (2017). "Quantitative susceptibility mapping differentiates between parkinsonian disorders." Parkinsonism Relat Disord **44**: 51-57.

Slawek, J., A. Roszmann, P. Robowski, M. Dubaniewicz, E. J. Sitek, K. Honczarenko, A. Gorzkowska, S. Budrewicz, M. Mak, M. Golab-Janowska, E. Koziorowska-Gawron, M. Drozdzik, M. Kurzawski, T. Bandurski and M. Bialecka (2013). "The impact of MRI white matter hyperintensities on dementia in Parkinson's disease in relation to the homocysteine level and other vascular risk factors." Neurodegener Dis **12**(1): 1-12.

Smith, S. M. (2002). "Fast robust automated brain extraction." Hum Brain Mapp **17**(3): 143-155.

Smith, S. M., M. Jenkinson, H. Johansen-Berg, D. Rueckert, T. E. Nichols, C. E. Mackay, K. E. Watkins, O. Ciccarelli, M. Z. Cader, P. M. Matthews and T. E. Behrens (2006). "Tract-based spatial statistics: voxelwise analysis of multi-subject diffusion data." Neuroimage **31**(4): 1487-1505.

Smith, S. M., M. Jenkinson, M. W. Woolrich, C. F. Beckmann, T. E. Behrens, H. Johansen-Berg, P. R. Bannister, M. De Luca, I. Drobnjak, D. E. Flitney, R. K. Niazy, J. Saunders, J. Vickers, Y. Zhang, N. De Stefano, J. M. Brady and P. M. Matthews (2004). "Advances in functional and structural MR image analysis and implementation as FSL." Neuroimage **23 Suppl 1**: S208-219.

Somme, J., J. C. Gomez-Esteban, B. Tijero, K. Berganzo, E. Lezcano and J. J. Zarranz (2013). "The applause sign and neuropsychological profile in progressive supranuclear palsy and Parkinson's disease." Clin Neurol Neurosurg **115**(8): 1230-1233.

Song, J. W. and K. C. Chung (2010). "Observational studies: cohort and case-control studies." Plast Reconstr Surg **126**(6): 2234-2242.

Soria, G., E. Aguilar, R. Tudela, J. Mullol, A. M. Planas and C. Marin (2011). "In vivo magnetic resonance imaging characterization of bilateral structural changes in experimental Parkinson's disease: a T2 relaxometry study combined with longitudinal diffusion tensor imaging and manganese-enhanced magnetic resonance imaging in the 6-hydroxydopamine rat model." Eur J Neurosci **33**(8): 1551-1560.

Spiegel, J., D. Hellwig, S. Samnick, W. Jost, M. O. Mollers, K. Fassbender, C. M. Kirsch and U. Dillmann (2007). "Striatal FP-CIT uptake differs in the subtypes of early Parkinson's disease." J Neural Transm (Vienna) **114**(3): 331-335.

Spillantini, M. G., R. A. Crowther, R. Jakes, M. Hasegawa and M. Goedert (1998). "alpha-Synuclein in filamentous inclusions of Lewy bodies from Parkinson's disease and dementia with lewy bodies." Proc Natl Acad Sci U S A **95**(11): 6469-6473.

Stamelou, M. and G. U. Hoeglinger (2013). "Atypical parkinsonism: an update." Curr Opin Neurol **26**(4): 401-405.

Stankovic, I., F. Krismer, A. Jesic, A. Antonini, T. Benke, R. G. Brown, D. J. Burn, J. L. Holton, H. Kaufmann, V. S. Kostic, H. Ling, W. G. Meissner, W. Poewe, M. Semnic, K. Seppi, A. Takeda, D. Weintraub, G. K. Wenning and M. S. A. S. G. Movement Disorders Society (2014). "Cognitive impairment in multiple system atrophy: a position statement by the Neuropsychology Task Force of the MDS Multiple System Atrophy (MODIMSA) study group." Mov Disord **29**(7): 857-867.

Stejskal, E. and J. Tanner (1965). "Spin diffusion measurements: Spin echoes in the presence of a time-dependent field gradient." Journal of Chemical Physics **42**: 288-292.

Suchowersky, O., S. Reich, J. Perlmutter, T. Zesiewicz, G. Gronseth, W. J. Weiner and N. Quality Standards Subcommittee of the American Academy of (2006). "Practice Parameter: diagnosis and prognosis of new onset Parkinson disease (an evidence-based review): report of the Quality Standards Subcommittee of the American Academy of Neurology." Neurology **66**(7): 968-975.

Surova, Y., M. Nilsson, J. Latt, B. Lampinen, O. Lindberg, S. Hall, H. Widner, C. Nilsson, D. van Westen and O. Hansson (2015). "Disease-specific structural changes in thalamus and dentatorubrothalamic tract in progressive supranuclear palsy." Neuroradiology **57**(11): 1079-1091.

Surova, Y., F. Szczepankiewicz, J. Latt, M. Nilsson, B. Eriksson, A. Leemans, O. Hansson, D. van Westen and C. Nilsson (2013). "Assessment of global and regional diffusion changes along white matter tracts in parkinsonian disorders by MR tractography." PLoS One **8**(6): e66022.

Szczepankiewicz, F., S. Lasic, D. van Westen, P. C. Sundgren, E. Englund, C. F. Westin, F. Stahlberg, J. Latt, D. Topgaard and M. Nilsson (2015). "Quantification of microscopic diffusion anisotropy disentangles effects of orientation dispersion from microstructure: applications in healthy volunteers and in brain tumors." Neuroimage **104**: 241-252.

Szczepankiewicz, F., J. Latt, R. Wirestam, A. Leemans, P. Sundgren, D. van Westen, F. Stahlberg and M. Nilsson (2013). "Variability in diffusion kurtosis imaging: impact on study design, statistical power and interpretation." Neuroimage **76**: 145-154.

Teune, L. K., A. L. Bartels, B. M. de Jong, A. T. Willemsen, S. A. Eshuis, J. J. de Vries, J. C. van Oostrom and K. L. Leenders (2010). "Typical cerebral metabolic patterns in neurodegenerative brain diseases." Mov Disord **25**(14): 2395-2404.

Tison, F., F. Yekhlef, V. Chrysostome and C. Sourgen (2000). "Prevalence of multiple system atrophy." Lancet **355**(9202): 495-496.

Tomlinson, C. L., R. Stowe, S. Patel, C. Rick, R. Gray and C. E. Clarke (2010). "Systematic review of levodopa dose equivalency reporting in Parkinson's disease." Mov Disord **25**(15): 2649-2653.

Tournier, J. D., F. Calamante and A. Connelly (2007). "Robust determination of the fibre orientation distribution in diffusion MRI: non-negativity constrained super-resolved spherical deconvolution." Neuroimage **35**(4): 1459-1472.

Tournier JD, C. F., Connelly A. (2012). "MRtrix: Diffusion tractography in crossing fiber regions." Int J Imaging Syst Technol **22**: 53-66.

Tripathi, M., V. Dhawan, S. Peng, S. Kushwaha, A. Batla, A. Jaimini, M. M. D'Souza, R. Sharma, S. Saw and A. Mondal (2013). "Differential diagnosis of parkinsonian syndromes using F-18 fluorodeoxyglucose positron emission tomography." Neuroradiology **55**(4): 483-492.

Tsukamoto, K., E. Matsusue, Y. Kanasaki, S. Kakite, S. Fujii, T. Kaminou and T. Ogawa (2012). "Significance of apparent diffusion coefficient measurement for the differential diagnosis of multiple system atrophy, progressive supranuclear palsy, and Parkinson's disease: evaluation by 3.0-T MR imaging." Neuroradiology **54**(9): 947-955.

Tuite, P. J., S. Mangia and S. Michaeli (2013). "Magnetic Resonance Imaging (MRI) in Parkinson's Disease." J Alzheimers Dis Parkinsonism **Suppl 1**: 001.

Ubhi, K., P. Low and E. Masliah (2011). "Multiple system atrophy: a clinical and neuropathological perspective." Trends Neurosci **34**(11): 581-590.

Umesh Rudrapatna, S., T. Wieloch, K. Beirup, K. Ruscher, W. Mol, P. Yanev, A. Leemans, A. van der Toorn and R. M. Dijkhuizen (2014). "Can diffusion kurtosis imaging improve the sensitivity and specificity of detecting microstructural alterations in brain tissue chronically after experimental stroke? Comparisons with diffusion tensor imaging and histology." Neuroimage **97**: 363-373.

Wadia, P. M., P. Howard, M. Q. Ribeirro, J. Robblee, A. Asante, D. J. Mikulis and A. E. Lang (2013). "The value of GRE, ADC and routine MRI in distinguishing Parkinsonian disorders." Can J Neurol Sci **40**(3): 389-402.

Wahlund, L. O., F. Barkhof, F. Fazekas, L. Bronge, M. Augustin, M. Sjogren, A. Wallin, H. Ader, D. Leys, L. Pantoni, F. Pasquier, T. Erkinjuntti, P. Scheltens and C. European Task Force on Age-Related White Matter (2001). "A new rating scale for age-related white matter changes applicable to MRI and CT." Stroke **32**(6): 1318-1322.

Vaillancourt, D. E., M. B. Spraker, J. Prodoehl, I. Abraham, D. M. Corcos, X. J. Zhou, C. L. Comella and D. M. Little (2009). "High-resolution diffusion tensor imaging in the substantia nigra of de novo Parkinson disease." Neurology **72**(16): 1378-1384.

Wakana, S., H. Jiang, L. M. Nagae-Poetscher, P. C. van Zijl and S. Mori (2004). "Fiber tract-based atlas of human white matter anatomy." Radiology **230**(1): 77-87.

Wallis, L. I., M. N. Paley, J. M. Graham, R. A. Grunewald, E. L. Wignall, H. M. Joy and P. D. Griffiths (2008). "MRI assessment of basal ganglia iron deposition in Parkinson's disease." J Magn Reson Imaging **28**(5): 1061-1067.

Van Camp, N., I. Blockx, M. Verhoye, C. Casteels, F. Coun, A. Leemans, J. Sijbers, V. Baekelandt, K. Van Laere and A. Van der Linden (2009). "Diffusion tensor imaging

in a rat model of Parkinson's disease after lesioning of the nigrostriatal tract." NMR Biomed **22**(7): 697-706.

Wang, J., Q. X. Yang, X. Sun, J. Vesek, Z. Mosher, M. Vasavada, J. Chu, S. Kanekar, V. Shivkumar, K. Venkiteswaran and T. Subramanian (2015). "MRI evaluation of asymmetry of nigrostriatal damage in the early stage of early-onset Parkinson's disease." Parkinsonism Relat Disord **21**(6): 590-596.

Wang, J. J., W. Y. Lin, C. S. Lu, Y. H. Weng, S. H. Ng, C. H. Wang, H. L. Liu, R. H. Hsieh, Y. L. Wan and Y. Y. Wai (2011). "Parkinson disease: diagnostic utility of diffusion kurtosis imaging." Radiology **261**(1): 210-217.

Wang, Y., S. R. Butros, X. Shuai, Y. Dai, C. Chen, M. Liu, E. M. Haacke, J. Hu and H. Xu (2012). "Different iron-deposition patterns of multiple system atrophy with predominant parkinsonism and idiopathetic Parkinson diseases demonstrated by phase-corrected susceptibility-weighted imaging." AJNR Am J Neuroradiol **33**(2): 266-273.

Vanhoutte, G., S. Pereson, Y. P. R. Delgado, P. J. Guns, B. Asselbergh, J. Veraart, J. Sijbers, M. Verhoye, C. Van Broeckhoven and A. Van der Linden (2013). "Diffusion kurtosis imaging to detect amyloidosis in an APP/PS1 mouse model for Alzheimer's disease." Magn Reson Med **69**(4): 1115-1121.

Ward, C. D. and W. R. Gibb (1990). "Research diagnostic criteria for Parkinson's disease." Adv Neurol **53**: 245-249.

Varrone, A., K. L. Marek, D. Jennings, R. B. Innis and J. P. Seibyl (2001). "[(123)I]beta-CIT SPECT imaging demonstrates reduced density of striatal dopamine transporters in Parkinson's disease and multiple system atrophy." Mov Disord **16**(6): 1023-1032.

Watanabe, H., Y. Saito, S. Terao, T. Ando, T. Kachi, E. Mukai, I. Aiba, Y. Abe, A. Tamakoshi, M. Doyu, M. Hirayama and G. Sobue (2002). "Progression and prognosis in multiple system atrophy: an analysis of 230 Japanese patients." Brain **125**(Pt 5): 1070-1083.

Wenning, G. K., C. Colosimo, F. Geser and W. Poewe (2004). "Multiple system atrophy." Lancet Neurol **3**(2): 93-103.

Wenning, G. K., F. Geser, F. Krismer, K. Seppi, S. Duerr, S. Boesch, M. Kollensperger, G. Goebel, K. P. Pfeiffer, P. Barone, M. T. Pellecchia, N. P. Quinn, V. Koukouni, C. J. Fowler, A. Schrag, C. J. Mathias, N. Giladi, T. Gurevich, E. Dupont, K. Ostergaard, C. F. Nilsson, H. Widner, W. Oertel, K. M. Eggert, A. Albanese, F. del Sorbo, E. Tolosa, A. Cardozo, G. Deuschl, H. Hellriegel, T. Klockgether, R. Dodel, C. Sampaio, M. Coelho, R. Djaldetti, E. Melamed, T. Gasser, C. Kamm, G. Meco, C. Colosimo, O. Rascol, W. G. Meissner, F. Tison, W. Poewe and G. European Multiple System Atrophy Study (2013). "The natural history of multiple system atrophy: a prospective European cohort study." Lancet Neurol **12**(3): 264-274.

Whitwell, J. L., G. U. Hoglinger, A. Antonini, Y. Bordelon, A. L. Boxer, C. Colosimo, T. van Eimeren, L. I. Golbe, J. Kassubek, C. Kurz, I. Litvan, A. Pantelyat, G. Rabinovici, G. Respondek, A. Rominger, J. B. Rowe, M. Stamelou, K. A. Josephs and P. S. P. S. G. Movement Disorder Society-endorsed (2017). "Radiological biomarkers for diagnosis in PSP: Where are we and where do we need to be?" Mov Disord.

Wichmann, T., Delong MR (2002). Neurocircuitry of Parkinson's Disease. Neuropsychopharmacology: The Fifth Generation of Progress. K. L. Davis, Charney D, Coyle JT, Nemeroff C. Philadelphia, PA: Lippincott, Williams, &Wikins**:** 1761-1780.

Williams, D. R., R. de Silva, D. C. Paviour, A. Pittman, H. C. Watt, L. Kilford, J. L. Holton, T. Revesz and A. J. Lees (2005). "Characteristics of two distinct clinical phenotypes in pathologically proven progressive supranuclear palsy: Richardson's syndrome and PSP-parkinsonism." Brain **128**(Pt 6): 1247-1258.

Williams, D. R. and A. J. Lees (2009). "Progressive supranuclear palsy: clinicopathological concepts and diagnostic challenges." Lancet Neurol **8**(3): 270-279.

Visser, M., J. Marinus, A. M. Stiggelbout and J. J. Van Hilten (2004). "Assessment of autonomic dysfunction in Parkinson's disease: the SCOPA-AUT." Mov Disord **19**(11): 1306-1312.

Wu, B., W. Li, A. Guidon and C. Liu (2012). "Whole brain susceptibility mapping using compressed sensing." Magn Reson Med **67**(1): 137-147.

Yablonskiy, D. A. and A. L. Sukstanskii (2010). "Theoretical models of the diffusion weighted MR signal." NMR Biomed **23**(7): 661-681.

Yang, J., N. Shao, J. Li and H. Shang (2014). "Voxelwise meta-analysis of white matter abnormalities in progressive supranuclear palsy." Neurol Sci **35**(1): 7-14.

Zalewski, N., H. Botha, J. L. Whitwell, V. Lowe, D. W. Dickson and K. A. Josephs (2014). "FDG-PET in pathologically confirmed spontaneous 4R-tauopathy variants." J Neurol **261**(4): 710-716.

Zhan, W., G. A. Kang, G. A. Glass, Y. Zhang, C. Shirley, R. Millin, K. L. Possin, M. Nezamzadeh, M. W. Weiner, W. J. Marks, Jr. and N. Schuff (2012). "Regional alterations of brain microstructure in Parkinson's disease using diffusion tensor imaging." Mov Disord **27**(1): 90-97.

Zhang, H., T. Schneider, C. A. Wheeler-Kingshott and D. C. Alexander (2012). "NODDI: practical in vivo neurite orientation dispersion and density imaging of the human brain." Neuroimage **61**(4): 1000-1016.

Zhang, J., Y. Zhang, J. Wang, P. Cai, C. Luo, Z. Qian, Y. Dai and H. Feng (2010). "Characterizing iron deposition in Parkinson's disease using susceptibility-weighted imaging: an in vivo MR study." Brain Res **1330**: 124-130.

Zhang, Y., I. W. Wu, D. Tosun, E. Foster, N. Schuff and I. Parkinson's Progression Markers (2016). "Progression of Regional Microstructural Degeneration in Parkinson's Disease: A Multicenter Diffusion Tensor Imaging Study." PLoS One **11**(10): e0165540.

Zhuo, J., S. Xu, J. L. Proctor, R. J. Mullins, J. Z. Simon, G. Fiskum and R. P. Gullapalli (2012). "Diffusion kurtosis as an in vivo imaging marker for reactive astrogliosis in traumatic brain injury." Neuroimage **59**(1): 467-477.

Ziegler, D. A., J. S. Wonderlick, P. Ashourian, L. A. Hansen, J. C. Young, A. J. Murphy, C. K. Koppuzha, J. H. Growdon and S. Corkin (2013). "Substantia nigra volume loss before basal forebrain degeneration in early Parkinson disease." JAMA Neurol **70**(2): 241-247.

Zigmond, A. S. and R. P. Snaith (1983). "The hospital anxiety and depression scale." Acta Psychiatr Scand **67**(6): 361-370.

Zigmond, M., Burke RE (2002). Pathophysiology of Parkinson's Diasese. Neuropsychopharmacology: The Fifth Generation of Progress. K. Davis, Charley D, Coyle JT, Nemeroff C. Philadelphia, PA: Lippincott, Williams, % Wilkins**:** 1781-1794.

Paper I

OPEN ACCESS Freely available online

PLOS ONE

Assessment of Global and Regional Diffusion Changes along White Matter Tracts in Parkinsonian Disorders by MR Tractography

Yulia Surova[1,2*], Filip Szczepankiewicz[3], Jimmy Lätt[4], Markus Nilsson[5], Bengt Eriksson[1,6], Alexander Leemans[7], Oskar Hansson[1,6], Danielle van Westen[4,8☯], Christer Nilsson[6☯]

1 Department of Clinical Sciences, Neurology, Lund University, Lund, Sweden, **2** Department of Neurology Lund, Skåne University Hospital, Lund, Sweden, **3** Department of Medical Radiation Physics, Lund University, Lund, Sweden, **4** Center for Medical Imaging and Physiology, Skåne University Hospital, Lund, Sweden, **5** Lund University Bioimaging Center, Lund University, Lund, Sweden, **6** Clinical Memory Research Unit, Department of Clinical Sciences Malmö, Lund University, Sweden, **7** Image Sciences Institute, University Medical Center Utrecht, Utrecht, The Netherlands, **8** Department of Clinical Sciences, Diagnostic Radiology, Lund University, Lund, Sweden

Abstract

Purpose: The aim of the study was to determine the usefulness of diffusion tensor tractography (DTT) in parkinsonian disorders using a recently developed method for normalization of diffusion data and tract size along white matter tracts. Furthermore, the use of DTT in selected white matter tracts for differential diagnosis was assessed.

Methods: We quantified global and regional diffusion parameters in major white matter tracts in patients with multiple system atrophy (MSA), progressive nuclear palsy (PSP), idiopathic Parkinson's disease (IPD) and healthy controls). Diffusion tensor imaging data sets with whole brain coverage were acquired at 3 T using 48 diffusion encoding directions and a voxel size of $2\times2\times2$ mm^3. DTT of the corpus callosum (CC), cingulum (CG), corticospinal tract (CST) and middle cerebellar peduncles (MCP) was performed using multiple regions of interest. Regional evaluation comprised projection of fractional anisotropy (FA), mean diffusivity (MD), radial diffusivity (RD) and the apparent area coefficient (AAC) onto a calculated mean tract and extraction of their values along each structure.

Results: There were significant changes of global DTT parameters in the CST (MSA and PSP), CC (PSP) and CG (PSP). Consistent tract-specific variations in DTT parameters could be seen along each tract in the different patient groups and controls. Regional analysis demonstrated significant changes in the anterior CC (MD, RD and FA), CST (MD) and CG (AAC) of patients with PSP compared to controls. Increased MD in CC and CST, as well as decreased AAC in CG, was correlated with a diagnosis of PSP compared to IPD.

Conclusions: DTT can be used for demonstrating disease-specific regional white matter changes in parkinsonian disorders. The anterior portion of the CC was identified as a promising region for detection of neurodegenerative changes in patients with PSP, as well as for differential diagnosis between PSP and IPD.

Citation: Surova Y, Szczepankiewicz F, Lätt J, Nilsson M, Eriksson B, et al. (2013) Assessment of Global and Regional Diffusion Changes along White Matter Tracts in Parkinsonian Disorders by MR Tractography. PLoS ONE 8(6): e66022. doi:10.1371/journal.pone.0066022

Editor: Wang Zhan, University of Maryland, College Park, United States of America

Received February 16, 2013; **Accepted** April 30, 2013; **Published** June 13, 2013

Funding: This research was supported by the Swedish Parkinson foundation, the Swedish Science Council grants through the Linnaeus project BAGADILICO, the Swedish Parkinson Academy and research funds from province of Skåne University Hospital and state grants (inclusively ALF) and in part by the Swedish Cancer Society (GrantNo CAN 2009/1076 and CAN 2012/597). The funders had no role in study design, data collection and analysis, decision to publish and preparation of the manuscript.

Competing Interests: The authors have declared that no competing interests exist.

* E-mail: yulia.surova@med.lu.se

☯ These authors contributed equally to this work.

Introduction

Idiopathic Parkinson's disease (IPD), progressive supranuclear palsy (PSP) and multiple system atrophy (MSA), are the most common neurodegenerative disease entities in what is often called parkinsonian disorders. Outside specialized centers and in the early stages of the diseases, clinical differential diagnosis can often be difficult because of similarity of symptoms and lack of diagnostic markers. Several imaging methods have been shown to be of benefit in the differential diagnosis of different parkinsonian disorders [1]. Diffusion tensor imaging (DTI) [2–3] with calculation of the fractional anisotropy (FA) and mean diffusivity (MD) have been used in the diagnostic evaluation of IPD, PSP and MSA [4–10]. Measurement of MD in basal ganglia structures can differentiate between IPD and MSA/PSP, while FA and MD values within specific white matter tracts can be helpful in differentiating PSP and the parkinsonian variant of MSA (MSA-P) from both each other and from IPD [11–19]. Few studies have been performed using diffusion tensor tractography (DTT) [20] in parkinsonian disorders. In a pilot study, we have previously shown that disease-specific degenerative changes can be demonstrated by DTT in MSA and PSP [4] and some of these findings have

recently been confirmed [21–22]. However, global measurements of diffusion parameters in whole white matter tracts might overlook regional changes along a tract [23–24].

The aim of the present study was to investigate diffusion properties in major white matter tracts of patients with different parkinsonian disorders, employing DTT with an alternative processing scheme to be able to investigate both global and regional changes in larger nerve tracts [25–32]. We focused on three conventional parameters: FA, MD and radial diffusivity (RD) as well as a new measure of tract cross-sectional surface area - the apparent area coefficient (AAC) [30]. We demonstrate both tract-specific and disease-specific variations in DTT parameters along white matter tracts, which might form a basis for future studies of differential diagnosis and disease monitoring in parkinsonian disorders.

Materials and Methods

Ethics Statement

The Ethics Committee of Lund University approved this study. All study participants gave written consent for participation in the study, which was performed in accordance with the provisions of the Helsinki Declaration.

Subjects

The study included 54 subjects: thirty-eight patients presenting parkinsonian syndromes and sixteen healthy controls. Patients were recruited from the Neurology and Memory Clinics at Skåne University Hospital and Landskrona Hospital, Sweden. Patients with a clinical diagnosis of probable IPD (n = 10), PSP (n = 16) and MSA-P (n = 12) according to established criteria [33–35] were included in the study. Clinical diagnoses were made by two neurologists experienced in parkinsonian disorders (C.N. and B.E). Out of the 16 patients with a diagnosis of probable PSP, all presented gradually progressive disorders with an age of onset 40 years or older, symmetry of symptoms (rigidity, bradykinesia); all patients presented both gaze palsy and prominent postural instability with falls within the first year of disease onset, and no response to dopaminergic drugs. All patients with MSA-P showed progressive akinesia and rigidity, urinary incontinence or incomplete bladder emptying after 1 year of disease onset as well as orthostatic hypotension, with no patients showing falls or gaze palsy in the first year of the disease. All patients with IPD showed good clinical improvement after administration of levodopa in respect to baseline conditions. Healthy controls matched for age and gender were recruited from the Swedish population registry. All healthy controls had a normal neurological examination and structural brain MRI, with no history of neurological or psychiatric disease.

Data Acquisition

A 3 T Philips MR scanner, equipped with an eight-channel head coil, was used for the study. DTI was performed using a single-shot EPI sequence with diffusion encoding in 48 directions (b values 0 and 800 s/mm^2) [36]. A b-value of 800 s/mm^2 was selected to shorten the acquisition times. While the most commonly used b-value is 1000 s/mm^2, DTI is expected to work well with b-values at least in the range b = 700–1200 s/mm^2. However, lower b-values are expected to result in slightly higher values of the mean diffusivity [37]. The reconstructed voxel size was $2\times2\times2$ mm^3, and 60 slices were acquired. In order to shorten acquisition time and reduce susceptibility distortions, a SENSE factor of 2.5 was applied in the phase-encoding direction (anterior–posterior). The acquisition time for the DTI sequence was 6 min 49 s. The axial slices in the DTI volume were aligned with the posterior outline of the cranial brain stem.

Data Processing and Fibre Tracking

Subject motion and eddy-current correction was performed in Elastix [38], as implemented in ExploreDTI [28], taking the b-matrix reorientation into account [39]. Whole-brain tractography was generated using ExploreDTI [28], with FA and angular threshold values of 0.2 and 30°, respectively. Multiple regions-of-interest (ROIs) were delineated on the directionally color-coded FA images, in order to extract three bilateral fibre structures: the middle cerebellar peduncle (MCP), the cingulum (CG), and the corticospinal tract (CST). In addition, the mid-sagittal segment (14 mm) of the corpus callosum (CC) was extracted. In addition to these four structures, the SCP and the ICP were also identified with the help of published DTI brain atlases [40–41]. However, the variability in tractography outcome of SCP and ICP was too high to permit any reliable analysis. As such, these structures were not considered for further investigation in this study.

Tractography of the frontal and parietal cingulum (CG) on each side was performed using colour-coded FA-maps. First, two ROIs were placed in the transversal plane to select the anterior part of the CG, which runs parallel to the genu of the corpus callosum; the most rostral part was not included. Then four ROIs were placed in the coronal plane at equal intervals along the superior part of the CG. Finally, two ROIs were placed in the transversal plane defining the posterior CG where it arches around the splenium of the CC. The descending part of the CG was not included. The data for CG were excluded in two patients with MSA-P and one patient with PSP due to incomplete tracking.

For the CST, we extracted the supratentorial portion of CST only, in order to limit variability caused by tracking over long distances [32]. For this purpose, three ROIs used as AND-gates in the tractography were placed in the axial plane, including the posterior limb of the internal capsule, centrum semiovale and the ipsilateral precentral gyrus (primary motor cortex), respectively. The CC was manually subdivided into five areas, according to Hofer's scheme [42], although we treated CC3 and CC4 as one segment in the analysis. The anterior part of CC was defined as CC1–CC2, posterior – CC3–CC5. For the MCP two ROIs were placed: at the level of the pontine crossing fibres and at the level of the deep nuclei.

In order to assess the variation of FA, MD, and RD along the white matter structures, the parameters were projected onto a calculated mean tract, which is a single tract that resembles the major features of each individual white matter structure in 3D space. This enables the evaluation of diffusion parameters as a function of position along the tract. The normalization was based on the position of the explicit landmarks. The method has been used previously [28,30]. In principle, the method and workflow corresponds to the framework presented by Colby et al. [24], although no explicit tract resampling was performed. In addition to the diffusion parameters, we also calculated the cross-sectional area of the tract as a function of position, here denoted the apparent area coefficient (AAC) [30]. The value of the AAC was calculated from the track points passing through cross-sections of the tract, as shown in Fig. 1. FA, MD, RD and AAC will be referred to as DTT parameters. The CC was not analyzed in regard to AAC due to geometric limitations in the quantification of the structure's apparent area along the mean track. Since we wanted to evaluate variations along the CC in an anterior-posterior direction the mean track of the CC was constructed differently than in the other pathways, i.e. with an orientation perpendicular to the fibre orientation. Thereby, the AAC, defined

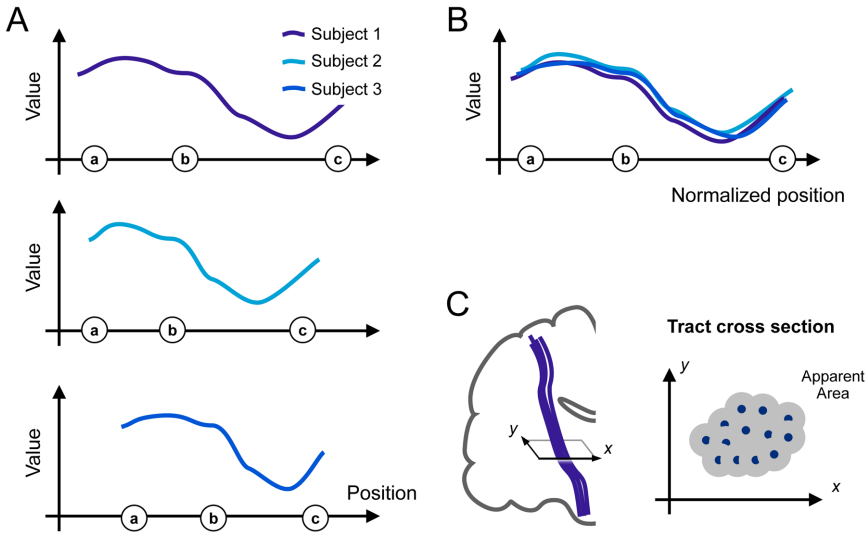

Figure 1. Schematic illustration of the method used to display the variation of the diffusion parameters along the tracts. Projection of diffusion parameters to a mean track resulted in individual parameter-versus-position plots (A), which were associated to the positions of the landmarks, shown as letters a-b-c in circles along the x-axis. The positions were normalized by interpolating the data so that the interval lengths a–b and b–c became equal in all individuals (B). Finally, the apparent area coefficient (AAC) of the tracts was calculated from cross sections of the tracts, where each individual track point (C, blue points) contributed to the total area coefficient with a weight of πr^2, with r = 0.5 mm. Only non-overlapping parts of the subareas contributed to the total area coefficient.
doi:10.1371/journal.pone.0066022.g001

as the cross-sectional area of the tract in a plane with a normal given by the direction of the mean track, was not defined.

The mean values of FA, MD, RD and AAC from the tracts of the right and left hemisphere were treated as independent variables. In the cases where significant differences were found they were then included into a binary logistic regression analysis. This procedure was used as parkinsonian disorders affect both hemispheres, often asymmetrically, although there may be a similar extent of atrophy bilaterally in later stages. DTT parameters for the different groups were plotted as a function of the position along the mean track, with the distances between the anatomical landmarks scaled according to their average relative distance.

Statistical Analysis

Statistical analysis was performed with SPSS Statistics 20 for Windows (IBM Corporation, Somers, NY, USA). Differences between groups in demographic and clinical categorical variables were analyzed by Fisher's Exact test. The Kruskall-Wallis test was used to compare average FA, MD, RD and AAC values in whole tracts between the PSP, MSA-P, IPD and control groups. Where significant differences were found, group comparisons were performed using the Mann–Whitney *U*-test. An adjustment for multiple comparisons between the 4 control/patient categories (i.e. 6 comparisons) was made, leading to an adjusted significance level of $P = 0.008$ using Bonferroni correction. The average median values for the DTI parameters from the corresponding whole tracts of both hemispheres were reported. For statistical evaluation of differences in regional diffusion data between diagnostic subgroups, Mann-Whitney *U*-test was performed for each point along each white matter tract. Comparisons were made between controls and the respective disease groups at a significance level of $P<0.05$. To further study the regional variation within the CC, MD and FA in the anterior and posterior parts of CC were compared. Bee swarm box plots were applied to display the data graphically.

To study the ability of DTT measurements to distinguish IPD from PSP, univariate binary logistic regression analysis was performed with five diffusion parameter values that were significantly different between PSP and IPD, based on the results of Mann-Whitney *U*-test. All of these five models of binary logistic regression analysis were adjusted for age and sex. The sensitivity, specificity and the optimal cutoff level of DTI values chosen by the models were calculated with receiver operator characteristic curve analysis (ROC), as a measure of the usefulness of DTT in selected tracts as a diagnostic tool for individual cases.

Results

Demographic and clinical data of patients and controls are reported in Table 1. There were no significant differences in age, gender ratio or disease duration between the IPD, MSA-P and PSP groups.

Analysis of global values of DTT parameters was made by comparing median values in whole white matter tracts for the different disease groups. The most prominent differences were detected in FA, MD and RD values in the CC in patients with PSP compared with both IPD and controls. In addition, comparing PSP patients to IPD showed a significantly lower AAC in the CG and an increase of MD in the CST. There were no significant

Table 1. Demographic data and clinical diagnosis.

	CTR (n = 16)	IPD (n = 10)	MSA-P (n = 12)	PSP (n = 16)	p
Sex female:male	7:9	4:6	8:4	9:7	0.583[a]
Age (years)	67 (63–73)	68 (59–70)	63 (56–75)	68 (65–72)	0.385[b]
Disease duration(years)	–	4.5 (2.0–7.5)	3.0 (2.2–5.0)	3.5 (2.2–4.0)	0.273[b]

There were no significant differences in demographic data between the controls and the different disease groups. All values expressed as medians, values in parenthesis indicate 25–75 percentiles.
[a]P values refer to Fisher's Exact test,
[b]P values refer to Kruskal-Wallis test, where controls were excluded from the group comparisons of disease duration. IPD, idiopathic Parkinson's disease; PSP, progressive supranuclear palsy; MSA-P, multiple system atrophy, parkinsonian variant; CTR, healthy controls.
doi:10.1371/journal.pone.0066022.t001

differences between PSP and MSA-P patients. We also found significantly higher AAC in the CG of patients with IPD compared to controls. MSA patients showed a significantly higher RD in the CST compared to IPD. There was an increase in MD and decrease in AAC in the MCP in MSA compared to IPD patients, which did not reach statistical significance. The median values of diffusion data and AAC for the whole tracts are summarized in Table 2.

Concerning the regional analysis along white matter tracts, there were consistent variations of the DTT parameters along each tract, as determined by visual inspection, which were very similar in the different patient groups and controls. Each tract and parameter had its characteristic "2D-profile" along its length (Fig. 2). The exception was the diffusion values from CC in the PSP group that differed significantly in shape from the other groups (see below and Fig. 2). For all parameters, there were differences in FA and RD values between the left and right CG (Fig. 3) and, to a lesser degree, for MD in the CST (data not shown), which were consistent throughout the control and patient groups (Fig. 3). Although all statistically significant differences between controls and disease groups are depicted in Fig. 2, only continuous changes encompassing more than 2 cm along a tract were considered of significance for further analysis. There was a trend towards lower AAC in both the MSA and PSP groups in MCP, which was not significant (Fig. 2). In PSP, significant changes were seen for AAC in the CG and for MD in the CST. However, the most striking finding was a marked increase in MD and RD, and a corresponding reduction of FA, in the anterior and central parts of the CC in PSP.

Table 2. DTT parameters in white matter tracts.

		Group			
Tract	**Parameter**	**CTR**	**IPD**	**MSA-P**	**PSP**
CG	FA	0.50 (0.49–0.51)	0.51 (0.48–0.54)	0.47 (0.43–0.50)	0.46 (0.44–0.50)
	MD	0.83 (0.82–0.83)	0.83 (0.80–0.88)	0.84 (0.82–0.90)	0.85 (0.82–0.89)
	RD	0.58 (0.56–0.59)	0.57 (0.53–0.61)	0.62 (0.56–0.65)	0.62 (0.58–0.66)
	AAC	2.61 (2.51–2.78)	2.96[c] (2.72–3.04)	2.81 (2.36–2.99)	2.44[be] (2.27–2.72)
CST	FA	0.54 (0.53–0.55)	0.54 (0.54–0.57)	0.53 (0.51–0.54)	0.55 (0.53–0.58)
	MD	0.79 (0.78–0.82)	0.79 (0.77–0.80)	0.82 (0.80–0.84)	0.84[abe] (0.81–0.87)
	RD	0.52 (0.50–0.54)	0.52 (0.49–053)	0.55[d] (0.53–0.57)	0.55 (0.51–0.58)
	AAC	3.92 (3.59–4.70)	3.84 (3.60–4.22)	4.07 (3.82–4.61)	4.07 (3.59–4.47)
MCP	FA	0.61 (0.59–0.63)	0.59 (0.58–0.60)	0.58 (0.54–0.63)	0.59 (0.58–0.61)
	MD	0.74 (0.70–0.76)	0.72 (0.71–0.80)	0.80 (0.73–0.85)	0.77 (0.74–0.79)
	RD	0.43 (0.41–0.47)	0.44 (0.43–0.50)	0.46 (0.44–0.56)	0.47 (0.43–0.50)
	AAC	5.07 (4.77–5.27)	5.52 (4.92–5.69)	4.67 (4.38–5.27)	4.81 (4.41–5.14)
CC	FA	0.63 (0.60–0.65)	0.65 (0.62–0.67)	0.62 (0.60–0.63)	0.56[ab] (0.53–0.61)
	MD	1.04 (0.99–1.10)	1.02 (0.96–1.07)	1.06 (1.02–1.13)	1.15[abe] (1.08–1.26)
	RD	0.61 (0.56–0.69)	0.58 (0.52–0.64)	0.63 (0.59–0.69)	0.73[ab] (0.65–0.87)

Fractional anisotropy (FA), mean and radial diffusivity (MD, RD, 10^−3 mm^2/s) and apparent area coefficient (AAC) values in major white matter tracts. The medians of diffusion parameters are presented. For paired structures (CG, cingulum, CST, corticospinal tract, MCP, middle cerebellar peduncles), all values are estimated medians from the left and right tracts; values in parenthesis indicate 25–75 percentiles.
[a]CTR/PSP, P≤0.008;
[b]IPD/PSP, P≤0.002;
[c]CTR/IPD, P = 0,002;
[d]IPD/MSA, P = 0.007, Mann-Whitney *U* test.
[e]IPD/PSP, P<0.05, binary logistic regression analysis, age/sex adjusted. Abbreviations: IPD, idiopathic Parkinson's disease; PSP, progressive supranuclear palsy; MSA-P, multiple system atrophy, parkinsonian variant; CTR, healthy controls.
doi:10.1371/journal.pone.0066022.t002

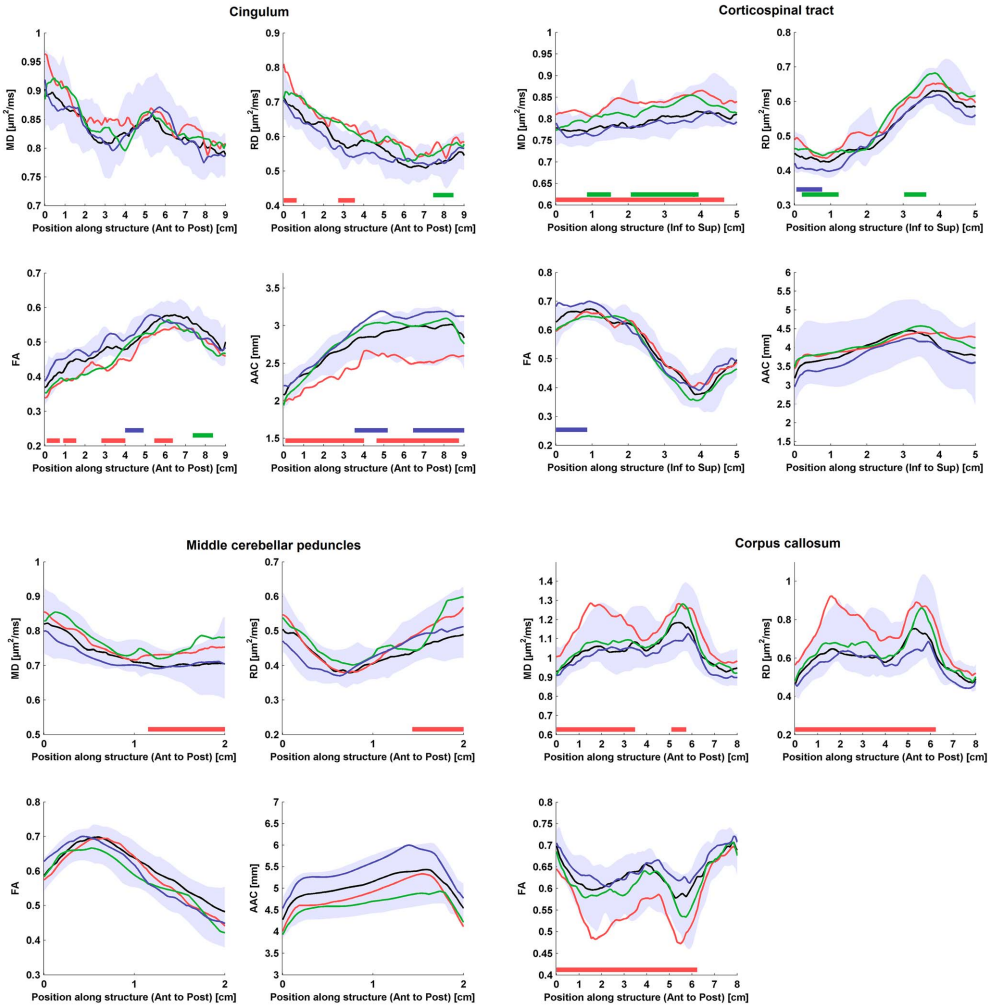

Figure 2. Comparisons between diffusion parameters and apparent area coefficient (AAC) in patients with Parkinsons's disease (IPD – blue lines), multiple system atrophy (MSA – green lines), progressive supranuclear palsy (PSP – red lines) and controls (CTR – black lines). The lines show the median of diffusion parameters as a function of distance. The colored area shows the 10–90% confidence interval of the median in CTR. Panel A-C show mean diffusivity (MD), fractional anisotropy (FA), radial diffusivity (RD) and AAC in the cingulum, corticospinal tract, middle cerebellar peduncles and the corpus callosum, respectively. Values for AAC could not be calculated for the corpus callosum (see Methods). Positions with significant difference from controls ($P<0.05$, Mann–Whitney *U*-test) along tracts are marked with horizontal bars placed just above the x-axis, color-coded according to disease. Significant differences extending continuously for more than five mm along a tract were found for AAC in the cingulum, MD in the corticospinal tract, and RD, MD and FA in the corpus callosum in PSP.
doi:10.1371/journal.pone.0066022.g002

Based on the Mann-Whitney *U*-test, five models of univariate binary logistic regression analysis were performed in order to test the potential of using diffusion parameters for differential diagnosis of IPD and PSP. AAC in the CG, MD in the CST, MD in the CC, RD in the CC and FA in the CC were included in the models, see Statistical analysis. A summary of the results is shown in Table 3, with details of each comparison given below. Logistic regression analysis confirmed that the AAC in the CG, the MD in CST and the MD in the CC could significantly ($P<0.025$) discriminate PSP from IPD (Table 3). The sensitivity and specificity for all these parameters, calculated using a ROC curve analysis, showed the optimal cutoff levels (with an area under the ROC curve of 0.85–

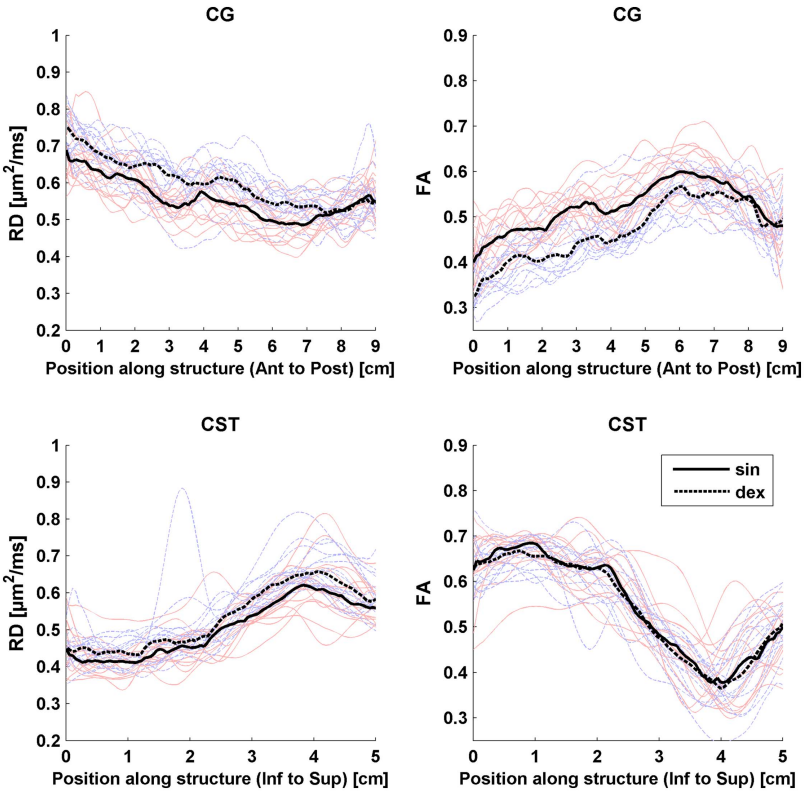

Figure 3. The plots show radial diffusivity (RD) and fractional anisotropy (FA) as functions of position along the cingulum (CG) (upper panels) and corticospinal tract (CST) (lower panels) from the right and left hemispheres in controls. Measurements from the right hemisphere are shown in blue and from the left side in red lines, respectively. The dashed and solid black lines represent the median value in each position of the left and right hand side tracts, respectively. The horizontal axis shows the position along CG in anterior – posterior direction. Distances 0–6 cm correspond approximately to the frontal part of the CG and 6–9 cm corresponds to the parietal part of the CG. For CST the horizontal axis shows the position along CST in inferior – superior direction. Distances 0–3 cm correspond approximately to the infracallosal part of the CST and 3–5 cm corresponds to the supracallosal part of the CST.
doi:10.1371/journal.pone.0066022.g003

0.88) to discriminate PSP from IPD with a sensitivity of 81–94% and a specificity of 80%. This correctly classified 80–87% of PSP and IPD subjects.

To further evaluate the differences in regional values of diffusion parameters along white matter tracts demonstrated above, diffusion parameters from the anterior and posterior part of CC were compared separately. The MD in the anterior part of CC, tested in the model of binary logistic regression, age and sex adjusted, showed the same significant trend toward discrimination of PSP and IPD as the MD in the whole CC. MD in the posterior part of the CC did not reach significance in the binary logistic regression model. Bee swarm box plots showed substantial overlap between the different groups (Fig. 4). The controls also showed large variation of diffusion parameter values.

Discussion

Diffusion tensor imaging has emerged as a powerful tool for detecting early degenerative changes in both normal aging [43–44] and neurodegenerative disease [45,46]. Studies have shown that diffusion changes can be detected before atrophy or signal changes can be seen on standard MRI sequences [46–47]. It is therefore natural that DTI has been used to explore diffusion changes also in parkinsonian disorders [48–50].

The first study that demonstrated diffusion changes in the parkinsonian brain was Yoshikawa et al. [50], using a ROI-based approach. They showed that by placing small ROIs along the presumed position of the nigrostriatal tract, reduced ADC and increased FA could be seen in both patients with IPD and PSP compared to controls. DTI with manual placement of ROIs has since then dominated and has been applied to both subcortical nuclei and white matter tracts, as reviewed above. Although most

Table 3. Use of DTT parameters for differential diagnosis.

Structure	Parameter	AUC (ROC)	Cutoff	Sensitivity, %	Specificity, %	Observed clinical diagnosis	Predicted		Percentage correct diagnosis, %	Overall percentage correct diagnosis, %
							Clinical diagnosis			
							IPD	PSP		
CG Whole*	AAC	0,88	2,730	87	80	IPD	8	2	80	80
						PSP	3	12	80	
CST Whole*	MD	0,85	0,801	94	80	IPD	7	3	70	87
						PSP	3	13	81	
CC Whole*	MD	0,85	1,072	81	80	IPD	7	3	70	81
						PSP	2	14	87	

Mean diffusivity (MD, 10^−3 mm^2/s) and apparent area coefficient (AAC) differentiating PSP from IPD. CG – cingulum, CST – corticospinal tract, CC – corpus callosum, PSP – progressive supranuclear palsy, AUC – area under curve, ROC – receiver operating characteristic analysis.

*Significant differences between PSP and IPD, P<0,05, using binary logistic regression, adjusted for age and sex. There were no age/sex differences between IPD and PSP groups together with chosen MR parameters.

doi:10.1371/journal.pone.0066022.t003

studies have focused on group differences between controls and disease groups, there have been attempts to determine cut-off values for diffusion parameters in specific structures that can aid in the differential diagnosis between IPD and atypical parkinsonian disorders such as MSA and PSP. While measurements of FA and MD in the putamen in most cases can differentiate MSA and PSP from IPD and controls [12,51], other studies have targeted the middle and superior cerebellar peduncles to differentiate between MSA and PSP [4,13,52].

Using DTI with a ROI-based approach is time-consuming and has the additional disadvantage of only capturing a small part of a white matter tract. With larger ROIs there is a risk that included voxels might contain signal from adjacent tissue including other tracts, nuclei or CSF, a problem which becomes even more pronounced when investigating smaller white matter tracts [53]. In addition, ROI-based approaches also result in loss of data on local variations in diffusion parameters [23]. To address this issue some studies have used tract-based spatial statistics (TBSS) for analysis of DTI-data between groups [54–55]. TBSS captures regional variations along white matter tracts which can be correlated to clinical symptoms in comparisons between groups [55], but does not allow for specific analysis of tracts in individual patients.

DTT allows for delineation and separate analysis of diffusion parameters and structure in discrete white matter tracts [24,27,28]. It has so far only been used in a limited number of studies in parkinsonian disorders [1,4,21,23]. Although previous studies have demonstrated regional variations along normal white matter tracts as well as in neurodegenerative disease [23,32,55], most studies to date have used the mean value of diffusion parameters in the whole tract for analysis. In addition, a quantitative measure of tract size has largely been lacking.

In this study, we applied a new approach for visualization and quantitative evaluation of DTT parameters along white matter tracts in patients with parkinsonian disorders as a function of distance from specific anatomical landmarks [27,28,31]. The procedure overcomes existing limitations of user-specified region definition or full-brain registration. The tracking takes only a few seconds on a standard PC and the whole process including ROI specifications, DTT parameter calculation, tracking, and storing fibres into a database takes a few minutes per subject. Our results demonstrate that the method is highly reproducible and captures known variations along specific white matter tracts. The difference between the right and left cingulum shown here has previously been demonstrated in healthy adults [56], as has variations along the corticospinal tract [32]. It is interesting that these variations change or disappear in PSP where the disease process often involves both these pathways. The numerical values for FA and MD in the whole tracts showed good agreement with published data from normal individuals in the age group 40–65 years for CG, CST and MCP [57]. Our present method of analysis seems most suitable for analysis of larger white matter tracts. Diffusion data from tractography of the SCP and ICP resulted in very large variations in diffusion parameters precluding any further statistical analysis. Current research in our group addresses the issues of developing more advanced schemes for fibre tract alignment and validation of fibre bundles obtained by tracking in comparison to co-registered structural image data.

There are results from other studies, suggesting that the MCP has the best diagnostic accuracy in discriminating MSA from IPD and PSP [13]. Regional analysis in our study showed that DTT parameters appeared to be changed along the entire or larger part of the MCP (MD, RD and AAC) in MSA-P, compared to controls, although the changes were non-significant. In fact, significant differences were only found for the posterior MCP in patients with

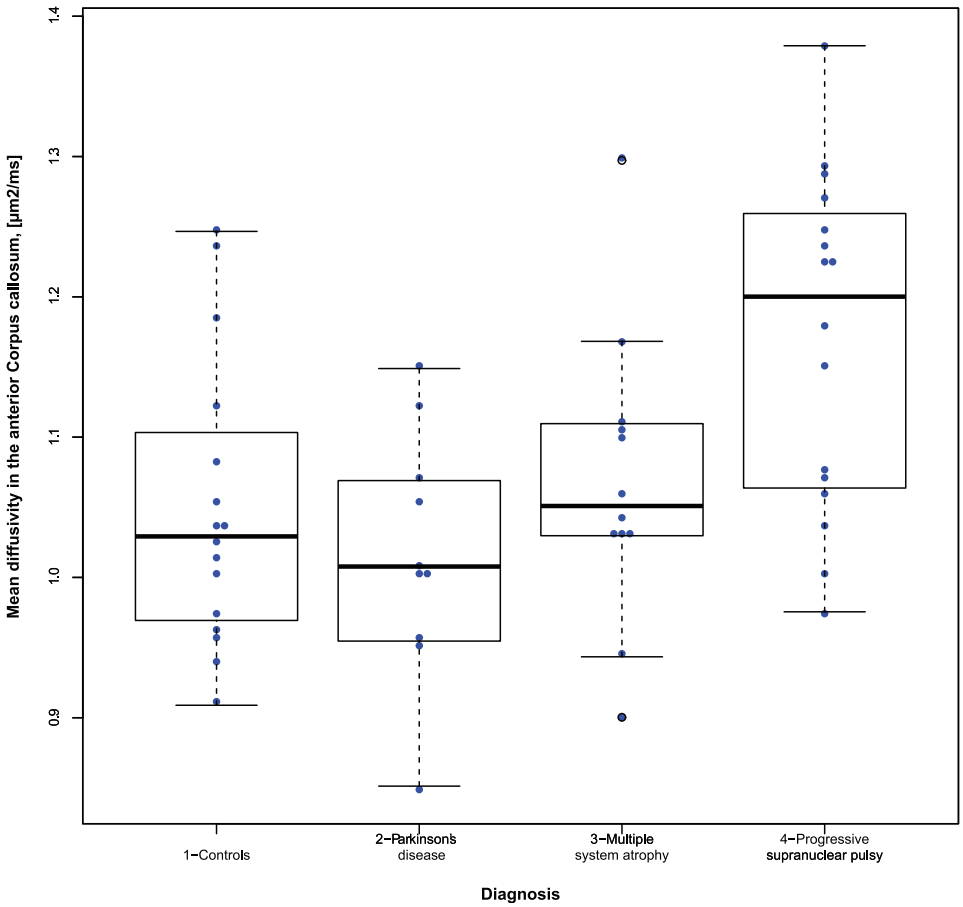

Figure 4. Beeswarm box-plot comparing mean diffusivity and fractional anisotropy in the anterior part of corpus callosum between patients with Parkinson's disease, multiple system atrophy, progressive supranuclear palsy and controls. Horizontal lines that intersect the boxes are medians. The top of the boxes is the 75th percentile and the bottom the 25th percentile. The whiskers above and below boxes represent maximum and minimum values when there are no outliers. If outliers are present the whisker on the appropriate side is taken to 1.5×IQR from the quartile. Outliers are labeled with open circles.
doi:10.1371/journal.pone.0066022.g004

PSP. Degeneration of the olivopontocerebellar system, including the pontine neurons and transverse fibres, is highly variable and mostly less severe in MSA-P as compared to the cerebellar form of MSA (MSA-C), which can explain the variation and overlap with controls and other disease groups [58–60]. Our results to a certain degree support that the pathological process affects the pons and cerebellum also in MSA-P, but that the discriminatory potential for differential diagnosis is limited.

The current study using DTT demonstrates that the CC is the structure that best differentiates PSP from IPD and MSA, as has previously been found in studies using DTI [6,7,12,21,54]. In addition, our study indicates that the most prominent changes in diffusion parameters compared to other parkinsonian disorders occur in the anterior part of CC in PSP, in keeping with the well-known involvement of the frontal lobes in this disease [54,61,62]. Interestingly, reduced FA values in the genu of CC has recently been reported in patients with Parkinson's disease with dementia (PDD) and dementia with Lewy bodies (DLB) as well [63–64]. In addition, Kamagata et al. demonstrated reduced FA in the anterior CG of patients with PD [65], a finding which was not reproduced in the present study.

We also found that MD values in the CST can help to discriminate IPD and PSP. It is well established that CST can be affected in PSP [4]. The use of AAC as a measure of tract diameter appears to be a useful addition to DTT. Although this study was mainly exploratory (hypothesis-generating), comparing diffusion parameters at group level, we have also demonstrated significant discriminatory power for differentiation of IPD and PSP using

AAC in CG as well as MD in CST and CC. These results should be treated with caution considering the limited number of cases in each group, but may add useful information for future studies.

Measurement of DTT parameters in whole white matter tracts was sufficient for detecting clinically important differences between patient groups, while regional analysis of diffusion data helped to determine the location of the changes. Our results highlight the need to consider differences in diffusion properties along major white matter tracts and the possibility of asymmetry between the left and right hemispheres both in patients and healthy controls. The large degree of overlap in diffusion parameter values between individuals limits the usefulness of the method as a diagnostic biomarker on its own. However, DTT parameters could still be used together with other clinical, biochemical and imaging markers for diagnostic purposes. Large inter-individual differences in clinical signs and biomarker values are common in neurodegenerative disease as well as in other biological systems. For this reason even extreme outliers were included in the analysis. It is important to note the large variation in diffusion parameter values also in neurologically healthy elderly persons.

Several limitations of our study should be mentioned. First, the relatively small number of patients limits generalization of the findings. Moreover, positioning of the ROIs was performed manually and errors could be introduced by limited intrarater reliability. Also, statistical analysis within small ROIs including only a few voxels might be very sensitive to partial volume effects, limiting the method to the study of larger tracts. Although all patients fulfilled clinical research criteria for diagnosis of their respective disorder, they might still vary substantially in disease stage, rate of progression and clinical symptoms. Additionally, none of the included subjects had their diagnosis confirmed by autopsy. However, diagnosis of MSA and PSP by an experienced clinician yields sensitivities of 88% and 84% (positive predictive values of a clinical diagnosis of MSA and PSP in this study were 86 and 80%, respectively) [66]. Finally, we acknowledge that DTI is not capable of unambiguously characterizing the white matter microstructure in regions of complex fibre architecture [67–68] and that more advanced diffusion approaches could be preferable for reconstructing tract pathways [69–71]. Notwithstanding the low specificity in assessing the cause of the observed diffusion abnormalities [72], DTI may still exhibit a high sensitivity, which has shown to be useful in several applications [73–74].

In summary, we have shown that DTT has the potential as a tool for assessing pathway-specific abnormalities in parkinsonian disorders on both an individual and group level. The ability to visualize and quantify global and regional DTT parameters in specific white matter tracts could improve differential diagnosis and also help to explain the underlying anatomical mechanisms of individual clinical phenotypes. Additional studies are required to validate the research findings and to determine whether DTI/DTT can detect diffusion changes in very early stages of parkinsonian disorders.

Author Contributions

Conceived and designed the experiments: CN DvW OH. Performed the experiments: YS FS. Analyzed the data: YS. Contributed reagents/materials/analysis tools: CN BE DvW JL MN AL OH. Wrote the paper: YS CN.

References

1. Piccini P, Brooks DJ (2006) New developments of brain imaging for Parkinson's disease and related disorders. Mov Disord 21: 2035–41.
2. Basser PJ, Mattiello J, LeBihan D (1994) MR Diffusion Tensor Spectroscopy and Imaging. Biophysical Journal 66: 259–67.
3. Tournier JD, Mori S, Leemans A (2011) Diffusion Tensor Imaging and Beyond. Magn Reson Med 65: 1532–56.
4. Nilsson C, Markenroth Bloch K, Brockstedt S, Latt J, Widner H, et al. (2007) Tracking the neurodegeneration of parkinsonian disorders – a pilot study. Neuroradiology 49: 111–19.
5. Seppi K, Schocke MF, Mair KJ, Esterhammer R, Scherfler C, et al. (2006) Progression of putaminal degeneration in multiple system atrophy: a serial diffusion MR study. Neuroimage 31: 240–45.
6. Wang J, Wai Y, Lin WY, Ng S, Wang CH, et al. (2010) Microstructural changes in patients with progressive supranuclear palsy: a diffusion tensor imaging study. J Magn Reson Imaging 32: 69–75.
7. Padovani A, Borroni B, Brambati SM, Agosti C, Broli M, et al. (2006) Diffusion tensor imaging and voxel based morphometry study in early progressive supranuclear palsy. J Neurol Neurosurg Psychiatry 77: 457–63.
8. Peran P, Cherubini A, Assogna F, Piras F, Quattrocchi C, et al. (2010) Magnetic resonance imaging markers of Parkinson's disease nigrostriatal signature. Brain 133: 3423–33.
9. Zhan W, Kang GA, Glass GA, Zhang Y, Shirley C, et al. (2012) Regional alterations of brain microstructure in Parkinson's diseases using diffusion tensor imaging. Mov Disord 1: 90–97.
10. Vaillancourt DE, Spraker MB, Prodoehl J, Abraham I, Corcos DM, et al. (2009) High-resolution diffusion tensor imaging in the substantia nigra of de novo Parkinson disease. Neurology 72: 1378–84.
11. Nicoletti G, Tonon C, Lodi R, Condino F, Manners D, et al. (2008) Apparent diffusion coefficient of the superior cerebellar peduncle differentiates progressive supranuclear palsy from Parkinson's disease. Mov Disord 23: 2370–76.
12. Kollensperger M, Seppi K, Liener C, Boesch S, Heute D, et al. (2007) Diffusion weighted imaging best discriminates PD from MSA-P: A comparison with tilt table testing and heart MIBG scintigraphy. Mov Disord 22: 1771–76.
13. Paviour DC, Thornton JS, Lees AJ, Jäger HR (2007) Diffusion-weighted magnetic resonance imaging diffentiates parkinsonian variant of multiple-system atrophy from progressive supranuclear palsy. Mov Disord 22: 68–74.
14. Erbetta A, Mandelli ML, Savoiardo M, Grisoli M, Bizzi A, et al. (2009) Diffusion tensor imaging shows different topographic involvement of the thalamus in progressive supranuclear palsy and corticobasal degeneration. Am J Neuroradiol 30: 1482–87.
15. Ito S, Makino T, Shirai W, Hattori T (2008) Diffusion tensor analysis of corpus callosum in progressive supranuclear palsy. Neuroradiology 50: 981–85.
16. Tha KK, Terae S, Yabe I, Miyamoto T, Soma H, et al. (2010) Microstructural white matter abnormalities of multiple system atrophy: in vivo topographic illustration by using diffusion-tensor MR imaging. Radiology 255: 563–9.
17. Shiga K, Yamada K, Yoshikawa K, Mizuno T, Nishimura T, et al. (2005) Local tissue anisotropy decreases in cerebellopetal fibres and pyramidal tract in multiple system atrophy. J Neurol 252: 589–96.
18. Schocke MF, Seppi K, Esterhammer R, Kremser C, Mair KJ, et al. (2004) Trace of diffusion tensor differentiates the Parkinson variant of multiple system atrophy and Parkinson's disease. Neuroimage 21: 1443–51.
19. Schocke MF, Seppi K, Esterhammer R, Kremser C, Jaschke W, et al. (2002) Diffusion-weighted MRI differentiates the Parkinson variant of multiple system atrophy from PD. Neurology 58: 575–80.
20. Mori S, Crain BJ, Chacko VP, van Zijl PC (1999) Three-dimensional tracking of axonal projections in the brain by magnetic resonance imaging. Ann Neurol 45: 265–9.
21. Canu E, Agosta F, Baglio F, Galantucci S, Nemni R, et al. (2011) Diffusion tensor magnetic resonance imaging tractography in progressive supranuclear palsy. Mov Disord 26: 1751–5.
22. Makino T, Ito S, Kumabara S (2011) Involvement of pontine transverse and longitudinal fibers in multiple system atrophy: a tractography-based study. J Neurol Sci 303: 61–6.
23. Kvickström P, Eriksson B, van Westen D, Lätt J, Elfgren C, et al. (2011) Selective frontal neurodegeneration of the inferior fronto-occipital fasciculus in progressive supranuclear palsy (PSP) demonstrated by diffusion tensor tractography. BMC Neurology. 26: 11–13.
24. Colby JB, Soderberg L, Lebel C, Dinov ID, Thompson PM, et al. (2012) Along-tract statistics allow for enhanced tractography analysis. Neuroimage 59: 3227–42.
25. Lim KO, Hedehus M, Moseley M, de Crespiqny A, Sullivan EV, et al. (1999) Compromised white matter tract integrity in schizophrenia inferred from diffusion tensor imaging. Arch Gen Psychiatry 56: 367–374.
26. Xu D, Mori S, Solaiyappan M, van Zijl PC, Davatzikos C (2002) A framework for callosal fiber distribution analysis. Neuroimage 17: 1131–43.
27. Fillard P, Gilmore J, Piven J, Lin WL, Gerig G (2003) Quantitative analysis of white matter fiber properties along geodesic paths. In: Ellis RE, Peters TM, editors. Medical Image Computing and Computer-Assisted Intervention (MICCAI 03). Lecture Notes in Computer Science, Volume 2879. Heidelberg: Springer-Verlag. 16–23.

28. Leemans A, Jeurissen B, Sijbers J, Jones DK (2009) ExploreDTI: a graphical toolbox for processing, analyzing, and visualizing diffusion MR data. In Proc Intl Soc Mag Reson Med 3537.
29. Szczepankiewicz F, Leemans A, Sundgren P, Wirestam R, Ståhlberg F, et al. (2012) Power and variability analysis in diffusion kurtosis imaging: Sample size estimation in three white matter structures. In Proc Intl Soc Mag Reson Med 3628.
30. Mårtensson J, Nilsson M, Ståhlberg F, Sundgren P, Nilsson C, et al. (2013) Spatial analysis of diffusion tensor tractography statistics along the inferior fronto-occipital fasciculus with application in progressive supranuclear palsy. MAGMA (In press).
31. Mårtensson J, Nilsson M, Elfgren C, Landqvist M, Ståhlberg F, et al. (2011) Spatial analysis of diffusion tensor tractography depicts local white matter changes. In Proc Intl Soc Mag Reson Med 4876.
32. Reich DS, Smith SA, Jones CK, Zackowski KM, van Zijl PC, et al. (2006) Quantitative Characterization of the Corticospinal Tract at 3 Tesla. Am J Neuroradiol 27: 2168–78.
33. Calne DB, Snow BJ, Lee C (1992) Criteria for diagnosing Parkinson's disease. Ann Neurol 32: S125–7.
34. Litvan I, Agid Y, Calne D, Campbell G, Dubois B, et al. (1996) Clinical research criteria for the diagnosis of progressive supranuclear palsy (Steele-Richardson-Olszewski syndrome): report of the NINDS-SPSP International Workshop. Neurology 47: 1–9.
35. Gilman S, Low PA, Quinn N, Albanese A, Ben-Shlomo Y, et al. (1999) Consensus statement on the diagnosis of multiple system atrophy. J Neurol Sci 163: 94–8.
36. Jones DK, Leemans A (2010) Diffusion tensor imaging. Methods Mol Biol 711: 127–44.
37. Nucifora PG, Verma R, Lee SK, Melhem ER (2007) Diffusion-tensor MR imaging and tractography: exploring brain microstructure and connectivity. Radiology 245: 127–44.
38. Klein S, Staring M, Murphy K, Viergever MA, Pluim JP (2010) Elastix: A toolbox for intensitybased medical image registration. IEEET. Med Imaging 29: 195–205.
39. Leemans A, Jones DK (2009) The B-matrix must be rotated when correcting for subject motion in DTI data. Magn Reson Med 61: 1336–49.
40. Stieltjes B, Kaufmann WE, van Zijl PC, Fredericksen K, Pearlson GD, et al. (2001) Diffusion tensor imaging and axonal tracking in the human brainstem. Neuroimage 14: 723–35.
41. Wakana S, Jiang H, Nagae-Poetscher LM, van Zijl PC, Mori S (2004) Fiber tract-based atlas of human white matter anatomy. Radiology 230: 77–87.
42. Hofer S, Frahma J (2006) Topography of the human corpus callosum revisited: comprehensive fiber tractography using diffusion tensor magnetic resonance imaging. Neuroimage 32: 989–94.
43. Hsu JL, Van Hecke W, Bai CH, Lee CH, Tsai YF, et al. (2010) Microstructural white matter changes in normal aging: a diffusion tensor imaging study with higher-order polynomial regression models. Neuroimage 49: 32–43.
44. Hsu JL, Leemans A, Bai CH, Lee CH, Tsai YF, et al. (2008) Gender differences and age-related white matter changes of the human brain: a diffusion tensor imaging study. Neuroimage 39: 566–77.
45. Zhang Y, Schuff N, Jahng GH, Bayne W, Mori S, et al. (2007) Diffusion tensor imaging of cingulum fibers in mild cognitive impairment and Alzheimer disease. Neurology 68: 13–9.
46. Muller MJ, Greverus D, Weibrich C, Dellani PR, Scheurich A, et al. (2007) Diagnostic utility of hippocampal size and mean diffusivity in amnestic MCI. Neurobiol Aging 28: 398–403.
47. Salat DH, Lee SY, Yu P, Setty B, Rosas HD, et al. (2009) DTI in development and aging. In: Johansen-Berg H and Behrens TEJ (eds) Diffusion MRI. From quantitative measurement to in vivo neuroanatomy. Amsterdam, Elsevier/ Academic Press. 205–36.
48. Van Camp N, Blockx I, Verhoye M, Casteels C, Coun F, et al. (2009) Diffusion tensor imaging in a rat model of Parkinson's disease after lesioning of the nigrostriatal tract. NMR Biomed 22: 697–706.
49. Wang HC, Hsu JL, Leemans A (2012) Diffusion Tensor Imaging of Vascular Parkinsonism: Structural Changes in Cerebral White Matter and the Association With Clinical Severity. Arch Neurol 23: 1–9.
50. Yoshikawa K, Nakata Y, Yamada K, Nakagawa M (2004) Early pathological changes in the parkinsonian brain demonstrated by diffusion tensor. Neurol Neurosurg Psychiatry 75: 481–4.
51. Seppi K, Schocke MF, Esterhammer R, Kremser C, Brenneis C, et al. (2003) Diffusion-weighted imaging discriminates progressive supranuclear palsy from PD, but not from the parkinson variant of multiple system atrophy. Neurology 60: 922–7.
52. Tsukamoto K, Matsusue E, Kanasaki Y, Kakite S, Fujii S, et al. (2012) Significance of apparent diffusion coefficient measurement for the differential diagnosis of multiple system atrophy, progressive supranuclear palsy, and Parkinson's disease: evaluation by 3.0 T MR imaging. Neuroradiology 54: 947–55.
53. Vos SB, Jones DK, Viergever MA, Leemans A (2011) Partial volume effect as a hidden covariate in DTI analyses. Neuroimage 55: 1566–76.
54. Knake S, Belke M, Menzler K, Pilatus U, Eqqert KM, et al. (2010) In Vivo Demonstration of Microstructural Brain Pathology in Progressive Supranuclear Palsy: A DTI Study Using TBSS. Mov Disord 25: 1232–8.
55. Whitwell JL, Master AV, Avula R, Kantarci K, Eqqers SD, et al. (2011) Clinical correlates of white matter tract degeneration in progressive supranuclear palsy. Arch Neurol 68: 753–60.
56. Gong G, Jiang T, Zhu C, Zang Y, Wanq F, et al. (2005) Asymmetry analysis of cingulum based on scale-invariant parameterization by diffusion tensor imaging. Hum Brain Mapp 24: 92–8.
57. Lee CEC, Danielian LE, Thomasson D, Baker EH (2009) Normal regional fractional anisotropy and diffusion coefficient of the brain measured on a 3TMR scanner. Neuroradiology 51: 3–9.
58. Kume A, Takahashi A, Hashizume Y (1993) Neuronal cell loss of the striatonigral system in multiple system atrophy. J Neurol Sci 117: 33–40.
59. Wenning GK, Tison F, Ben Shlomo Y, Daniel SE, Quinn NP (1997) Multiple system atrophy: a review of 203 pathologically proven cases. Mov Disord 12: 133–47.
60. Köllensperger M, Geser F, Ndayisaba JP, Boesch S, Seppi K, et al. (2010) Presentation, diagnosis and management of multiple system atrophy in Europe: final analysis of the European multiple system atrophy registry. Mov Disord 25: 2604–12.
61. Brenneis C, Seppi K, Schocke M, Benke T, Wenning GK, et al. (2004) Voxel based morphometry reveals a distinct pattern of frontal atrophy in progressive supranuclear palsy. J Neurol Neurosurg Psychiatry 75: 246–9.
62. Cordato NJ, Duggins AJ, Halliday GM, Morris JG, Pantelis C (2005) Clinical deficits correlate with regional cerebral atrophy in progressive supranuclear palsy. Brain 128: 1259.
63. Kamagata K, Motoi Y, Tomiyama H, Abe O, Ito K, et al. (2013) Relationship between cognitive impairment and white-matter alteration in Parkinson's disease with dementia: tract-based spatial statistics and tract-specific analysis. Eur Radiol 13: In press.
64. Hattori T, Orimo S, Aoki S, Ito K, Abe O et al. (2012) Cognitive status correlates with white matter alteration in Parkinson's disease. Hum Brain Mapp 33: 727–39.
65. Kamagata K, Motoi Y, Abe O, Shimoji K, Hori M et al. (2012) White matter alteration of the cingulum in Parkinson disease with and without dementia: evaluation by diffusion tensor tract-specific analysis. Am J Neuroradiology 33: 890–95.
66. Hughes AJ, Daniel SE, Ben Shlomo Y, Lees AJ (2000) The accuracy of diagnosis of parkinsonian syndromes in a specialist movement disorder service. Brain 125: 861–70.
67. Jeurissen B, Leemans A, Tournier JD, Jones DK, Sijbers J (2012) Investigating the prevalence of complex fiber configurations in white matter tissue with diffusion magnetic resonance imaging. Hum Brain Mapp 19. doi: 10.1002/ hbm.22099.
68. Vos SB, Jones DK, Jeurissen B, Vierqever MA, Leemans A (2012) The influence of complex white matter architecture on the mean diffusivity in diffusion tensor MRI of the human brain. Neuroimage 59: 2208–16.
69. Descoteaux M, Deriche R, Knösche TR, Anwander A (2009) Deterministic and probabilistic tractography based on complex fibre orientation distributions. IEEE Trans Med Imaging 28: 269–86.
70. Jeurissen B, Leemans A, Jones DK, Tournier JD, Sijbers J (2011) Probabilistic fiber tracking using the residual bootstrap with constrained spherical deconvolution. Hum Brain Mapp 32: 461–79.
71. Wedeen VJ, Wang RP, Schmahmann JD, Benner T, Tsenq WY, et al. (2008) Diffusion spectrum magnetic resonance imaging (DSI) tractography of crossing fibers. Neuroimage 41: 1267–77.
72. Hrabětová S, Nicholson C (2007) Biophysical Properties of Brain Extracellular Space Explored with Ion-Selective Microelectrodes, Integrative Optical Imaging and Related Techniques. In: Michael AC, Borland LM, editors. Electrochemical Methods for Neuroscience. Boca Raton (FL): CRC Press; Chapter 10.
73. Douaud G, Jbabdi S, Behrens TE, Menke RA, Gass A, et al. (2011) DTI measures in crossing-fibre areas: increased diffusion anisotropy reveals early white matter alteration in MCI and mild Alzheimer's disease. Neuroimage 55: 880–90.
74. Deprez S, Billiet T, Sunaert S, Leemans A (2013) Diffusion tensor MRI of chemotherapy-induced cognitive impairment in non-CNS cancer patients: a review. Brain Imaging Behav 18: In press.

Paper II

Neuroradiology
DOI 10.1007/s00234-015-1563-z

DIAGNOSTIC NEURORADIOLOGY

Disease-specific structural changes in thalamus and dentatorubrothalamic tract in progressive supranuclear palsy

Yulia Surova[1,2] · Markus Nilsson[3] · Jimmy Lätt[4] · Björn Lampinen[5] · Olof Lindberg[6] · Sara Hall[1,2] · Håkan Widner[1,2] · Christer Nilsson[2,6] · Danielle van Westen[1,4] · Oskar Hansson[6,7]

Received: 28 April 2015 / Accepted: 12 July 2015

Abstract
Introduction The aim of this study is to identify disease-specific changes of the thalamus, basal ganglia, pons, and midbrain in patients with progressive supranuclear palsy (PSP), Parkinson's disease (PD), and multiple system atrophy with predominant parkinsonism (MSA-P) using diffusion tensor imaging and volumetric analysis.
Methods MRI diffusion and volumetric data were acquired in a derivation of 30 controls and 8 patients with PSP and a validation cohort comprised of controls (n=21) and patients with PSP (n=27), PD (n=10), and MSA-P (n=11). Analysis was performed using regions of interest (ROI), tract-based spatial statistic (TBSS), and tractography and results compared between diagnostic groups.
Results In the derivation cohort, we observed increased mean diffusivity (MD) in the thalamus, superior cerebellar peduncle, and the midbrain in PSP compared to controls. Furthermore, volumetric analysis showed reduced thalamic volumes in PSP. In the validation cohort, the observations of increased MD were replicated by ROI-based analysis and in the thalamus by TBSS-based analysis. Such differences were not found for patients with PD in any of the cohorts. Tractography of the dentatorubrothalamic tract (DRTT) showed increased MD in PSP patients from both cohorts compared to controls and in the validation cohort in PSP compared to PD and MSA patients. Increased MD in the thalamus and along the DRTT correlated with disease stage and motor function in PSP.
Conclusion Patients with PSP, but not PD or MSA-P, exhibit signs of structural abnormalities in the thalamus and in the DRTT. These changes are associated with disease stage and impaired motor function.

Keywords Diffusion tensor imaging · Tractography · Tract-based spatial statistics · Progressive supranuclear palsy

✉ Yulia Surova
yulia.surova@med.lu.se

[1] Department of Clinical Sciences, Lund University, Lund, Sweden
[2] Department of Neurology, Skåne University Hospital, 221 85 Lund, Sweden
[3] Lund University Bioimaging Center, Lund University, Lund, Sweden
[4] Center for Medical Imaging and Physiology, Skåne University Hospital, Lund, Sweden
[5] Department of Medical Radiation Physics, Lund University, Lund, Sweden
[6] Department of Clinical Sciences, Malmö, Lund University, Malmö, Sweden
[7] Memory Clinic, Skåne University Hospital, Lund, Sweden

Introduction

Progressive supranuclear palsy syndrome (PSP) is a slowly progressing fatal neurodegenerative disease with characteristic neuropathological features including the formation of tau-containing neurofibrillary tangles and neuropil threads in the basal ganglia and brainstem structures [1–3]. According to neuropathological studies, the highest level of tau-pathology in PSP is found in the substantia nigra, globus pallidus, subthalamic nucleus, red nucleus (RN), brainstem tegmentum, and dentate nucleus [4, 5]. The thalamus often also exhibits neuronal loss and gliosis, in particular, the ventral anterior (VA) and ventral lateral (VL) thalamic nuclei [6]. PSP can often be difficult to distinguish clinically from other movement disorders, e.g., Parkinson's disease (PD), multiple

Published online: 08 August 2015

system atrophy (MSA), and corticobasal degeneration (CBD), especially during early stages due to overlapping symptomatology. Patients with PSP exhibit motor symptoms, such as early development of postural instability, falls and rigidity and bradykinesia, as well as cognitive symptoms [3]. Fluorodeoxyglucose positron emission tomography (FDG-PET) has indicated reduced metabolism in the caudate nucleus, thalamus, and midbrain in PSP with thalamic hypometabolism correlating with impaired balance [7–9].

Diffusion tensor imaging (DTI) with estimation of parameters fractional anisotropy (FA) and mean diffusivity (MD) [10] has been used to study potential microstructural changes indicating neuronal pathway loss in the basal ganglia, midbrain, and pons in patients with PSP. Increased values of MD have been found in the thalamus, putamen, dorsal pons, and midbrain in PSP compared with controls [11–13]. Reduced values of FA have been observed in some white matter tracts, such as the superior cerebellar peduncles (SCP), corpus callosum, and inferior longitudinal fasciculus, as well as in the thalamus [14] with DTI parameters in the SCP differentiating PSP from other neurodegenerative diseases such as PD, MSA, and CBD [15–17].

Here, we aim at extending the previously reported findings of microstructural changes in subcortical structures by comparing diffusion parameter estimates from patients with PSP, MSA and PD, and controls and relating these findings to clinical symptoms. Two cohorts, with images acquired in different scanners with different protocols, were used in order to be able to study the reproducibility of the results, especially as the cohorts were quite modest in size. DTI parameters were quantified in the caudate head, putamen, and whole thalamus, as well as separately in some thalamic nuclei, the RN, SCP, deep cerebellar nuclei, pons, and midbrain, using region of interest (ROI) analysis, as well as in the dentatorubrothalamic tract (DRTT) [18] using tractography. Furthermore, tract-based spatial statistics (TBSS) analysis was employed to compare DTI parameters in the thalamus. Seemingly, we investigated whether the changes in DTI parameters were associated with severity of motor symptoms. We demonstrate specific diffusion changes in the thalamus and DRTT in patients with PSP that correlate with an increase in disease severity and worsening of motor function.

Materials and methods

Subjects

The derivation cohort included 38 subjects, 8 patients with probable PSP that were diagnosed according to the National Institute of Neurological Disorders and Stroke (NINDS) criteria [3], and 30 healthy age- and sex-matched controls. Healthy controls had no previous neurologic or psychiatric diseases. Adjunctive inclusion criteria for patients with PSP were a poor or absent response to levodopa. All patients were recruited at Skåne University Hospital. Patients and controls were evaluated using clinical assessments, among these, the Hoehn and Yahr staging scale (H&Y) [19], the Schwab and England activities of daily living scale (S&E) [20], as well as the Unified Parkinson's Disease Rating Scale (UPDRS)-3 [21] on the on stage. The tandem gait test [22] was included to assess disturbances in balance. Cognitive function was assessed by Mini Mental State Examinations (MMSE) [23] and The Quick Test of Cognitive Speed (AQT) [24]. In addition, the PSP rating scale (PSPRS) was administered to PSP patients [25]. Patients were evaluated three times at typical intervals of 2 years, but here, we report on the PSPRS score closest to the MRI scan date (Table 1). The PSPRS comprises 28 items in six areas, the History and daily activities, the Mentation, the Bulbar, the Ocular motor, the Limb motor, and the Gate and midline with the total score ranging from 0 (normal) to 100. There was no attempt to evaluate patients off medication.

In the validation cohort, participants were recruited from the Neurology and Memory Clinics at Skåne University Hospital, Sweden, between 2008 and 2011. For the present work, 69 subjects were included, with a clinical diagnosis of probable PD (n=10), probable PSP (n=27), or probable MSA-P (parkinsonian variant of MSA) (n=11). In addition, neurologically healthy controls were recruited (n=21). Clinical diagnosis was assessed by neurologists experienced in parkinsonian disorders according to NINDS criteria [3, 26, 27]. Postmortem diagnoses were available from one PSP and one MSA-P cases. Controls, age- and sex-matched, were recruited from the Swedish population registry and had no previous neurologic or psychiatric diseases. The H&Y [19] and the S&E [20] were assessed retrospectively from medical records, without any information about on/off state during visit to doctor.

Since vascular lesions could mimic parkinsonism or be subclinical in healthy subjects, patients with anatomic MRI abnormalities and vascular lesions in midbrain and basal ganglia were ruled out by an experienced neuroradiologist who evaluated MRI scans for each subject in both cohorts.

Data acquisition and processing

In the derivation cohort, imaging was performed using a 3 T Siemens Skyra MR scanner equipped with a 20 channel head coil. The DTI data were collected using a single-shot EPI (TE/TR 70/7500 ms/ms) sequence with diffusion encoding in 30 directions using b values of 0 and 1000 s/mm^2, IPAT factor of 2, voxel size of $2\times2\times2$ mm^3, with an acquisition time 4 min 15 s. In the validation cohort, imaging was performed

Table 1 Case demographics, brainstem measurements, and volumetric data for controls and cases of two cohorts

	Derivation cohort			Validation cohort				
	CTR (*n*=30)	PSP (*n*=8)	*P*	CTR (*n*=21)	PD (*n*=10)	PSP (*n*=27)	MSA-P (*n*=11)	*P*
Gender female:male	16:14	4:4	0.59[a]	9:12	4:6	13:14	7:4	0.68[a]
Age, years	69 (67–72)	70 (68–75)	0.38[c]	69 (65–76)	68 (59–70)	68 (65–71)	64 (56–76)	0.21[b]
Disease duration, years	n.d.	5 (4–7)		n.d.	4 (2–7)	3 (2–4)	3 (3–5)	0.54[b]
Hoehn and Yahr	0	4 (3–5)		0	2 (1–3)	3 (3–4)	3 (3–4)	≤0.00[bdf]
Schwab and England, IQL	100	55 (22–87)	≤0.00[c]	100	90 (90–100)	70 (60–80)	70 (70–80)	≤0.00[bcdefh]
Pons area, mm^2	525 (490–546)	434 (402–527)	0.01[c]	531 (505–556)	519 (477–536)	474 (418–515)	485 (429–522)	≤0.00[bce]
Midbrain area, mm^2	108 (97–126)	71 (46–80)	0.00[c]	117 (103–126)	116 (108–161)	63 (55–71)	113 (103–132)	≤0.00[bcdg]
Midbrain/pons ratio	0.21 (0.19–0.25)	0.16 (0.11–0.18)	<0.001[c]	0.21 (0.20–0.24)	0.24 (0.21–0.31)	0.14 (0.12–0.15)	0.22 (0.21–0.25)	≤0.00[bcdg]
Thalamus, cm^3	9.3±0.7	7.9±0.5	<0.001[c]	8.7±0.7	10.1±1.0	8.3±1.3	8.9±1.1	<0.01[dh]
Caudate nucleus, cm^3	4.4±0.4	3.7±0.4	0.001[c]	4.4±4.5	4.7±6.6	4.2±0.8	4.0±0.6	0.23[b]
Putamen, cm^3	5.7±0.5	4.7±0.5	0.001[c]	5.5±0.6	6.1±0.7	4.7±1.2	4.6±0.7	<0.01[def]
Globus pallidus, cm^3	2.2±0.2	1.7±0.4	0.001[c]	2.2±0.5	2.2±0.2	1.8±0.6	1.8±0.6	<0.01[cdf]
UPDRS motor score, IQL	0 (0–2)	43 (32–57)	<0.001[c]	n.d.	n.d.	n.d.	n.d.	
Tandem gait test, IQL	0	3 (2–3)	<0.001[c]	n.d.	n.d.	n.d.	n.d.	
MMSE score, IQL	29 (28–30)	26 (20–27)	<0.001[c]	n.d.	n.d.	n.d.	n.d.	
AQT color-form, sec	62 (57–68)	218 (90–296)	<0.001[c]	n.d.	n.d.	n.d.	n.d.	

All values expressed as medians, values in parenthesis indicate 25–75th percentiles, except volumetric measurement, which expressed as mean±standard deviation

Abbreviations: *PD* Parkinson's disease, *PSP* progressive supranuclear palsy, *MSA-P* multiple system atrophy, parkinsonian variant, *CTR* healthy controls, *MMSE* Mini Mental State Examination, *AQT* Quick Test of Cognitive Speed, *UPDRS* Unified Parkinson's Disease Rating Scale

[a] Fisher's exact test

[b] Kruskal-Wallis test, controls were excluded from the group comparisons of disease duration and Hoehn and Yahr scale

[c] PSP/CTR

[d] PSP/PD

[e] MSA-P/CTR

[f] MSA-P/PD

[g] MSA-P/PSP

[h] PD/CTR. Mann–Whitney *U* test

using a 3 T Philips Achieva MR scanner, equipped with an eight-channel head coil. DTI data were collected using a single-shot EPI sequence (TE/TR 90/7840 ms/ms) with diffusion encoding in 48 directions, *b* values of 0 and 800 s/mm^2, and SENSE factor of 2.5; 60 slices were acquired with voxel size 2×2×2 mm^3. The lower *b* value in the validation cohort was used to reduce the acquisition time. However, this will result in slightly higher values for MD [28] and thus values for MD from the derivation and validation cohorts are expected to differ. Subject motion and eddy-current correction was performed using ElastiX [29], and parameter maps were calculated using in-house developed software. For tractography, data was processed using MRtrix (Brain Research Institute, Melbourne, Australia, http://www.brain.org.au/software/) [30], including constrained spherical deconvolution (CSD) to model multiple fiber orientations in each voxel.

Volumetric data were acquired in the derivation cohort using a MPRAGE sequence with TR/TE 7/3 ms, flip angle 9°, resolution 1×1×1 mm^3 and in validating cohort using a T1-weighted TFE sequence with TR/TE 8/4 ms, flip angle 10°, resolution 1×1×1 mm^3.

Analysis of diffusion parameters

a) ROI-based analysis

For ROI-based estimation of diffusion parameters, ROIs were outlined manually on parameter maps by one trained investigator (YS). All ROIs were outlined twice with an interval of 3 months (average intra-rater variability >0.9 for all ROIs). FA- and directionally color-encoded FA maps were used to outline all ROIs, except for the RN and deep cerebellar nuclei (DCN), where the non-diffusion-weighted map was used (Fig. 1). The ROI size was adjusted in each subject to maximize coverage of each structure, while minimizing partial volume effects from neighboring areas. Contamination from cerebrospinal fluid (CSF), which has isotropic diffusion with a high MD, was avoided by excluding voxels adjacent to the third and lateral ventricles.

The head of the caudate nucleus was delineated in a single slice at the level where it was most conspicuous. The thalamus and putamen were delineated in 5–8 consecutive slices at the level of the internal capsule, the thalamus adjacent to the interthalamic adhesion, and the putamen to the extreme capsule. The VA and VL nuclei of the thalamus (VAVL) were identified on FA color maps as green voxels (Fig. 1) [31, 32], in the anterior part of the lateral thalamus close to the genu of the internal capsule, while excluding the three most medial voxels that were regarded to comprise the medial dorsal nuclei. The lateral posterior nucleus (LP) and ventral posterior (VP) nuclear complex of the thalamus (LPVP) were identified on FA color maps as violet voxels (Fig. 1) [31, 32] adjacent to the posterior limb of the internal capsule and anterior to the pulvinar in red. The RN was identified as a circular area of signal hypointensity in the midbrain on non-diffusion-weighted maps and delineated in at least two consecutive axial slices. The SCP was delineated on two consecutive sagittal slices. The midbrain and the pons were delineated on five consecutive sagittal

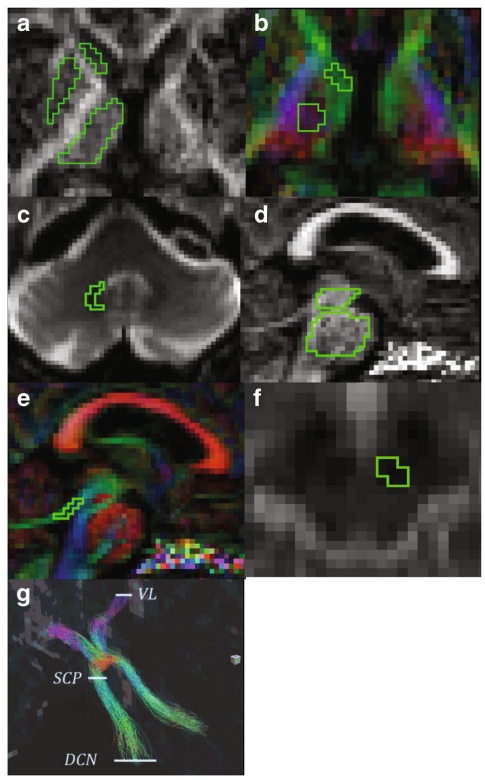

Fig. 1 Region of interests in subcortical structures and the superior cerebellar peduncle and tractography of the dentatorubrothalamic tract. Region of interests (ROIs) are placed in **a** the putamen, caudate head, thalamus; **b** the ventral anterior and ventral lateral nuclei of the thalamus (VL), *green colored voxels* and the lateral posterior nucleus and ventral posterior nuclear complex of the thalamus, *violet colored voxels*; **c** the red nucleus; **d** the pons and midbrain; **e** superior cerebellar peduncle (SCP); **f** deep cerebellar nuclei (DCN); **g** the left and right dentatorubrothalamic tract defined by ROIs were placed in DCN, SCP, and contralateral VL

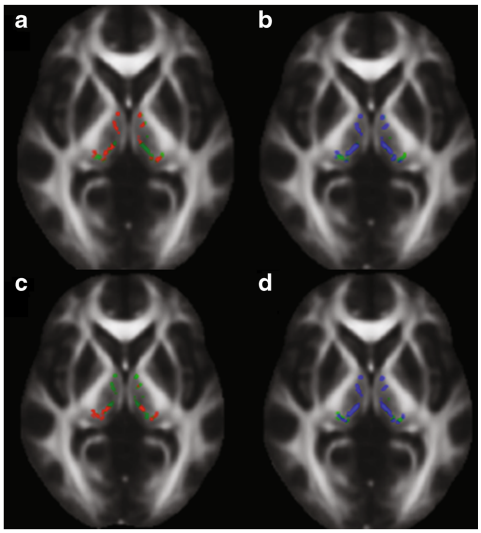

Fig. 2 Areas in thalamus with significantly decreased fractional anisotropy and increased mean diffusivity in patients with progressive supranuclear palsy when compared to healthy controls. Results of the tract-based spatial statistics (TBSS) analysis in the thalamus, showing regions of significant decreased fractional anisotropy (*red voxels*) and increased mean diffusivity (*blue voxels*) in patients with progressive supranuclear palsy when compared to healthy controls. **a** and **b** correspond to the derivation cohort, while **c** and **d** correspond to the validation cohort. *Green voxels* are voxels on the TBSS-skeleton where no significance was found

slices, with ROIs including the whole structure. The manual approach proposed by Oba et al. [33] was used to identify the boundaries of the pons and the midbrain. For each structure, the average FA and MD value from the right and left hemisphere was calculated.

b) tract-based spatial statistics analysis

TBSS (v 1.03), part of the FRMIB Software Library (FSL), was employed as a complementary analysis tool for diffusion parameters in the thalamus. Comparisons were performed in PSP vs controls in the derivation cohort and in PSP vs controls, PD and MSA-P in the validation cohort (Fig. 2) [34]. FA and MD maps were registered onto the 1 mm^3 FMRIB58 FA template in MNI152 standard space, using the linear and nonlinear registration tools FLIRT and FNIRT [35, 36]. Before registration, the diffusion maps were masked with the FSL Brain Extraction Tool (BET) [37]. The normalized maps were skeletonized by projection onto the FMRIB58 template skeleton. Finally, the skeletonized maps were masked to include only voxels from the thalamus. The masking was done using the left and right thalamus regions in the MNI152 space Harvard-Oxford subcortical atlas, together with the requirement that the MD of the normalized maps must be less than unity in the control subjects of the derivation cohort [38].

c) Tractography of the DRTT

For probabilistic tractography of the DRTT, its inferior and superior part were constructed each using a seed ROI placed in the DCN and VAVL of the contralateral thalamus, respectively, and an include ROI in the SCP (Fig. 1). The left and right DRTT were then constructed by combining the inferior and superior DRTT into one tract, selecting fibers passing through include ROIs in these three locations, DCN, SCP, and VAVL. All tracts were visually inspected. The tractography procedure did not generate tracts in two controls from the derivation cohort (unilaterally) as well as in four PSP patients (one patient bilaterally and three unilateral) and one control (unilateral) in the validation cohort.

Volumetric analysis

The diameter and area of the midbrain and pons, the midsagittal slice were assessed according to Oba [33]. Thus, measurements included the antero-posterior diameter of the midbrain (AP-diameter), the distance between the interpeduncular fossa, and the aqueduct in the midbrain proper without the quadrigeminal plate (IF-AQ-diameter), the surface of the pons (P-area), and the surface of the midbrain (M-area) [33, 39]. The P/M ratio was calculated as the ratio of the P-area to the M-area. Measurements were performed twice and median values were used.

Automated volumetric measurement was performed with FIRST [40]. Correction for intracranial volume (ICV) was achieved by multiplying each volume with the scaling factor that estimates the scaling between the subject's image and standard space and that is provided by the sienax toolbox [41]. The mean volume of the right and left thalamus, caudate nucleus, putamen, and globus pallidus were used.

Statistical analysis

Statistical analysis was performed with SPSS Statistics 20 for Windows (IBM Corporation, Somers, NY, USA). Within each cohort, differences between groups in demographic and clinical categorical variables were analyzed using the Fisher's exact test for dichotomized data and Kruskal-Wallis test

followed by Mann–Whitney *U* test for continuous data. Correlation between diffusion parameters and clinical scores was tested using Spearman correlation (Spearman's Rho). The level of significance was set to $P<0.05$ in the derivation and $P<0.008$ in the validation cohorts. An adjustment for multiple comparisons between the 4 control/patient categories (i.e., 6 comparisons) was made in the validation cohort, leading to an adjusted significance level of $P=0.008$ using Bonferroni correction. Correlation between diffusion parameters and PSPRS items was tested with linear logistic regression. Adjustment for age was performed by binary logistic regression analysis with diffusion parameter values that were significantly different between groups, based on the results of Mann–Whitney *U* test. For comparison between PSP and controls, effect sizes were computed in the form of differences in diffusional parameters group means.

To study the ability of DTI and DTT measurements to distinguish PSP from controls, MSA-P and PD in the validation cohort, receiver operator characteristic curve analysis (ROC) was performed.

Statistical processing of TBSS data was performed using Threshold-Free Cluster Enhancement of FSL Randomize (v 2.9), with 7500 permutations for the null distribution [42]. Finally, for each comparison and diffusion parameter, we computed effect sizes in the form of difference in group means in the skeletonized space in the thalamus region.

Results

Demographics

Demographic clinical data of patients and controls in both cohorts are reported in Table 1. Study participants of the derivation cohort were more extensively characterized compared to the validation cohort. Age, gender, and disease duration were similar in the PD, MSA-P, and PSP groups in both cohorts; however, patients with PSP and MSA-P were more disabled compared to controls as well as patients with PD.

Diffusion parameters

a) Region of interests based analysis

In the derivation cohort, we found that patients with PSP have increased MD in the whole thalamus, the thalamic nuclei (VAVL and LPVP), and the midbrain (Table 2). Significant changes of MD (increase with 9–12 %) were found in the caudate head, thalamus, VAVL, LPVP, and midbrain. Values of FA were reduced with 12–19 % for the SCP and midbrain in PSP patients.

In the validation cohort, patients with PSP showed higher MD values in the whole thalamus, the VAVL nuclei of the thalamus and the midbrain compared to controls, patients with PD, and patients with MSA-P (Table 2). Patients with MSA-P displayed higher MD values in the pons than controls and patients with PD but not compared to patients with PSP (Table 2). The values of MD in PSP were increased with 6–9 % in the putamen, thalamus, VAVL, LPVP, and pons and with 12–15 % for midbrain, SCP, and red nucleus. Values of FA in PSP were reduced with 5–6 % in the putamen and VAVL, with 11–15 % in midbrain and SCP.

In the patients with PSP, MD changes in the thalamus did not correlate with volumetric measurements in any of the cohorts.

b) tract-based spatial statistics analysis

In the derivation cohort, PSP patients showed significantly higher MD than controls in 75 % of the skeletonized voxels in the thalamus (Fig. 2). In the validation cohort, patients with PSP were found to have a higher MD in the thalamus than controls (75 % significant voxels). In the derivation cohort, a higher MD was also found in the PSP group compared to both PD (67 % significant voxels) and MSA-P (53 % significant voxels). Furthermore, a reduced FA was observed in PSP vs controls in both cohorts and in PSP vs IPD in the derivation cohort (30–50 % significant voxels).

c) Tractography of the DRTT

As many of the changes in diffusion parameters in patients with PSP observed above were localized in structures associated with the DRTT (i.e., SCP, midbrain, and ventral thalamus); probabilistic tractography of this tract was performed. In the derivation cohort, elevation in MD and reduction of FA was seen in patients with PSP, even though it only reached significance on the right side ($P<0.05$) (Table 2 and Fig. 3c, d). Value of FA was reduced with 19 %, and value of MD was increased with 14 % for right DRTT in PSP patients. Similar to the derivation cohort, tractography of the DRTT in patients with PSP in the validation cohort exhibited reduced FA and increased MD in the DRTT on both sides when compared to both controls and patients with PD or MSA-P (Table 2 and Fig. 3a, b). The values of FA were reduced with 21–28 %, and values

Table 2 Regional fractional anisotropy and mean diffusivity values in two cohorts

Region	Parameter	Derivation cohort		Validation cohort			
	FA	CTR	PSP	CTR	PD	PSP	MSA-P
Caudate head		0.16 (0.14–0.18)	0.18 (0.15–0.20)	0.16 (0.14–0.20)	0.17 (0.14–0.19)	0.18 (0.15–0.20)	0.16 (0.15–0.21)
Putamen		0.15 (0.14–0.17)	0.16 (0.13–0.19)	0.19 (0.17–0.20)	0.20 (0.18–0.22)	0.18 (0.17–0.20)[c]	0.22 (0.20–0.24)
Thalamus		0.29 (0.28–0.31)	0.28 (0.25–0.30)	0.32 (0.30–0.33)	0.31 (0.30–0.33)	0.30 (0.29–0.33)	0.31 (0.29–0.33)
VAVL		0.28 (0.26–0.30)	0.27 (0.24–0.30)	0.31 (0.30–0.33)	0.32 (0.29–0.34)	0.29 (0.26–0.32)[a]	0.31 (0.29–0.33)
LPVP		0.27 (0.25–0.29)	0.26 (0.24–0.28)	0.29 (0.26–0.32)	0.31 (0.29–0.33)	0.31 (0.29–0.33)	0.31 (0.29–0.35)
Red nucleus		0.45 (0.40–0.52)	0.45 (0.40–0.51)	0.54 (0.49–0.58)	0.53 (0.47–0.54)	0.50 (0.45–0.56)	0.51 (0.43–0.56)
SCP		0.66 (0.62–0.68)	0.54 (0.42–0.70)[a]	0.78 (0.75–0.82)	0.79 (0.71–0.84)	0.66 (0.60–0.71)[bc]	0.75 (0.73–0.76)
Pons		0.35 (0.34–0.38)	0.33 (0.32–0.36)	0.41 (0.39–0.46)	0.40 (0.37–0.44)	0.39 (0.36–0.42)	0.39 (0.34–0.39)
Midbrain		0.40 (0.36–0.42)	0.35 (0.30–0.38)[a]	0.45 (0.43–0.48)	0.47 (0.45–0.48)	0.40 (0.38–0.43)[abc]	0.45 (0.43–0.49)
DRTT left		0.38 (0.33–0.39)	0.33 (0.25–0.38)	0.38 (0.35–0.40)	0.39 (0.36–0.41)	0.30 (0.27–0.34)[abc]	0.37 (0.31–0.38)
DRTT right		0.37 (0.33–0.40)	0.30 (0.26–0.35)[a]	0.36 (0.33–0.37)	0.38 (0.36–0.44)	0.26 (0.24–0.29)[abc]	0.32 (0.31–0.36)[c]
	MD						
Caudate head		0.68 (0.66–0.73)	0.74 (0.63–0.79)[a]	0.79 (0.76–0.87)	0.81 (0.77–0.91)	0.82 (0.75–0.96)	0.76 (0.68–0.85)
Putamen		0.68 (0.64–0.71)	0.70 (0.66–0.76)	0.81 (0.75–0.86)	0.78 (0.76–0.86)	0.86 (0.80–0.96)[a]	0.88 (0.84–1.04)[ed]
Thalamus		0.71 (0.69–0.73)	0.79 (0.71–0.89)[a]	0.79 (0.75–0.82)	0.77 (0.76–0.81)	0.84 (0.79–0.88)[abc]	0.78 (0.77–0.80)
VAVL		0.72 (0.70–0.74)	0.81 (0.71–0.89)[a]	0.79 (0.76–0.81)	0.79 (0.77–0.83)	0.86 (0.82–0.93)[abc]	0.80 (0.76–0.83)
LPVP		0.70 (0.68–0.72)	0.77 (0.71–0.93)[a]	0.76 (0.72–0.81)	0.71 (0.70–0.75)	0.81 (0.76–0.89)[bc]	0.74 (0.74–0.75)
Red nucleus		0.48 (0.43–0.53)	0.55 (0.42–0.59)	0.53 (0.45–0.60)	0.53 0.48–0.58)	0.61 (0.55–0.68)[a]	0.61 (0.52–0.62)
SCP		0.82 (0.76–0.86)	0.85 (0.79–1.11)	0.83 (0.76–0.88)	0.82 (0.76–0.89)	0.94 (0.90–1.10)[ab]	0.92 (0.87–0.97)[d]
Pons		0.63 (0.60–0.66)	0.65 (0.62–0.70)	0.72 (0.70–0.75)	0.72 (0.70–0.75)	0.76 (0.72–0.79)[a]	0.75 (0.75–0.78)[de]
Midbrain		0.68 (0.66–0.72)	0.74 (0.71–0.81)[a]	0.74 (0.73–0.76)	0.73 (0.71–0.76)	0.83 (0.80–0.85)[abc]	0.75 (0.70–0.78)
DRTT left		0.89 (0.84–0.93)	1.02 (0.86–1.18)	1.1 (1.02–1.15)	1.03 (0.97–1.11)	1.37 (1.27–1.52)[abc]	1.21 (1.02–1.23)[c]
DRTT right		0.87 (0.80–0.93)	0.99 (0.82–1.07)[a]	1.16 (1.05–1.20)	1.06 (0.99–1.10)	1.50 (1.34–1.55)[abc]	1.22 (1.16–1.30)[c]

MD (10^–3 mm^2/s). All values expressed as medians, values in parenthesis indicate 25–75th percentiles. FA values in caudate head and putamen are low and should therefore be interpreted with caution

Abbreviations: *FA* fractional anisotropy, *MD* mean diffusivity, *VAVL* ventral anterior and ventral lateral nuclei of the thalamus, *LPVP* lateral posterior nucleus and ventral posterior nuclear complex of the thalamus, *SCP* superior cerebellar peduncle, *DRTT* dentatorubrothalamic tract, *PD* Parkinson's disease, *PSP* progressive supranuclear palsy, *MSA-P* multiple system atrophy, parkinsonian variant, *CTR* healthy control

[a] PSP/CTR

[b] PD/PSP

[c] PSP/MSA-P

[d] MSA-P/CTR

[e] MSA-P/PD. Mann–Whitney *U* test

of MD in PSP were increased with 24–29 % in the left and right DRTT.

Volumetric measurements

The volumes of the thalamus, the putamen, and the globus pallidus were reduced in patients with PSP in both cohorts (Table 1). The midbrain area was reduced in patients with PSP when compared to PD, MSA-P, and control subjects (Table 1). In patients with MSA-P (validation cohort only), the volumes of the putamen and the globus pallidus were reduced (Table 1). Only the thalamic volume and the midbrain area were specifically reduced in PSP.

Correlation between clinical scales and diffusion parameters of thalamus and dentatorubrothalamic tract in progressive supranuclear palsy

In the derivation cohort, increased MD in the whole thalamus, VAVL, and LPVP correlated with increased disease stage (H&Y) and with reduced rating scores of activities of daily living (S&E) (Spearman's Rho=−0.732–0.756, $P<0.05$). Very similar findings were obtained in the validation cohort. There was a negative correlation between MD and disease

stage (H&Y) in PSP patients in the validation cohort, similar to that in the derivation cohort, for values obtained in the whole thalamus and in the VAVL nuclei (Spearman's Rho= 0.456 and 0.431, P=0.017 and P=0.025, respectively). Further, higher MD in the LPVP correlated negatively with functional measures of activity of daily living (S&E) (Spearman's Rho=−0.467 and −0.489, P=0.014 and P= 0.010, respectively).

The thalamic volume correlated with neither S&E nor H&Y (both cohorts).

In the derivation cohort, the patients with PSP were also assessed with other clinical rating scales including UPDRS and the PSP rating scale. We found that worse motor performance (UPDRS-3) was associated with increased MD in the whole thalamus, VAVL, and LPVP (Spearman's Rho=0.714–0.772, P<0.05) and reduced FA in the whole thalamus

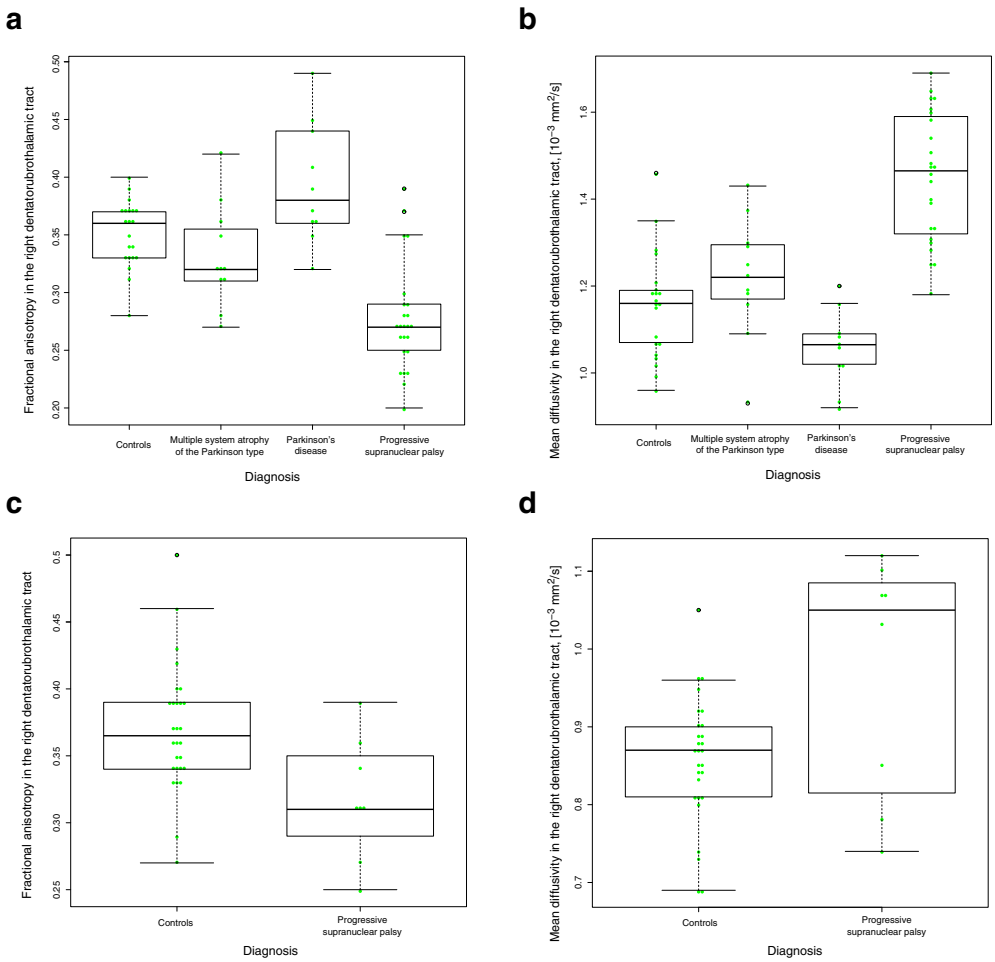

Fig. 3 Fractional anisotropy and mean diffusivity in dentatorubrothalamic tract in derivation and validation cohorts. **a** Fractional anisotropy values in the right dentatorubrothalamic tract validation cohort. **b** Mean diffusivity values in the right dentatorubrothalamic tract validation cohort, [10^–3 mm^2/s]. **c** Fractional anisotropy values in the right dentatorubrothalamic tract derivation cohort. **d** Mean diffusivity values in the right dentatorubrothalamic tract derivation cohort, [10^–3 mm^2/s]

(Spearman's Rho=−0.762, P=0.028). Impaired balance (Tandem Gait Test) correlated with increased MD in the whole thalamus, VAVL, LPVP, but also with MD in the right DRTT (Spearman's Rho=0.791–0.828, P<0.05). Further, we found significant correlations between diffusion changes in thalamus (whole thalamus and VAVL) and the items in the PSP rating scale (Table 3). As depicted in Fig. 4, linear regression showed highly significant positive linear correlation between MD in the thalamus in patients with PSP and the PSP rating scale total score and strong negative linear relationship between FA in the thalamus in PSP and the PSP rating scale total score.

Diagnostic accuracy of diffusion parameters of the midbrain, dentatorubrothalamic tract, and thalamus in progressive supranuclear palsy

Diffusion parameters from the validation cohort, that showed the most extensive differences between PSP and other diagnostic groups, were tested separately in the ROC analysis for diagnostic accuracy (Table 4).

When using the MD in the midbrain, we found that it could differentiate PSP from controls with an area under the curve (AUC) of 0.86 (Table 4), PSP from MSA-P and PD with an AUC of 0.90 (Table 4), and PSP from all groups of 0.88 (Table 4).

When using the MD in the right DRTT, we found that it could differentiate PSP from controls with an AUC of 0.95 (Table 4). Similar results were obtained when PSP separated from MSA-P and PD (Table 4) and when PSP separated from all groups (Table 4).

When using MD in the thalamus, we found that it could differentiate PSP from controls with an AUC of 0.77 (Table 4). Similar results were obtained when PSP separated from MSA-P and PD (Table 4) and when PSP separated from all groups (Table 4).

Discussion

We have performed a study comprising two cohorts with similar demographic characteristics, comparing DTI and volumetric measurements. We derived and validated changes of MD in the thalamus, in the VAVL and LVLP thalamic nuclei and in the DRTT in PSP. Importantly, these changes were specific for PSP and correlated highly with the PSP rating scale. Furthermore, these changes were not correlated with the atrophy of thalamus and seem associated with worse motor symptoms and impaired balance.

Neurodegeneration of the thalamic nuclei in PSP has been described in a few small autopsy studies [6, 43, 44]. Tau-containing neurofilaments (NFTs) have been shown in many nuclei of the thalamus in patients with PSP. In some cases, the loss of nerve cells was severe in the dorsal part of lateral and ventral nuclei with concomitant fibrillary gliosis. Further, a comparative neuropathological study comparing cases with PD and PSP found tau-pathology in all ventral thalamic nuclei in PSP with neuronal loss most evident in the ventrolateral posterior nuclei [45]. In vivo, DTI changes in PSP have previously been shown in the thalamus when compared to controls [12, 14, 17]. Our results corroborate these findings and further suggest that changes of MD in the thalamus, in the VAVL, and LVLP thalamic nuclei are specific for PSP when compared to the other major parkinsonian disorders such as PD and MSA-P.

The present findings of changes of DTI parameters in the SCP, midbrain, and ventral thalamic nuclei in PSP suggested structural damage along the DRTT. The DRTT projects from the dentate nucleus of the cerebellum, through the SCP toward the red nucleus (with axon collaterals to this nucleus) and then proceeds superiorly to the contralateral ventral lateral and anterior nuclei of the thalamus. Degeneration of DRTT has previously been shown neuropathologically in 10 cases with PSP where degeneration and activated microglia along this tract

Table 3 Spearman's correlation coefficient (Rho) describing the association of diffusion tensor imaging parameters mean diffusivity and fractional anisotropy with the Progressive Supranuclear Palsy Rating Scale items scores

PSPRS items	PSPRS items scores	FA		MD	
		Thalamus	VAVL	Thalamus	VAVL
History	7.25±4.62	−0.383	−0.575	0.611	0.659
Mentation	4.25±3.88	−0.849‡	−0.506	0.892‡	0.892‡
Bulbar	2±1.6	−0.835†	−0.933‡	0.651	0.749†
Ocular motor	8.88±2.85	−0.759†	−0.313	0.699	0.723†
Limb motor	5.75±1.67	−0.776†	−0.325	0.801†	0.776†
Gate and midline	11±7.19	−0.735†	−0.578	0.783†	0.807†
Total	39.13±18.11	−0.833†	−0.738†	0.905‡	0.929‡

PSPRS items scores expressed as mean±standard deviation. No correction for multiple comparisons was done

Abbreviations: *PSPRS* Progressive Supranuclear Palsy Rating Scale, *MD* mean diffusivity, *FA* fractional anisotropy, *VAVL* ventral anterior and ventral lateral nuclei of thalamus

†P<0.05, ‡P<0.01, Spearman's correlation coefficient

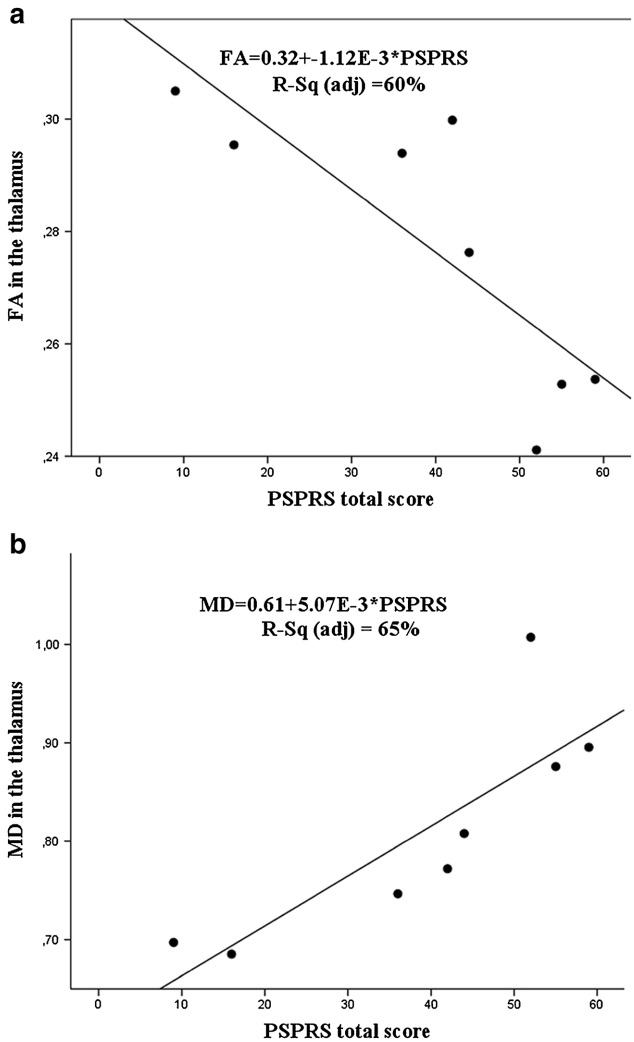

Fig. 4 Correlation between the progressive supranuclear palsy rating score and fractional anisotropy and mean diffusivity in the thalamus for the patients with progressive supranuclear palsy in derivation cohort. **a** The regression line (*black line*) with a 95 % confidence interval (CI) shows an association between higher progressive supranuclear palsy rating score (PSPRS) and reduced fractional anisotropy in the thalamus. The correlation coefficient value is 0.81 and 60 % of variance is explained. **b** The regression line (*black line*) with a 95 % CI shows an association between higher PSPRS score and elevated mean diffusivity in the thalamus. The correlation coefficient value is 0.84 and 65 % of variance is explained

were found [46]. Using tractography, we demonstrate reduced FA and elevated MD in the DRTT in PSP, which was confirmed in two different cohorts (Table 2; Fig. 3). Further, the quite high diagnostic accuracy obtained using the MD in the DRTT and MD in the midbrain, and to a lesser degree the MD of thalamus (Table 4), warrants further studies investigating the clinical diagnostic utility of these measures. To our knowledge, this study was first to using tractography to show changes in diffusion parameters along the DRTT in patients with PSP but not the first to show diffusion changes in regional parts of the DRTT [14].

The motor and pre-motor cortex receives thalamic inputs especially from the ventral thalamic nuclei (i.e., the "motor thalamus") and changes in motor cortical activation are associated with the clinical features of rigidity, bradykinesia, and postural instability in both PSP and PD [45]. In this context, it is interesting to note that we found that increased MD in ventral thalamic nuclei was very consistently associated with worse motor symptoms in PSP. The ventral thalamic nuclei receive input, e.g., from the basal ganglia (globus pallidus) via the thalamic fasciculus and from the cerebellum via the DRTT.

Table 4 Diagnostic accuracy of mean diffusivity in the thalamus, the right dentatorubrothalamic tract, and midbrain

	ROC (95 % CI)	Cutoff MD [$\mu m^2/ms$]	Sensitivity %	Specificity %
PSP vs controls				
Thalamus	0.77 (0.64–0.91)	0.80	74	67
DRTT R	0.95 (0.88–1.00)	1.23	96	81
Midbrain	0.86 (0.74–0.98)	0.77	85	81
PSP vs PD and MSA-P				
Thalamus	0.81 (0.68–0.93)	0.79	81	77
DRTT R	0.94 (0.87–1.0)	1.25	92	81
Midbrain	0.90 (0.88–0.99)	0.78	81	81
PSP vs PD, MSA-P, and controls				
Thalamus	0.79 (0.68–0.9)	0.8	74	71
DRTT R	0.94 (0.89–0.99)	1.24	96	79
Midbrain	0.88 (0.79–0.97)	0.77	85	79

Values refer to the validation cohort

Abbreviations: *PSP* progressive supranuclear palsy, *PD* Parkinson's disease, *MSA-P* multiple system atrophy, parkinsonian variant, *DRTT R* right dentatorubrothalamic tract, *ROC* receiver operator curve analysis, *MD* mean diffusivity, *CI* confidence interval

It has been suggested that the DRTT is important for postural stability. Our finding that increased MD in the DRTT is associated with impaired balance (poor performance on the tandem gait test) in patients with PSP might suggest that these changes are associated with postural instability and falls in PSP. This finding is in agreement with a previous study showing that imbalance and falls in PSP are associated with thalamic dysfunction visualized with FDG-PET, suggesting that brainstem-thalamic loops play an important role in postural imbalance and falls in PSP [9].

In the present study, we also found that the volumes of the putamen and the globus pallidus are reduced in both MSA-P and PSP, but that the volumes of the thalamus and the midbrain are selectively reduced in PSP, which is in agreement with a previous study [47]. The volumetric changes of the thalamus were not associated with clinical assessment scales in PSP, which was in sharp contrast to diffusion measures (especially MD) in the same structure, indicating that DTI more reliably detect meaningful changes in the thalamus of patients with PSP.

Our DTI results of ROI-based analysis of diffusion changes in thalamus are in agreement with the TBSS analysis of thalamus. Interestingly, our DTI results of MD changes in the infratentorial part of the DRTT in patients with PSP are in agreement with previously published results of the TBSS study [48] where patients with PSP showed white matter (WM) changes encompassing the inferior part of this tract. Our results are also in line with a previous report from another TBSS study [49] showing widespread changes in white matter tracts in both PSP and MSA patients, not found in patients with PD.

Our study has some limitations. First, the PSP group is small in the derivation cohort. However, there are previous studies demonstrating that with effect sizes above 5 %, as few as 4–7 individuals are needed when analyzing MD values in white matter structures [50]. Although the coefficients of variation were slightly higher in the structures we analyzed, the reduction in MD in PSP compared to controls in derivation cohort was up to 15 %. Given that the results were reproduced in the validation cohort, we are confident in the reliability of the results. Second, when using small cohort number, the main limitation is the risk of type II errors, not type I errors. The strength of the present study was also that the results from the derivation cohort were reproduced in the validation cohort. However, the correlations performed only in the derivation cohort (i.e., correlations with UPDRS, PSP rating scale, and tandem gate) should be interpreted with caution until validated in other cohorts. Third, manual placements of ROIs for DTI analyses can be subjective, but the ROI-based analyses of the present study resulted in high intra-rater reliability and the results were validated by the automatic TBSS analysis. Finally, clinical diagnostic criteria were used for patient collection without neuropathological confirmation in the study, thus misdiagnosis cannot be excluded. However, in two cases (one with PSP and one with MSA-P) that underwent neuropathological examination the clinical diagnoses were confirmed.

Conclusions

We investigated disease-specific structural changes in thalamus and dentatorubrothalamic tract in PSP. In a cohort with 8 PSP patients and 30 controls, we found elevated MD in the thalamus, SCP, midbrain, and of the DRTT in patients with PSP. Increased MD in the thalamus and in the DRTT

correlated with impaired motor function or balance in patients with PSP. Volumetric analysis showed reduced thalamic volumes in PSP. The DTI and volumetric findings were successfully reproduced in a validation cohort with 27 PSP patients and 21 controls. In addition, we found that most of these changes were specific to PSP and not found in patients with PD or MSA-P, which indicates that MD changes in thalamus and DRTT might be specific to impaired motor function and balance. Future studies need to be performed to examine whether changes in DTI parameters in the thalamus could be part of an MRI protocol for differential diagnosis of PSP vs PD and MSA-P. Further studies are also needed to confirm that alterations in thalamus and the DRTT are associated with impaired motor function and balance in PSP.

Acknowledgments The authors thank Ann Johansson and Katarina Johansson, Research Nurses in the Neurology Department, without whom completion of this study would never have been possible. The study was supported by the European Research Council, the Swedish Research Council, The Parkinson Foundation of Sweden, The Michael J Fox Foundation, the Crafoord Foundation, the Swedish Brain Foundation and the Swedish Federal Government under the ALF agreement. The funding sources had no role in the design and conduct of the study, in the collection, analysis, interpretation of the data or in the preparation, review or approval of the manuscript.

Ethical standards and patient consent We declare that all human and animal studies have been approved by the Ethics Committee at Lund University and have therefore been performed in accordance with the ethical standards laid down in the 1964 Declaration of Helsinki and its later amendments. We declare that all patients gave informed consent prior to inclusion in this study.

Conflict of interest We declare that we have no conflict of interest.

References

1. Steele JC, Richardson JC, Olszewski J (1964) Progressive supranuclear palsy. A heterogeneous degeneration involving the brainstem, basal ganglia and cerebellum with vertical gaze and pseudobulbar palsy, nuchal dystonia and dementia. Arch Neurol 10:333–59
2. Dickson DW, Ahmed Z, Algom AA et al (2010) Neuropathology of variants of progressive supranuclear palsy. Curr Opin Neurol 23: 394–400
3. Litvan I, Agid Y, Calne D et al (1996) Clinical research criteria for the diagnosis of progressive supranuclear palsy (Steele-Richardson-Olszewski syndrome): report of the NINDS-PSP International Workshop. Neurology 47:1–9
4. Wakabayashi K, Takahashi H (2004) Pathological heterogeneity in progressive supranuclear palsy and corticobasal degeneration. Neuropathology 24:79–86
5. Williams DR, Lees AJ (2009) Progressive supranuclear palsy: clinicopathological concepts and diagnostic challenges. Lancet Neurol 8:270–79
6. Dickson DW, Rademakers R, Hutton ML (2007) Progressive supranuclear palsy: pathology and genetics. Brain Pathol 17:74–82
7. Srulijes K, Reimold M, Liscic RM et al (2012) Fluorodeoxyglucose positron emission tomography in Richardson's syndrome and progressive supranuclear palsy-parkinsonism. Mov Disord 27:151–5
8. Zalewski N, Botha H, Whitwell JL et al (2014) FDG-PET in pathologically confirmed spontaneous 4R-tauopathy variants. J Neurol 261:710–6
9. Zwergal A, la Fougère C, Lorenzl S et al (2011) Postural imbalance and falls in PSP correlate with functional pathology of the thalamus. Neurology 77:101–9
10. Basser PJ, Mattiello J, LeBihan D (1994) MR diffusion tensor spectroscopy and imaging. Biophys J 66:259–67
11. Hess CP, Christine CW, Apple AC et al (2014) Changes in the thalamus in atypical parkinsonism detected using shape analysis and diffusion tensor imaging. AJNR Am J Neuroradiol 35:897–903
12. Saini J, Bagapally BS, Sandhya M et al (2012) In vivo evaluation of white matter pathology in patients of progressive supranuclear palsy using TBSS. Neuroradiology 54:771–80
13. Wang J, Wai Y, Lin WY et al (2010) Microstructural changes in patients with progressive supranuclear palsy: a diffusion tensor imaging study. J Magn Reson Imaging 32:69–75
14. Whitwell JL, Avula R, Master A et al (2011) Disrupted thalamocortical connectivity in PSP: a resting-state fMRI, DTI, and VBM study. Parkinsonism Relat Disord 17:599–605
15. Blain CR, Barker GJ, Jarosz JM et al (2006) Measuring brain stem and cerebellar damage in parkinsonian syndromes using diffusion tensor MRI. Neurology 67:2199–205
16. Nilsson C, Markenroth Bloch K, Brockstedt S et al (2007) Tracking the neurodegeneration of parkinsonian disorders—a pilot study. Neuroradiology 49:111–9
17. Erbetta A, Mandelli ML, Savoiardo M et al (2009) Diffusion tensor imaging shows different topographic involvement of the thalamus in progressive supranuclear palsy and corticobasal degeneration. AJNR Am J Neuroradiol 30:1482–7
18. Kwon HG, Hong JH, Hong CP et al (2011) Dentatorubrothalamic tract in human brain: diffusion tensor tractography study. Neuroradiology 53:787–91
19. Hoehn MM, Yahr MD (1967) Parkinsonism: onset, progression and mortality. Neurology 17:427–442
20. Schwab RS, England AC (1969) Projection technique for evaluating surgery in Parkinson's Disease. In: Gillingham FJ, Donaldson IML (eds) Third symposium of Parkinson's disease. Edinburgh, Scotland, pp 152–57
21. Fahn S, Elton RL, members of the UPDRS development committee (1987) Unified Parkinson's Disease Rating Scale. In: Fahn S, Marsden CD, Goldstein M, Calne DB (eds) Recent developments in Parkinson's Disease, vol 2. Macmillan Healthcare Information, Florham Park, NJ, pp 153–63
22. Fregly AR (1974) Vestibular ataxia and its measurement in man. In: Kornhuber HH (ed) Handbook of sensory physiology. Springer, Berlin, pp 321–60
23. Folstein SE, McHugh PR (1975) "Mini-mental state": a practical method for grading the cognitive state of patients for the clinician. J Psychiatr Res 12:189–98
24. Nielsen NP, Wiig EH, Warkentin S et al (2004) Clinical utility of color-form naming in Alzheimer's disease: preliminary evidence. Percept Mot Skills 99:1201–4
25. Golbe LI, Ohman-Strickland PA (2007) A clinical rating scale for progressive supranuclear palsy. Brain 130:1552–65
26. Calne DB, Snow BJ, Lee C (1992) Criteria for diagnosing Parkinson's disease. Ann Neurol 32:S125–7

27. Gilman S, Wenning GK, Low PA et al (2008) Second consensus statement on the diagnosis of multiple system atrophy. Neurology 71:670–676
28. Nucifora PG, Verma R, Lee SK, Melhem ER (2007) Diffusion-tensor MR imaging and tractography: exploring brain microstructure and connectivity. Radiology 245:367–84
29. Klein S, Staring M, Murphy K et al (2010) Elastix: a toolbox for intensity-based medical image registration. IEEE Trans Med Imaging 29:196–205
30. Tournier JD, Calamante F, Connelly A (2007) Robust determination of the fibre orientation distribution in diffusion MRI: non-negativity constrained super-resolved spherical deconvolution. Neuroimage 35:1459–72
31. Wiegell MR, Tuch DS, Larsson HB et al (2003) Automatic segmentation of thalamic nuclei from diffusion tensor magnetic resonance imaging. Neuroimage 19:391–401
32. Unrath A, Klose U, Grodd W et al (2008) Directional colour encoding of the human thalamus by diffusion tensor imaging. NeurosciLett 434:322–7
33. Oba H, Yagishita A, Terada H et al (2005) New and reliable MRI diagnosis for progressive supranuclear palsy. Neurology 64:2050–55
34. Smith SM, Jenkinson M, Johansen-Berg H et al (2006) Tract-based spatial statistics: voxelwise analysis of multi-subject diffusion data. NeuroImage 31:1487–1505
35. Andersson JLR, Jenkinson M, Smith S (2012) Non-linear optimisation. FMRIB Technical Report TR07JA1 2007a http://wwwfmriboxacuk/analysis/techrep Accessed(3 September 2012)
36. Andersson JLR, Jenkinson M, Smith S (2012) Non-linear registration, aka Spatial normalisation. FMRIB Technical Report TR07JA2. 2007b. http://www.fmrib.ox.ac.uk/analysis/techrep Accessed 3 September 2012
37. Smith SM (2002) Fast robust automated brain extraction. Human Brain Mapping 17:143–155
38. Smith SM, Jenkinson M, Woolrich MW et al (2004) Advances in functional and structural MR image analysis and implementation as FSL. Neuroimage 23:S208–S219
39. Quattrone A, Nicoletti G, Messina D et al (2008) MR imaging index for differentiation of progressive supranuclear palsy from Parkinson disease and the Parkinson variant of multiple system atrophy. Radiology 246:214–21
40. Patenaude B, Smith SM, Kennedy D et al (2011) A Bayesian model of shape and appearance for subcortical brain. NeuroImage 56:907–22
41. Buckner RL, Head D, Parker J et al (2004) A unified approach for morphometric and functional data analysis in young, old, and demented adults using automated atlas-based head size normalization: reliability and validation against manual measurement of total intracranial volume. Neuroimage 23:724–38
42. Winkler AM, Ridgway GR, Webster MA et al (2014) Permutation inference for the general linear model. NeuroImage 92:381–397
43. Henderson JM, Carpenter K, Cartwright H et al (2000) Loss of thalamic intralaminar nuclei in progressive supranuclear palsy and Parkinson's disease: clinical and therapeutic implications. Brain 123:1410–21
44. Kobayashi Z, Akaza M, Ishihara S et al (2013) Thalamic hypoperfusion in early stage of progressive supranuclear palsy (Richardson's syndrome): Report of an autopsy-confirmed case. J Neurol Sci 335:224–7
45. Halliday GM, Macdonald V, Henderson JM (2005) A comparison of degeneration in motor thalamus and cortex between progressive supranuclear palsy and Parkinson's disease. Brain 128:2272–80
46. Ishizawa K, Dickson DW (2001) Microglial activation parallels system degeneration in progressive supranuclear palsy and corticobasal degeneration. J Neuropathol Exp Neurol 60:647–57
47. Messina D, Cerasa A, Condino F et al (2011) Patterns of brain atrophy in Parkinson's disease, progressive supranuclear palsy and multiple system atrophy. Parkinsonism and Related Disorders 17:172–6
48. Tessitore A, Giordano A, Caiazzo G et al (2014) Clinical correlations of microstructural changes in progressive supranuclear palsy. Neurobiol Aging 35:2404–10
49. Worker A, Blain C, Jarosz J et al (2014) Diffusion tensor imaging of Parkinson's disease, multiple system atrophy and progressive supranuclear palsy: a tract-based spatial statistics study. PLoS One 9(11), e112638
50. Heiervang E, Behrens TEJ, Mackay CE et al (2006) Between session reproducibility and between subject variability of diffusion MR and tractography measures. NeuroImage 33:867–877

Paper III

PLOS ONE

RESEARCH ARTICLE

Alterations of Diffusion Kurtosis and Neurite Density Measures in Deep Grey Matter and White Matter in Parkinson's Disease

Yulia Surova[1,2]*, Björn Lampinen[3], Markus Nilsson[4], Jimmy Lätt[5], Sara Hall[1,2], Håkan Widner[1,2], Swedish BioFINDER study, Danielle van Westen[1,4], Oskar Hansson[6,7]

1 Department of Clinical Sciences, Lund, Lund University, Lund, Sweden, **2** Department of Neurology, Skåne University Hospital, Lund, Sweden, **3** Department of Medical Radiation Physics, Lund University, Lund, Sweden, **4** Lund University Bioimaging Center, Lund University, Lund, Sweden, **5** Center for Medical Imaging and Physiology, Skåne University Hospital, Lund, Sweden, **6** Department of Clinical Sciences, Malmö, Lund University, Malmö, Sweden, **7** Memory Clinic, Skåne University Hospital, Malmö, Sweden

* yulia.surova@med.lu.se

Citation: Surova Y, Lampinen B, Nilsson M, Lätt J, Hall S, Widner H, et al. (2016) Alterations of Diffusion Kurtosis and Neurite Density Measures in Deep Grey Matter and White Matter in Parkinson's Disease. PLoS ONE 11(6): e0157755. doi:10.1371/journal.pone.0157755

Editor: Alexander Leemans, University Medical Center Utrecht, NETHERLANDS

Received: February 20, 2016

Accepted: June 3, 2016

Published: June 30, 2016

Data Availability Statement: To protect study participant information, data are available on request. The corresponding author of the paper (Yulia Surova yulia.surova@med.lu.se) or the PI of the BIOFINDER study http://biofinder.se (Oskar Hansson oskar.hansson@med.lu.se) should be contacted for data requests.

Funding: The study was supported by the European Research Council, the Swedish Research Council, The Parkinson Foundation of Sweden, the Swedish Brain Foundation, the Swedish Cancer Society (grant no. CAN 2009/1076), the Swedish Foundation for

Abstract

In Parkinson's disease (PD), pathological microstructural changes occur and such changes might be detected using diffusion magnetic resonance imaging (dMRI). However, it is unclear whether dMRI improves PD diagnosis or helps differentiating between phenotypes, such as postural instability gait difficulty (PIGD) and tremor dominant (TD) PD. We included 105 patients with PD and 44 healthy controls (HC), all of whom underwent dMRI as part of the prospective Swedish BioFINDER study. Diffusion kurtosis imaging (DKI) and neurite density imaging (NDI) analyses were performed using regions of interest in the basal ganglia, the thalamus, the pons and the midbrain as well as tractography of selected white matter tracts. In the putamen, the PD group showed increased mean diffusivity (MD) ($p = .003$), decreased fractional anisotropy (FA) ($p = .001$) and decreased mean kurtosis (MK), compared to HC ($p = .024$). High MD and a low MK in the putamen were associated with more severe motor and cognitive symptomatology ($p < .05$). Also, patients with PIGD exhibited increased MD in the putamen compared to the TD patients ($p = .009$). In the thalamus, MD was increased ($p = .001$) and FA was decreased ($p = .032$) in PD compared to HC. Increased MD and decreased FA correlated negatively with motor speed and balance ($p < .05$). In the superior longitudinal fasciculus (SLF), MD ($p = .019$) and f_{iso} were increased in PD compared to HC ($p = .03$). These changes correlated negatively with motor speed ($p < .002$) and balance ($p < .037$). However, most of the observed changes in PD were also present in cases with either multiple system atrophy (n = 11) or progressive supranuclear palsy (n = 10). In conclusion, PD patients exhibit microstructural changes in the putamen, the thalamus, and the SLF, which are associated with worse disease severity. However, the dMRI changes are not sufficiently specific to improve the diagnostic work-up of PD. Longitudinal studies should evaluate whether dMRI measures can be used to track disease progression.

Strategic Research (AM13-0090), and the Swedish Federal Government under the ALF Agreement. The funding sources had no role in the design and conduct of the study; in the collection, analysis, interpretation of the data; or in the preparation, review, or approval of the manuscript.

Competing Interests: The authors have declared that no competing interests exist.

Introduction

Parkinson's disease (PD) is the second most common neurodegenerative disorder, with a prevalence of approximately 1% in the population older than 60 years. It is classically characterized by resting tremor, slowness of initial movement, rigidity, and general postural instability [1]. Microstructural changes include neuronal loss in the substantia nigra [2]. The loss of cells results in profound dopamine depletion in the motor region of the striatum [3], with nigral projections to the putamen being most affected [4]. Neuropathology reports in PD have shown that the thalamus and the putamen are also affected [4, 5]. Post-mortem diagnosis of PD requires evidence of cell loss in the substantia nigra, aggregated α-synuclein deposits accumulated in neurites (Lewy neurites) and in neuronal somata (Lewy bodies). The clinical signs and symptoms of PD vary considerably, and are assumingly caused by differences in the degeneration pattern of the nigrostriatal dopaminergic system and other subcortical neuronal systems [6–8]. A number of proposals divide patients with PD into the tremor dominant (TD) and postural instability gait difficulty (PIGD) subtypes [6, 7]. As of yet, no study has assessed if there are differences in measures from diffusion MRI (dMRI) between PIGD and TD.

Conventional magnetic resonance imaging (MRI) has been unsuccessful in detecting pathophysiologic changes in PD. However, several changes have been found in measures from dMRI techniques. Using diffusion tensor imaging (DTI), spatially resolved micro-structural brain damage has been identified in PD [9]. Overall, DTI measures tend to show consistent results of changes in brain regions involved in the basal ganglia circuit, including an elevation of mean diffusivity (MD) and a reduction of fractional anisotropy (FA) [9, 10]. However, a recent meta-analysis of FA changes in the substantia nigra has questioned the stability and validity of this measure as a PD biomarker [10]. Several studies have reported increased MD and reduced FA in the caudate nucleus, the putamen, the globus pallidus and the thalamus in PD [11–16]. Other reports have shown normal dMRI in the striatum of PD [17, 18]. Together these somewhat divergent results call for large prospective studies to investigate dMRI changes in PD. On the other hand, the patterns of change seem to be more robust in atypical parkinsonian disorders like progressive supranuclear palsy (PSP) or multiple system atrophy (MSA), with changes in dMRI measures reported in the basal ganglia regions such as the putamen and the thalamus [19–25], but also in the caudate nucleus and the globus pallidus [14, 26, 27]. Interestingly, DTI measures in the basal ganglia are promising for differentiating atypical parkinsonian disorders from PD [10].

Changes in FA and MD have also been observed in several brain white matter (WM) tracts in PD. Compared to healthy controls (HC), patients with PD exhibit increased MD and reduced FA in the superior longitudinal fasciculus (SLF), the genu of the corpus callosum (CC), and in the cingulum (CG) [28]. Interestingly, Zheng et al. [29] showed that executive function, linguistic performance, attention, and memory were positively correlated with FA and negatively correlated with MD in relevant WM tracts, consistent with the expectation that FA decreases and MD increases with increased levels of neurodegeneration and neurocognitive dysfunction.

Changes in diffusion kurtosis, which quantifies non-Gaussian water diffusion [30], have not yet been well studied in PD. Wang et al. [24] demonstrated elevated mean kurtosis (MK) in the putamen and in the substantia nigra in PD. Reduced FA and MK have been found in PD patients in WM structures such as the cingulate fiber tracts [28], the anterior part of the inferior fronto-occipital fasciculus (IFOF), the anterior SLF, the anterior and superior corona radiata, parts of the genu and body of the CC, and part of the parietal WM (part of the posterior SLF) [28].

In this explorative study, we aimed to extend the previously reported findings of dMRI changes in grey matter (GM) and brain WM tracts in PD. To this end, multi-shell dMRI data

were obtained from a large sample of PD patients, as well as from healthy controls. The data were analyzed using diffusion kurtosis imaging (DKI) to obtain MD, FA and MK, and neurite density imaging (NDI) [31] to obtain the neurite density index (f_{ic}) and the partial fraction of free water (f_{iso}). Values of these parameters were obtained in GM structures by drawing regions of interest (ROI) in the basal ganglia, the thalamus, the midbrain and the pons. In WM, parameter values were obtained in tracts defined using tractography and included the cingulum (CG), the CC, the fornix, the SLF, the inferior longitudinal fasciculus (ILF), the IFOF, the uncinate fasciculus (UF), and the corticospinal tract (CST). First, we investigated whether diffusion changes in subcortical GM structures and WM tracts could be found in PD compared to HC, and found changes in putamen, thalamus, and SLF. Second, we studied whether these changes were different between the PIGD and TD subtypes, as well as between PD and patients with PSP or MSA. Third, we tested whether the diffusion changes in PD were associated with motor or cognitive deficits.

Materials and Methods

Ethics Statement

This study was approved by the Ethics Committee at Lund University and performed in accordance with the Helsinki Declaration. All participants gave written informed consent prior to participation.

Participants

In this case-control study participants were recruited from the Neurology Clinic at Skåne University Hospital, Sweden, between 2008 and 2015 as part of the prospective and longitudinal Swedish BioFINDER study (http://www.biofinder.se) [32]. For the present work, 105 subjects were included with a clinical diagnosis of probable PD. The diagnosis was made by neurologists trained in movement disorder diagnostics according to the National Institute of Neurological Disorders and Stroke (NINDS) criteria of PD [33]. Neurologically HC were recruited (n = 44), who did not have any objective cognitive or parkinsonian symptoms. In addition, we included patients with a clinical diagnosis of probable PSP (n = 10) and MSA (n = 11) who fulfilled the NINDS criteria of either PSP or MSA [34, 35]. Motor function, disease stage and disability was evaluated using e.g. Unified Parkinson's disease rating scale motor part (UPDRS-III) [36], Hoehn and Yahr staging scale (H&Y), the Schwab and England activities of daily living scale (S&E) [37], and the timed up and go test [38, 39]. The tandem gait test [40] was done to assess disturbances in balance and gait. Cognitive assessments were conducted by trained physicians using a standardized battery, including Mini Mental State Examinations (MMSE), The Quick Test of Cognitive Speed (AQT) test [41], and the memory subtests of the Alzheimer's Disease Assessment Scale (ADAS-Cog, which consist of a 10 word delayed recall). To ensure standardization, assessments were conducted during patients "on" medication state, or fully responding to their PD medications (in the "on" state). At the time of testing, none of the patients exhibited any dyskinesia, dystonia, or other signs of involuntary movement.

Classification into postural instability gait disorder and tremor dominant subtypes of patients with Parkinson's disease. The UPDRS-III motor score was used to compute a mean tremor score of the following 9 tremor items: right and left arm tremor as determined by history, during patients "on" and "off" medication state. Tremor at rest of either lips, face or chin tremor, tremor in all 4 limbs, and action or postural tremor on both arms were determined by the investigator during examination. A mean score of 5 PIGD items were computed: falling, freezing, and walking difficulty by history, during patients "on" and "off" medication state. Gait and postural instability were determined during patients' examination). When the ratio of

the mean tremor score divided by the PIGD score was greater than or equal to 1.5, study participants were assigned to the TD subgroup [6]. When this ratio was equal to or less than 1.0, study participants were assigned to the PIGD subgroup [6]. Patients with mixture phenotype were ignored when comparing PIGD to TD.

MRI data acquisition and post-processing

Imaging was performed on a 3 T Siemens Skyra MR scanner equipped with a 20 channel head coil. The diffusion MRI protocol comprised 99 DWI volumes, where the choice of *b*-values and encoding directions was inspired by Poot et al. [42]. In total, three volumes were acquired with $b = 0$ s/mm^2, while the remaining 96 volumes were acquired using *b*-values of 250, 500, 1000, and 2750 s/mm^2, distributed over 6, 6, 20, and 64 directions, respectively. A single-shot spin-echo with EPI read-out was used, with the following settings: TR = 8100 ms, TR = 103 ms, voxel size = 2.3×2.3×2.3 mm^3, FOV = 294×294×120 mm^3, iPAT = 2, and partial Fourier factor = 6/8. The imaging volume comprised 52 contiguous axial slices adjusted to include the whole cerebrum. Total acquisition time was approximately 14 minutes. Motion and eddy current distortions were corrected using an extrapolation-based method for improved high *b*-value performance [11]. In this procedure, the diffusion-weighted images were modulated with the Jacobian determinant of the transformation matrix [43]. In order to mitigate the potential effects of Gibbs ringing artifacts, image volumes were smoothed using an isotropic 3D Gaussian kernel with a full-width at half maximum of 2.3 mm [44–46]. Smoothing with a kernel of this size has little effect on sensitivity and specificity [47], and is thus not expected to significantly influence the parameter precision. DKI analysis was performed to obtain maps of FA, MK, and MD, using in-house developed software which fitted the diffusion and kurtosis tensors by nonlinear optimization as in Lätt et al [48]. The fitting only allowed positive values of the diffusion tensor eigenvalues. In a small number of voxels where the kurtosis was below zero, the fitting was repeated after additional smoothing was performed. NDI analysis [31], a simplification of the NODDI analysis [49], was performed to obtain maps of the neurite density index (f_{ic}) and the partial fraction of free water (f_{iso}). NDI utilizes a concept from solid-state NMR called powder averaging [50], where the MR signal is averaged across all rotations of a sample. In dMRI, we average across encoding directions for each b-value, which induces complete orientation dispersion in each voxel. This concept has previously been applied in diffusion MRI to analyze microscopic diffusion anisotropy [51, 52]. Here, we use it to simplify the NODDI model in order to speed up the analysis by predicting the MR signal in terms of only three model parameters (S_0, f_{ic}, and f_{iso}), according to

$$S = S_0(f_{iso}\exp(-bD_{iso}) + (1 - f_{iso})(f_{ic}A_{ic} + (1 - f_{ic})A_{ec})) \quad (1)$$

where the attenuation A of the intra-neurite and extracellular components were given by

$$A_x = \exp(-b\mathrm{MD}_x)h(\alpha_x) \quad (2)$$

and

$$h(\alpha) = \sqrt{\frac{\pi}{4\alpha}}\exp(\alpha/3)\mathrm{erf}(\sqrt{\alpha}) \quad (3)$$

Here, erf is the error function and $\alpha_x = b\,(\mathrm{AD}_x - \mathrm{RD}_x)$ where AD_x and RD_x are the axial and radial diffusivities, respectively, from which the mean diffusivity is calculated according to $\mathrm{MD}_x = (\mathrm{AD}_x + 2\,\mathrm{RD}_x)/3$. [53]. Just as for the NODDI model, we assumed $\mathrm{AD}_{ic} = \mathrm{AD}_{ec} = 1.7$ μm^2/ms, $\mathrm{RD}_{ic} = 0$, and $\mathrm{RD}_{ec} = (1 - f_{ic})\,\mathrm{AD}_{ec}$. Just as for NODDI, NDI is built on the assumption that the diffusivities are identical inside and outside the axons, which is not necessarily

true and may thus bias the estimated parameters [54, 55]. Accordingly, the values of the obtained parameters should be interpreted as phenomenological fit parameters rather than in terms of absolute quantification of specific features of the tissue microstructure.

All calculations were performed using in-house developed software, implemented in Matlab (The Mathworks, Natick, MA, USA).

All relevant data are within the paper. The raw imaging data are available for researchers who meet the criteria for access to confidential data and are granted accessed by the local data access committee.

Region of interest analysis of diffusion parameters

ROI based analysis of grey matter. All ROIs were outlined manually (Fig 1) in the subject's native space using MK and directionally color-encoded FA (DEC) maps, with the exception of the red nucleus and the substantia nigra, where the non-diffusion weighted b_0 map was used. ROI size was adjusted in order to maximize coverage of each structure in each subject, while minimizing partial-volume effects from neighboring areas. Contamination from cerebrospinal fluid (CSF), which has isotropic diffusion with a high MD, was avoided by excluding voxels adjacent to the third and lateral ventricles. Slice selection for ROI delineation was performed with respect to standard neuroanatomical criteria [56]. The head of the caudate nucleus was delineated in one slice at the level where it was most conspicuous. The thalamus was

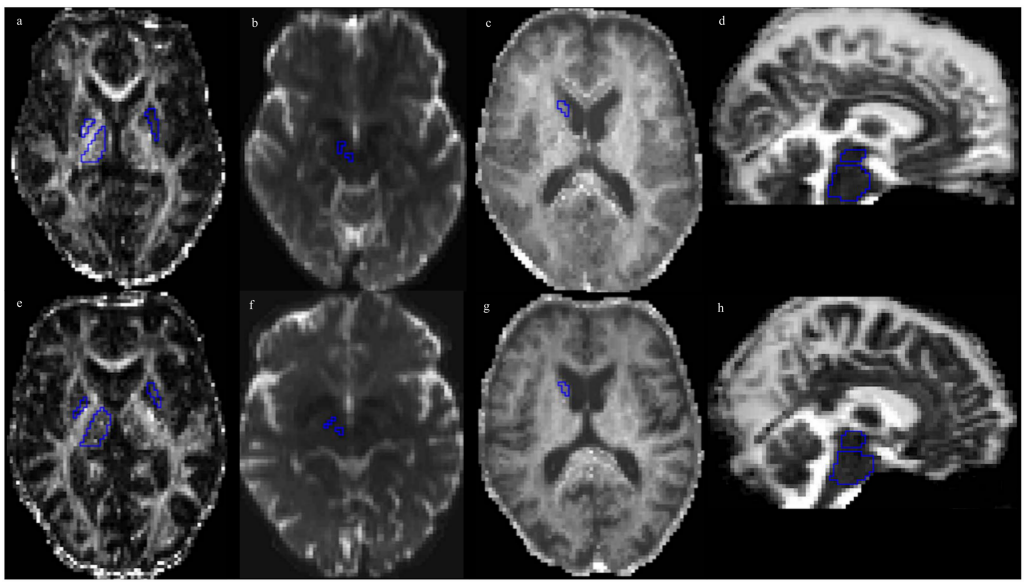

Fig 1. Parameter maps for both PD patients and healthy controls with key ROIs examined. ROIs for measurement in the anatomical areas reported in Table 2, overlaid on the FA, b_0, MK and MD maps from a 66-year-old healthy male participant (panels a-e), and a 66-year-old male PD patient (panels f-j). In panels (a) and (f), ROIs are placed in the pallidum and the thalamus (right), and the putamen (left) on the FA-map; in panels (b) and (g) in the substantia nigra and red nucleus (right) on the b_0-map; in panels (c) and (h) in the caudate head (right) on the MK map; and in panels (d) and (i) in the pons and midbrain on the MD map.

doi:10.1371/journal.pone.0157755.g001

delineated in 5–8 consecutive slices at the level of the internal capsule and adjacent to the interthalamic adhesion. The globus pallidus and the putamen were delineated in one slice, and were adjusted to the extreme capsule. The red nucleus was identified as a circular area of signal hypointensity in the midbrain on b_0 maps and delineated in one axial slice. The substantia nigra was identified as an area of signal hypointensity in the midbrain on b_0 maps and delineated in one axial slice. The midbrain and the pons were delineated in 8 consecutive sagittal slices, with the boundaries identified using the manual approach proposed by Oba et al. [57]. For each structure, the average MK, MD, FA value and NDI parameters from the right and left hemisphere was calculated. All ROIs were redrawn 8 weeks later on the same images, by the same investigator (intra-rater variability > 0.9 for all ROIs), and the average values from paired ROIs were used for analysis. The image-presentation order was randomized, and the investigator was blinded to the order. In the substantia nigra, red nucleus and globus pallidus, and midbrain, the signal-to-noise ratio (SNR) was approximately 50% of that in the thalamus, and 25–35% of that in WM (data not shown). The low SNR in these structures was suspected of causing artificial changes in FA, MD and MK (S1 File, S1 Fig), wherefore the structures were excluded from the analysis, besides the substantia nigra.

Tractography of brain white matter tracts. Tractography was performed using deterministic tracking based on constrained spherical deconvolution (CSD) [58], generating the left and right anterior half of the dorsal CG, the posterior half of the CG, the hippocampal CG, the SLF, the ILF, the IFOF, the UF, the CST and the CC. The fornix was generated using probabilistic tractography. The ROIs used to define the seed region for each tract, and to segment the tract based on logical operations, were defined in MNI152 standard-space [59] and warped back to native space utilizing the warp-fields generated by FLIRT and FNIRT [60].

All tracts were generated using one seed-ROI covering the full extent of the expected tract, and then further defined using logical AND- and NOT-ROIs. The subdivisions of the CG were defined according to Jones et al. [61], using two NOT-ROIs, one at its most anterior border and one at the rostral-caudal midpoint of the dorsal CG. The posterior CG was defined using two NOT-ROIs, one at the rostral-caudal midpoint of the dorsal CG and one at the dorsal border of the splenium. The hippocampal CG was defined using two NOT-ROIs, one at the dorsal border of the splenium of the CC and one at the level of the mesencephalon. The fornix was defined using two AND-ROIs and one NOT-ROI. The first AND-ROI was located at the level of the corpus fornicis, inferior to the anterior pillars, and the second was located at the level of the crus fornicis, inferior to the splenium of the CC. The NOT-ROI was located anterior to the anterior pillars, inferior to the crus fornicis and through the CC. The CC was defined using NOT-ROIs located just above its anterior, posterior, superior and inferior borders. Furthermore, AND-ROIs were used to include its 2 cm wide central portion. The SLF was defined according to Wakana et al. [62], using one AND-ROI in the frontal lobe at the level of the rostral-caudal midpoint of the CC, and one AND-ROI located just anterior to the posterior border of the Sylvian fissure. The ILF was defined using one AND-ROI anteriorly in the temporal lobe and one AND-ROI in the occipital lobe 2 cm posterior to the sagittal stratum. The IFOF was defined using one AND-ROI in the frontal lobe located inferior to the anterior-inferior border of the CC and one AND-ROI in the occipital lobe at the level of the sagittal stratum. The UF was defined using two AND-ROIs, one located in the frontal lobe 1 cm anterior to the CC, and one located in the temporal lobe at the level of central pons. In addition, a NOT-ROI was placed in the midsagittal plane, as well as posterior to the UF In addition, for the SLF, the ILF, the IFOF and the UF, a NOT-ROI was placed in the midsagittal plane. The CST was defined using one AND-ROI located in the thalamus and a second AND-ROI located in the motor cortex at the level of the hand area.

The average parameter estimates for each WM tract were used in the subsequent analysis.

Statistical analysis

Statistical analysis was performed with SPSS Statistics 20 for Windows (IBM Corporation, Somers, NY, USA). Using the Mann-Whitney *U* test, comparisons of demography, clinical categorical variables and dMRI parameters were performed for: PD vs. HC, PIGD vs. TD, PD vs. PSP as well as PD vs. MSA. Correlations between diffusion parameters and clinical scores were tested for using Spearman's rho (R_s). Proportions were compared using Pearson's chi-squared test. For the dMRI parameter comparisons that came out significant using non-parametric testing, a one-way analysis of covariance (ANCOVA) was also conducted in order to control for the effects of gender and age. MD in the thalamus, MK and FA in the putamen, MD and f_{iso} in the SLF, and f_{ic} in CST were all non-normally distributed, hence logarithmic transformation was performed before analysis with ANCOVA. The significance level was set to 0.05. In addition, the effect sizes were calculated for significant changes in dMRI parameters.

Univariate binary logistic regression analysis was performed to study the ability of DKI measures to distinguish PD from HC. Based on the ANCOVA, significantly different dMRI parameters were assigned to binary logistic regression analysis. The model where PD was compared to HC was adjusted for age and sex. Adjusting for sex was performed since the patient group had a larger proportion of men. To assess the usefulness of DKI as a diagnostic tool for individual cases, the sensitivity, specificity and the optimal cutoff level of the DKI values were calculated for selected regions with receiver operator characteristic curve analysis (ROC). Multiple comparison correction was not applied in this explorative study.

Results

Demographics

Demographics for the HC and PD groups are given in Table 1. The PD and HC groups did not differ significantly by age, but there was a significant difference in gender distribution (Pearson's $c^2 = 5.4$, $p < .05$), with a higher proportion of men in the PD group. The PIGD group performed worse on tests reflecting gait and balance (timed up and go and tandem gait tests) and a cognitive function (AQT) compared to the TD group.

Table 1. Demographic data and biomarker levels for the diagnostic groups.

	HC (n = 44)	PD (n = 105)	*p*-value (PD vs. HC)	PIGD (n = 47)	TD (n = 50)	*p*-value (PIGD vs.TD)
Gender female: male	25: 19	61: 44	0.02 [a]	20:27	15:35	0.07 [a]
Age (years)	66 ± 8	66 ± 11	0.475[b]	66 ± 11	66 ±11	0.767 [b]
Disease duration (years)	ND	5 ± 4		5 ± 5	5 ± 3	0.266 [b]
Hoehn and Yahr stage	ND	2 ± 1		2 ± 1	2 ± 1	0.001[b]
Schwab and England	100	90 ± 9	<0.001 [b]	87 ± 11	93 ± 6	0.001[b]
UPDRS-III motor score	2 ± 2	13 ± 10	<0.001 [b]	13 ± 11	13 ± 8	0.734 [b]
Tandem gait test "on"	0.21 ± 0.5	0.66 ± 1	0.006 [b]	0.96 ± 1.2	0.34 ± 0.6	0.005 [b]
Timed up and go test "on" (seconds)	8 ± 1	10 ± 2	<0.00 [b]	10 ± 3	9 ± 2	0.031 [b]
MMSE score	28 ± 2	28 ± 2	0.887 [b]	28 ± 2	28 ± 1	0.731 [b]
Memory delayed recall (ADAS-Cog)	2 ± 2	4 ± 7	0.031 [b]	3 ± 3	3 ± 2	0.901 [b]
AQT	61 ± 14	70 ± 18	0.011 [b]	73 ± 22	67 ± 15	0.024 [b]

Values are given as mean ±SD. UPDRS-III, Unified Parkinson's disease rating scale motor part; MMSE, Mini Mental State Examination test; ADAS-Cog, Alzheimer's Disease Assessment Scale; AQT, the Quick Test of Cognitive Speed (AQT) test; HC, healphy controls; PD, Parkinson's disease; PIGD, postural instability gait difficulty; TD, tremor dominant; SD, standard deviation; ND, not done.

[a] Pearson's chi-square

[b] Mann-Whitney U test.

doi:10.1371/journal.pone.0157755.t001

Differences in dMRI parameters in PD compared to HC

Table 2 shows the comparisons in GM structures between PD and HC. In the putamen, MD was increased with 8% and FA was decreased with 9% in PD compared to HC (Mann-Whitney *U* test, $p < .003$; ANCOVA, $p < .005$). The PD group also exhibited a 6% decrease of the MK in the putamen compared to HC (Mann-Whitney *U* test, $p < .05$; ANCOVA, $p < .001$). In the thalamus, MD was increased with 4%, and FA was decreased with 3%, in PD compared to HC (Mann-Whitney *U* test, $p < .05$; ANCOVA, $p < .001$, $p < .05$, respectively). There were no significant age- and gender-adjusted differences in dMRI parameters in the caudate head or the pons between the two groups. There were no significant differences ($p < .05$, ANCOVA) in NDI parameters in the caudate head, thalamus, putamen, and pons found in PD. In the caudate head, the f_{iso} was decreased with 2% and in the thalamus, f_{iso} was increased with 2% in PD ($p < .05$, Mann-Whitney U test, $p > .05$, ANCOVA).

Table 2. Diffusion magnetic resonance measures in patients with Parkinson's disease (PD) and healthy controls (HC). The PD group was also divided into those with postural instability and gait difficulty (PIGD) and tremor-dominant (TD) phenotypes.

Structure	Parameter	HC (n = 44)	PD (n = 105)	*p*-value [a] (PD vs. HC)	PIGD (n = 47)	TD (n = 50)	*p*-value [a] (PIGD vs.TD)
Substantia nigra	FA	0.64 ± 0.10	0.62 ± 0.11	0.571	0.62 ± 0.1	0.62 ± 0.11	0.971
Caudate head	FA	0.23 ± 0.04	0.22 ± 0.04	0.390	0.22 ± 0.03	0.23 ± 0.04	0.170
Putamen	FA	0.23 ± 0.04	0.20 ± 0.03	**0.001** [b]	0.20 ± 0.33	0.21 ± 0.03	0.170
Thalamus	FA	0.37 ± 0.02	0.36 ± 0.02	**0.032** [b]	0.36 ± 0.02	0.36 ± 0.02	0.683
Pons	FA	0.52 ± 0.02	0.51 ± 0.02	0.524	0.51 ± 0.03	0.51 ± 0.02	0.829
Substantia nigra	MD	0.45 ± 0.12	0.48 ± 0.12	0.251	0.49 ± 0.1	0.48 ± 0.12	0.885
Caudate head	MD	0.80 ± 0.12	0.83 ± 0.14	0.138	0.84 ± 0.15	0.82 ± 0.14	0.269
Putamen	MD	0.78 ± 0.10	0.80 ± 0.14	**0.003** [b]	0.88 ± 0.17	0.81 ± 0.10	**0.009** [c]
Thalamus	MD	0.77 ± 0.05	0.80 ± 0.05	**<0.001** [b]	0.82 ± 0.05	0.80 ± 0.05	0.052
Pons	MD	0.70 ± 0.04	0.71 ± 0.05	0.165	0.71 ± 0.05	0.70 ± 0.05	0.549
Substantia nigra	MK	ND	ND		ND	ND	
Caudate head	MK	0.92 ± 0.11	0.95 ± 0.11	0.253	0.94 ± 0.10	0.94 ± 0.11	0.776
Putamen	MK	1.24 ± 0.19	1.16 ± 0.15	**0.024** [b]	1.12 ± 0.13	1.18 ± 0.17	0.101
Thalamus	MK	1.19 ± 0.09	1.16 ± 0.10	0.066	1.15 ± 0.10	1.17 ± 0.10	0.569
Pons	MK	1.52 ± 0.11	1.55 ± 0.15	0.238	1.53 ± 0.15	1.57 ± 0.16	0.356
Substantia nigra	NDI f_{ic}	ND	ND		ND	ND	
Caudate head	NDI f_{ic}	0.66 ± 0.08	0.62 ± 0.15	0.168	0.60 ± 0.15	0.63 ± 0.16	0.330
Putamen	NDI f_{ic}	0.77 ± 0.13	0.74 ± 0.12	0.119	0.73 ± 0.11	0.74 ± 0.12	0.762
Thalamus	NDI f_{ic}	0.72 ± 0.07	0.72 ± 0.07	0.874	0.72 ± 0.07	0.73 ± 0.07	0.423
Pons	NDI f_{ic}	0.94 ± 0.05	0.95 ± 0.04	0.123	0.95 ± 0.04	0.95 ± 0.04	0.979
Substantia nigra	NDI f_{iso}	ND	ND		ND	ND	
Caudate head	NDI f_{iso}	± 0.08	0.10 ± 0.08	0.038	0.01 ± 0.09	0.01 ± 0.08	0.539
Putamen	NDI f_{iso}	0.11 ± 0.08	0.12 ± 0.09	0.987	0.13 ± 0.11	0.11 ± 0.08	0.569
Thalamus	NDI f_{iso}	0.09 ± 0.04	0.11 ± 0.03	0.024	0.11 ± 0.04	0.10 ± 0.03	0.784
Pons	NDI f_{iso}	0.10 ± 0.03	0.11 ± 0.03	0.122	0.11 ± 0.03	0.11 ± 0.03	0.445

MD [10^-9 m^2/s]. Values are given as mean ± SD. FA, fractional anisotropy; MD, mean diffusivity; MK, mean kurtosis; NDI f_{iso} and f_{ic}, neurite density imaging measures; ND, not done.

[a] *p*, Mann-Whitney U test.

[b] $p < .05$, ANCOVA (age/gender adjusted).

[c] $p < .05$, ANCOVA (age adjusted).

P-values given in bold were significant when both using Mann-Whitney U test and ANCOVA.

doi:10.1371/journal.pone.0157755.t002

Table 3. Diffusion kurtosis imaging measures in white matter structures in patients with Parkinson's disease (PD) and healthy controls (HC).

Region	Parameter	HC (n = 44)	PD (n = 105)	*p*-value [a](PD vs. HC)
Cingulum anterior	FA	0.35 ± 0.03	0.34 ± 0.05	0.927
Cingulum posterior	FA	0.49 ± 0.03	0.49 ± 0.03	0.987
Cingulum hippocampus	FA	0.38 ± 0.03	0.40 ± 0.04	0.041
Fornix	FA	0.30 ± 0.04	0.30 ± 0.04	0.753
Corpus callosum	FA	0.55 ± 0.03	0.56 ± 0.04	0.280
SLF	FA	0.46 ± 0.03	0.46 ± 0.03	0.731
ILF	FA	0.45 ± 0.04	0.44 ± 0.05	0.070
IFOF	FA	0.51 ± 0.03	0.50 ± 0.08	0.148
Uncinate Fasciculus	FA	0.39 ± 0.03	0.39 ± 0.03	0.224
CST	FA	0.40 ± 0.12	0.38 ± 0.13	0.141
Cingulum anterior	MD	0.90 ± 0.05	0.89 ± 0.10	0.874
Cingulum posterior	MD	0.80 ± 0.04	0.81 ± 0.05	0.208
Cingulum hippocampus	MD	0.87 ± 0.07	0.88 ± 0.07	0.728
Fornix	MD	1.75 ± 0.24	1.73 ± 0.25	0.744
Corpus callosum	MD	1.26 ± 0.11	1.26 ± 0.12	0.698
SLF	MD	0.81 ± 0.05	0.84 ± 0.05	**0.019** [b]
ILF	MD	0.97 ± 0.10	0.99 ± 0.13	0.034
IFOF	MD	0.95 ± 0.06	0.95 ± 0.15	0.254
Uncinate Fasciculus	MD	0.91 ± 0.06	0.94 ± 0.07	0.063
CST	MD	0.68 ± 0.19	0.67 ± 0.24	0.057
Cingulum anterior	MK	0.84 ± 0.06	0.83 ± 0.10	0.914
Cingulum posterior	MK	1.09 ± 0.07	1.09 ± 0.08	0.607
Cingulum hippocampus	MK	1.00 ± 0.08	1.01 ± 0.09	0.275
Fornix	MK	0.77 ± 0.08	0.79 ± 0.07	0.179
Corpus callosum	MK	0.90 ± 0.06	0.91 ± 0.06	0.397
SLF	MK	1.18 ± 0.05	1.17 ± 0.06	0.234
ILF	MK	1.02 ± 0.06	1.00 ± 0.12	0.454
IFOF	MK	1.01 ± 0.04	1.00 ± 0.16	0.970
Uncinate Fasciculus	MK	1.03 ± 0.05	1.02 ± 0.06	0.379
CST	MK	1.16 ± 0.06	1.14 ± 0.14	0.429

MD [10^-9 m^2/s]. Values are given as mean ± SD. ILF, inferior longitudinal fasciculus; IFOF, inferior fronto-occipital fasciculus; SLF, superior longitudinal fasciculus; CST, corticospinal tract; FA, fractional anisotropy; MD, mean diffusivity; MK, mean kurtosis; NDI f_{iso} and f_{ic}, neurite density imaging measures.

[a] p, Mann-Whitney U test.

[b] $p < .05$, ANCOVA (age and gender adjusted).

P-values given in bold were significant when both using Mann-Whitney U test and ANCOVA.

doi:10.1371/journal.pone.0157755.t003

The comparisons in WM tracts between PD and HC are presented in Tables 3 and 4. In SLF, the MD was increased with 4% and f_{iso} was increased with 9% (Mann-Whitney U test and ANCOVA, $p < .05$) in PD. In CST, f_{ic} was significantly decreased with 3% (Mann Whitney U test and ANCOVA, $p < .05$ both) (Table 4).

Differences in dMRI parameters in PIGD compared to TD

The comparisons in GM structures between PIGD and TD are shown in Table 2. Compared to TD, patients with the PIGD phenotype exhibited a 7% increase in MD in the putamen (Mann-Whitney U test, $p < .01$). The difference remained significant after adjusting for age

Table 4. Neurite density imaging (NDI) measures in white matter structures in patients with Parkinson's disease (PD) and healthy controls (HC).

Region	Parameter	HC (n = 44)	PD (n = 105)	*p*-value [a] (PD vs. HC)
Cingulum anterior	NDI f_{ic}	0.58 ± 0.10	0.57 ± 0.07	0.340
Cingulum posterior	NDI f_{ic}	0.71 ± 0.12	0.72 ± 0.06	0.582
Cingulum hippocampus	NDI f_{ic}	0.72 ± 0.13	0.75 ± 0.07	0.658
Fornix	NDI f_{ic}	0.71 ± 0.09	0.72 ± 0.1	0.472
Corpus callosum	NDI f_{ic}	0.76 ± 0.13	0.76 ± 0.09	0.675
SLF	NDI f_{ic}	0.72 ± 0.04	0.70 ± 0.09	0.351
ILF	NDI f_{ic}	0.64 ± 0.05	0.62 ± 0.08	0.167
IFOF	NDI f_{ic}	0.65 ± 0.04	0.64 ± 0.08	0.184
Uncinate Fasciculus	NDI f_{ic}	0.64 ± 0.04	0.63 ± 0.06	0.225
CST	NDI f_{ic}	0.73 ± 0.04	0.71 ± 0.06	**0.043** [b]
Cingulum anterior	NDI f_{iso}	0.11 ± 0.03	0.10 ± 0.03	0.268
Cingulum posterior	NDI f_{iso}	0.10 ± 0.03	0.10 ± 0.03	0.484
Cingulum hippocampus	NDI f_{iso}	0.14 ± 0.04	0.14 ± 0.04	0.923
Fornix	NDI f_{iso}	0.50 ± 0.09	0.49 ± 0.11	0.724
Corpus callosum	NDI f_{iso}	0.29 ± 0.04	0.29 ± 0.05	0.690
SLF	NDI f_{iso}	0.11 ± 0.03	0.12 ± 0.03	**0.030** [b]
ILF	NDI f_{iso}	0.15 ± 0.04	0.16 ± 0.04	0.134
IFOF	NDI f_{iso}	0.14 ± 0.03	0.15 ± 0.03	0.226
Uncinate Fasciculus	NDI f_{iso}	0.13 ± 0.03	0.14 ± 0.03	0.112
CST	NDI f_{iso}	0.11 ± 0.03	0.12 ± 0.03	0.060

Values are given as mean ± SD. ILF, inferior longitudinal fasciculus; IFOF, inferior fronto-occipital fasciculus; SLF, superior longitudinal fasciculus; CST, corticospinal tract; FA, fractional anisotropy; MD, mean diffusivity; MK, mean kurtosis; NDI f_{iso} and f_{ic}, neurite density imaging measures.

[a] *p*, Mann-Whitney U test.

[b] $p < .05$, ANCOVA (age and gender adjusted). P-values given in bold were significant when both using Mann-Whitney U test and ANCOVA.

doi:10.1371/journal.pone.0157755.t004

(ANCOVA, $p < .05$). There were no differences in dMRI parameters in the analyzed WM tracts between the two groups (data not shown).

Correlations between clinical scores and dMRI parameters in PD

Next we analyzed correlations between the dMRI parameters that were changed in PD compared to HC (according to the analyses above) with clinical measures of motor and cognitive function.

Putamen: Increased MD correlated significantly with a worse motor function, as measured by H&Y ($R_s = .297$, $p < .005$), UPDRS-III motor score ($R_s = .192$, $p < .05$), tandem gait ($R_s = .439$, $p < .001$), and timed up and go ($R_s = .443$, $p < .001$) tests (Fig 2).

MK correlated negatively with the disease duration ($R_s = -.206$, $p < .05$). Furthermore, increased MD correlated with impaired cognitive speed and attention, as measured by AQT ($R_s = .219$, $p < .05$). Decreased MK was associated with reduced memory performance, as measured by ADAS-Cog item 3 ($R_s = .258$, $p < .01$). In summary, a high MD and a low MK in the putamen are associated with more severe motor and cognitive symptomatology.

Thalamus: Increased MD correlated significantly with a worse motor speed and balance, as measured by the Hand test ($R_s = -.243$, $p < .05$), tandem gait and timed up and go tests ($R_s = .222$, $p = .05$ and $R_s = .399$, $p < .001$, respectively, Fig 2). Decreased FA also correlated negatively with timed up and go test ($R_s = -.226$, $p < .05$).

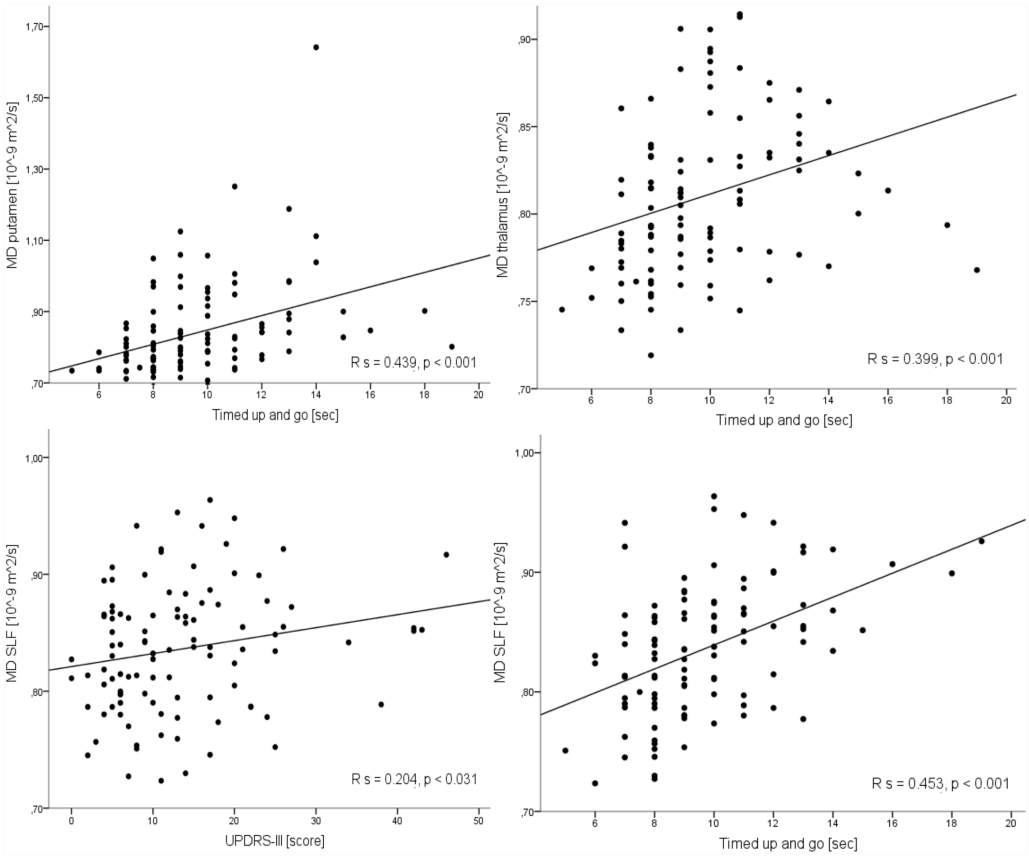

Fig 2. Correlation between mean diffusivity (MD) in the putamen, thalamus and superior longitudinal fasciculus (SLF) with the time up and go test score and between the MD in the SLF with Unified Parkinson's disease rating scale motor part (UPDRS-III) score. A moderate positive correlation was found between MD in the putamen, thalamus and SLF and time up and go test score. A moderate positive correlation was found between the MD in the SLF and UPDRS-III scale score. R_s, Spearman's rho.

doi:10.1371/journal.pone.0157755.g002

SLF: Increased MD correlated significantly with the worsening of the motor function, as measured by H&Y, UPDRS-III motor score, tandem gate, timed up and go tests and the cognitive function, as measured by AQT and ADAS-Cog (R_s = .204–358, $p < .05$). Increased f_{iso} correlated significantly with the worsening of the motor function, as measured by tandem gate and timed up and go tests and the cognitive function, as measured by ADAS-Cog (R_s = .205–325, $p < .05$). Increased f_{iso} correlated significantly with the worsening of the cognitive function as measured by MMSE (R_s = −.202, $p < .05$). In the caudate head and thalamus, f_{iso} did not correlate neither with disease duration nor with clinical scales.

Table 5. Differences between patients with Parkinson's disease (PD) and cases with progressive supranuclear palsy (PSP) or multiple system atrophy (MSA).

	PD (n = 105)	PSP (n = 10)	MSA (n = 11)	*p*-value (PD vs PSP)	*p*-value (PD vs MSA)
Gender female: male	44: 61	5: 5	5: 6	1.000 [a]	0.527 [a]
Age (years)	66 ± 11	73 ± 6	63 ± 10	0.037	0.302
Disease duration (years)	5 ± 4	7 ± 2	6 ± 4	0.051	0.299
Hoehn and Yahr	2 ± 1	4 ± 1	4 ± 1	<0.001	<0.001
Schwab and England	90 ± 9	58 ± 35	67 ± 22	<0.002	<0.001
UPDRS-III motor score	13 ± 10	39 ± 14	34 ± 19	<0.001	<0.001
FA putamen	0.20 ± 0.03	0.23 ± 0.06	0.26 ± 0.03	0.053	**<0.001** [c]
MD putamen	0.80 ± 0.14	0.88 ± 0.33	0.83 ± 0.15	0.275	0.276
MK putamen	1.14 ± 0.15	1.35 ± 0.25	1.34 ± 0.17	**0.012** [b]	**0.001** [c]
FA thalamus	0.36 ± 0.02	0.34 ± 0.04	0.35 ± 0.01	0.204	**0.034** [c]
MD thalamus	0.80 ± 0.05	0.87 ± 0.11	0.84 ± 0.06	**0.044** [b]	0.08
MD SLF	0.84 ± 0.05	0.89 ± 0.09	0.84 ± 0.04	**0.024** [b]	0.984
NDI f_{ic} CST	0.71 ± 0.06	0.69 ± 0.07	0.71 ± 0.04	0.473	0.875
NDI f_{iso} SLF	0.12 ± 0.03	0.12 ± 0.01	0.13 ± 0.04	0.164	0.638

MD [10^-9 m^2/s]. Values are given as mean ± SD. UPDRS-III, Unified Parkinson's disease rating scale motor part; FA, fractional anisotropy; MD, mean diffusivity; DKI, Diffusion Tensor Imaging; dMRI, diffusion magnetic resonance imaging; SLF, superior longitudinal fasciculus; CST, corticospinal tract; NDI f_{iso} and f_{ic}, neurite density imaging measures; SD, standard deviation.

[a] Pearson's chi-square. *p*-value, Mann-Whitney U test.

[b] PD/PSP,

[c] PD/MSA,

$p < .05$, ANCOVA (age adjusted). P-values given in bold were significant when both using Mann-Whitney U test and ANCOVA.

doi:10.1371/journal.pone.0157755.t005

Differences in dMRI parameters in PD compared to PSP or MSA

To study whether the observed differences in dMRI parameters were specific for PD, we also investigated the same parameters in patients with PSP and MSA and compared these values to the ones obtained in the PD group. The results are given in table 5. In summary, only FA and MK of putamen seem to be specifically changed in PD where both these parameters are reduced indicating microstructural damage. All of the other changes observed in PD were also found to be changed in PSP and MSA in the same direction and often even more pronounced such as MD in the thalamus or putamen.

Diagnostic accuracy of the studied dMRI parameters in identification of PD

Based on the ANCOVA test, the univariate binary logistic regression analysis were performed in order to test the potential of dMRI parameters for the differential diagnosis of PD vs. HC. MD and MK in the putamen were included in the models, see Statistical analysis. A summary of the results is shown in S1 Table. Logistic regression analysis confirmed that the MD and MK in the putamen could significantly ($p < .05$) discriminate PD from HC. The sensitivity and specificity for these parameters, calculated using a ROC curve analysis, showed the optimal cutoff level of 0.79 for MD and of 1.18 for MK in putamen (with an area under the ROC curve of 0.62–0.65) to discriminate PD from HC with a sensitivity and specificity of around 60%.

Discussion

We investigated disease-specific structural changes in deep grey matter and white matter in patients with PD. In this cohort with 105 patients with PD and 44 healthy controls, we found that MD in the thalamus was increased and FA was decreased in PD. These parameters correlated significantly with the worsening of motor speed and balance. In the putamen, MD was increased and FA and MK were decreased in PD. These changes were associated with worsening of motor speed, balance, and cognitive function. Further, in the white matter of PD patients, MD and f_{iso} in the SLF were increased and correlated significantly with worsening of motor speed, balance, and cognitive function. Further, we found that MD in the putamen was increased in PIGD compared to the TD. However, most changes except those of MD and MK in the putamen were not specific to PD but also found in MSA or PSP.

The present results confirm those of recent DTI studies showing that the increased MD and decreased FA in the thalamus and putamen can be found in patients with PD [12–16, 63]. Nevertheless, DTI studies have shown inconsistent results regarding the microstructural alterations in these regions, as there are some studies that showed no changes in dMRI measures in the striatum between controls and PD patients [17, 18]. Nicoletti et al. [17] investigated 16 patients with PD and 15 HC. Paviour et al. [18] investigated only 12 PD and 7 HC. These limited statistical power due to the small group sizes may explain why no effects were found in these studies. Szczepankiewicz et al. [64] showed that group sizes above 15 are required to detect effects of 5% with a power of 90% in large tract structures. Smaller ROIs, and lower SNR at 1.5 T, as was used in these studies, would lead to ever stronger requirements on group size to attain sufficient power. Thus these inconsistencies in the results may be due to differences in sample size and sample characteristics, as well as methodological differences between ROI analysis and voxel-based analysis. However, the present results indicate that there are indeed significant, although not very prominent, dMRI changes in the putamen and thalamus in PD, which may be related to progressive degeneration of nigrostriatal dopaminergic neurons. Our study did not find FA difference in any WM region between groups, and only found elevated MD and f_{iso} in SLF and reduced f_{ic} in CST in patients with PD compared to HC (Table 4). The reason for this discrepancy is not clear. That fact that our study did not find FA difference in any region between groups and only found the MD alteration is in line with the previous report that used Tract-Based Spatial Statistics (TBSS) analysis [63]. Other TBSS study reported only the FA alteration in WM in PD patients [65]. We therefore now caution the interpretation of these findings. In fact, the SLF is composed of 4 bundles of axons, connecting multiple frontal and prefrontal regions with superior temporal and parietal areas [66]. As a consequence of its structural heterogeneity, it is related to a range of premotor, motor, visuospatial, and auditory functions [66]. This probably can explain the clinical correlations we found with dMRI alterations in SLF. Previous studies have indeed found correlation between SLF and deficits in premotor functions and visuospatial perception in PD [67–70].

We did not find any clear diagnostic utility of measuring of MD and FA in the caudate nucleus, putamen, globus pallidus or substantia nigra when identifying PD. This finding is partly in agreement with Wang et al. [24]. Further, Kamagata et al [65], showed reduced MK in the frontal, parietal, occipital, right temporal white matter, posterior corona radiata and SLF in a PD group compared with a control group when using tract-based spatial statistics. these changes were not observed in the present study. However, the PD patients in the present study had less motor symptoms and/or shorter disease duration, which could explain these discrepancies. Considered together, the results might suggest that alterations of MK in basal ganglia and white matter probably might not improve the diagnostic work-up of early PD. However,

such alterations may be are related to the disease severity of PD since we found that MK of putamen in PD patients correlate with disease duration and congnitive performance.

The clinical heterogeneity of PD is well recognized [6–8]. Early postural instability and gait involvement in PIGD dominant PD has been associated with a worse prognosis for motor and cognitive function, whereas the TD form of PD might be more benign [6–8]. Our results showed that MD in the putamen was increased in PIGD when compared to the TD. One possible explanation for the differences between the PIGD and TD might be the distinctly different patterns of neurodegeneration. In a study by Jellinger et al. [7] patients with PIGD demonstrated more severe cell loss in the ventrolateral part of SNpc, which projects to the dorsal putamen. One can speculate that pathology at the substantia nigra level could affect the discharge to the putamen as well as the degree of the subtle diffusion changes of putamen. Potentially 7 Tesla MRI that could assay more subtle changes in grey matter organization, and assessment of the alignment of fibers in white matter by novel dMRI techniques [64] might add some of the evidence. Even though we found several changes in dMRI in putamen, thalamus and SLF in PD, these changes were quite modest compared to controls and most of these changes were also observed in MSA or PSP. Consequently, we believe that dMRI of white matter tracts or the grey matter of the basal ganglia are unlikely to be used in the clinic to reliably detect early PD. However, it is intriguing that almost all dMRI abnormalities in PD correlate significantly with motor and cognitive function. Especially increased MD in putamen, thalamus and SLF was associated with worse motor functions (UPDRS-III motor score, tandem gate, and timed up and go test) as well as with worse cognitive function (MMSE, AQT, and memory delayed recall part of ADAS-cog), suggesting that better microstructural integrity as measured by diffusion MRI correlates with better clinical function. Several potential disease-modifying therapies for PD, like immunotherapy against α-synuclein, are currently being developed [71]. It will be very important to establish methods that objectively and reliably can tract the disease progression over time to be able to evaluate the effects of such treatments. Maybe dMRI in the basal ganglia could be included in such analyses, besides PET imaging of the integrity dopaminergic neurons, since the intersubject variability in dMRI parameters is much larger than the intrasubject variability [64]. However, longitudinal studies in PD evaluating the change in dMRI over 2–4 year is needed before such conclusions can be drawn.

The data reported in present study suggested that NDI measures in the basal ganglia are not useful for detection of PD patients. However, we did not assess NDI in the substantia nigra, because the low SNR in the substantia nigra was suspected of causing artificial changes in NDI. Using NODDI, Kamagata et al. [72] found lower V_{ic} (f_{ic} in our study) in the contralateral substantia nigra part compacta (SNpc) and putamen in PD patients. V_{ic} might be an indirect measure of nigrostriatal microstructural changes such as cell loss, morphological changes in dendritic length, and loss of dendritic spines and could be associated with disease severity in PD [72], indicating that NODDI in the substantia nigra might be useful for early diagnosis of PD as well as assessment of its subsequent progression. However, achieving sufficient SNR for accurate quantification of the neurite density in this iron-rich structure is challenging.

There are limitations with the study. The data was obtained in 2.3×2.3×2.3 mm^3 voxels. The rather large voxel size implies that partial volume effects may be present in spite of efforts to avoid inclusion of surrounding structures during ROI placement. Another limitation was that the significance threshold was not corrected for multiple comparisons. This omission was motivated by the explorative nature of this study where we wanted to minimize the type II error rate. Furthermore, correcting for multiple comparisons would only strengthen the main conclusion that the magnitude of dMRI changes in PD are too small to be used to reliably detect early PD in a clinical setting. In addition, the analyses of disease stage-related microstructural changes dMRI is cross-sectional and need to be replicated and confirmed in

longitudinal studies. Lastly, the ROIs were drawn manually by one author, and therefore the reproducibility of the measurements was uncertain. Rater bias was prevented by blinding, and the intra-rater variability coefficient was larger than 0.9 for all ROIs.

Conclusions

The present study shows significant changes in dMRI parameters in the putamen, thalamus and SLF in PD. Most of the changes were modest in magnitude, and dMRI is unlikely to be useful in order to reliably detect early PD. However, changes in dMRI parameters correlated with worse motor and cognitive function in PD. Consequently, future longitudinal studies are needed to determine whether dMRI can be used to reliably track the disease progression of PD, and thereby might be of used in clinical trials, evaluating novel therapies with potential disease-modifying effects.

Supporting Information

S1 Fig. The correlation between the signal-to-noise ratio of globus pallidus relative to white matter and the mean diffusivity. PAL, globus pallidus; MD, mean diffusivity; SNR, signal-to-noise ratio. Lower values of MD were clearly associated to lower SNR.
(TIF)

S1 File. Increased iron in substantia nigra reduces the signal-to-noise ratio.
(DOCX)

S1 Table. Use of DKI parameters in differential diagnosis. Mean diffusivity (MD, 10^9 mm^2/s) and mean kurtosis (MK), differentiating patients with Parkinson disease (PD) from healthy controls (HC); PD from patients with progressive supranuclear palsy (PSP) and multiple system atrophy (MSA). AUC, area under curve; DKI, diffusion kurtosis imaging; ROC, receiver operating characteristic analysis. *Significant differences between PD vs HC and PD vs PSP and MSA, $p < 0.05$, using binary logistic regression, adjusted for age and sex (PD vs HC) and adjusted for age (PD vs PSP and MSA).
(DOCX)

Acknowledgments

The authors sincerely thank the study participants and research nurse Katarina Johansson.

Author Contributions

Conceived and designed the experiments: HW DvW OH. Performed the experiments: YS BL DvW. Analyzed the data: YS BL DvW. Contributed reagents/materials/analysis tools: SH JL DvW MN OH. Wrote the paper: YS MN DvW OH. Designed the software used in analysis: BL MN.

References

1. de Lau LM, Breteler MM. Epidemiology of Parkinson's disease. Lancet Neurol. 2006; 5(6):525–35. doi: 10.1016/S1474-4422(06)70471-9 PMID: 16713924.
2. Damier P, Hirsch EC, Agid Y, Graybiel AM. The substantia nigra of the human brain. I. Nigrosomes and the nigral matrix, a compartmental organization based on calbindin D(28K) immunohistochemistry. Brain. 1999; 122 (Pt 8):1421–36. PMID: 10430829.
3. Kish SJ, Shannak K, Hornykiewicz O. Uneven pattern of dopamine loss in the striatum of patients with idiopathic Parkinson's disease. Pathophysiologic and clinical implications. N Engl J Med. 1988; 318 (14):876–80. doi: 10.1056/NEJM198804073181402 PMID: 3352672.

4. Braak H, Ghebremedhin E, Rub U, Bratzke H, Del Tredici K. Stages in the development of Parkinson's disease-related pathology. Cell Tissue Res. 2004; 318(1):121–34. doi: 10.1007/s00441-004-0956-9 PMID: 15338272.
5. Goedert M, Spillantini MG, Del Tredici K, Braak H. 100 years of Lewy pathology. Nat Rev Neurol. 2013; 9(1):13–24. doi: 10.1038/nrneurol.2012.242 PMID: 23183883.
6. Jankovic J, McDermott M, Carter J, Gauthier S, Goetz C, Golbe L, et al. Variable expression of Parkinson's disease: a base-line analysis of the DATATOP cohort. The Parkinson Study Group. Neurology. 1990; 40(10):1529–34. PMID: 2215943.
7. Jellinger KA. Post mortem studies in Parkinson's disease—is it possible to detect brain areas for specific symptoms? J Neural Transm Suppl. 1999; 56:1–29. PMID: 10370901.
8. Selikhova M, Williams DR, Kempster PA, Holton JL, Revesz T, Lees AJ. A clinico-pathological study of subtypes in Parkinson's disease. Brain. 2009; 132(Pt 11):2947–57. doi: 10.1093/brain/awp234 PMID: 19759203.
9. Brooks DJ. Technology insight: imaging neurodegeneration in Parkinson's disease. Nat Clin Pract Neurol. 2008; 4(5):267–77. doi: 10.1038/ncpneuro0773 PMID: 18382437.
10. Cochrane CJ, Ebmeier KP. Diffusion tensor imaging in parkinsonian syndromes: a systematic review and meta-analysis. Neurology. 2013; 80(9):857–64. doi: 10.1212/WNL.0b013e318284070c PMID: 23439701; PubMed Central PMCID: PMCPMC3598454.
11. Nilsson M, Szczepankiewicz F, van Westen D, Hansson O. Motion and eddy-current correction in high b-value diffusion MRI: Systematic registration errors and how to avoid them. Proceedings of the ISMRM. 2014:2569.
12. Peran P, Cherubini A, Assogna F, Piras F, Quattrocchi C, Peppe A, et al. Magnetic resonance imaging markers of Parkinson's disease nigrostriatal signature. Brain. 2010; 133(11):3423–33. doi: 10.1093/brain/awq212 PMID: 20736190.
13. Planetta PJ, Schulze ET, Geary EK, Corcos DM, Goldman JG, Little DM, et al. Thalamic projection fiber integrity in de novo Parkinson disease. AJNR Am J Neuroradiol. 2013; 34(1):74–9. doi: 10.3174/ajnr.A3178 PMID: 22766668; PubMed Central PMCID: PMCPMC3669594.
14. Schocke MF, Seppi K, Esterhammer R, Kremser C, Mair KJ, Czermak BV, et al. Trace of diffusion tensor differentiates the Parkinson variant of multiple system atrophy and Parkinson's disease. Neuroimage. 2004; 21(4):1443–51. doi: 10.1016/j.neuroimage.2003.12.005 PMID: 15050569.
15. Youn J, Lee JM, Kwon H, Kim JS, Son TO, Cho JW. Alterations of mean diffusivity of pedunculopontine nucleus pathway in Parkinson's disease patients with freezing of gait. Parkinsonism Relat Disord. 2015; 21(1):12–7. doi: 10.1016/j.parkreldis.2014.10.003 PMID: 25455691.
16. Zhan W, Kang GA, Glass GA, Zhang Y, Shirley C, Millin R, et al. Regional alterations of brain microstructure in Parkinson's disease using diffusion tensor imaging. Mov Disord. 2012; 27(1):90–7. doi: 10.1002/mds.23917 PMID: 21850668; PubMed Central PMCID: PMCPMC4472452.
17. Nicoletti G, Lodi R, Condino F, Tonon C, Fera F, Malucelli E, et al. Apparent diffusion coefficient measurements of the middle cerebellar peduncle differentiate the Parkinson variant of MSA from Parkinson's disease and progressive supranuclear palsy. Brain. 2006; 129(Pt 10):2679–87. doi: 10.1093/brain/awl166 PMID: 16815875.
18. Paviour DC, Thornton JS, Lees AJ, Jager HR. Diffusion-weighted magnetic resonance imaging differentiates Parkinsonian variant of multiple-system atrophy from progressive supranuclear palsy. Mov Disord. 2007; 22(1):68–74. doi: 10.1002/mds.21204 PMID: 17089396.
19. Hess CP, Christine CW, Apple AC, Dillon WP, Aminoff MJ. Changes in the thalamus in atypical parkinsonism detected using shape analysis and diffusion tensor imaging. AJNR Am J Neuroradiol. 2014; 35(5):897–903. doi: 10.3174/ajnr.A3832 PMID: 24356677.
20. Meijer FJ, van Rumund A, Tuladhar AM, Aerts MB, Titulaer I, Esselink RA, et al. Conventional 3T brain MRI and diffusion tensor imaging in the diagnostic workup of early stage parkinsonism. Neuroradiology. 2015; 57(7):655–69. doi: 10.1007/s00234-015-1515-7 PMID: 25845807; PubMed Central PMCID: PMCPMC4495265.
21. Rizzo G, Martinelli P, Manners D, Scaglione C, Tonon C, Cortelli P, et al. Diffusion-weighted brain imaging study of patients with clinical diagnosis of corticobasal degeneration, progressive supranuclear palsy and Parkinson's disease. Brain. 2008; 131(Pt 10):2690–700. doi: 10.1093/brain/awn195 PMID: 18819991.
22. Saini J, Bagepally BS, Sandhya M, Pasha SA, Yadav R, Pal PK. In vivo evaluation of white matter pathology in patients of progressive supranuclear palsy using TBSS. Neuroradiology. 2012; 54(7):771–80. doi: 10.1007/s00234-011-0983-7 PMID: 22160214.

23. Stebbins GT, Goetz CG, Carrillo MC, Bangen KJ, Turner DA, Glover GH, et al. Altered cortical visual processing in PD with hallucinations: an fMRI study. Neurology. 2004; 63(8):1409–16. PMID: 15505157.

24. Wang JJ, Lin WY, Lu CS, Weng YH, Ng SH, Wang CH, et al. Parkinson disease: diagnostic utility of diffusion kurtosis imaging. Radiology. 2011; 261(1):210–7. doi: 10.1148/radiol.11102277 PMID: 21771952.

25. Surova Y, Nilsson M, Latt J, Lampinen B, Lindberg O, Hall S, et al. Disease-specific structural changes in thalamus and dentatorubrothalamic tract in progressive supranuclear palsy. Neuroradiology. 2015; 57(11):1079–91. doi: 10.1007/s00234-015-1563-z PMID: 26253801; PubMed Central PMCID: PMCPMC4626534.

26. Erbetta A, Mandelli ML, Savoiardo M, Grisoli M, Bizzi A, Soliveri P, et al. Diffusion tensor imaging shows different topographic involvement of the thalamus in progressive supranuclear palsy and corticobasal degeneration. AJNR Am J Neuroradiol. 2009; 30(8):1482–7. doi: 10.3174/ajnr.A1615 PMID: 19589886.

27. Piattella MC, Upadhyay N, Bologna M, Sbardella E, Tona F, Formica A, et al. Neuroimaging evidence of gray and white matter damage and clinical correlates in progressive supranuclear palsy. J Neurol. 2015; 262(8):1850–8. doi: 10.1007/s00415-015-7779-3 PMID: 25980906.

28. Weingarten CP, Sundman MH, Hickey P, Chen NK. Neuroimaging of Parkinson's disease: Expanding views. Neurosci Biobehav Rev. 2015; 59:16–52. doi: 10.1016/j.neubiorev.2015.09.007 PMID: 26409344.

29. Zheng Z, Shemmassian S, Wijekoon C, Kim W, Bookheimer SY, Pouratian N. DTI correlates of distinct cognitive impairments in Parkinson's disease. Hum Brain Mapp. 2014; 35(4):1325–33. doi: 10.1002/hbm.22256 PMID: 23417856; PubMed Central PMCID: PMCPMC3664116.

30. Jensen JH, Helpern JA. MRI quantification of non-Gaussian water diffusion by kurtosis analysis. NMR Biomed. 2010; 23(7):698–710. doi: 10.1002/nbm.1518 PMID: 20632416; PubMed Central PMCID: PMCPMC2997680.

31. Lampinen B, van Westen D, Ståhlberg F, Lätt J, Hansson O, Nilsson M. Neurite Density Imaging (NDI): rapid acquisition and estimation of the intracellular volume fraction. Proceedings of the ISMRM. 2015:2772.

32. Hall S, Surova Y, Ohrfelt A, Zetterberg H, Lindqvist D, Hansson O. CSF biomarkers and clinical progression of Parkinson disease. Neurology. 2015; 84(1):57–63. doi: 10.1212/WNL.0000000000001098 PMID: 25411441; PubMed Central PMCID: PMCPMC4336091.

33. Gelb DJ, Oliver E, Gilman S. Diagnostic criteria for Parkinson disease. Arch Neurol. 1999; 56(1):33–9. PMID: 9923759.

34. Gilman S, Wenning GK, Low PA, Brooks DJ, Mathias CJ, Trojanowski JQ, et al. Second consensus statement on the diagnosis of multiple system atrophy. Neurology. 2008; 71(9):670–6. doi: 10.1212/01.wnl.0000324625.00404.15 PMID: 18725592; PubMed Central PMCID: PMCPMC2676993.

35. Litvan I, Agid Y, Calne D, Campbell G, Dubois B, Duvoisin RC, et al. Clinical research criteria for the diagnosis of progressive supranuclear palsy (Steele-Richardson-Olszewski syndrome): report of the NINDS-SPSP international workshop. Neurology. 1996; 47(1):1–9. PMID: 8710059.

36. Fahn S, Elton RL, Members of the UPDRS development committee. Unified Parkinson's Disease Rating Scale. In: Fahn S, Marsden CD, Goldstein M, Calne DB, editor. Recent developments in Parkinson's Disease, vol 2. Florham Park, NJ: Macmillan Healthcare Information; 1987. p. 153–63.

37. Schwab RS, England AC. Projection technique for evaluating surgery in Parkinson's disease. In: Gillingham FJ, Donaldson IML, editor. Third Symposium of Parkinson's disease Edinburgh: E & S Livingstone; 1969. p. 152–7.

38. Lim LI, van Wegen EE, de Goede CJ, Jones D, Rochester L, Hetherington V, et al. Measuring gait and gait-related activities in Parkinson's patients own home environment: a reliability, responsiveness and feasibility study. Parkinsonism Relat Disord. 2005; 11(1):19–24. doi: 10.1016/j.parkreldis.2004.06.003 PMID: 15619458.

39. Podsiadlo D, Richardson S. The timed "Up & Go": a test of basic functional mobility for frail elderly persons. J Am Geriatr Soc. 1991; 39(2):142–8. PMID: 1991946.

40. Fregly AR. Vestibular ataxia and its measurement in man. In: K HH, editor. Handbook of Sensory Physiology. Berlin: Springer; 1974. p. 321–60.

41. Nielsen NP, Wiig EH, Warkentin S, Minthon L. Clinical utility of color-form naming in Alzheimer's disease: preliminary evidence. Percept Mot Skills. 2004; 99(3 Pt 2):1201–4. doi: 10.2466/pms.99.3f.1201-1204 PMID: 15739845.

42. Poot DH, den Dekker AJ, Achten E, Verhoye M, Sijbers J. Optimal experimental design for diffusion kurtosis imaging. IEEE Trans Med Imaging. 2010; 29(3):819–29. doi: 10.1109/TMI.2009.2037915 PMID: 20199917.

43. Jones DK, Cercignani M. Twenty-five pitfalls in the analysis of diffusion MRI data. NMR Biomed. 2010; 23(7):803–20. doi: 10.1002/nbm.1543 PMID: 20886566.

44. Veraart J, Fieremans E, Jelescu IO, Knoll F, Novikov DS. Gibbs ringing in diffusion MRI. Magn Reson Med. 2015. doi: 10.1002/mrm.25866 PMID: 26257388.

45. Perrone D, Aelterman J, Pizurica A, Jeurissen B, Philips W, Leemans A. The effect of Gibbs ringing artifacts on measures derived from diffusion MRI. Neuroimage. 2015; 120:441–55. doi: 10.1016/j.neuroimage.2015.06.068 PMID: 26142273.

46. Kellner E, Dhital B, Kiselev VG, Reisert M. Gibbs-ringing artifact removal based on local subvoxel-shifts. Magn Reson Med. 2015. doi: 10.1002/mrm.26054 PMID: 26745823.

47. Van Hecke W, Leemans A, De Backer S, Jeurissen B, Parizel PM, Sijbers J. Comparing isotropic and anisotropic smoothing for voxel-based DTI analyses: A simulation study. Hum Brain Mapp. 2010; 31 (1):98–114. doi: 10.1002/hbm.20848 PMID: 19593775.

48. Latt J, Nilsson M, Wirestam R, Stahlberg F, Karlsson N, Johansson M, et al. Regional values of diffusional kurtosis estimates in the healthy brain. J Magn Reson Imaging. 2013; 37(3):610–8. doi: 10.1002/jmri.23857 PMID: 23055442; PubMed Central PMCID: PMCPMC3596978.

49. Zhang H, Schneider T, Wheeler-Kingshott CA, Alexander DC. NODDI: practical in vivo neurite orientation dispersion and density imaging of the human brain. Neuroimage. 2012; 61(4):1000–16. doi: 10.1016/j.neuroimage.2012.03.072 PMID: 22484410.

50. Edén M. Computer Simulations in Solid-State NMR. III. Powder Averaging. Concepts in Magnetic Resonance Part A. 2002; 18A(1):24–55.

51. Jespersen SN, Lundell H, Sonderby CK, Dyrby TB. Orientationally invariant metrics of apparent compartment eccentricity from double pulsed field gradient diffusion experiments. NMR Biomed. 2013; 26 (12):1647–62. doi: 10.1002/nbm.2999 PMID: 24038641.

52. Lasic S, Szczepankiewicz F, Eriksson S, Nilsson M, Topgaard D. Microanisotropy imaging: quantification of microscopic diffusion anisotropy and orientational order parameter by diffusion MRI with magic-angle spinning of the q-vector. Frontiers in Physics | Biophysics. 2014; 27:1–14. doi: 10.3389/fphy.2014.00011

53. Eriksson S, Lasic S, Nilsson M, Westin CF, Topgaard D. NMR diffusion-encoding with axial symmetry and variable anisotropy: Distinguishing between prolate and oblate microscopic diffusion tensors with unknown orientation distribution. J Chem Phys. 2015; 142(10):104201. doi: 10.1063/1.4913502 PMID: 25770532; PubMed Central PMCID: PMCPMC4359170.

54. Jelescu IO, Veraart J, Adisetiyo V, Milla SS, Novikov DS, Fieremans E. One diffusion acquisition and different white matter models: how does microstructure change in human early development based on WMTI and NODDI? Neuroimage. 2015; 107:242–56. doi: 10.1016/j.neuroimage.2014.12.009 PMID: 25498427; PubMed Central PMCID: PMCPMC4300243.

55. Jelescu IO, Veraart J, Fieremans E, Novikov DS. Degeneracy in model parameter estimation for multi-compartmental diffusion in neuronal tissue. NMR Biomed. 2016; 29(1):33–47. doi: 10.1002/nbm.3450 PMID: 26615981.

56. Talairach J, Tournoux P. Co-Planar Stereotaxic Atlas of the Human Brain: 3-Dimensional Proportional System: an Approach to Cerebral Imaging. New York: Thieme Medical Publishers; 1988.

57. Oba H, Yagishita A, Terada H, Barkovich AJ, Kutomi K, Yamauchi T, et al. New and reliable MRI diagnosis for progressive supranuclear palsy. Neurology. 2005; 64(12):2050–5. doi: 10.1212/01.WNL.0000165960.04422.D0 PMID: 15985570.

58. Tournier JD C F, Connelly A.. MRtrix: Diffusion tractography in crossing fiber regions. Int J Imaging Syst Technol. 2012; 22:53–66.

59. Mazziotta J, Toga A, Evans A, Fox P, Lancaster J, Zilles K, et al. A probabilistic atlas and reference system for the human brain: International Consortium for Brain Mapping (ICBM). Philos Trans R Soc Lond B Biol Sci. 2001; 356(1412):1293–322. doi: 10.1098/rstb.2001.0915 PMID: 11545704; PubMed Central PMCID: PMCPMC1088516.

60. Andersson JLR, Smith, S, Jenkinson, M. Non-linear registration, aka Spatial normalisation. 2012 3 September. Report No.: FMRIB Technical Report TR07JA1. 2007b.

61. Jones DK, Christiansen KF, Chapman RJ, Aggleton JP. Distinct subdivisions of the cingulum bundle revealed by diffusion MRI fibre tracking: implications for neuropsychological investigations. Neuropsychologia. 2013; 51(1):67–78. doi: 10.1016/j.neuropsychologia.2012.11.018 PMID: 23178227; PubMed Central PMCID: PMCPMC3611599.

62. Wakana S, Caprihan A, Panzenboeck MM, Fallon JH, Perry M, Gollub RL, et al. Reproducibility of quantitative tractography methods applied to cerebral white matter. Neuroimage. 2007; 36(3):630–44. doi: 10.1016/j.neuroimage.2007.02.049 PMID: 17481925; PubMed Central PMCID: PMCPMC2350213.

63. Kim HJ, Kim SJ, Kim HS, Choi CG, Kim N, Han S, et al. Alterations of mean diffusivity in brain white matter and deep gray matter in Parkinson's disease. Neurosci Lett. 2013; 550:64–8. doi: 10.1016/j.neulet.2013.06.050 PMID: 23831353.

64. Szczepankiewicz F, Latt J, Wirestam R, Leemans A, Sundgren P, van Westen D, et al. Variability in diffusion kurtosis imaging: impact on study design, statistical power and interpretation. Neuroimage. 2013; 76:145–54. doi: 10.1016/j.neuroimage.2013.02.078 PMID: 23507377.

65. Kamagata K, Tomiyama H, Hatano T, Motoi Y, Abe O, Shimoji K, et al. A preliminary diffusional kurtosis imaging study of Parkinson disease: comparison with conventional diffusion tensor imaging. Neuroradiology. 2014; 56(3):251–8. doi: 10.1007/s00234-014-1327-1 PMID: 24468858.

66. Makris N, Kennedy DN, McInerney S, Sorensen AG, Wang R, Caviness VS Jr., et al. Segmentation of subcomponents within the superior longitudinal fascicle in humans: a quantitative, in vivo, DT-MRI study. Cereb Cortex. 2005; 15(6):854–69. doi: 10.1093/cercor/bhh186 PMID: 15590909.

67. Bruck A, Kurki T, Kaasinen V, Vahlberg T, Rinne JO. Hippocampal and prefrontal atrophy in patients with early non-demented Parkinson's disease is related to cognitive impairment. J Neurol Neurosurg Psychiatry. 2004; 75(10):1467–9. doi: 10.1136/jnnp.2003.031237 PMID: 15377698; PubMed Central PMCID: PMCPMC1738757.

68. Farina E, Gattellaro G, Pomati S, Magni E, Perretti A, Cannata AP, et al. Researching a differential impairment of frontal functions and explicit memory in early Parkinson's disease. Eur J Neurol. 2000; 7 (3):259–67. PMID: 10886309.

69. Lee CS, Samii A, Sossi V, Ruth TJ, Schulzer M, Holden JE, et al. In vivo positron emission tomographic evidence for compensatory changes in presynaptic dopaminergic nerve terminals in Parkinson's disease. Ann Neurol. 2000; 47(4):493–503. PMID: 10762161.

70. Taylor AE, Saint-Cyr JA, Lang AE. Frontal lobe dysfunction in Parkinson's disease. The cortical focus of neostriatal outflow. Brain. 1986; 109 (Pt 5):845–83. PMID: 3779372.

71. Levin J, Schmidt F, Boehm C, Prix C, Botzel K, Ryazanov S, et al. The oligomer modulator anle138b inhibits disease progression in a Parkinson mouse model even with treatment started after disease onset. Acta Neuropathol. 2014; 127(5):779–80. doi: 10.1007/s00401-014-1265-3 PMID: 24615514; PubMed Central PMCID: PMCPMC3984662.

72. Kamagata K, Hatano T, Okuzumi A, Motoi Y, Abe O, Shimoji K, et al. Neurite orientation dispersion and density imaging in the substantia nigra in idiopathic Parkinson disease. Eur Radiol. 2015. doi: 10.1007/s00330-015-4066-8 PMID: 26515546.

Paper IV

Neuroradiology (2018) 60:247–254
https://doi.org/10.1007/s00234-017-1971-3

DIAGNOSTIC NEURORADIOLOGY

Alteration of putaminal fractional anisotropy in Parkinson's disease: a longitudinal diffusion kurtosis imaging study

Yulia Surova[1,2] · Markus Nilsson[3] · Björn Lampinen[4] · Jimmy Lätt[5] · Sara Hall[6,7] · Håkan Widner[1,2] · Danielle van Westen[1,4] · Oskar Hansson[6,7]

Received: 11 September 2017 / Accepted: 22 December 2017 / Published online: 24 January 2018

Abstract

Purpose In Parkinson's disease (PD), pathological microstructural changes occur that may be detected using diffusion magnetic resonance imaging (dMRI). However, there are few longitudinal studies that explore the effect of disease progression on diffusion indices.

Methods We prospectively included 76 patients with PD and 38 healthy controls (HC), all of whom underwent diffusion kurtosis imaging (DKI) as part of the prospective Swedish BioFINDER study at baseline and 2 years later. Annualized rates of change in DKI parameters, including fractional anisotropy (FA), mean diffusivity (MD), and mean kurtosis (MK), were estimated in the gray matter (GM) by placing regions of interest (ROIs) in the basal ganglia and the thalamus, and in the white matter (WM) by tract-based spatial statistics (TBSS) analysis.

Results When adjusting for potential confounding factors (age, gender, baseline-follow-up interval, and software upgrade of MRI scanner), only a decrease in FA in the putamen of PD patients ($\beta = -0.248$, $P < .01$) over 2 years was significantly different from the changes observed in HC over the same time period. This 2-year decrease in FA in the putamen in PD correlated with higher L-dopa equivalent dose at baseline (Spearman's rho = .399, $P < .0001$).

Conclusion The study indicates that in PD microstructural changes in the putamen occur selectively over a 2-year period and can be detected with DKI.

Keywords Parkinson's disease · Diffusion kurtosis imaging · Tractography · Tract-based spatial statistics

Electronic supplementary material The online version of this article (https://doi.org/10.1007/s00234-017-1971-3) contains supplementary material, which is available to authorized users.

✉ Yulia Surova
yulia.surova@med.lu.se

[1] Department of Clinical Sciences, Lund, Lund University, Lund, Sweden

[2] Department of Neurology Lund, Skåne University Hospital, 221 85 Lund, Sweden

[3] Center for Medical Imaging and Physiology, Skåne University Hospital, Lund, Sweden

[4] Lund University Bioimaging Center, Lund University, Lund, Sweden

[5] Department of Medical Radiation Physics, Lund University, Lund, Sweden

[6] Department of Clinical Sciences, Malmö, Lund University, Malmö, Sweden

[7] Memory Clinic, Skåne University Hospital, Lund, Sweden

Introduction

Parkinson's disease (PD) is an incurable disorder that affects about ten million people worldwide [13]. There is a need for objective methods to track the disease progression over time in the symptomatic phase of patients with PD, to be used when evaluating novel disease-modifying therapies. Although longitudinal studies using positron emission tomography (PET) have been conducted in PD [29], radiation risk, cost, and infrastructural support limit their clinical utility. Diffusion magnetic resonance imaging (dMRI) is a non-invasive and widely accessible imaging modality, which makes it suited for longitudinal studies. A few studies have indicated that diffusion tensor imaging (DTI) might have a potential to track the disease progression in patients with PD [24, 28, 46]. Diffusion kurtosis imaging (DKI) is an extension of DTI [15] that has been suggested to be more sensitive in detecting and differentiating alterations of tissue microstructure [3, 47] and in PD

patients [17, 45]. However, DKI tends to show inconsistent results in brain regions involved in the basal ganglia circuit in PD. Cross-sectional studies in patients with PD have reported increased mean diffusional kurtosis (MK) in basal ganglia, thalamus, and sensorimotor cortex [20, 43, 45], lower MK in white matter (WM) regions [17, 18], or no differences in MK in WM and deep gray matter in PD [37]. DKI has also been suggested as being sensitive to alpha-synuclein accumulation in transgenetic mice [21]. However, there are to our knowledge no longitudinal DKI studies available in PD.

To investigate the link between diffusional changes and PD progression and to distinguish between the concomitant effects of normal aging and disease evolution over time, a longitudinal approach involving both PD patients and normal subjects is the most appropriate study design. Investigation of the longitudinal cerebral alterations occurring in PD ideally includes baseline and follow-up data [23] using the same MRI scanner.

Thus, a 2-year prospective and longitudinal study was conducted on a cohort of PD patients and controls. A follow-up period of approximately 2 years is often used in trials evaluating novel disease-modifying therapies in neurodegenerative disorders such as PD. Effects of disease progression and normal aging on DKI measures in the basal ganglia, the thalamus, and cerebral WM tracts were investigated. Our specific aim was to determine whether there are specific DKI changes over time in PD patients when compared to healthy elderly over a 2-year time period.

Materials and methods

Ethics statement

This study was approved by the Ethics Committee at Lund University and performed in accordance with the Helsinki Declaration. All participants gave written informed consent prior to participation.

Participants

In this case-control study, participants were recruited from the Neurology Clinic at Skåne University Hospital, Sweden, as part of the prospective and longitudinal Swedish BioFINDER study (www.biofinder.se) [12]. As of November 2016, 229 individuals had been included in the Parkinson sub-study of BioFINDER, of which 67 did not perform DKI at baseline, 39 did not perform DKI during follow-up, and 8 cases did not pass QC (Online Resource 1). Consequently, we included 76 patients with PD and 38 healthy controls. For the present work, 76 subjects were included with a clinical diagnosis of probable PD. The diagnosis was made by neurologists trained in movement disorder diagnostics according to the National Institute of Neurological Disorders and Stroke (NINDS) criteria of PD [10]. Neurologically healthy controls (HC), who did not have any objective cognitive or parkinsonian symptoms, were also recruited ($n = 38$). All 114 subjects had clinical assessments and were scanned on two occasions on average 25.3 months apart, with a standard deviation of 4. 3 months. Motor function and disease stage were evaluated using, e.g., Unified Parkinson's disease rating scale motor part (UPDRS-III) [7] and Hoehn and Yahr staging scale (H&Y) [14]. The total score from the motor section of the UPDRS III was broken down into subscales for bradykinesia, rigidity, tremor, gait posture [32]. Cognitive assessments were conducted by trained physicians using a Mini Mental State Examinations (MMSE) [9]. To ensure standardization, assessments were conducted during patients "on" medication state, or fully responding to their PD medications (in the "on" state). The daily L-dopa equivalent dose (LEDD) was calculated (Table 1) [39]. At the time of testing, none of the patients exhibited any dyskinesia, dystonia, or other signs of involuntary movement.

MRI data acquisition

Imaging was performed on a 3 T Siemens Magnetom Skyra MR scanner equipped with a 20 channel head coil. The dMRI protocol comprised 99 DWI volumes, where the choice of b-values and encoding directions was inspired by Poot et al. [31]. In total, three volumes were acquired with $b = 0$ s/mm^2, while the remaining 96 volumes were acquired using b-values of 250, 500, 1000, and 2750 s/mm^2, distributed over 6, 6, 20, and 64 directions, respectively. A single-shot spin-echo with mono-polar diffusion encoding and EPI read-out was used for the acquisition with the following settings: voxel size = 2.3 × 2.3 × 2.3 mm^3, FOV = 294 × 294 × 120 mm^3, iPAT = 2, and partial Fourier factor = 6/8. The imaging volume comprised 52 contiguous axial slices adjusted to include the whole cerebrum. Total acquisition time was approximately 14 min. The study was initiated with the scanner on software version Syngo MR D11, but was later upgraded to version D13, and later again to E11. The upgrades resulted in slight changes of the repetition time (TR) and echo time (TE). For the D11, D13, and E11 versions, TR was set to 7500, 8100, and 8100 ms, respectively, while TE was set to 103, 103, and 104 ms, respectively. Some participants were scanned on baseline with D11 and on follow-up with D13 (28 HC and 41 PD), some made both baseline and follow-up scans on D13 (10 HC and 12 PD), while others made baseline scans on D13 and follow-up on E11 (23 PD). This was corrected for in the analysis, as described under the "analysis" section.

Table 1 Subject characteristic

	Healthy controls ($n = 38$)		Parkinson's patients ($n = 76$)				
	Baseline	Year 2	Baseline	Year 2	Group effect	Time effect	Interaction
Age, years	66.4 (8.1)	–	65.0 (10.8)	–	.801	–	–
Sex (male/female)	16:22	–	52:24	–	.009	–	–
dMRI interval, month	–	25.9 (2.3)	–	25.3 (4.3)	.414	–	–
Disease duration, years	–	–	5.5 (3.6)	7.5 (3.6)	–	< .001	–
Bradykinesia	0 (.0)	0 (.0)	.7 (0.7)	.8 (.9)	< .001	.360	.360
Rigidity	.5 (.9)	.1 (.4)	1.8 (2.5)	1.9 (2.5)	< .001	.383	.293
Tremor	.0 (.3)	.1 (.4)	3.8 (3.3)	3.1 (3.1)	< .001	.256	.221
Gait/posture	.0 (.2)	.0 (.2)	.6 (1.0)	.8 (1.1)	< .001	.313	.313
Hoehn and Yahr stage	–	–	1.8 (.6)	2.0 (.9)	–	.237	–
UPDRS motor, score	1.4 (2.5)	1.7 (2.2)	12.5 (8.6)	14.0 (10.3)	< .001	.215	.347
MMSE, score	28.2 (1.6)	29.0 (1.2)	29.2 (4.5)	29.3 (4.7)	.390	.006	.024
$LEDD_{TOTAL}$, mg	–	–	527.4 (374.9)	705.8 (350.6)	–	< .001	–

UPDRS-III unified Parkinson's disease rating scale motor part, *MMSE* Mini Mental State Examination test, *LEDD* daily L-dopa equivalent dose

Post-processing

Motion and eddy-current distortions were corrected using volume registration to extrapolated references, which is a method particularly well suited for high b-value data acquired in elderly subjects with atrophy [26]. In this procedure, the diffusion-weighted images were modulated with the Jacobian determinant of the transformation matrix [16]. In order to mitigate the potential effects of Gibbs ringing artifacts, image volumes were smoothed using an isotropic 3D Gaussian kernel with a full-width at half maximum of 2.3 mm [19, 30, 41]. Smoothing with a kernel of this size has little effect on sensitivity and specificity [40] and is thus not expected to significantly influence the parameter precision. DKI analysis was performed to obtain maps of fractional anisotropy (FA), MK, and mean diffusivity (MD), using in-house developed software which fitted the diffusion and kurtosis tensors by non-linear optimization as in [22]. The fitting only allowed positive values of the diffusion tensor eigenvalues. In a small number of voxels where the kurtosis was below zero, the fitting was repeated after additional smoothing was performed.

Longitudinal change was assessed in maps produced by coregistering by registering the data from the two time points. To reduce measurement bias, baseline and follow-up FA volumes were both registered to a subject-specific time-averaged template, after which the transform from the FA registration was applied to other contrasts. The template was created by, for each subject, computing and applying the transform that took the baseline volume half-way to the follow-up volume, and vice versa for the follow-up volume, and averaging the two. These registration steps were performed using non-linear registration with the FNIRT tool from FSL. All subsequent analysis was based on data in this subject-specific time-averaged space.

Analysis

ROI based analysis of gray matter

Our a-priori hypothesis defined the caudate, putamen, globus pallidum, thalamus, substantia nigra, and red nucleus as regions of interest for PD follow-up. Our ROI-selection was based on a-priori hypothesis concerning four brain circuits or regions. The first was the cortico-basal ganglia circuit, which consists of the striatum (caudate nucleus and putamen), globus pallidus, and thalamus [33]. The second and third regions included the midbrain and the pons, which have also been implicated in PD [4, 11]. The fourth region comprised the red nucleus, which according to Braak has not been implicated in PD [4] and thus served as a reference region." DKI values were obtained by region of interest (ROI) analysis. One experienced rater drew all ROIs manually according to Surova et al. [37] in the subject-specific time-average data. The same ROIs could thus be applied to both time points. The rater was blinded to the group (HC or patient). Separate ROIs were drawn in the left and the right hemispheres. Because of the presence of bilateral disease in all patients, laterality was not considered in the current study. Values from left and right hemispheres were thus averaged to obtain the final value for analysis. Intra-rater reliability for the ROI placement procedures were assessed on 23 randomly chosen participants using the FA, MD, and MK of the left-side ROIs as a quantitative measure and the mean interclass correlation coefficients for each ROI are presented in (Online Resource 2).

Tract-based spatial statistics analysis of white matter

We assessed differences in two-year changes in major WM tracts between PD and HC using tract-based spatial statistics (TBSS) (v 1.03), part of the FRMIB Software Library (FSL), which is a registration tool for improved voxel-wise comparisons between multiple subjects. The TBSS procedure involved registration of 2-year difference maps of FA, MK, and MD onto the 1 mm^3 FMRIB58 FA template in MNI152 standard space, using the linear and non-linear registration tools FLIRT and FNIRT [1]. Before registration, the diffusion maps were masked with the FSL Brain Extraction Tool (BET) [35]. The normalized maps were then skeletonized by projection onto the FMRIB58 template skeleton. The skeletonized maps were subjected to voxel-wise comparison between PD and HC using FSL Randomize with 7500 permutations [44]. The procedure corrected for multiple comparisons using threshold-free cluster enhancement [36] and included age, gender, and software upgrade of the MRI scanner as covariates. TBSS analyses were done blinded for diagnosis.

Analysis of white matter hyperintensities

Analysis of white matter hyperintensities (WMH) was rated according to the scales of Fazekas [8] and Wahlund [42].

Statistical analysis

Statistical analysis of ROI data was performed with SPSS Statistics 20 for Windows (IBM Corporation, Somers, NY, USA). Demographic and clinical differences between groups were analyzed with either repeated measures ANOVA or Pearson's chi-squared test. Correlations between diffusion parameters and clinical scores were tested for using the linear correlation coefficient (R2 Linear) and Spearman's rho (R_s). The change over time in the mean values (FA, MK, and MD) of the caudate nucleus, putamen, pallidum, thalamus, substantia nigra, and red nucleus were compared between the diagnostic groups using ANCOVA with age, gender, baseline follow-up interval, and software upgrade of MRI scanner included as covariates. Study participants who were scanned with the same scanner software version in baseline and follow-up was coded as "0," while those were scanned with different software versions were coded as "1." Significance threshold was set to 0.05. Multiple comparison correction was not applied to the reported p values. The TBSS analysis, however, inherently corrects for multiple comparisons through the threshold-free cluster enhancement procedure, as now mentioned above.

Results

Demographic and clinical

Table 1 shows the demographic and clinical characteristics of HC and patients with PD at baseline and after 2 years. There was no group difference in age but there was a significant difference in gender distribution (Pearson's $c^2 = 7.2$, $P = .009$), with a higher proportion of men in the PD group.

The PD group had higher UPDRS III total and sub-scores ($P < .001$) compared with HC. An effect of time was found for the MMSE ($P = .006$), due to an increase in the HC group over the 2 years, and for LEDD in the PD group ($P < .001$), amounting to a daily LEDD increase by approximately 35% (180 mg). There were no other significant changes in any other clinical or demographic data over time (Table 1).

ROI based analysis of deep GM

Changes in DKI parameters were observed in both PD patients and controls over the 2-year period. Specifically, reductions in MD and increases in MK and FA were found in many brain regions (Online Resource 3). However, when comparing the changes in dMRI parameters in PD over 2 years to the changes observed in controls over the same time period, we only found a decrease in FA in the putamen in PD (ANCOVA, $\beta = -.248$, $P = .001$). Figure 1 illustrates FA changes in the putamen for PD and HC. There were no other significant longitudinal changes observed in PD when compared to controls, including in the white matter (Online Resource 3).

Tract-based spatial statistics analysis of white matter

There were no significant longitudinal changes in either MD, FA, or MK in the WM observed in PD patients compared to controls.

Correlation between clinical and DKI changes

Two-year change in FA in the putamen in PD patients correlated with LEDD at baseline (R2 linear = − 0.184; $R_s = -0.399$, $P < .0001$) (Fig. 2) and LEDD at follow-up (data not shown). No correlations were found between DKI parameters and UPDRS III, H&Y, and MMSE. Also no correlations were found between change in DKI parameters versus change in UPDRS III, H&Y, and MMSE.

Analysis of WMH

The amount of WMHs did not show any statistically significant difference between controls and patients with PD (data not shown).

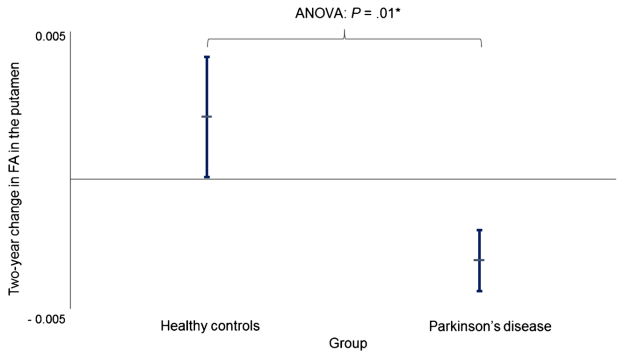

Fig. 1 Two-year change of fractional anisotropy (FA) in the putamen in patients with Parkinson's disease (PD) and healthy controls (HC). Differences in absolute values of FA (values from 2-year MRI minus values from baseline) in the putamen between patients with PD and HCs were analyzed using ANCOVA A modest significant difference was found between PD and HC ($\beta = -0.248$, $P = 0.01$). Lines extending vertically indicate standard error of mean. Horizontal lines that intersect the vertical lines are means

Discussion

We investigated disease-specific structural changes in deep GM and WM in patients with PD over a two-year period. In this cohort with 76 patients with PD and 38 controls, we found a selective reduction in FA in the putamen in PD that correlated with increased LEDD at baseline and follow-up. As the increased LEDD at follow-up is most probably the marker for disease progression, it might be that the decreased FA in the putamen at follow-up has some clinical relevance, especially if this result is confirmed by other studies. This result can be related to a recent longitudinal study that found an increased MD over 6 years in the anterior putamen in patients with PD [6] that correlated with UPDRS scoring [6]. Chan et al did not have controls [6], however, therefore their results may be affected by normal aging and system update effects such as those demonstrated here. Finally, our study did not show any significant diffusion changes in white matter over time in PD when compared to the changes observed in controls, which is in agreement with a previous study [34].

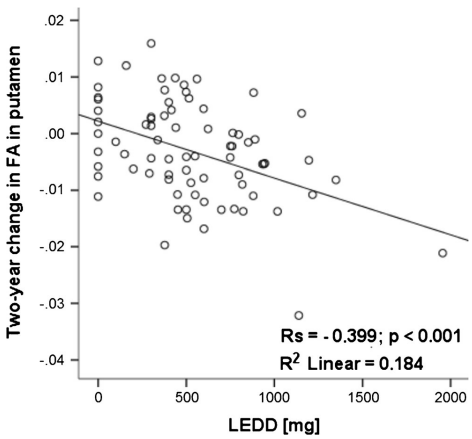

Fig. 2 Correlation between 2-year change in fractional anisotropy (FA) in the putamen with the daily L-dopa equivalent dose (LEDD) at baseline. A moderate positive correlation was found between 2-year change in FA in the putamen and LEDD at baseline in PD. R2 linear, linear correlation coefficient; Rs, Spearman's rho

The observed putaminal FA changes may be related to the progressive loss of dopaminergic nerve terminals in the putamen that occurs in PD patients [5, 27]. Axonal damage or demyelination, with disruption of the axonal membrane and myelin sheath, causes a reduction in the water diffusivity restriction that results in decreased FA indices [2, 25, 37].

Since diffusion changes in PD patients involve both aging and the specific disease evolution, longitudinal follow-up including age-matched controls is warranted to take both factors into account, as done in the present study. Since no significant age-related putaminal FA changes were observed in the control group, it is likely that the disease itself is the main explanation.

The current cohort was similarly matched to controls as in the recent longitudinal DTI reports in PD patients. However, the current study deviates from previous longitudinal reports at several points [6, 23, 24, 28, 34, 46]. The PD patients in the current cohort had longer disease duration, compared to some [24, 46], but shorter compared to other previous studies [6, 23, 34]. The time between dMRI scans was longer, compared to in Ofori et al. [28], Loane et al. [24] and Zhang et al. [46]. Benefits of the current study include using the DKI sequence, which can assess both classic diffusion measurements (FA and MD) as well as MK. Our study is the first longitudinal DKI study. This is the reason that our study benefits from increased power via its longitudinal design. Furthermore, compared to other longitudinal DTI studies, the patients in

the current study did not refrain from antiparkinsonian medication prior to scanning; therefore, we cannot objectively compare the different PD cohorts regarding disease severity. The most notable difference in findings is the lack of diffusion changes in the substantia nigra in the current report, which stands in contrast to previous results [23, 24, 46]. Zhang et al. [46] demonstrated an FA reduction in the substantia nigra of 3.6 ± 1.4%/year from baseline, and increased radial and axial diffusivity in the thalamus of 8.0 ± 2.9%/year and 4.0 ± 1.5%/year, respectively. Such discrepancies were possibly caused by differences in dMRI techniques (DTI in Zhang et al. and DKI in our study). Another possible reason could be that the study of Zhang et al. was multicenter (16 US sites, 5 European, 1 Australian), which can influence the interplay between selected image acquisition parameters and factors including signal-to-noise ratio, image resolution, image distortion and thus, the results derived.

Our study has a number of limitations. First, because the PD diagnoses were not histopathologically confirmed, there is a possibility of misdiagnosis. However, the validity of the PD diagnosis is strengthened by the observation that, after being followed for 25 months, all patients continued to respond satisfactorily to antiparkinsonian therapy and remained free of signs that are atypical Parkinsonism. Another limitation is that the ROIs on gray matter were drawn manually, which could lead to larger variability and bias. However, the interclass correlation coefficients indicated a low variability from this source when it came to putamen (0.81–0.91). Finally, since the study is longitudinal in nature, there is always a risk that those patients with a more severe disease progression drop out of the study, which might cause a selection bias of those still remaining in the study.

Conclusion

Our longitudinal 2-year study of a relatively large cohort of PD patients provides evidence that DKI of the putamen can be used to detect disease progression in symptomatic PD patients. If this finding is replicated in other prospective and longitudinal DKI studies of PD patients and age-matched controls, DKI of putamen might be considered as a secondary outcome measure in clinical trials evaluating novel disease-modifying therapies. However, future studies also need to compare the accuracy of diffusion imaging of putamen with volumetric measures of the basal ganglia when it comes to tracking disease progression.

Acknowledgements The authors thank Ann Johansson and Katarina Johansson, research nurses in the Neurology Department.

Compliance with ethical standards

Funding YS and SH have been funded for this study by the Swedish federal government under the ALF agreement.

Conflict of interest The authors declare that they have no conflict of interest.

Ethical approval All procedures performed in the studies involving human participants were in accordance with the ethical standards of the institutional and/or national research committee and with the 1964 Helsinki Declaration and its later amendments or comparable ethical standards.

Informed consent Informed consent was obtained from all individual participants included in the study.

References

1. Andersson, J. L. R., Smith, S, Jenkinson, M. (2012). Non-linear optimisation
2. Arfanakis K, Haughton VM, Carew JD, Rogers BP, Dempsey RJ, Meyerand ME (2002) "Diffusion tensor MR imaging in diffuse axonal injury." AJNR Am J Neuroradiol 23(5):794–802
3. Bester M, Jensen JH, Babb JS, Tabesh A, Miles L, Herbert J, Grossman RI, Inglese M (2015) Non-Gaussian diffusion MRI of gray matter is associated with cognitive impairment in multiple sclerosis. Mult Scler 21(7):935–944. https://doi.org/10.1177/1352458514556295
4. Braak H, Del Tredici K, Rub U, de Vos RA, Jansen Steur EN, Braak E (2003) Staging of brain pathology related to sporadic Parkinson's disease. Neurobiol Aging 24(2):197–211. https://doi.org/10.1016/S0197-4580(02)00065-9
5. Bruck A, Aalto S, Rauhala E, Bergman J, Marttila R, Rinne JO (2009) A follow-up study on 6-[18F]fluoro-L-dopa uptake in early Parkinson's disease shows nonlinear progression in the putamen. Mov Disord 24(7):1009–1015. https://doi.org/10.1002/mds.22484
6. Chan LL, Ng KM, Yeoh CS, Rumpel H, Li HH, Tan EK (2016) Putaminal diffusivity correlates with disease progression in Parkinson's disease: prospective 6-year study. Medicine (Baltimore) 95(6):e2594. https://doi.org/10.1097/MD.0000000000002594
7. Fahn S, Elton RL, Members of the UPDRS development committee (1987) Unified Parkinson's disease rating scale. In: Fahn S, Marsden CD, Goldstein M, Calne DB (eds) Recent developments in Parkinson's disease, vol 2. Macmillan Healthcare Information, Florham Park, pp 153–163
8. Fazekas F, Chawluk JB, Alavi A, Hurtig HI, Zimmerman RA (1987) MR signal abnormalities at 1.5 T in Alzheimer's dementia and normal aging. AJR Am J Roentgenol 149(2):351–356. https://doi.org/10.2214/ajr.149.2.351

9. Folstein MF, Folstein SE, McHugh PR (1975) "Mini-mental state". A practical method for grading the cognitive state of patients for the clinician. J Psychiatr Res 12(3):189–198. https://doi.org/10.1016/0022-3956(75)90026-6
10. Gelb DJ, Oliver E, Gilman S (1999) Diagnostic criteria for Parkinson disease. Arch Neurol 56(1):33–39. https://doi.org/10.1001/archneur.56.1.33
11. Goedert M, Spillantini MG, Del Tredici K, Braak H (2013) 100 years of Lewy pathology. Nat Rev Neurol 9(1):13–24. https://doi.org/10.1038/nrneurol.2012.242
12. Hall S, Surova Y, Ohrfelt A, Zetterberg H, Lindqvist D, Hansson O (2015) CSF biomarkers and clinical progression of Parkinson disease. Neurology 84(1):57–63. https://doi.org/10.1212/WNL.0000000000001098
13. Hermanns M (2011) Weathering the storm: living with Parkinson's disease. J Christ Nurs 28(2):76–82; quiz 83-74. https://doi.org/10.1097/CNJ.0b013e31820b8d9f
14. Hoehn MM, Yahr MD (1967) Parkinsonism: onset, progression and mortality. Neurology 17(5):427–442. https://doi.org/10.1212/WNL.17.5.427
15. Jensen JH, Helpern JA, Ramani A, Lu H, Kaczynski K (2005) Diffusional kurtosis imaging: the quantification of non-Gaussian water diffusion by means of magnetic resonance imaging. Magn Reson Med 53(6):1432–1440. https://doi.org/10.1002/mrm.20508
16. Jones DK, Cercignani M (2010) Twenty-five pitfalls in the analysis of diffusion MRI data. NMR Biomed 23(7):803–820. https://doi.org/10.1002/nbm.1543
17. Kamagata K, Tomiyama H, Motoi Y, Kano M, Abe O, Ito K, Shimoji K, Suzuki M, Hori M, Nakanishi A, Kuwatsuru R, Sasai K, Aoki S, Hattori N (2013) Diffusional kurtosis imaging of cingulate fibers in Parkinson disease: comparison with conventional diffusion tensor imaging. Magn Reson Imaging 31(9):1501–1506. https://doi.org/10.1016/j.mri.2013.06.009
18. Kamagata K, Tomiyama H, Hatano T, Motoi Y, Abe O, Shimoji K, Kamiya K, Suzuki M, Hori M, Yoshida M, Hattori N, Aoki S (2014) A preliminary diffusional kurtosis imaging study of Parkinson disease: comparison with conventional diffusion tensor imaging. Neuroradiology 56(3):251–258. https://doi.org/10.1007/s00234-014-1327-1
19. Kellner E, Dhital B, Kiselev VG, Reisert M (2016) Gibbs-ringing artifact removal based on local subvoxel-shifts. Magn Reson Med 76(5):1574–1581. https://doi.org/10.1002/mrm.26054
20. Khairnar A, Ruda-Kucerova J, Szabo N, Drazanova E, Arab A, Hutter-Paier B, Neddens J, Latta P, Starcuk Z Jr, Rektorova I (2016) Early and progressive microstructural brain changes in mice overexpressing human alpha-Synuclein detected by diffusion kurtosis imaging. Immun, Brain Behav
21. Khairnar A, Ruda-Kucerova J, Szabo N, Drazanova E, Arab A, Hutter-Paier B, Neddens J, Latta P, Starcuk Z Jr, Rektorova I (2017) Early and progressive microstructural brain changes in mice overexpressing human alpha-Synuclein detected by diffusion kurtosis imaging. Brain Behav Immun 61:197–208. https://doi.org/10.1016/j.bbi.2016.11.027
22. Latt J, Nilsson M, Wirestam R, Stahlberg F, Karlsson N, Johansson M, Sundgren PC, van Westen D (2013) Regional values of diffusional kurtosis estimates in the healthy brain. J Magn Reson Imaging 37(3):610–618. https://doi.org/10.1002/jmri.23857
23. Lenfeldt N, Larsson A, Nyberg L, Birgander R, Forsgren L (2015) Fractional anisotropy in the substantia nigra in Parkinson's disease: a complex picture. Eur J Neurol 22(10):1408–1414. https://doi.org/10.1111/ene.12760
24. Loane C, Politis M, Kefalopoulou Z, Valle-Guzman N, Paul G, Widner H, Foltynie T, Barker RA, Piccini P (2016) Aberrant nigral diffusion in Parkinson's disease: a longitudinal diffusion tensor imaging study. Mov Disord 31(7):1020–1026. https://doi.org/10.1002/mds.26606
25. Mamere AE, Saraiva LA, Matos AL, Carneiro AA, Santos AC (2009) "Evaluation of delayed neuronal and axonal damage secondary to moderate and severe traumatic brain injury using quantitative MR imaging techniques." AJNR Am J Neuroradiol 30(5):947–952
26. Nilsson, M., Szczepankiewicz F, van Westen D, Hansson O (2014). Motion and eddy-current correction in high b-value diffusion MRI: systematic registration errors and how to avoid them. Proceedings of the ISMRM: 2569
27. Nurmi E, Ruottinen HM, Bergman J, Haaparanta M, Solin O, Sonninen P, Rinne JO (2001) Rate of progression in Parkinson's disease: a 6-[18F]fluoro-L-dopa PET study. Mov Disord 16(4):608–615. https://doi.org/10.1002/mds.1139
28. Ofori E, Pasternak O, Planetta PJ, Li H, Burciu RG, Snyder AF, Lai S, Okun MS, Vaillancourt DE (2015) Longitudinal changes in free-water within the substantia nigra of Parkinson's disease. Brain 138(Pt 8):2322–2331
29. Pavese N, Rivero-Bosch M, Lewis SJ, Whone AL, Brooks DJ (2011) Progression of monoaminergic dysfunction in Parkinson's disease: a longitudinal 18F-dopa PET study. NeuroImage 56(3):1463–1468. https://doi.org/10.1016/j.neuroimage.2011.03.012
30. Perrone D, Aelterman J, Pizurica A, Jeurissen B, Philips W, Leemans A (2015) The effect of Gibbs ringing artifacts on measures derived from diffusion MRI. NeuroImage 120:441–455. https://doi.org/10.1016/j.neuroimage.2015.06.068
31. Poot DH, den Dekker AJ, Achten E, Verhoye M, Sijbers J (2010) Optimal experimental design for diffusion kurtosis imaging. IEEE Trans Med Imaging 29(3):819–829. https://doi.org/10.1109/TMI.2009.2037915
32. Prodoehl J, Spraker M, Corcos D, Comella C, Vaillancourt D (2010) Blood oxygenation level-dependent activation in basal ganglia nuclei relates to specific symptoms in de novo Parkinson's disease. Mov Disord 25(13):2035–2043. https://doi.org/10.1002/mds.23360
33. Redgrave P, Rodriguez M, Smith Y, Rodriguez-Oroz MC, Lehericy S, Bergman H, Agid Y, DeLong MR, Obeso JA (2010) Goal-directed and habitual control in the basal ganglia: implications for Parkinson's disease. Nat Rev Neurosci 11(11):760–772. https://doi.org/10.1038/nrn2915
34. Rossi ME, Ruottinen H, Saunamaki T, Elovaara I, Dastidar P (2014) Imaging brain iron and diffusion patterns: a follow-up study of Parkinson's disease in the initial stages. Acad Radiol 21(1):64–71. https://doi.org/10.1016/j.acra.2013.09.018
35. Smith SM (2002) Fast robust automated brain extraction. Hum Brain Mapp 17(3):143–155. https://doi.org/10.1002/hbm.10062
36. Smith SM, Nichols TE (2009) Threshold-free cluster enhancement: addressing problems of smoothing, threshold dependence and localisation in cluster inference. NeuroImage 44(1):83–98. https://doi.org/10.1016/j.neuroimage.2008.03.061
37. Surova Y, Lampinen B, Nilsson M, Latt J, Hall S, Widner H, Swedish Bio FS, van Westen D, Hansson O (2016) Alterations of diffusion kurtosis and neurite density measures in deep grey matter and white matter in Parkinson's disease. PLoS One 11(6):e0157755. https://doi.org/10.1371/journal.pone.0157755
38. Tievsky AL, Ptak T, Farkas J (1999) "Investigation of apparent diffusion coefficient and diffusion tensor anisotrophy in acute and chronic multiple sclerosis lesions." AJNR Am J Neuroradiol 20(8):1491–1499
39. Tomlinson CL, Stowe R, Patel S, Rick C, Gray R, Clarke CE (2010) Systematic review of levodopa dose equivalency reporting in Parkinson's disease. Mov Disord 25(15):2649–2653. https://doi.org/10.1002/mds.23429
40. Van Hecke W, Leemans A, De Backer S, Jeurissen B, Parizel PM, Sijbers J (2010) Comparing isotropic and anisotropic smoothing for

voxel-based DTI analyses: a simulation study. Hum Brain Mapp 31(1):98–114. https://doi.org/10.1002/hbm.20848

41. Veraart J, Fieremans E, Jelescu IO, Knoll F, Novikov DS (2016) Gibbs ringing in diffusion MRI. Magn Reson Med 76(1):301–314. https://doi.org/10.1002/mrm.25866
42. Wahlund LO, Barkhof F, Fazekas F, Bronge L, Augustin M, Sjogren M, Wallin A, Ader H, Leys D, Pantoni L, Pasquier F, Erkinjuntti T, Scheltens P, C. European Task Force on Age-Related White Matter (2001) A new rating scale for age-related white matter changes applicable to MRI and CT. Stroke 32(6): 1318–1322. https://doi.org/10.1161/01.STR.32.6.1318
43. Wang JJ, Lin WY, Lu CS, Weng YH, Ng SH, Wang CH, Liu HL, Hsieh RH, Wan YL, Wai YY (2011) Parkinson disease: diagnostic utility of diffusion kurtosis imaging. Radiology 261(1):210–217. https://doi.org/10.1148/radiol.11102277
44. Winkler AM, Ridgway GR, Webster MA, Smith SM, Nichols TE (2014) Permutation inference for the general linear model. NeuroImage 92:381–397. https://doi.org/10.1016/j.neuroimage.2014.01.060
45. Zhang G, Zhang Y, Zhang C, Wang Y, Ma G, Nie K, Xie H, Liu J, Wang L (2015) Diffusion kurtosis imaging of substantia Nigra is a sensitive method for early diagnosis and disease evaluation in Parkinson's disease. Parkinsons Dis 2015:207624
46. Zhang Y, Wu IW, Tosun D, Foster E, Schuff N, I. Parkinson's Progression Markers (2016) Progression of regional microstructural degeneration in Parkinson's disease: a multicenter diffusion tensor imaging study. PLoS One 11(10):e0165540. https://doi.org/10.1371/journal.pone.0165540
47. Zhuo J, Xu S, Proctor JL, Mullins RJ, Simon JZ, Fiskum G, Gullapalli RP (2012) Diffusion kurtosis as an in vivo imaging marker for reactive astrogliosis in traumatic brain injury. NeuroImage 59(1):467–477. https://doi.org/10.1016/j.neuroimage.2011.07.050

Paper V

Quantitative susceptibility mapping (QSM) in parkinsonism – potentially improving diagnostics

Authors: Henrik Sjöström, MD; Yulia Surova, MD; Markus Nilsson, PhD; Tobias Granberg, MD, PhD; Eric Westman, PhD; Danielle van Westen, MD, PhD; Per Svenningsson, MD, PhD; Oskar Hansson, MD, PhD

Henrik Sjöström, Karolinska Institutet, Department of Clinical Neuroscience; Karolinska University Hospital, Department of Neurology.
Yulia Surova, Lund University, Department of Clinical Sciences, Clinical memory Research Unit; Skåne University Hospital, Neurology Clinic.
Markus Nilsson, Lund University, Lund University Bioimaging Center.
Tobias Granberg, Karolinska Institutet, Department of Clinical Neuroscience; Karolinska University Hospital, Department of Radiology.
Eric Westman, Karolinska Institutet, Department of Neurobiology, Care Sciences and Society, Division of Clinical Geriatrics; King's College London, Institute of Psychiatry, Psychology and Neuroscience, Centre for Neuroimaging Sciences, Department of Neuroimaging.
Danielle van Westen, Lund University, Department of Clinical Sciences, Diagnostic Radiology; Skåne University Hospital, Department for Image and Function.
Per Svenningsson, Karolinska Institutet, Department of Clinical Neuroscience; Karolinska University Hospital, Department of Neurology.
Oskar Hansson, Lund University, Department of Clinical Sciences, Clinical memory Research unit; Skåne University Hospital, Memory Clinic.

Title character count: 93

Number of references: 29
Number of tables: 2
Number of figures: 4

Word count abstract: 244
Word count paper: 2611

Corresponding Author:
Henrik Sjöström
Department of Neurology, R54
Karolinska University Hospital
141 86 Stockholm, Sweden
Phone +46 702 24 40 09
E-mail: henrik.sjostrom@ki.se

Henrik Sjöström henrik.sjostrom@ki.se
Yulia Surova yulia.surova@med.lu.se
Markus Nilsson markus.nilsson@med.lu.se
Tobias Granberg tobias.granberg@ki.se
Eric Westman eric.westman@ki.se
Danielle van Westen danielle.van_westen@med.lu.se
Per Svenningsson per.svenningsson@ki.se
Oskar Hansson oskar.hansson@med.lu.se

Statistical analysis conducted by Henrik Sjöström, MD, Karolinska Institutet.
Search terms: MRI [120], Parkinson's disease [165], Progressive supranuclear palsy [166], Multiple system atrophy [172]

Author contributions:
Henrik Sjöström, study concept and design, data processing, statistical analysis, drafting of initial manuscript.
Yulia Surova, acquisition of data, data processing, revision of manuscript for intellectual content.
Markus Nilsson, acquisition of data, revision of manuscript for intellectual content.
Tobias Granberg, study concept and design, revision of manuscript for intellectual content.
Eric Westman study concept and design, revision of manuscript for intellectual content.
Danielle van Westen, study concept and design, acquisition of data, revision of manuscript for intellectual content.
Per Svenningsson, study concept and design, study funding, revision of manuscript for intellectual content.
Oskar Hansson, study concept and design, study funding, acquisition of data, revision of manuscript for intellectual content.

Author disclosures:
Henrik Sjöström – Reports no disclosures.
Yulia Surova – Reports no disclosures.
Markus Nilsson – Reports no disclosures.
Tobias Granberg – Reports no disclosures.
Eric Westman – Reports no disclosures.
Danielle van Westen – Reports no disclosures.
Per Svenningsson – Reports no disclosures.
Oskar Hansson – OH has acquired research support (for the institution) from Roche, GE Healthcare, Biogen, AVID Radiopharmaceuticals, Fujirebio, and Euroimmun. In the past 2 years, he has received consultancy/speaker fees (paid to the institution) from Lilly, Roche, and Fujirebio.

Study funding:
Study funded by the European Research Council, the Swedish Research Council, the Parkinson foundation of Sweden, the Parkinson research foundation, the Marianne and Marcus Wallenberg foundation, the Swedish Brain Foundation, the Skåne University Hospital Foundation, and the Swedish federal government under the ALF agreement. PS is a Wallenberg Clinical Scholar.

Abstract

Objective: To evaluate the use of quantitative susceptibility mapping (QSM) for differential diagnosis in Parkinson's disease (PD), Progressive supranuclear palsy (PSP) and Multiple system atrophy (MSA).

Methods: We included 133 patients with PD, 11 with PSP, 10 with MSA and 44 healthy controls. All participants underwent MRI as part of the prospective Swedish BioFINDER study. Magnitude and high-pass filtered phase images from susceptibility-weighted MRI were processed into susceptibility maps using an in-house developed pipeline.

Results: We found that susceptibility patterns in deep structures differed between groups. PSP had higher susceptibility in globus pallidus, substantia nigra, red nucleus and dentate nucleus compared to all other groups, as well as higher putaminal susceptibility compared to PD and controls. We also found higher putaminal susceptibility in MSA compared to PD and controls, and higher susceptibility in substantia nigra and dentate nucleus compared to PD. Utilizing all regions in a discriminant analysis between PSP and PD, a sensitivity of 100% and specificity of 97% was achieved. Using all regions to separate PSP from MSA, we found a sensitivity of 91% and specificity of 90%. We also found correlations between disease severity measured by UPDRS-III and putaminal susceptibility in PD.

Conclusions: Susceptibility in deep nuclei seems promising in the diagnostics of atypical parkinsonism, especially in PSP where both high sensitivity and specificity was achieved. Correlations between susceptibility and disease severity within groups might indicate a possibility that QSM could be valuable in monitoring disease progression and in clinical trials.

Introduction

The most common cause of parkinsonism is idiopathic Parkinson's disease (PD), that must be differentiated from progressive supranuclear palsy (PSP) and multiple system atrophy (MSA).[1] A correct and early diagnosis is important for optimal patient care and for enrolment in clinical trials.[2] However, the parkinsonian disorders may be hard to distinguish from each other, especially in the early stages. Patients with MSA typically develop autonomic dysfunction in combination with parkinsonian or cerebellar symptoms,[3] whereas patients with PSP patients commonly exhibit vertical gaze palsy in addition to postural instability and falls.[4] In suspected parkinsonian disorders, MRI is commonly performed as part of the clinical investigation. Structural images, however, lack accuracy in separating these conditions at early stages.[5] Other MRI techniques including diffusion weighted imaging, presence of swallow-tail sign on susceptibility-weighted images (SWI) and neuromelanin-sensitive imaging show varying potential.[6–10]

Quantitative susceptibility mapping (QSM) is a technique where phase MRI data is processed to yield susceptibility maps. The quantitative maps correlate well to tissue iron content.[11] Iron accumulation is common in neurodegenerative disorders, and QSM has been used to investigate changes in the substantia nigra in PD.[12,13] While QSM is commonly gathered through dedicated data acquisition, routine clinical SWI sequence may be used for quantitative measurements. We have previously showed that PSP and MSA exhibit characteristic susceptibility patterns in a retrospective pilot study using such data.[14] The aim of this study is to corroborate and extend these findings in a larger prospective cohort, investigate a new brain region, and to further evaluate the diagnostic performance.

Methods

Participants

Participants were prospectively recruited from the Neurology Clinic at Skåne University Hospital, Sweden, between the years 2008 and 2017, as part of the Swedish BioFINDER study (http://www.biofinder.se).[15] As of July 4th 2017, a total of 356 individuals had been included. 67 dropped out of the study before MRI examination; 42 declined MRI examination, 13 had DBS prior to study, 8 had cancer, 2 had pacemakers, 1 received a transplantation and 1 had a subdural hematoma. After excluding 23 individuals with other or unclear diagnoses, we selected 134 patients with PD, 11 with PSP, 10 with MSA and 44 healthy controls for this current study. The diagnosis of PD was established by a movement disorder specialist according to the National Institute of Neurological Disorders and Stroke (NINDS) criteria.[16] The included patients with PSP and MSA met the conditions for probable disease, as determined by a movement disorder specialist, according to their respective diagnostic criteria.[17,18]

Clinical assessments

Patients and healthy controls underwent a series of clinical tests and rating scales, including motor tests with Unified Parkinson's Disease Rating Scale Part III (UPDRS-III) and Hoehn & Yahr. To assess cognitive ability a standard battery of tests, including Mini-Mental State Examination (MMSE), were conducted by a trained physician. Presence of dementia was assessed and recorded. All tests were conducted in "on state" to ensure standardization. None of the participants exhibited signs of involuntary movements, such as dyskinesia or dystonia, during testing. The clinical tests were conducted in relatively close proximity to the MRI examination (median: 1.2 months before MRI, interquartile range (IQR): 3.6 months before to 2.0 months after MRI)

Standard protocol approvals, registrations, and patient consents

The study was approved by the ethics committee at Lund University and performed in accordance with the Helsinki Declaration. All participants gave signed informed consent before participating.

MRI protocol

Brain imaging was performed on a 3 T Siemens Skyra MRI scanner equipped with a 20-channel head coil (Siemens Medical Systems, Erlangen, Germany). High-resolution 3D SWI sequences were used to obtain magnitude and high-pass filtered phase images (repetition time 27 ms, echo time 20 ms, flip angle 15°, voxel size 0.86 x 0.86 x 1.5 mm^3). We also acquired high-resolution 3D T1-weighted images using magnetization-prepared rapid gradient-echo (MPRAGE) (repetition time 1900 ms, echo time 2.54 ms, inversion time 900 ms, flip angle 9°, voxel size 1 x 1 x 1 mm^3) for volumetric analysis.

Image processing

The phase and magnitude data was processed using an in-house developed pipeline consisting of FSL (version 5.0.8, http://www.fmrib.ox.ac.uk/fsl), MATLAB (version R2015a, MathWorks, Natick, USA) and STISuite (version 2.2, Duke University, Durham, North Carolina, USA).[19,20] These methods have been thoroughly described and illustrated in a previous study.[14] To summarize, brain masks were created through FSL-BET using the magnitude images.[21] The masks were then three-dimensionally eroded to ensure that no extra-cerebral tissue was present within the mask. The masks were applied to the phase images which were unwrapped using Laplacian techniques and thereafter processed using the Variable-kernel Sophisticated Harmonic Artifact Reduction on Phase data method (V-SHARP) to remove unwanted background phase. Finally, the inverse solution from field to

source was calculated using the improved sparse linear equation and least-squares method (iLSQR).[19,20,22,23]

The segmentation process is illustrated in Figure 1. The image analysis was conducted blinded to the diagnosis and in a randomized order for all participants. Automated segmentation of the globus pallidus and putamen was performed using FSL-FIRST on the T1-weighted volumes.[24] The magnitude images were then registered to the T1-weighted volumes and the resulting transformation applied to the susceptibility maps.[25] The masks from the automated segmentations were then manually adjusted by a resident in neurology (H.S.) to ensure good fit with the susceptibility maps using ITK-SNAP (version 3.2.0, http://www.itksnap.org).[26] The remaining regions of interest (ROI), consisting of the substantia nigra, the red nucleus and the cerebellar dentate nucleus, were manually delineated by a specialist in neurology (Y.S.) using in-house developed segmentation software. As shown in Figure 1, these regions were segmented directly on the susceptibility maps. Parameter estimates were extracted as averages of the paired structures. The selection of these particular regions was based on findings in a previous study,[14] where differences between the groups were found in globus pallidus, putamen, substantia nigra and the red nucleus. The dentate nucleus was added since PSP is known to exhibit tau pathology in this structure[4] and the region might also be interesting in MSA considering that a subtype has prominent cerebellar involvement.[27] Additionally, ROIs were manually placed in the frontal horns of the lateral ventricles by a resident in neurology (H.S.) and all other susceptibility values were normalized to this reference region.

Statistical analysis

Statistical analysis was performed using SPSS (version 24.0 for Mac, IBM Corp., Armonk, NY, USA). Gender distribution between the groups was assessed using Pearson's χ^2 test and possible differences in age by one-way ANOVA. One-way ANCOVA was used to investigate differences in susceptibility between the groups and pairwise comparisons were performed within the ANCOVA using least significant difference (LSD). Area under receiver operating characteristic curves (AUC) and discriminant analysis were used to evaluate diagnostic performance. Pearson partial correlation tests were conducted to test for correlations between susceptibility levels and clinical scales, and between disease duration and susceptibility levels. For the pairwise comparisons we employed a Bonferroni-corrected α-value of 0.05/30 = 0.0017 to determine statistical significance. A p-value < 0.05 was considered significant unless otherwise mentioned.

Results

Demographics

The demographics of the participants are presented in Table 1. There was no significant difference in age ($F_{3,195} = 1.842$, $p = 0.141$ assessed by one-way ANOVA) between the groups. There was a difference in gender distribution ($p = 0.026$ assessed by Pearson's χ^2 test), with more male participants in the PD group, thus a one-way ANCOVA was used to correct for gender and age in the group comparisons.

Group differences

As shown in Figure 2 there were significant group differences in all ROIs; globus pallidus ($F_{3,193} = 6.474$, $p < 0.001$), putamen ($F_{3,193} = 32.920$, $p < 0.001$), substantia nigra ($F_{3,193} = 22.968$, $p < 0.001$), red nucleus ($F_{3,193} = 43.137$, $p < 0.001$) and dentate nucleus ($F_{3,193} =$

26.291, $p < 0.001$). Significant effects of age were found in the putamen ($p < 0.001$), red nucleus ($p < 0.001$) and dentate nucleus ($p = 0.004$). No significant effects of gender were found in any of the regions. Further analyses revealed that the PSP group showed higher susceptibility in the red nucleus compared to all other groups (all p-values < 10^-4) and in globus pallidus, putamen, substantia nigra and the dentate nucleus compared to PD and controls (all p-values < 0.0001). We also found higher putaminal susceptibility in MSA compared to PD ($p < 0.0001$) and healthy controls ($p < 0.0001$), and higher susceptibility in substantia nigra ($p = 0.0006$) and the dentate nucleus ($p < 0.0001$) compared to PD. We found no significant differences between the PD group and the control group in any of the ROI. Representative susceptibility maps of the different groups are presented in Figure 3.

Diagnostic performance

Diagnostic performance in the different regions between the groups was evaluated using the area under ROC-curves, AUC. Cut-off levels were chosen to yield a differentiation as close to perfect as possible by selecting the point on the ROC curve closest to the upper left corner. The ROC-curves and associated results are reported in Figure 4A-F. To further investigate diagnostic accuracy, we also performed discriminant analysis between each of the three patient groups and the controls, using all of the five ROI. In the discriminant analysis, prior probabilities were set to "all groups equal" to correct for unbalanced group sizes. In classifying PSP vs. PD, we found a sensitivity of 100%, a specificity of 97.0% and a total of 97.2% cases correctly classified. With leave-one-out cross-validation (LOOCV), results were unchanged. When classifying PSP vs. MSA, a sensitivity of 90.9% and a specificity of 90.0% were achieved, with 90.5% of cases correctly classified. In the LOOCV of this classification we found a sensitivity of 81.8%, a specificity of 90.0% and a total of 85.7% cases correctly classified. Results from all discriminant analyses are reported in Table 2.

Correlations between susceptibility and clinical scores

In the PD group, we evaluated correlations between susceptibility levels in the different regions and the clinical scores from UPDRS-III and Hoehn & Yahr ratings. Due to the small number of subjects with PSP and MSA, no correlation tests were carried out in these groups. For this analysis, we used Pearson partial correlation while controlling for age, gender and disease duration. There was a significant correlation between putaminal susceptibility and UPDRS-III in the PD ($R = 0.213$, $p = 0.015$). The remaining tests between susceptibility levels and UPDRS-III or Hoehn & Yahr did not show any significant correlations. We also assessed correlations between disease duration and regional susceptibility while controlling for age and gender. In these tests, we found significant correlations in the PD group in the globus pallidus ($R = 0.198$, $p = 0.023$) and in the substantia nigra ($R = 0.251$, $p = 0.004$). Plots of the significant correlations are shown in Figure 4G-I.

Discussion

We have processed magnitude and high-pass filtered phase data from standard clinical SWI sequences to demonstrate different patterns in parenchymal susceptibility between the different parkinsonian disorders and healthy controls. We can here show a very promising performance in the separation of PSP from the other groups both using cutoffs on ROC-curves and with discriminant classification analysis. When comparing PSP to PD, we find a diagnostic performance with sensitivity 90.9% and specificity 97.0% in the substantia nigra, sensitivity 100% and specificity 91.0% in the red nucleus, and sensitivity 90.9% and specificity 89.6% in the dentate nucleus. The diagnostic performance is increased when including susceptibility levels from all studied regions in discriminant analyses where we have shown a sensitivity of 100% and specificity of 97.0% using LOOCV, for differentiating PSP from PD. We find these levels of diagnostic performance impressive and reviewing

literature we find that these results are comparable to the performance of midbrain-pons area and MR Parkinsonism Index (MRPI) measurements.[28] Combining morphological analyses such as the MRPI with QSM to potentially increase the diagnostic accuracy even further is an interesting direction for future studies. Moreover, it will be important to perform comparative studies in patients with classical Richardson PSP to other subtypes of PSP and patients with corticobasal syndrome.[29] The elevated susceptibility in the putamen and the dentate nucleus in MSA are coherent with pathological processes in these conditions,[27] and thus potential biomarkers. Considering that differentiating early PSP and MSA is a common clinical problem, we believe that analyzing the susceptibility patterns could possibly be of use in these situations. Further studies on possible and early disease would be needed to evaluate this. We also show correlations between UPDRS-III-scores and putaminal susceptibility in the PD group which is consistent with findings in an earlier study[14] and with pathological processes in PD.[1] The correlations between disease duration and susceptibility levels in globus pallidus and the substantia nigra suggests that susceptibility gradually increases with the disease progression.

This work is an extension and validation of a previous study,[14] where a smaller and less coherent retrospective cohort was studied. We are able to show that the majority of these findings persist in this larger and improved study. Here, the participants have been recruited prospectively and all were imaged on the same MRI scanner with a SWI sequence with the same acquisition parameters, which was not the case in the earlier study. We have also used blinding of diagnosis during all segmentation processing. Considering known pathologies in PSP and cerebellar involvement in variants of MSA, we also expanded the number of investigated regions to include the cerebellar dentate nucleus.[4,27] The major findings of the

previous study, with markedly elevated susceptibility levels in mesencephalic nuclei in PSP compared to all other groups, have been corroborated in this larger cohort.

One limitation of this study is the use of SWI-based high-pass filtered phase images. The filtering process can remove local field inhomogeneities together with background phase and because of this reduce the susceptibility contrast, which could lessen the ability to find differences between groups. We have, however, been able to demonstrate highly significant differences and diagnostic separation between the groups with these methods. Considering this filtered nature of the phase images, the yielded susceptibility maps can be considered to reflect apparent susceptibility rather than actual susceptibility. Moreover, this apparent susceptibility is not directly comparable to the susceptibility obtained from QSM based on unfiltered phase data. The images on which our findings are based are representative for a clinical setting where SWI is frequently used. With this in mind, we believe that the approach demonstrated herein could also be used on other material and neurological diseases where magnitude and phase data from SWI have already been acquired. In contrast to other studies using QSM in Parkinson's disease,[12,13] we did not find a susceptibility difference in the substantia nigra between PD and controls. We believe this might in part be due to lower susceptibility contrast due to the filtered phase data in this study. To evaluate susceptibility mapping as an early diagnostic marker, further studies are needed with individuals in early disease stages. Longitudinal studies in parkinsonian disorders are also needed to further assess the ability of these methods to monitor disease progression or measure treatment effects in trials.

In summary, we show different patterns of brain susceptibility between these conditions, reflecting underlying regional differences in pathological processes and brain iron

accumulation. We believe that these differences in susceptibility, particularly in the mesencephalic region, could be of great use in the diagnostics of parkinsonian disorders, especially when faced with the diagnostic challenge of separating PSP from other parkinsonian disorders and healthy individuals. This is very important in the clinical care of these patients considering optimization of medication and involvement of different health professions such as physiotherapists, nutritionists, psychologists and speech-language therapists. It is also of importance to have an early and correct diagnosis when considering inclusion of patients in clinical trials.

Acknowledgments

We want to thank the participants and their families for making this study possible.

References

1. Kalia LV, Lang AE. Parkinson's disease. Lancet. 2015;386:896–912.

2. Eschlböck S, Krismer F, Wenning GK. Interventional trials in atypical parkinsonism. Parkinsonism Relat Disord. 2016;22 Suppl 1:S82-92.

3. Wenning GK, Colosimo C, Geser F, Poewe W. Multiple system atrophy. Lancet Neurol. 2004;3:93–103.

4. Williams DR, Lees AJ. Progressive supranuclear palsy: clinicopathological concepts and diagnostic challenges. Lancet Neurol. 2009;8:270–279.

5. Broski SM, Hunt CH, Johnson GB, Morreale RF, Lowe VJ, Peller PJ. Structural and functional imaging in parkinsonian syndromes. Radiographics. 2014;34:1273–1292.

6. Sako W, Abe T, Murakami N, et al. Imaging-based differential diagnosis between multiple system atrophy and Parkinson's disease. J Neurol Sci. 2016;368:104–108.

7. Surova Y, Nilsson M, Lätt J, et al. Disease-specific structural changes in thalamus and dentatorubrothalamic tract in progressive supranuclear palsy. Neuroradiology. 2015;57:1079–1091.

8. Bae YJ, Kim J-M, Kim E, et al. Loss of Nigral Hyperintensity on 3 Tesla MRI of Parkinsonism: Comparison With (123) I-FP-CIT SPECT. Mov Disord. 2016;31:684–692.

9. Reiter E, Mueller C, Pinter B, et al. Dorsolateral nigral hyperintensity on 3.0T susceptibility-weighted imaging in neurodegenerative Parkinsonism. Mov Disord. 2015;30:1068–1076.

10. Heim B, Krismer F, De Marzi R, Seppi K. Magnetic resonance imaging for the diagnosis of Parkinson's disease. J Neural Transm (Vienna). 2017;124:915–964.

11. Langkammer C, Schweser F, Krebs N, et al. Quantitative susceptibility mapping (QSM) as a means to measure brain iron? A post mortem validation study. Neuroimage. 2012;62:1593–1599.

12. Barbosa JHO, Santos AC, Tumas V, et al. Quantifying brain iron deposition in patients with Parkinson's disease using quantitative susceptibility mapping, R2 and R2. Magn Reson Imaging. 2015;33:559–565.

13. Murakami Y, Kakeda S, Watanabe K, et al. Usefulness of Quantitative Susceptibility Mapping for the Diagnosis of Parkinson Disease. AJNR Am J Neuroradiol. Epub 2015 Mar 12.

14. Sjöström H, Granberg T, Westman E, Svenningsson P. Quantitative susceptibility mapping differentiates between parkinsonian disorders. Parkinsonism Relat Disord. 2017;44:51–57.

15. Hall S, Surova Y, Öhrfelt A, Zetterberg H, Lindqvist D, Hansson O. CSF biomarkers and clinical progression of Parkinson disease. Neurology. 2015;84:57–63.

16. Gelb DJ, Oliver E, Gilman S. Diagnostic criteria for Parkinson disease. Arch Neurol. 1999;56:33–39.

17. Litvan I, Agid Y, Calne D, et al. Clinical research criteria for the diagnosis of progressive supranuclear palsy (Steele-Richardson-Olszewski syndrome): report of the NINDS-SPSP international workshop. Neurology. 1996;47:1–9.

18. Gilman S, Wenning GK, Low PA, et al. Second consensus statement on the diagnosis of multiple system atrophy. Neurology. 2008;71:670–676.

19. Li W, Wu B, Liu C. Quantitative susceptibility mapping of human brain reflects spatial variation in tissue composition. Neuroimage. 2011;55:1645–1656.

20. Li W, Wang N, Yu F, et al. A method for estimating and removing streaking artifacts in quantitative susceptibility mapping. Neuroimage. 2015;108:111–122.

21. Smith SM. Fast robust automated brain extraction. Hum Brain Mapp. 2002;17:143–155.

22. Li W, Avram AV, Wu B, Xiao X, Liu C. Integrated Laplacian-based phase unwrapping and background phase removal for quantitative susceptibility mapping. NMR Biomed. 2014;27:219–227.

23. Wu B, Li W, Guidon A, Liu C. Whole brain susceptibility mapping using compressed sensing. Magn Reson Med. 2012;67:137–147.

24. Patenaude B, Smith SM, Kennedy DN, Jenkinson M. A Bayesian model of shape and appearance for subcortical brain segmentation. Neuroimage. 2011;56:907–922.

25. Jenkinson M, Bannister P, Brady M, Smith S. Improved optimization for the robust and accurate linear registration and motion correction of brain images. Neuroimage. 2002;17:825–841.

26. Yushkevich PA, Piven J, Hazlett HC, et al. User-guided 3D active contour segmentation of anatomical structures: significantly improved efficiency and reliability. Neuroimage. 2006;31:1116–1128.

27. Ahmed Z, Asi YT, Sailer A, et al. The neuropathology, pathophysiology and genetics of multiple system atrophy. Neuropathol Appl Neurobiol. 2012;38:4–24.

28. Whitwell JL, Höglinger GU, Antonini A, et al. Radiological biomarkers for diagnosis in PSP: Where are we and where do we need to be? Mov Disord. 2017;32:955–971.

29. Boxer AL, Yu J-T, Golbe LI, Litvan I, Lang AE, Höglinger GU. Advances in progressive supranuclear palsy: new diagnostic criteria, biomarkers, and therapeutic approaches. Lancet Neurol. 2017;16:552–563.

Legends to figures

Figure 1. Segmentation processing. Automated segmentation of globus pallidus (blue) and putamen (magenta) on T1-weighted image and manual editing to unsure fit to susceptibility map (A). Manual segmentation of substantia nigra (green), the red nucleus (red) and the dentate nucleus (yellow) on the susceptibility maps (B).

Figure 2. Susceptibility distributions and differences. Susceptibility distributions in the different groups in globus pallidus (A), putamen (B), substantia nigra (C), the red nucleus (D) and the dentate nucleus (E). Red line denotes the median and blue lines the interquartile range. Significant differences between the groups (F). Abbreviations: PD = Parkinson's disease; PSP = progressive supranuclear palsy; MSA = multiple system atrophy; CTRL = control; ppm = parts per million.

Figure 3. Representative susceptibility maps and plots of correlation. Representative susceptibility maps from the different groups showing higher susceptibility in the red nucleus in PSP, higher susceptibility in the dentate nucleus in PSP and MSA, and higher putaminal susceptibility in MSA compared to PD and controls. Top row showing the level of the lentiform nuclei, middle row mesencephalon and bottom row cerebellum. Abbreviations: PD = Parkinson's disease; PSP = progressive supranuclear palsy; MSA = multiple system atrophy.

Figure 4. Receiver operating characteristic (ROC) curves showing diagnostic performance. Receiver operating characteristic (ROC) displaying diagnostic separation in all regions between PSP and PD (A), PSP and MSA (B), PSP and controls (C), MSA and PD

(D), MSA and controls (E), controls and PD (F). Scatter plots showing significant correlations from the Pearson partial correlation tests (G-I). * indicates that the AUC, sensitivity and sensitivity shown are for the reversed comparison. Abbreviations: PD = Parkinson's disease; PSP = progressive supranuclear palsy; MSA = multiple system atrophy; ROI = region of interest; AUC = area under curve; Sens. = sensitivity; Spec. = specificity; GP = globus pallidus; PUT = putamen; SN = substantia nigra; RN = red nucleus; DN = dentate nucleus; UPDRS-III = unified Parkinson's disease rating scale part III; susc. = susceptibility; ppm = parts per million.

Demographic variables	PD	PSP	MSA	Controls
Participants, N	134	11	10	44
Age at clinical visit, y, mean ± SD	66.9 ± 9.6	72.2 ± 5.5	63.4 ± 11.4	66.0 ± 7.8
Gender, F/M; Female, %	48/86; 35	6/5; 55	6/4; 60	26/18; 59
Disease duration, y, mean ± SD	6.0 ± 5.0	5.5 ± 2.8	4.7 ± 2.2	N/A
UPDRS-III, score, median (IQR)	13.5 (7-22.25)	36 (28-58)	38.5 (24-52.5)	1 (0-2)
Hoehn & Yahr, score, median (IQR)	2 (1-2.5)	4 (3.5)	4 (3-5)	0 (0-0)
MMSE, score, median (IQR)	28 (27-29)	27 (19-28)	29 (26.75-29)	29 (28-30)
Dementia, N	18	4	0	0

Table 1. Demographic characteristics of study participants. Abbreviations: IQR = interquartile range; UPDRS-III = unified Parkinson's disease rating scale part III; MMSE = mini-mental state examination; PD = Parkinson's disease; PSP = progressive supranuclear palsy; MSA = multiple system atrophy.

	Sensitivity	Specificity	Correctly classified	LOOCV Sensitivity	LOOCV Specificity	LOOCV Correctly classified
PSP vs. PD	100%	97.0%	97.2%	100%	97.0%	97.2%
PSP vs. MSA	90.9%	90.0%	90.5%	81.8%	90.0%	85.7%
MSA vs. PD	70.0%	94.8%	93.1%	60.0%	94.8%	92.4%
PSP vs. Control	100%	97.7%	98.2%	81.8%	95.5%	92.7%
MSA vs. Control	70.0%	88.6%	85.2%	70.0%	88.6%	85.2%
PD vs. Control	61.9%	56.8%	60.7%	59.7%	54.5%	58.4%

Table 2. Results from discriminant analyses. Abbreviations: PD = Parkinson's disease; PSP = progressive supranuclear palsy; MSA = multiple system atrophy; LOOCV = leave-one-out cross-validation.

Figure 1

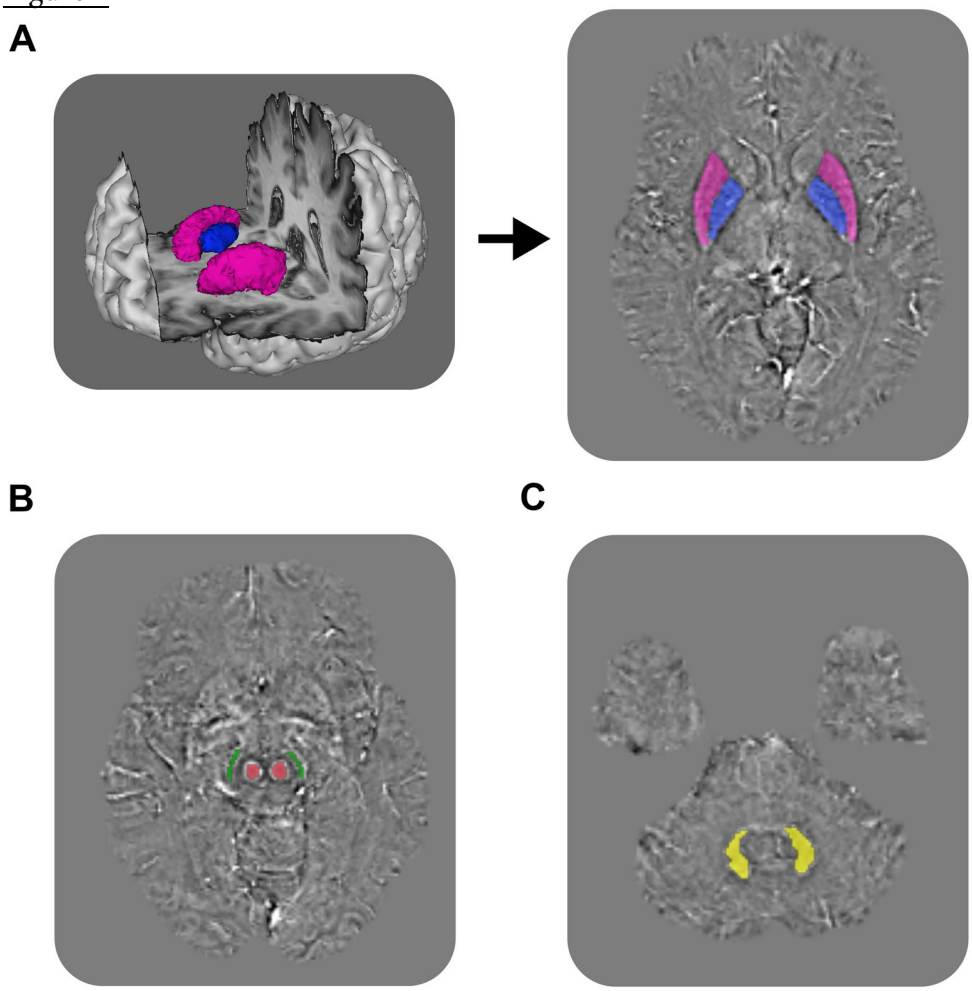

Figure 2

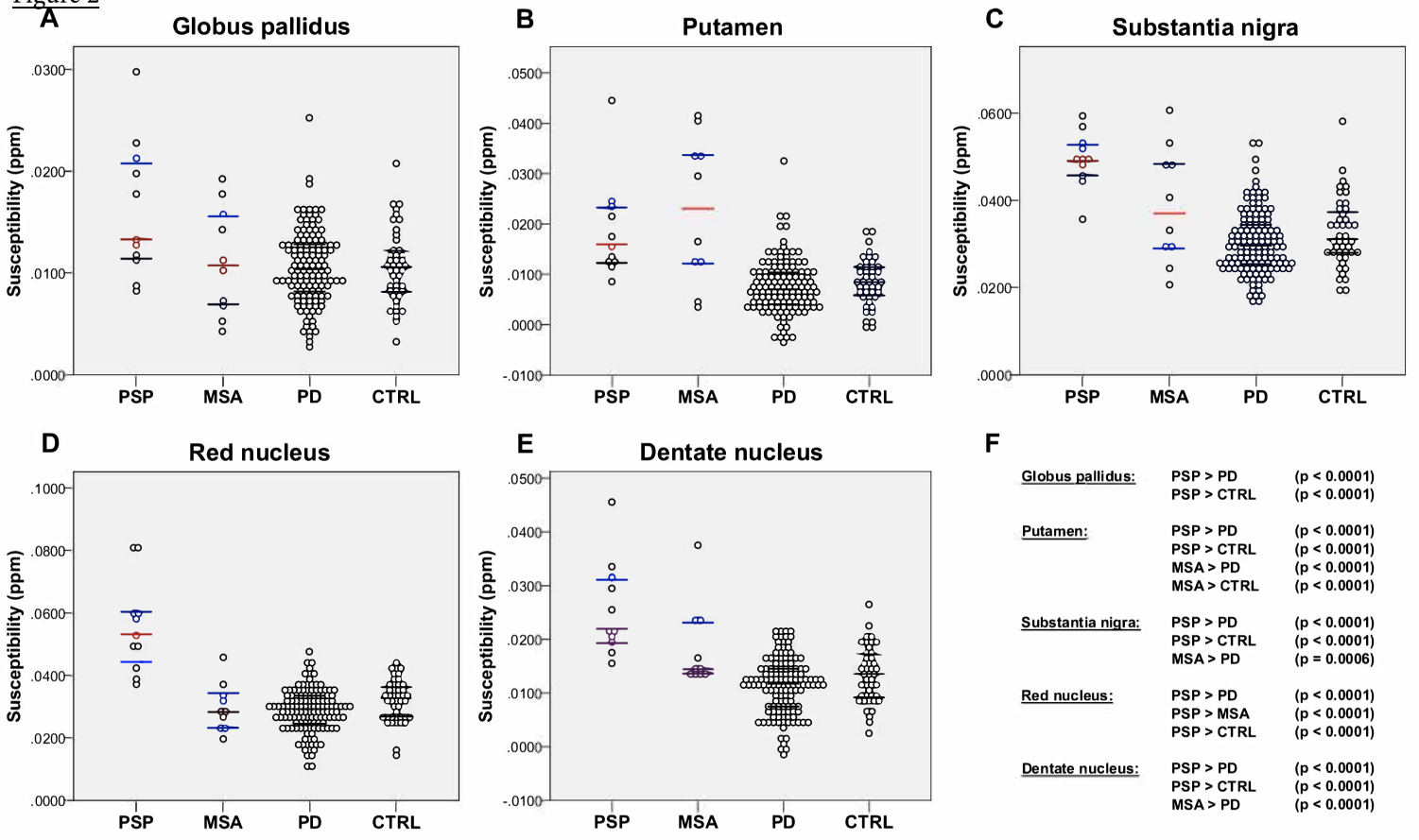
A
Globus pallidus
Susceptibility (ppm)
.0300
.0200
.0100
.0000
PSP
MSA
PD
CTRL
B
Putamen
Susceptibility (ppm)
.0500
.0400
.0300
.0200
.0100
.0000
-.0100
PSP
MSA
PD
CTRL
C
Substantia nigra
Susceptibility (ppm)
.0600
.0400
.0200
.0000
PSP
MSA
PD
CTRL
D
Red nucleus
Susceptibility (ppm)
.1000
.0800
.0600
.0400
.0200
.0000
PSP
MSA
PD
CTRL
E
Dentate nucleus
Susceptibility (ppm)
.0500
.0400
.0300
.0200
.0100
.0000
-.0100
PSP
MSA
PD
CTRL
F
Globus pallidus: PSP > PD (p < 0.0001)
PSP > CTRL (p < 0.0001)
Putamen: PSP > PD (p < 0.0001)
PSP > CTRL (p < 0.0001)
MSA > PD (p < 0.0001)
MSA > CTRL (p < 0.0001)
Substantia nigra: PSP > PD (p < 0.0001)
PSP > CTRL (p < 0.0001)
MSA > PD (p = 0.0006)
Red nucleus: PSP > PD (p < 0.0001)
PSP > MSA (p < 0.0001)
PSP > CTRL (p < 0.0001)
Dentate nucleus: PSP > PD (p < 0.0001)
PSP > CTRL (p < 0.0001)
MSA > PD (p < 0.0001)

Figure 3

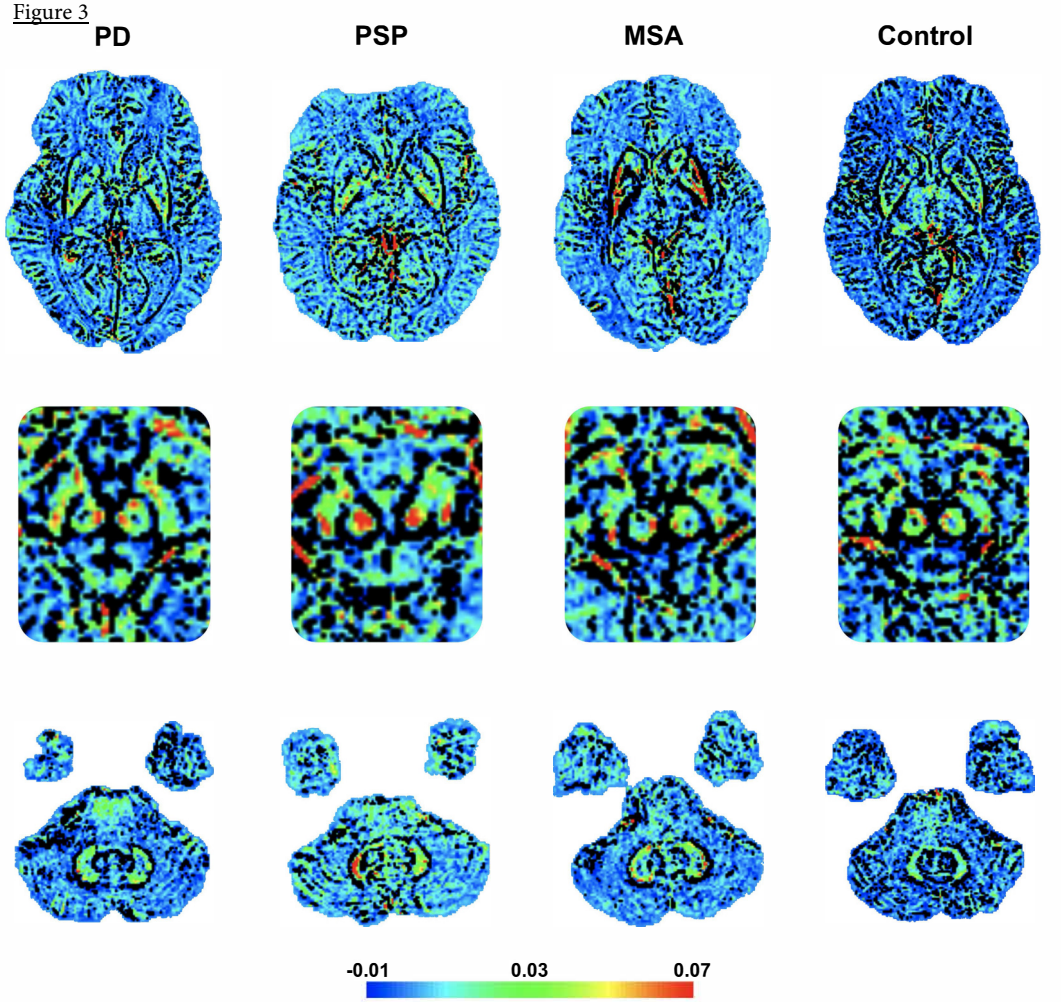

Figure 4

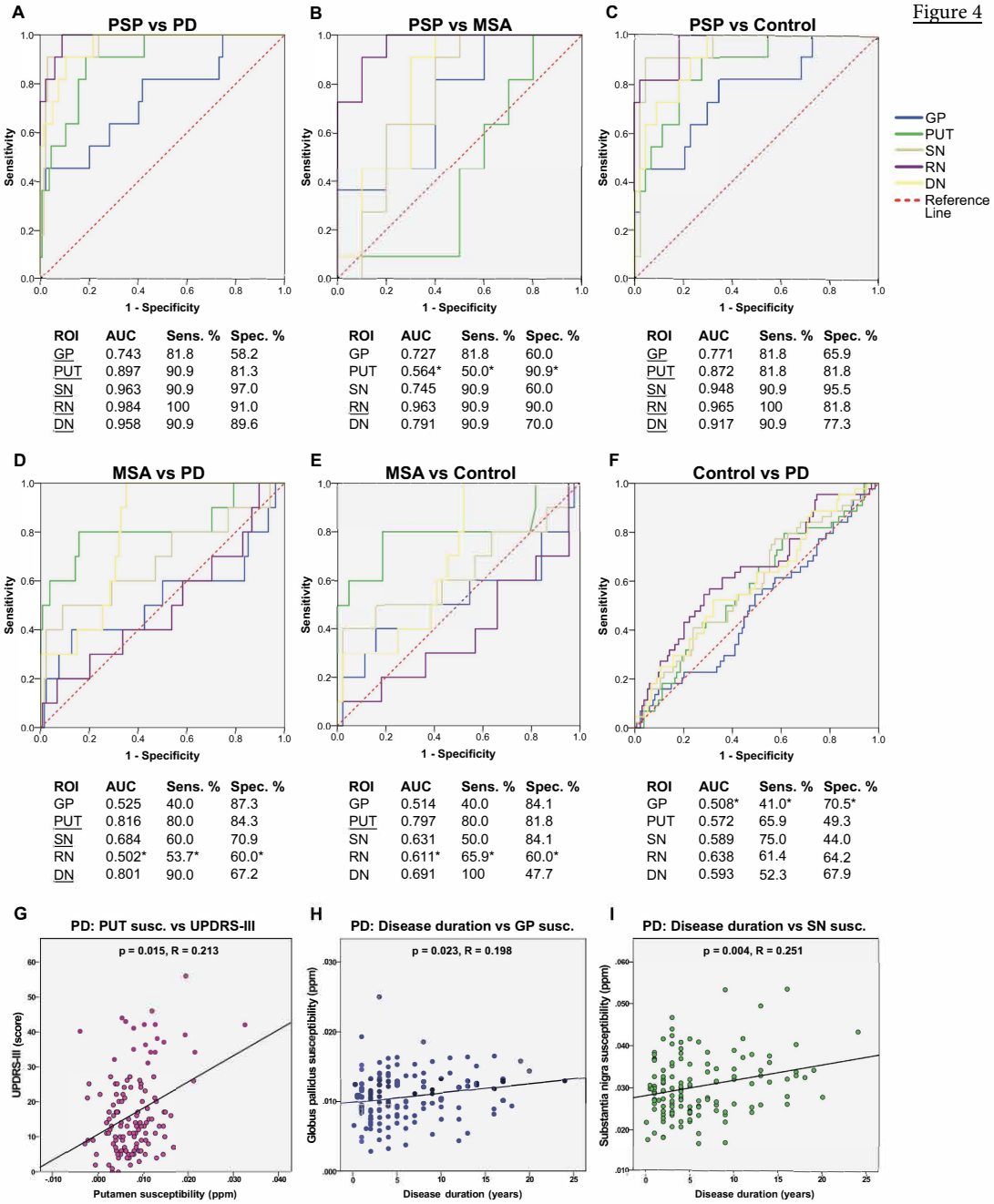

ROI	AUC	Sens. %	Spec. %
GP	0.743	81.8	58.2
PUT	0.897	90.9	81.3
SN	0.963	90.9	97.0
RN	0.984	100	91.0
DN	0.958	90.9	89.6

ROI	AUC	Sens. %	Spec. %
GP	0.727	81.8	60.0
PUT	0.564*	50.0*	90.9*
SN	0.745	90.9	60.0
RN	0.963	90.9	90.0
DN	0.791	90.9	70.0

ROI	AUC	Sens. %	Spec. %
GP	0.771	81.8	65.9
PUT	0.872	81.8	81.8
SN	0.948	90.9	95.5
RN	0.965	100	81.8
DN	0.917	90.9	77.3

ROI	AUC	Sens. %	Spec. %
GP	0.525	40.0	87.3
PUT	0.816	80.0	84.3
SN	0.684	60.0	70.9
RN	0.502*	53.7*	60.0*
DN	0.801	90.0	67.2

ROI	AUC	Sens. %	Spec. %
GP	0.514	40.0	84.1
PUT	0.797	80.0	81.8
SN	0.631	50.0	84.1
RN	0.611*	65.9*	60.0*
DN	0.691	100	47.7

ROI	AUC	Sens. %	Spec. %
GP	0.508*	41.0*	70.5*
PUT	0.572	65.9	49.3
SN	0.589	75.0	44.0
RN	0.638	61.4	64.2
DN	0.593	52.3	67.9

Errata

Errata in Paper II

In Paper II, In Discussion is said LVLP. This should be LPVP. Also in Fig.1 legends, **c** is said red nucleus, and **f** is said for deep cerebellar nuclei. This should be **c** for deep cerebellar nuclei and **f** for red nucleus.

Errata in Paper III

In Paper III, S1 Table is called Use of DKI parameters in differential diagnosis. This should be called Use of DKI parameters in differential diagnosis of patients with Parkinson's disease from healthy controls.

Also in the same table legend is said: Mean diffusivity (MD, 10^9 mm^2/s) and mean kurtosis (MK), differentiating patients with Parkinson disease (PD) from healthy controls (HC); PD from patients with progressive supranuclear palsy (PSP) and multiple system atrophy (MSA). AUC, area under curve; DKI, diffusion kurtosis imaging; ROC, receiver operating characteristic analysis. Significant differences between PD vs HC and PD vs PSP and MSA, $p < 0.05$, using binary logistic regression, adjusted for age and sex (PD vs HC) and adjusted for age (PD vs PSP and MSA).

This should be: Mean diffusivity [MD, 10^-9 m^2/s] and mean kurtosis (MK). AUC, area under curve; DKI, diffusion kurtosis imaging; ROC, receiver operating characteristic analysis. *Significant differences between patients with Parkinson's diseases from healthy controls, $p < .05$, using binary logistic regression, adjusted for age and sex.

In Results, Hand test should be called CAPSIT-PD test. CAPSIT-PD (Hagell 2000) test should be listed in the Material and Methods.